UNIVERSITY OF CAPE COAST

MATHEMATICAL MODEL OF IMMUNE RESPONSE TO HEPATITIS B VIRUS AND LIVER CANCER CO-EXISTENCE DYNAMICS IN THE PRESENCE OF TREATMENT

BY

PAUL CHATAA

Thesis submitted to the Department of Mathematics of the School of Physical Sciences, College of Agriculture and Natural Sciences, University of Cape Coast, in partial fulfilment of the requirements for the award of Doctor of Philosophy degree in Mathematics

JULY 2024

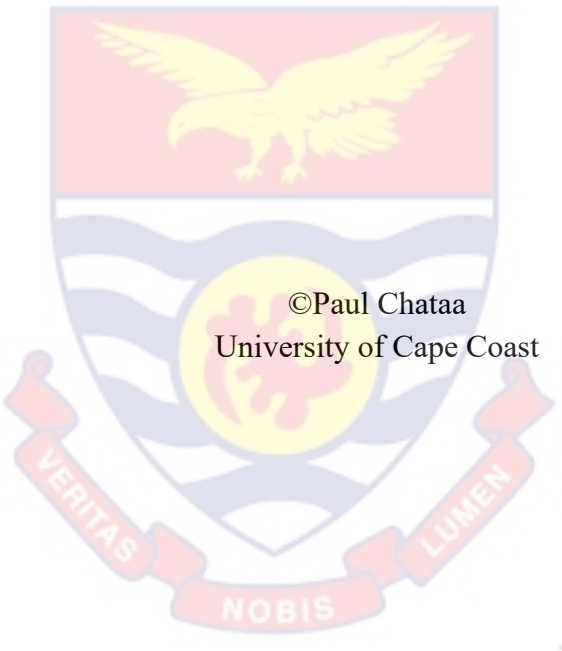

DECLARATION

Candidate's Declaration

I hereby declare that this thesis is the result of my own original research and that no part of it has been presented for another degree in this university or elsewhere.

Candidate's Signature ..... Date .....

Name: Paul Chataa

Supervisors' Declaration

We hereby declare that the preparation and presentation of the thesis were supervised in accordance with the guidelines on supervision of thesis laid down by the University of Cape Coast.

Principal Supervisor's Signature ..... Date .....

Name: Dr. Samuel Mindakifoe Naandam

Co-Supervisor's Signature ..... Date: .....

Name: Dr. Francis Tanam Djankpa

ABSTRACT

The principal method for modeling the spread of infectious diseases generally involves the application of ordinary differential equations. Studies have demonstrated that an effective strategy for refining certain mathematical models is the integration of fractional-order differential equations. To gain a more profound understanding of the interactions between the hepatitis B virus (HBV), liver cancer, and immune system cells, a mathematical model that combined both ordinary and fractional differential equations was investigated. This model was closely aligned with experimental data on viral DNA load. The work concentrated on four qualitative scenarios: the innate immune response, adaptive immune response, cytokine response, and the coexistence of infection dynamics. Unlike earlier models, liver cells were classified into distinct stages of infection. For populations of non-pathogenic macrophages in the presence and absence of malignant cells, the study calculated the invasion probability for transmission dynamics, represented by the control reproduction number, $\mathcal{R}_c$. The iterated two-step Adams-Bashforth method was employed for numerical simulations using the ABC fractional derivative in the Caputo sense, while the Latin Hypercube Sampling (LHS) and Partial Rank Correlation Coefficients (PRCC) techniques were utilized for parameter sensitivity analysis. The work identified the key transmission mechanism of viral load and proposed an optimal therapeutic method for viral treatment. Model parameters were estimated using nonlinear least squares fitting of longitudinal data (serum HBV DNA viral load) from existing literature. Finally, the study compared the classical-order model system with the ABC fractional differential equations model system to determine which offered superior performance. Both methods were evaluated using simulation results of the state variables, revealing that the fractional model provides more detailed results than the classical model.

KEY WORDS

Chronicity

Iterative Method

Interleukin-10

Lagrange Interpolation

Macrophages

Ulam-Hyers Stability

ACKNOWLEDGEMENTS

I wish to convey my profoundest appreciation to my supervisors, Dr. Samuel Mindakifoe Naandam and Dr. Francis Tanam Djankpa, for acquainting me with the discipline of mathematical biology and allowing me to work on various fascinating projects. I am immensely thankful for their insightful feedback, guidance, encouragement, and dedication. May God bless them with good health and enrich their lives. I would additionally like to articulate my utmost and most profound gratitude to Professor Bismark Oduro for his invaluable guidance, mentorship, and support throughout the course of my dissertation. His insightful advice, encouragement, and patience have been essential to my development as a researcher. My sincere thanks also go to Professor Ernest Yankson, Dean of the School of Physical Sciences, for his valuable academic contributions throughout this research. Additionally, I extend my heartfelt thanks to the staff and lecturers of the Mathematics Department. I am particularly grateful to Nicholas Opoku for his comments, feedback, and support throughout this dissertation.

This dissertation would have been inconceivable without the extraordinary support I received from my family, particularly my brother, Mr. Yaw Chataa. I am profoundly grateful for his steadfast assistance, relentless encouragement, and fervent prayers.

DEDICATION

To my family

TABLE OF CONTENTS

LIST OF TABLES

LIST OF FIGURES

LIST OF ABBREVIATIONS

ESLD	End-Stage Liver Disease
NK	Natural Killer
DNA	Deoxyribonucleic Acid
HBV	Hepatitis B Virus
HCC	Hepatocellular Carcinoma
LHBs	Large Hepatitis B surface Protein
RNA	Ribonucleic Acid
MHC	Major Histocompatibility Complex
WHO	World Health Organisation
LHS	Latin Hypercube Sampling
PRCC	Partial Rank Correlation Coefficients
UH	Ulam-Hyers Stability
AUC	Area Under the Curve
PC	Percentage Change

CHAPTER ONE

INTRODUCTION

This dissertation investigates the immune response to the simultaneous presence of hepatitis B virus (HBV) and liver carcinoma through a deterministic modeling framework utilizing both classical-order and fractional-order analyses. Our objective is to formulate and evaluate an epidemiological model that integrates immunological dynamics and cancer progression, employing both fractional-order and classical differential and integral operators novel areas in the realm of mathematical biology. The research encompasses an introduction to the topic, a delineation of the problem, the aims and significance of the study, and a comprehensive outline of the thesis structure.

Background to the Study

Hepatitis B, a hepatic viral infection, can evolve into both acute and chronic conditions, resulting in significant health repercussions. As detailed by Ciupe et al. (2014), this ailment causes approximately $750,000$ fatalities annually, with around $300,000$ of these deaths attributable to hepatic cirrhosis and hepatocellular carcinoma (HCC) (Guidotti & Chisari, 2001). This pathogen is presumed to impact approximately one-third of the worldwide populace, rendering it not merely one of the most primordial but also among the most hazardous viral menaces to human well-being (Ciupe, Ribeiro, Nelson, Dusheiko, & Perelson, 2007). Based on projections from the World Health Organization (WHO), approximately 1.5 million novel cases of hepatitis B are documented annually, resulting in a prevalence of 296 million individuals enduring chronic infection (World Health Organization, 2019). In 2019 alone, hepatitis B accounted for 820,000 fatalities, primarily attributable to hepatic fibrosis and hepatocellular malignancy, the most prevalent form of liver neoplasm (World Health Organization, 2019). The global mortality from liver cancer is substantial, with projections indicating that this figure will continue to escalate. Among the individuals affected, 6.3% are also co-infected with hepatitis B. Conversely, hepatitis B prevalence is relatively low in Europe and North America, with rates below

1%. Nonetheless, the disease remains a major health challenge in Asia and Africa, where the incidence of chronic infection is between 5 and 10 per 100 adults.

The hepatitis B virus (HBV), classified within the hepadnaviridae family, is the etiological agent responsible for hepatitis B infection. Due to its predominantly double-stranded DNA structure, once an individual is infected, the clearance of the hepatitis B virus becomes particularly arduous (Guidotti & Chisari, 2001). The incubation period for HBV ranges from 30 to 180 days. The virus can be detected approximately 30–60 days post-infection, and if transmission occurs during infancy or early childhood, it frequently establishes a persistent infection, leading to chronic hepatitis B in the majority of cases (around 90%) (Babiker et al., 2012; Nowak et al., 1996). Maternal-to-child transmission, primarily occurring during parturition, constitutes the foremost mechanism of infection in these initial developmental phases, leading to repetitive infection cycles and elevated chronicity rates. Horizontal transmission routes, including sexual contact among adults, intravenous drug use, exposure to contaminated blood products, and unhygienic practices, represent another vector of HBV dissemination. However, only 5–10% of adults subjected to these transmission routes develop chronic infection (Babiker et al., 2012; Nowak et al., 1996).

Adults generally recover from HBV infection when the immune system mounts an adequate and multifaceted response. This includes the activation of potent and diverse $CD4^+$ (T-helper 1) and $CD8^+$ (cytotoxic T lymphocyte) T-cell responses, production of neutralizing antibodies specific to the HBV surface antigen (HBsAg), and the secretion of antiviral cytokines within the liver, such as interferon-gamma (type-2 interferons) and tumor necrosis factor-alpha (TNF-α) (DeVico & Gallo, 2004; Nowak et al., 1996). These responses contribute to the generation of refractory hepatocytes that become resistant to reinfection (Su et al., 2012; Busca & Kumar, 2014). However, the precise roles of various immune system components, particularly the regulatory cytokine interleukin-10, in the initiation and resolution of HBV infections, remain inadequately understood. Unvaccinated neonates and immunosuppressed adults are more susceptible to progressing to chronic HBV

infection (Guidotti et al., 1994). In these individuals, both humoral and cellular immune responses are insufficiently effective, leading to persistent viral replication and continuous expression of HBsAg in the bloodstream (Guidotti & Chisari, 2001; Herbein & O'brien, 2000). The proportional influences of the immune system's heterogeneous constituents, especially the role of anti-inflammatory cytokines such as interleukin-10, in the advancement and chronicity of HBV infection, remain incompletely delineated.

The empirical investigation of the antibody-mediated immune response to hepatitis B virus (HBV) infection poses significant challenges. This complexity arises from the fact that free surface antigen antibodies are not discerned until subsequent to the resolution of HBV infection (Pawelek et al., 2012). However, both acute and chronic HBV infections are associated with circulating immune complexes that consist of antibodies bound to hepatitis B surface antigen (HBsAg), suggesting that antibody production occurs much earlier in the infection process than detectable and may contribute to the attenuation disease transmission dynamics (Ciupe, Ribeiro, Nelson, Dusheiko, & Perelson, 2007; Fatehi et al., 2022). Immune protection against HBV is conferred by HBsAg-specific antibodies, which possess neutralizing capabilities (Fatehi et al., 2022). Interestingly, the production of "subviral particles" (SVPs) increases exponentially in HBV infection compared to the generation of complete HBV virions (J. Hu & Liu, 2017; Fatehi et al., 2022). Sub-viral particles are viral particles that display HBV envelope proteins but lack the nucleocapsid and viral genetic material, rendering them non-infectious, and are produced by HBV-infected hepatocytes (Fatehi et al., 2020). Ongoing research aims to elucidate the mechanisms underlying their excessive production and their role in HBV pathogenesis (Murray & Goyal, 2015). Sub-viral particles may influence the immune response to HBV infection, potentially inducing immunological acquiescence during neonatal infection by delaying the generation of neutralizing antibodies. Furthermore, an abundance of SVPs can act as immunological decoys by sequestering neutralizing antibodies, thereby slowing the clearance of the virus from the host.

The hepatitis B virus employs host cellular machinery to facilitate its survival

and replication during infection. Once intracellular, the virus evades detection by immune surveillance, effectively shielding itself from the host's immunocompetent cells. In order to counteract this evasion, various components of the immune system synergistically mount a multi-layered defense across different stages of the infection. At the initial phase of infection, the innate immune response, involving natural killer (NK) cells and cytokine release, is pivotal in the host defense against a spectrum of viral infections, including SARS-CoV-2 (Covid-19), influenza, HIV, lymphocytic choriomeningitis virus (LCMV), and HBV. These innate immune mechanisms act to limit viral dissemination while simultaneously promoting the establishment of an adaptive immunological response. The NK cells specifically recognize virally infected cells by identifying reduced display of major histocompatibility complex (MHC) molecules on the cellular membrane, subsequently triggering the destruction of these compromised cells. Both NK cells and cytotoxic T lymphocytes (CTLs) harbor cytolytic effector molecules within granules that are mobilized and released upon interaction with an infected cell. Among these mediators, perforin, a pore-forming protein, disrupts the integrity of target cell membranes, enabling the entry of other cytotoxic molecules. The granules also contain enzymes known as granzymes, which infiltrate the target cell through perforin-created pores, inducing apoptosis and eliminating the infected cell.

Contrary to the typical progression of viral infections, the initial stages of hepatitis B virus (HBV) infection are characterized by a subdued production of interferon-α/β ($IFN_{\alpha/\beta}$) and a relatively slow rate of viral replication. Several hypotheses have been proposed to elucidate this anomaly. One theory posits that the virus may not immediately infiltrate hepatocytes but instead resides transiently in other tissues, while another suggests that the virus replicates at a significantly reduced rate during this phase (Perelson et al., 1996; Su et al., 2012). However, the precise biological transformations occurring during this period remain largely elusive. As HBV enters its exponential replication phase, the innate immune system, along with cytokine activity, is triggered (Busca & Kumar, 2014). This activation subsequently initiates the adaptive immune response, which includes antibody-mediated

neutralization of HBV surface antigen (HBsAg), thereby preventing the reinfection of hepatocytes. Furthermore, cytotoxic lymphocytes play a crucial role in eradicating infected cells while concurrently inducing cytokine production. Interestingly, cytotoxic lymphocytes not only eliminate HBV-infected hepatocytes but also facilitate non-cytolytic clearance of these cells (Busca & Kumar, 2014; Guidotti et al., 1994; Herbein & O'brien, 2000). In the evolving immune response to HBV, cytokines serve a pivotal function, inhibiting viral replication (Pawelek et al., 2012), stimulating antibody production, and activating natural killer (NK) cells and cytotoxic T lymphocytes (CTLs) (Ciupe, Ribeiro, Nelson, Dusheiko, & Perelson, 2007). Moreover, they aid in inducing immunity within target cells that have yet to be infected (Ramsay et al., 1993).

Tumorigenesis in the liver commences when a single hepatocyte undergoes aberrant growth. Based on its potential for metastasis, a tumor can be classified as benign, indicating it is non-cancerous with no propensity for metastasis; premalignant, suggesting it may develop into cancer; or malignant, indicating an aggressive capacity for rapid, uncontrolled growth and metastasis (Yang et al., 2020; Dehingia et al., 2021). Hepatocellular carcinoma (HCC), the medical term for primary liver cancer, represents a malignant neoplasm of the liver, which is the second-largest organ in the human body (Engelhart et al., 2011). Liver cancer ranks as the fifth leading cause of cancer-related mortality globally, constituting a significant public health concern, especially in low-resource settings where it receives insufficient attention. The scarcity of reliable epidemiological data on the incidence and prevalence of liver cancer impedes accurate projections of the HCC burden in developing countries. Consequently, the policy framework for the management and control of HCC is inadequate. This inadequacy is also evident in Ghana's approach to the management and control of HCC.

In developing regions, the majority of patients afflicted with hepatocellular carcinoma (HCC) present at medical facilities during advanced stages of the disease, resulting in exceedingly high mortality rates. Liver cancer is unique in that it can arise from both infectious and non-infectious etiologies. Key risk factors in-

clude chronic alcohol abuse and tobacco use. Due to its asymptomatic nature in early stages, HCC is often referred to as a "silent killer." Planning for the impact of HCC is challenging, as data for accurately estimating the incidence and prevalence of the disease within populations remains scarce. Proper estimation of the HCC burden is critical for effective allocation of healthcare resources, mobilization efforts, and the implementation of preventive strategies. Projections indicate that by 2030, liver and pancreatic cancers are expected to surpass breast, prostate, and colorectal cancers as the second and third leading causes of cancer-related mortality in the United States, respectively (Engelhart et al., 2011). The evolving epidemiological landscape, exacerbated by factors such as undetermined causes, inadequate prevention policies, insufficiently trained medical personnel, suboptimal monitoring, and a dearth of research, has rendered HCC a neglected non-communicable disease (NCD) in developing nations.

The application of advanced calculus has garnered significant scholarly attention and has been extensively utilized across various scientific domains. Researchers have employed modern calculus to construct mathematical models for a wide array of viral diseases. The majority of these mathematical modeling methodologies hinge on systems of differential equations, which may be linear or nonlinear, or on classical-order integral and differential equations. However, over the past three decades, fractional-order differential equations (FDEs) have been increasingly utilized to model complex real-world problems with greater precision and accuracy. The traditional integer-order mathematical framework may not always be suitable for capturing the intricacies of all systems. Consequently, fractional calculus has exerted a profound influence across multiple disciplines, including mechanics, chemistry, biology, and image processing. The utilization of fractional calculus enables the resolution of various physical challenges. In many scenarios, fractional-order differential equation (FODE) models exhibit superior alignment with real-world phenomena compared to their integer-order counterparts. This can be attributed to the fact that fractional derivatives and integrals allow for the incorporation of memory and hereditary effects, which are characteristic of most biological systems and infectious

disease processes. Additionally, FDEs provide a broader domain of stability relative to traditional differential equations. Moreover, unlike classical derivatives, which function as local operators, fractional derivatives serve as non-local operators. This non-locality permits fractional differential equations to represent epidemic models in a manner that is more realistic and comprehensive, accounting for both historical and current conditions.

The probability of eradicating hepatocellular carcinoma (HCC) diminishes significantly when hepatitis B virus (HBV) infection concomitantly occurs with hepatic carcinoma. Consequently, it is essential for the research consortium to conduct thorough inquiries into both hepatitis B and hepatic malignancy via clinical examinations and conceptual evaluations. The formulation of efficacious therapeutic interventions for hepatitis B and HCC constitutes a critical domain within medical research that will significantly enhance our understanding of tumor-immune system interactions. Despite the fact that a substantial proportion of individuals (approximately 90%) mount a robust and protective cell-mediated immune response that prevents the progression to chronic HBV infection, which is a precursor to HCC, hepatitis B remains one of the foremost causes of mortality worldwide, contributing to an estimated 3 million deaths annually (Guidotti & Chisari, 2001). The objective of this research was to explore the progression from acute HBV infection to chronic HBV infection, and ultimately to HCC, while examining the immune system's response to each of these stages. A more profound comprehension of the mechanisms governing immune response dynamics cells would enhance the immune system's capacity to control HBV in the early phases of infection and would elucidate how the virus evades both adaptive immunity and innate cytokine-mediated defenses. Consequently, we propose and analyze fractional and classical-order deterministic models to assess the impact of various immune response components on the co-dynamics of HBV and HCC in the context of therapeutic interventions.

Statement of the Problem

The World Health Organization (WHO) has instituted an ambitious target to eradicate hepatocellular carcinoma and hepatitis B virus (HBV) infection by the year

2030 (Vos et al., 2015; Fatehi et al., 2022). Current strategies for controlling the spread of HBV include the medical treatment of infected individuals and the immunization of neonates and vulnerable adults through the administration of the hepatitis B vaccine. Additionally, public health campaigns designed to raise awareness about the detrimental effects of alcohol consumption and smoking are employed as preventive measures to mitigate the risk of liver cancer and reduce the transmission of the virus. These prophylactic interventions aim to avert acute HBV infections and to prevent the recurrence of liver cirrhosis in individuals with pre-existing hepatic conditions. However, despite these efforts, the occurrence of hepatitis B and hepatic neoplasia remains profoundly elevated, with millions of novel instances and fatalities recorded annually. Although progress has been made toward the global elimination of HBV, the virus continues to pose a significant public health threat. As of 2019, an estimated 316 million individuals were living with chronic HBV infection globally (Sheena et al., 2022), reflecting a chronic HBV prevalence rate of approximately 4.1%.

Hepatocellular carcinoma (HCC), a predominant type of liver cancer, along with cirrhosis, constitutes the leading causes of mortality related to hepatitis B infection, according to the WHO (World Health Organization, 2019). Projections indicate that these diseases are likely to result in millions of additional fatalities in the coming years, underscoring the critical need for long-term strategies to manage HBV infection and liver cancer. Nevertheless, significant gaps remain in our understanding of the epidemiology of HBV and its disease course. There are unresolved questions about the virus's capacity to evade the immune system and progress to advanced stages, such as liver cirrhosis, HCC, and liver cancer. Despite these uncertainties, it is widely acknowledged that the application of mathematical modeling offers a robust approach for elucidating the epidemiological dynamics of HBV and liver cancer. This aligns with the notable successes observed through the integration of theoretical and empirical investigations in the realms of clinical and biological sciences. Researchers have recognized the critical role that mathematical models can play in epidemiological research. Consequently, gaining a deeper comprehen-

sion of the co-occurrence and interplay of HBV and liver cancer is essential for the development of effective fractional and classical order mathematical models that can accurately capture the dynamics of these disease processes.

During the acute phase of hepatitis B virus (HBV) infection, viral titers can surge to approximately 10^{10} HBV DNA copies per milliliter of plasma, persisting at elevated levels for several weeks as numerous hepatocytes become infected. Over time, viral titers diminish, and in roughly $85\% - 95\%$ of acutely infected adults, the virus is successfully eradicated. Individuals who achieve viral clearance generally exhibit more robust and diverse $CD4^+$ and $CD8^+$ T lymphocyte responses. Additionally, viral clearance in these patients is typically accompanied by an elevation in alanine aminotransferase (ALT) levels, indicative of hepatic injury and an active immune response mediated by cytotoxic cells. Although the immune system plays a crucial role in reducing viral titers, the exact mechanisms underlying this process remain incompletely elucidated.

Numerous mathematical models have been devised to investigate the transmission dynamics of HBV and hepatocellular carcinoma, as well as strategies for the prevention, treatment, and control of these diseases across various geographic regions. Utilizing systems of ordinary and partial differential equations, these models have yielded valuable insights into the impact of vaccination and therapeutic interventions as control measures for HBV infection and the management of liver cancer. Despite these contributions, existing modeling research has yet to result in the development of highly effective therapies for HBV and hepatocellular carcinoma. One conceivable rationale for this deficiency is that the majority of frameworks addressing HBV and hepatic malignancy neglect to integrate the impact of interleukin-10 and the differentiation pathways of naive T lymphocytes, which we have recognized as crucial components in devising effective therapeutic approaches for HBV and hepatic carcinoma.

Additionally, it is vital to acknowledge the paramount role that the immune system occupies in the evolution of hepatitis B virus (HBV) and hepatocellular carcinoma (HCC) infections. Interleukin-10 (I_{10}), a critical cytokine, regulates both

innate and adaptive immune responses, predominantly by imparting immunosuppressive and anti-inflammatory effects. Therefore, the development of a sophisticated model to analyze the regulatory functions of interleukin-10 and other immune mediators in orchestrating both cellular and humoral immunity would prove beneficial. This study formulated an advanced mathematical framework that incorporates interleukin-10 (I_{10}), naive T lymphocytes, antibodies, natural killer (NK) cells, effector B cells, and cytokines to investigate the immune system's multifaceted response to HBV and HCC infections. The research focuses on four pivotal domains: optimizing therapeutic interventions, evaluating the efficacy of fractional and classical-order models, elucidating the roles of innate immunity, humoral immunity, and cytokine-mediated pathways, and examining their coexistence in the complex dynamics of infection. The ultimate objective was to mitigate viral proliferation and minimize hepatic damage. Our model integrates several immune strategies, such as interferon-mediated immunity (type I and type II) to hinder viral replication by depleting the substrates necessary for viral synthesis (i.e., healthy hepatocytes), cell-mediated immunity (T lymphocytes, NK cells, effector B cells, interleukin-10 cells) to target and eliminate the source of viral generation (i.e., infected hepatocytes), and adaptive immunity (anti-HBV antibodies) to reduce the effective viral concentration. A distinctive feature of the model was its ability to simulate the impact of HBV infections on hepatocytes that have already undergone malignant transformation and how this interaction affects the overall population dynamics of liver cells.

Research Objectives

General objective

The primary aimed of this thesis is to mathematically examine the immune response in relation to the transmission dynamics of the hepatitis B virus and its co-existence with liver cancer.

Specific objectives

This research has the following specific objectives:

(1) to develop a classical and fractional order models, which takes into account the

important role played by various branches of the immune system in clearing HBV and liver cancer infections.

(2) to estimate the model parameters by fitting the model to HBV DNA viral load data and perform sensitivity analysis to determine the most sensitive parameters.

(3) to conduct numerical simulations on the model system to determine the transition time from acute infection to the chronic stage and to recommend a treatment strategy.

(4) to evaluate the classical-order and ABC fractional-order model systems to determine which one yields better results.

Significance of the Study

We can use mathematical models to evaluate the efficacy of various control and prevention efforts and to acquire a thorough knowledge of the dynamics of disease transmission. As far as we are aware, no mathematical model has been created that addresses the coexistence of the hepatitis B virus and liver cancer while considering the influence of innate, humoral, adaptive, and cytokine responses of the immune system. This research would aid medical professionals in their understanding of the immune system's defenses against the hepatitis B virus and liver cancer infection. The results of this research would give Ghanaian health officials a more comprehensive framework to create the best infectious disease policies. The study would also provide light on how medical facilities use their resources to hepatitis B and liver cancer patients who are receiving treatment. Finally, it would expand the body of knowledge on the hepatitis B virus and liver cancer infection and give researchers a platform to push the boundaries of knowledge in these two fields.

Delimitation

The thesis is limited to investigating the important role played by the immune system (i.e macrophages, T cells, NK cells, anti-bodies, effector B cells, interleukin-10, interferon-alpha and beta, interferon-gamma) in fighting hepatitis B virus and

liver cancer infections.

Limitation

This thesis has a limitation of accurate estimation of parameter values since we largely rely on patients DNA viral load data for parameter values for the numerical simulations which may be influenced by other factors.

Another significant limitation of this study is that the patient dataset used does not include individuals diagnosed with liver cancer. As such, the findings may not be directly applicable to patients with liver cancer, whose immune response and disease progression could differ substantially from those observed in our cohort. Future studies should aim to incorporate datasets that include patients with liver cancer to evaluate the generalizability of the results and to explore disease-specific dynamics.

Definitions of Terms

In this section, our focus lies on several significant definitions of factional derivatives concerning the Atangana-Baleanu and Caputo fractional operators, which are intended for application in the immune response to co-existing hepatitis B virus and liver cancer model systems.

Definition 1

Gamma Function: The Gamma function, denoted by $\Gamma(k)$, is a generalization of the factorial function when k is not an integer. Particularly, $\Gamma(x) = (n-1)!$ for $x \in \mathbb{N}$. For $k > 0$, it is defined as

$$\Gamma(k) = \int_0^\infty t^{k-1} e^{-k} dt.$$

Definition 2

Given a function $g : \mathbb{R}^+ \to \mathbb{R}$, then the fractional integral of order φ in Caputo sense is given as

$${}_0^C\mathbb{I}_t^\varphi [g(t)] = \frac{1}{\Gamma(\varphi)} \int_0^t (t-f)^{\varphi-1} g(f)\, df,$$

where Γ denote the gamma function and φ stands for the fractional order.

Definition 3

Given a function $g \in C^n$, then the Caputo derivative with order φ is given as

$$ {}_0^C\mathbb{D}_t^{\varphi}\left[g\left(t\right)\right] = \mathbb{I}^{n-\varphi}\mathbb{D}g\left(t\right) = \frac{1}{\Gamma\left(n-\varphi\right)}\int_0^t \frac{g^n\left(f\right)}{\left(t-f\right)^{\varphi-n+1}}df, $$

which is defined for the continuous function in absolute terms and $n-1 < \varphi < n \in N$. Here, ${}_0^C\mathbb{D}_t^{\varphi}\left[g\left(t\right)\right]$ approaches $g'(t)$ as φ approaches 1.

Definition 4

Sobolev Space: Let $p \in [1,\infty)$ and Ω be an open set of $\mathbb{R}$, the Sobolev Space $H^p\left(\Omega\right)$ is defined by $H^p\left(\Omega\right) = \{f \in L^2\left(\Omega\right) : \mathbb{D}^{\varphi}f \in L^2\left(\Omega\right) \quad \forall, |\varphi| \leq p\}$.

Definition 5

Let $h \in H'\left(a,b\right), \quad b > a$ be a function. Then the Caputo-Fabrizo derivative of order $\varphi \in (0,1)$ of a function h is defined as

$$ {}_a^{CF}\mathbb{D}_t^{\varphi}\left[h\left(t\right)\right] = \frac{P\left(\varphi\right)}{1-\varphi}\int_a^t h'\left(x\right)\exp\left[-\varphi\frac{t-x}{1-\varphi}\right]dx, $$

where $P(\varphi)$ is a normalization function satisfying $P(0) = P(1) = 1$.

Definition 6

The Caputo-Fabrizo fractional integral of order $\varphi \in (0,1)$ of a function h is defined as

$$ {}_a^{CF}\mathbb{I}_t^{\varphi}\left[h\left(t\right)\right] = \frac{2\left(1-\varphi\right)}{2\left(1-\varphi\right)P(\varphi)}h(t) + \frac{2\varphi}{(2-\varphi)P(\varphi)}\int_a^t h\left(\psi\right)d\psi, \quad t \geq 0. $$

Definition 7

Let $g \in H'\left(a,b\right), \quad a < b$ be a function and $\varphi \in (0,1)$. Then the Atangana-Baleanu derivative in Caputo sense of order φ of the function g is defined as

$$ {}_a^{ABC}\mathbb{D}_t^{\varphi}\left[g\left(t\right)\right] = \frac{G\left(\varphi\right)}{1-\varphi}\int_a^t g'\left(x\right)\mathbb{E}_{\varphi}\left[-\varphi\frac{\left(t-x\right)^{\varphi}}{1-\varphi}\right]dx, $$

where $G(\varphi)$ is a normalization function satisfying $G(0) = G(1) = 1$ and $\mathbb{E}_{\varphi}$ is the Mittag-Leffler function.

Definition 8

Let $g \in H'(a,b), \quad a < b$ be a function and $\varphi \in (0,1)$. Then the Atangana-Baleanu derivative in Riemann-Liouville sense of order φ of the function g is defined as

$$ {}^{ABR}_{a}\mathbb{D}^{\varphi}_{t}\left[g(t)\right] = \frac{G(\varphi)}{1-\varphi}\frac{d}{dt}\int_{a}^{t} g(x)\,\mathbb{E}_{\varphi}\left[-\varphi\frac{(t-x)^{\varphi}}{1-\varphi}\right]dx. $$

Definition 9

The Atangana-Baleanu fractional integral in Caputo sense is defined by

$$ {}^{ABC}_{a}\mathbb{I}^{\varphi}_{t}\left[g(t)\right] = \frac{(1-\varphi)}{G(\varphi)}g(t) + \frac{\varphi}{G(\varphi)\Gamma(\varphi)}\int_{a}^{t} g(\psi)\,(t-\psi)^{\varphi-1}\,d\psi. $$

Definition 10

The Laplace transform of the ABC derivative of the function $g(t)$ of order $\varphi > 0$ is defined as

$$ \mathscr{L}\{{}^{ABC}_{a}\mathbb{D}^{\alpha}_{t}g(t)\}(s) = B(\varphi)\frac{s^{\varphi}\mathscr{L}\{g(t)\}(s) - s^{\varphi-1}g(0)}{(1-\varphi)\,s^{\varphi}+\varphi}. $$

Theorem 1

For a continuous function g on $[a,b]$, the inequality given below holds on $[a,b]$:

$$ ||{}^{ABR}_{a}\mathbb{D}^{\varphi}_{t}\left[g(t)\right]|| \leq \frac{G(\varphi)}{1-\varphi}||g(t)||, \quad \textit{where} \quad ||g(t)|| = \max_{a\leq t\leq b}|g(t)|. $$

Theorem 2

The Atangana-Baleanu derivative in both Caputo and Riemann-Liouville sense satisfy Lipschitz condition

$$ ||{}^{ABC}_{a}\mathbb{D}^{\varphi}_{t}\left[g(t)\right] - {}^{ABC}_{a}\mathbb{D}^{\varphi}_{t}\left[h(t)\right]|| \leq k||g(t)-h(t)|| \quad \textit{and} $$

$$ ||{}^{ABR}_{a}\mathbb{D}^{\varphi}_{t}\left[g(t)\right] - {}^{ABR}_{a}\mathbb{D}^{\varphi}_{t}\left[h(t)\right]|| \leq k||g(t)-h(t)||. $$

The Mittag-Leffler function's one-parameter representations can be defined through power series

$$E_{\alpha}(t) = \sum_{k=0}^{\infty} \frac{t^k}{\Gamma(\alpha k + 1)}, \quad \alpha > 0, \tag{1}$$

while the two-parameter Mittag-Leffler is defined as

$$E_{\alpha,\beta}(t) = \sum_{k=0}^{\infty} \frac{t^k}{\Gamma(\alpha k + \beta)}, \quad \alpha > 0, \quad \beta > 0. \tag{2}$$

The exponential series defined by Eq. (2) gives a generalization of equation Eq. (1). As a result of the definition given in Eq. (2), the following relations hold:

$$E_{\alpha,\beta}(t) = \frac{1}{\Gamma(\beta)} + tE_{\alpha,\alpha+\beta}(t) \quad \text{and} \tag{3}$$

$$E_{\alpha,\beta}(t) = \beta E_{\alpha,\beta+1}(t) + \alpha t \frac{d}{dx} E_{\alpha,\beta+1}(t). \tag{4}$$

Observing from Eq. (4) implies that

$$\frac{d}{dx} E_{\alpha,\beta+1}(t) = \frac{1}{\alpha t} \left[E_{\alpha,\beta-1}(t) - \beta E_{\alpha,\beta+1}(t) \right]. \quad \text{So}$$

$$\frac{d}{dx} E_{\alpha,\beta}(t) = \frac{1}{\alpha t} \left[E_{\alpha,\beta-1}(t) - (\beta - 1) E_{\alpha,\beta}(t) \right].$$

Definition 11

The Laplace Transform can be used in differential equations to reduce a linear differential equations to an algebraic one which can then be solved by rules of algebra. The transform is written as follows

$$\mathscr{L}\{f(t)\} = F(s) = \int_0^{\infty} e^{-st} f(t) dt.$$

Whereas the Laplace transform of Caputo fractional derivatives is given by

$$\mathscr{L}\left[D^{\alpha}f(t)\right] = s^{\alpha}F(s) - \sum_{k=0}^{n-1} f^{k}(0)s^{\alpha-k-1}.$$

Lemma 1

Proposed by (Podlubny, 1998; Magin, 2004; Baleanu et al., 2012)

Let $\alpha > 0$, $\beta > 0$ and $m \in C$. We define

$$f(t) \quad = \quad t^{\beta-1}\mathbb{E}_{\alpha,\beta}\left(\pm mt^{\alpha}\right),$$

where $\mathbb{E}_{\alpha,\beta}(\cdot)$ represents the two-parameter Mittag-Leffler function. Its Laplace transform is defined as

$$\mathscr{L}\{f(t)\} \quad = \quad \frac{s^{\alpha-\beta}}{s^{\alpha} \pm m}.$$

Lemma 2

The solution of the following initial value problem for $\varphi \in (0, 1]$

$$\begin{cases} {}_{0}^{ABC}\mathbb{D}_{t}^{\varphi}\Phi(t) & = \Psi(t), \\ \Phi(0) & = \Phi_{0}, \end{cases}$$

is given by

$$\Phi(t) \quad = \quad \Phi_{0} + \frac{1-\varphi}{N(\varphi)}\Psi(t) + \frac{\varphi}{N(\varphi)}\frac{1}{\Gamma(\varphi)}\int_{0}^{t}(t-\theta)^{\varphi-1}\Psi(\theta)d\theta.$$

Organisation of the Study

The thesis is organized into five chapters. CHAPTER ONE provides the background of the study. In CHAPTER TWO, we present related literature on both fractional and classical mathematical models of hepatitis B and liver cancer transmission dynamics. CHAPTER THREE is devoted to the formulation and analysis of the classical-order model. We also extend the classical-order model to a fractional-order model and analyze its basic properties. Parameter estimation, numerical simu-

lations, and sensitivity analysis of the proposed model are carried out and discussed in CHAPTER FOUR. CHAPTER FIVE is dedicated to conclusions and recommendations.

CHAPTER TWO

LITERATURE REVIEW

Introduction

Hepatitis B and liver cancer are among the most insidious and lethal afflictions globally. This is largely due to the fact that many individuals infected with the hepatitis B virus are unaware of their condition. It is therefore crucial to investigate the patterns of their global dissemination. To achieve this effectively, it is essential to explore how various researchers have utilized mathematical modeling to tackle these issues and how their models can be adapted to aid in the eradication of liver cancer and hepatitis B. Our review indicates that numerous policymakers, analysts, and scholars have employed mathematical models to analyze the dynamics, outcomes, and impacts of liver cancer and hepatitis B over time within human populations, as well as to assess how these models address the response of health systems to such infections. Their primary objective has been to devise strategies for the prevention, diagnosis, and management of these severe diseases. Consequently, this chapter is dedicated to examining the empirical literature related to the pathophysiology of hepatitis B and liver cancer, the evolution of mathematical modeling as a tool for investigating persistent diseases, the integration of diverse therapeutic approaches as preventive strategies, and the response of health systems to these infections.

Immune System and its Constituents

The immune system is conceptualized as an intricate ensemble of biological mechanisms and structural entities within an organism, meticulously designed to counteract and neutralize potentially pathogenic entities. It is widely acknowledged that the immune system plays a pivotal role in maintaining human health by providing defense against deleterious agents such as bacteria, viruses, and other microorganisms (Guidotti & Chisari, 2001). This sophisticated network comprises a multitude of interconnected components that collectively safeguard the body against various pathogens, including bacteria, fungi, and viruses. Central to this defensive system are the thymus and bone marrow, which are instrumental in the development

and maturation of immune cells. The medullary cavity of the bones operates as the principal locus of genesis for both T and B lymphocytes, as well as other hematopoietic progenitor cells, thereby fulfilling a fundamental role in immunological efficacy. T lymphocytes migrate to the thymus for further maturation, while B lymphocytes remain within the bone marrow to undergo their developmental processes.

The thymus, located superior to the heart, posterior to the sternum, and between the pulmonary organs, consists of two lobe-shaped glands. Post-puberty, the thymus undergoes a progressive involution, gradually being substituted by connective tissue and adipose tissue. Thymosin, a hormone secreted by the thymus, facilitates the proliferation and differentiation of T lymphocytes. Within the thymic environment, T cells proliferate, acquire unique antigen receptors, and differentiate into subsets such as Helper T cells (T_1) and Cytotoxic T cells (T_2). These T cells express various surface proteins, including $CD4^+$ and $CD8^+$, essential for their functional roles. The thymus is responsible for generating the full complement of T cells necessary for an individual throughout puberty.

Upon completion of their maturation in the thymus and bone marrow, T and B lymphocytes transit to secondary lymphoid organs such as the spleen and lymph nodes, where they persist until activated by antigenic stimuli. The spleen, positioned in the upper left quadrant of the abdomen, posterior to the stomach and diaphragm, primarily functions in blood filtration. Lymph nodes, distributed throughout the body, serve as crucial sites for immune surveillance. The spleen also plays a role in the degradation of senescent erythrocytes by macrophages, large phagocytic cells specialized in engulfing pathogens, cellular debris, and foreign particles. Additionally, the spleen acts as a reservoir for white blood cells and platelets and contributes to the immune response by identifying potential pathogens.

The immune system's defensive mechanisms are categorized into two principal systems: innate (non-specific) and adaptive (specific) immunity. These systems comprise a diverse array of leukocytes, also known as white blood cells. Granulocytes, a subset of leukocytes, contain cytoplasmic granules with enzymatic activity and include neutrophils, basophils, and eosinophils. Conversely, cells of the adap-

tive immune system, often referred to as immune effector cells, execute specialized functions in response to specific antigens. Examples include T lymphocytes and B lymphocytes, which, alongside natural killer cells, perform targeted immune functions. Macrophages and neutrophils patrol tissues and the bloodstream, seeking and responding to potential threats. Upon encountering pathogens, these cells engage in interactions with other immune cells and perform phagocytosis. Furthermore, effector cells are instrumental in combating cancer cells, with activated B cells producing antibodies that facilitate the immune response, and activated T lymphocytes eliminating pathogens through cell-mediated mechanisms. Antigen-presenting cells (APCs), such as myeloid-derived suppressor cells, tumor-associated macrophages, regulatory T cells, and dendritic cells, are classified as non-effector cells. While non-effector cells do not possess direct tumor-killing capabilities, they play a role in modulating the immune response and can inadvertently support tumor growth during oncogenic processes.

Immune System Response to Hepatitis B Virus Infected Cells

It is broadly recognized that the immune system is crucial for human health as it provides defense against pathogenic entities such as bacteria, viruses, and other microorganisms (Guidotti & Chisari, 2001). Hepatitis B virus infection typically evolves through two principal stages: acute and chronic. An acute hepatitis B infection is marked by the transient presence (less than six months) of viral DNA, hepatitis B surface antigen (HBsAg), and hepatitis B envelope antigen (HBeAg), followed by their clearance and subsequent seroconversion to anti-HBsAg and anti-HBeAg. During convalescence, IgM antibodies to the hepatitis B core antigen (IgM anti-HBc) convert to IgG antibodies. This transition occurs within the initial six months of infection. Acute hepatitis B may resolve spontaneously within this period, with many patients asymptomatic and therefore not requiring treatment at this stage. As reported by Shepard et al. (2006), about 90% of adults will clear the infection naturally within the first six months (the acute phase) without necessitating therapy. If the immune system fails to eradicate the hepatitis B virus within this period, the infection becomes chronic.

At this stage, the virus may persist and not be eradicated spontaneously. Consequently, individuals with chronic hepatitis B will require sustained therapy to achieve a longer and healthier life (Wilson et al., 1998). Mahoney & Kane (1999) highlights that chronic hepatitis B leads to significant hepatic damage and contributes extensively to the global hepatitis burden. While some chronic hepatitis B patients may not display clinical or biochemical evidence of liver disease, others may experience symptoms such as chronic fatigue, anxiety, loss of appetite, and general malaise. This is in contrast to the acute phase, where symptoms may be absent. The severity of chronic hepatitis B infection can vary from moderate to severe depending on the individual's immune response. According to Hollinger & Liang (2001), chronic hepatitis B is associated with inflammatory liver conditions like cirrhosis and hepatocellular carcinoma (HCC). Mahoney & Kane (1999) further notes that individuals at elevated risk for HCC include adult males with a history of hepatitis B and chronic cirrhotic patients exposed to the virus during childhood. The risk of HCC is influenced by the individual's age, gender, ethnicity, and geographical location. Therefore, 90% of primary malignant liver tumors detected in adults are attributed to HCC (World Health Organization, 2002).

Various researchers have investigated different facets of HBV dynamics and immune responses during infection through mathematical modeling. To examine acute HBV infection and the impact of temporal delays in effector cell activation and proliferation, Ciupe, Ribeiro, Nelson, Dusheiko, & Perelson (2007); Ciupe, Ribeiro, Nelson, & Perelson (2007) modified a conventional immune response model to include delays in naive T cell recruitment. They subsequently analyzed the effects of pre-existing or vaccine-induced antibodies on HBV management (Ciupe et al., 2014). Instead of employing a mass-action model to address the limited liver capacity and susceptibility to HBV infection, Min et al. (2008) used a standard incidence function in their study of HBV transmission dynamics. Gourley et al. (2008) introduced a time-delayed version of the model proposed by Min et al. (2008). The model developed by Hews et al. (2010) provided a better fit to existing data and offered more accurate estimates of the basic reproduction number by incorporating a

standard incidence function and logistic growth for hepatocyte populations. In their study of HBV infection, Yousfi et al. (2011) explored potential limitations in the coordination among various branches of the adaptive immune response, particularly focusing on CTLs and antibodies.

Regarding the role of cytokines in modulating immune responses, Wiah et al. (2011) posited that, alongside the actions of cytotoxic T lymphocytes (CTLs) and antibodies on hepatitis B virus (HBV) infection, interferon cytokines α and β also aid in the eradication of the virus by transforming susceptible hepatocytes into cells resistant to infection. This methodology has been similarly adopted by other scholars (Dahari et al., 2009; Lewin et al., 2001; Sypsa et al., 2005), who integrated a constant rate of non-cytolytic clearance into their treatment frameworks. Kim et al. (2012) modified an earlier hepatitis C model to implicitly incorporate cytokines by permitting effector cells to facilitate a non-cytolytic recovery of infected cells.

An analytical framework for the antibody response post-hepatitis B virus (HBV) infection was formulated by (Ciupe et al., 2014) to investigate the mechanisms of immune protection. After identifying that the virus could evade neutralization by producing excessive quantities of non-infectious sub-viral particles bearing hepatitis B surface (HBs) proteins but lacking viral nucleic acids and nucleocapsid proteins they adjusted their model using data from seven adults identified during the acute infection phase. They demonstrated that viral clearance could be attained in individuals with high levels of anti-HBV antibodies, such as those who have been vaccinated, under the following conditions: Hepatitis B sub-viral particles are generated at two distinct rates: (1) slowly; (2) rapidly if anti-HBV antibodies are produced rapidly, exhibit high affinity, or if substantial levels of pre-existing HBV-specific antibodies are present at the time of infection, potentially due to prior vaccination. Additionally, they showed that when a robust cellular immune response addresses early infection, viral clearance can occur with low steady-state levels of anti-HBV antibodies, similar to those in uninfected individuals. They concluded that achieving HBV clearance necessitates higher antibody levels than those typically observed in clinical settings, as evidenced by many patients and most acutely infected indi-

viduals. Furthermore, they suggest that antibodies may function similarly to the $CD8$-antibody model, which implies that antibodies prevent re-infection and that cytotoxic effects are critical for initial viral control. The dynamics of their model correspond with the quantities and timing of antibodies seen in patients. Moreover, they assert that viral clearance remains attainable when pre-existing immunity from vaccination or cross-immunity results in elevated antibody levels early in infection, even if the virus generates a large quantity of sub-viral particles as a strategy to evade antibody-mediated defenses.

Immune System Response to Cancer Infected Cells

Hepatocellular carcinoma (HCC), commonly referred to as liver cancer, is a malignancy affecting the liver, the body's second largest organ. This neoplasm is considered one of the most lethal and challenging cancers to manage clinically. Projections indicate that by 2030, liver cancer is anticipated to surpass colorectal, breast, and prostate cancers as the second leading cause of cancer-related mortality in the United States, with pancreatic cancer following as the third (Rahib et al., 2014). Liver cancer is unique in that it originates from both infectious and non-infectious factors. According to the World Health Organization (WHO), cancer-related fatalities accounted for 8.8 million deaths in 2015 (Albertsen, 2003). By 2030, it is forecasted that there will be approximately 21.4 million cases and 13.5 million deaths globally due to cancer (R. M. Anderson & May, 1991). This scenario has spurred extensive research into the interplay between the immune system and tumor cells. The treatment of cancer remains one of the most formidable challenges in contemporary medicine. Therapeutic modalities include surgery, radiation, hormone therapy, virotherapy, chemotherapy (Kuznetsov et al., 1994), and, more recently, immunotherapy (de Pillis et al., 2006). Cancer arises from mutations or environmental factors that disrupt normal cellular functions, leading to malignant transformation. These alterations can be triggered by environmental carcinogens such as tobacco, UV radiation, X-rays, or various toxins, or by genetic mutations. Mutations and environmental exposures can activate or inactivate specific genes, leading to the oncogenic conversion of normal cells.

Typically, cancer therapies aim to eradicate malignant cells throughout the body while minimizing damage to healthy tissues. Chemotherapy remains a principal strategy, involving pharmacological agents designed to target and destroy tumor cells. However, these agents often adversely affect normal cells, resulting in a range of side effects, including drug resistance and recurrence (Bellomo et al., 2008). Consequently, immunotherapy has emerged as a promising alternative. Immunotherapy enhances the immune system's ability to identify and eliminate tumor cells through two principal approaches: active and passive immunotherapy. Passive immunotherapy involves the use of effector immune components to directly target tumor cells. This approach includes techniques such as chimeric antigen receptor [CAR]-T cell therapy and antibody-targeted treatments. Active immunotherapy, on the other hand, bolsters the immune system's capacity to recognize and combat cancer cells by stimulating immune system activity. This category includes cytokine therapies, adoptive cell therapies, and cancer vaccines (Martins et al., 2007).

Cancer vaccines enhance the responsiveness of cytotoxic T lymphocytes to tumor-specific antigens. Cytokines, essential signaling proteins produced by various cells including macrophages, B lymphocytes, and T lymphocytes, play a pivotal role in immune regulation. However, not all cytokines are approved for cancer treatment. The Food and Drug Administration (FDA) in the United States has authorized only two cytokines; interleukin-2 (IL-2) and interferon-alpha (IFN-α) due to their demonstrated clinical efficacy (Nagy, 2005). IL-2 primarily functions to activate T-cells and natural killer cells, which are instrumental in recognizing and eliminating tumor cells. Although IFN-α has a comparable response rate, it does not substantially enhance long-term survival (Mamat & Subiyanto, 2013; Sanmamed & Chen, 2018; Sharma & Samanta, 2013; de Pillis et al., 2008).

Numerous engineering and physical phenomena can be adeptly characterized and scrutinized through mathematical modeling. Conditions such as aortic aneurysm development (Hao et al., 2017), management of HIV infections (Ogunlaran & Oukouomi Noutchie, 2016), diabetes management (Shtylla et al., 2019), combating antibiotic resistant infections (Roberts et al., 2019), cardiac rhythms (Jones et al.,

2009), drug dispersion (Jones et al., 2009), hepatitis C virus (Elkaranshawy et al., 2019), and tumor proliferation and cancer treatment have all been elucidated using this technique. Scholars focusing on cancer biology primarily endeavor to develop mathematical models for the quantitative analysis of tumor growth and the response of cancer cells to various therapies.

Theoretical exploration of liver cancer via mathematical models provides a valuable approach to enhancing our understanding of tumor-immune dynamics. Despite substantial advancements in elucidating how tumors circumvent immune destruction, the mechanisms by which the immune system protects against malignancies remain incompletely understood. Thus, it is increasingly imperative to investigate the interaction between the immune system and malignant cells in vivo (Coskun et al., 2010; Spalding et al., 2008). Several studies have concentrated on the dynamic characteristics of the tumor-immune response system. To advance immunotherapy strategies, including dendritic cell vaccines, Qomlaqi et al. (2017) proposed a mathematical model delineating interactions between cancer cells and adaptive immune responses in murine models. Their model integrates interleukin-2 cytokines, tumor cells, natural killer cells, regulatory T cells, and both naive and mature helper T cells, as well as naive and mature cytotoxic T cells. Tumor growth due to internal pressure was explored by (Jones et al., 2009), incorporating tumor size, internal pressure, and nutrient concentration within a system of partial differential equations in the absence of therapeutic interventions (Tao et al., 2010). A statistical model for cancer mortality was investigated by Ghosh & Samanta (2019). A framework for immunotherapy using mature dendritic cells was proposed by Arabameri et al. (2018). A revised model incorporating the effects of INF-α and IL-2 was suggested by Mamat & Subiyanto (2013). To evaluate the influence of $CD4^+$ T cells, a model was initially developed by Eftimie et al. (2010) and subsequently refined by L. Anderson et al. (2015) and X. Hu & Jang (2018). $CD4^+$ T cells, serving as helper cells to activate $CD8^+$ T cells and safeguard against malignancies, also possess the ability to directly destroy tumor cells through cytokine secretion (L. Anderson et al., 2015; X. Hu & Jang, 2018; Mattes et al., 2003; Perez-Diez et al., 2007; S. Zhang et

al., 2009).

A mathematical model combining chemotherapy and immunotherapy for tumor growth was introduced by de Pillis et al. (2006). A model for radiation therapy, which considers the proportional impact on normal cells, was developed by (Freedman & Pinho, 2009). The mathematical model for bacille Calmette-Guérin (BCG) immunotherapy for superficial bladder cancer was analyzed by (Bunimovich-Mendrazitsky et al., 2007). Ghosh & Banerjee (2018) explored the role of antibodies in regulating malignancy proliferation. The impact of natural killer cells (NK), circulating lymphocytes, $CD8^+$ T cells, and CD4+ T cells on cancer cells was examined by Makhlouf et al. (2020), leading to the development of a treatment protocol that integrates chemotherapy, IL-2 cytokine therapy, and adoptive immunotherapy involving CD8+ and $CD4^+$ T cells. They further argued that $CD4^+$ T cells primarily eliminate tumor cells through cytokine production, in contrast to $CD8^+$ T cells.

Abernathy et al. (2020) investigated a modified nonlinear cancer model incorporating virotherapy, optimizing the dose for effective tumor eradication. (Cho & Levy, 2020) devised a cancer growth model incorporating targeted therapies and chemotherapy to analyze the competitive dynamics between malignant and healthy cells. Schlicke et al. (2021) calibrated the model using data from three patients with non-small cell lung cancer, developing a framework that incorporates various treatment options and assesses their outcomes. To quantitatively assess the relationship between cancer and the immune system, while accounting for antibodies, Ghosh & Banerjee (2018) developed a model reflecting these parameters. The model proposed by (Ivanov et al., 2009) was based on clinical evidence of antibodies directly eliminating malignant cells.

Kuznetsov et al. (1994) proposed a mathematical model for cytotoxic T lymphocytes and their response to an immunogenic tumor. They examined how the immune system influences tumor growth, the mechanisms through which tumors evade detection, and the development of dormant tumor states. Kirschner & Panetta (1998) utilized mathematical modeling to elucidate interactions among tumor cells, immune effector cells, and interleukin-2 (IL-2), addressing both long-term relapses

and short-term tumor growth fluctuations. The periodic dynamics within immune system models were explored by (Bodnar & Foryś, 2000b). A generic model of immune system dynamics, proposed by (Bodnar & Foryś, 2000a) within Marchuk's framework, illustrated various aspects of disease progression, oscillations, and recovery, and provided insights into the qualitative behavior of the model solutions. The spontaneous regression and growth of malignant tumors were conceptualized as a prey-predator system, where tumor cells are the prey and cytotoxic T-lymphocytes are the predators, incorporating stochastic elements to account for random fluctuations around the positive equilibrium point (Sarkar & Banerjee, 2005).

Modelling HBV and Liver Cancer via Classical Differential Operators

The correlation between hepatitis and malignancy within a homogeneous population, considering continuous influxes of cancer patients, was demonstrated by (Bhadauria, 2011) through the utilization of a nonlinear mathematical framework. Their study encompassed both vertical and horizontal transmission mechanisms of hepatitis within the community. By employing stability theory of differential equations, the equilibrium stability of the model was analyzed. Sensitivity analysis was conducted to evaluate how variations in system parameters influenced the endemic equilibrium. Additionally, the fourth-order Runge-Kutta method was applied to perform numerical simulations of the proposed model. A notable achievement of their model was quantifying the effect of hepatitis virus infections on cancer patients and its subsequent impact on increasing hepatitis outbreaks within the general populace. Their findings indicated that an increase in hepatitis infection transmission rates corresponded with a rise in the endemic infective population levels. This effect was further exacerbated when there was an elevated risk of hepatitis infection among cancer patients. Their study also highlighted that hepatitis B and C infections, which progress to liver cancer, facilitate a heightened prevalence of cancer cases within the population.

As part of oncolytic virotherapy, malignant tumor cells are targeted with viruses to induce infection and subsequent cell lysis while preserving healthy cells. This therapeutic approach also augments the immune system, enhancing the body's de-

fense mechanisms. Oncolytic virotherapy operates without the necessity for chemotherapy or radiation, simulating a virus's natural infection process. Abernathy et al. (2020) incorporated this treatment modality into their work, proposing a system of four nonlinear differential equations to model the implementation of virotherapy as an anti-cancer strategy. Their model elucidates the interactions between virions, effector T cells, infected tumor cells, and non-infected tumor cells.

To investigate the immune system dynamics and viral interactions during hepatitis B virus (HBV) infections, Long & Qi (2009) developed a mathematical model grounded in the pathophysiology, virology, and immunology of HBV. Specifically, they calibrated the noncytopathic effects of the cellular immune response to be proportional to the count of cytotoxic T lymphocytes (CTLs), rather than the product of CTL numbers and infected hepatocyte counts. The model underscored that robust immune responses are crucial for combating HBV infections. It also illustrated that vertical transmission of HBV results in a less severe, asymptomatic form of hepatitis, suggesting that both the absence of an antiviral immune response and the virus's persistence post-mother-infant transmission could be attributed to neonatal immune tolerance. In 85%–95% of adults, HBV infection typically leads to acute hepatitis followed by recovery, contingent upon the development of sufficient immune defenses. Recovery involves the generation of potent and diverse CD4 and CD8 T-cells, the synthesis of neutralizing antibodies against the HBV surface antigen (HBsAg), the production of antiviral cytokines such as tumor necrosis factor-alpha and interferon-gamma, and the establishment of resistance to reinfection. However, the exact proportional contributions of various immune system components, particularly the role of neutralizing antibodies in infection development and progression, remain inadequately understood. Further research is necessary to elucidate the specific roles of these immune system components during HBV infection.

To elucidate the intricacies of the immune system's response to hepatitis B virus (HBV) infections, Chenar et al. (2018) has extended the immune response model proposed by (Long & Qi, 2009) by incorporating additional immune system dynamics. Their enhanced model integrates the roles of cytokines alongside innate

and adaptive immune responses, with the primary aim of examining the synergistic interactions among disparate constituents of the immune system during HBV infections. Their research vividly illustrates the pivotal role of cytokines in modulating the immune system's response and controlling viral replication. Through a comprehensive stability analysis of multiple equilibrium states, the model was examined for conditions leading to periodic oscillations, infection eradication, or chronic infection persistence. The critical efficacy of therapeutic interventions, including interferon therapies and nucleoside analogs, was evaluated. Numerical simulations were employed to probe the interactions between cytokine-related parameters and the stability of the endemic equilibrium, with the objective of refining the understanding of cytokine involvement in the system's dynamics. Their results suggest that the endemic steady state can be stabilized by increasing the rates at which $IFN_{\frac{\alpha}{\beta}}$ and IFN_{γ} augment the cytolytic activity of NK cells or by enhancing the rates at which these interferons inhibit new virion production.

A notable feature of immunological dynamics is the non-instantaneous nature of several critical processes, such as the latency period between infection and cytotoxic T lymphocyte (CTL) recruitment, the generation of new virions post-cell infection, and the duration of viral cellular invasion. Therefore, (Chenar et al., 2018) can be extended mathematically by incorporating discretely distributed time delays for each associated process, thereby enhancing the model's realism and analytical complexity. It is well-established that antibodies bind to viral particles to form virus-antibody complexes rather than directly neutralizing the viruses. Since these complexes can dissociate and are not always stable, explicitly including them in the model could elucidate the dynamics more clearly. Despite their increased complexity, age-structured infectious disease models provide a more accurate depiction of disease transmission dynamics.

Building upon the aforementioned analysis, Fatehi et al. (2022) advanced the work of (Chenar et al., 2018) by incorporating the age distribution of infected cell populations, thereby accounting for the contributions of both humoral and cell-mediated immunity in the context of HBV infection. The model was adapted to re-

flect chronic infection, infection clearance, and exacerbations by adjusting immune response parameters. Initial validation of the model was conducted using publicly available patient data from acute infection phases. According to prevailing theories, $CD8^+$ T-cell depletion is associated with prolonged exposure to high antigen loads. The model was calibrated using viral load data from six patients recorded during the acute infection stage, with the initial viral load $V_c(0)$ treated as a variable. It was observed that patient 2 exhibited an earlier peak viral load compared to other patients, suggesting a potentially higher initial viral load. For patients 1, 3, 4, 5, and 6, the initial viral load was consistent with a value of 0.33 virions per milliliter, aligning with most literature findings, whereas for patient 2, the initial viral load was substantially higher at 10 virions per milliliter.

Analysis of the impact of non-infectious subviral particles and immune response exhaustion on immune response dynamics has been conducted. The comparative evaluation of various therapeutic interventions within the framework of this model reveals that therapies targeting specific stages of the viral life cycle are more efficacious than fatigue mitigation therapies, which are designed to address immune response depletion. Further results from the model suggest that initiating antiviral treatment during a period of declining viral load is more advantageous than starting therapy during periods of increasing viral load. The model demonstrates that expedited antibody production consistently leads to viral eradication, highlighting the potential effectiveness of antibody-based therapeutics currently in clinical trials (Fatehi et al., 2022).

Modeling HBV and Liver Cancer via Fractional Differential Operators

Fractional calculus, an extension of classical calculus, focuses on the operations of integration and differentiation of arbitrary orders (Nisar et al., 2022). During the 19th century, mathematicians developed fractional differential equations, fractional dynamics, and fractional geometry through the framework of fractional calculus. Presently, fractional calculus is applied across nearly all scientific disciplines. It is utilized to model phenomena in physics, engineering, and biology where traditional integer-order mathematical models prove inadequate. Consequently, disci-

plines such as mechanics, chemistry, biology, and image processing have significantly benefited from the adoption of fractional calculus. This approach addresses a range of issues, including historical and nonlocal effects, which are inadequately captured by integer-order derivatives. The Riemann-Liouville and Caputo fractional-order derivatives (RLFD) have been pivotal in the advancement of this research.

The incubation periods for bacteria, viruses, and vectors to acquire infectiousness exemplify how many biological systems exhibit memory effects or delayed responses (Sun et al., 2022). Fractional differential equation modeling of these systems provides distinct advantages over conventional integer-order models, which neglect such effects. Studying the immune system's response to cancer interactions is essential (Sun et al., 2022). A primary objective among researchers is to accurately model these interactions without overly complicating the mathematical framework.

Recently, there has been a growing focus on the issue of solitary kernels associated with fractional derivatives. To address this, (Amin et al., 2022) introduced a range of novel definitions. These new definitions, characterized by their nonsingular kernels, have had a profound impact. The Caputo-Fabrizio, Atangana-Baleanu (Atangana, 2018), and Caputo fractional derivatives (Kai, 2010) differ primarily in their underlying definitions: the Caputo-Fabrizio derivative is defined by an exponential decay law, the Atangana-Baleanu derivative by the Mittag-Leffler (ML) law, and the Caputo fractional derivative by a power law . Consequently, these fractional differential operators have been employed by researchers to tackle various practical challenges. For instance, Farman et al. (2021) explored the role of fractional time derivative operators in modeling anomalous diffusion. The study in (Ghanbari & Gómez-Aguilar, 2018) expanded on the model of nutrients, phytoplankton, and zooplankton using variable-order fractional differential operators. Additionally, (J. Gómez-Aguilar et al., 2019) applied robust methods to investigate the dynamics of fractional calcium oscillation models, focusing on controlling nonlinear fractional systems.

The influence of vitamins on tumor cell proliferation across various fractional orders was elucidated by (Ahmad et al., 2020), who explored a fractional-order

tumor-immune-vitamin model (TIVM) employing the Mittag-Leffler derivative. Utilizing adjusted parameters from the Caputo fractional-order model, Sweilam et al. (2020) developed a mathematical framework to control cancer cell dynamics. Their research incorporated optimal control strategies for a fractional-order delay model in oncological therapy. The primary aim of their study was to minimize tumor cell populations in the context of fractional optimal control problems (FOCPs) using the proposed paradigm. The fractional-order model proposed by Ahmad et al. (2020) incorporates two immune effectors interacting with cancer cells.

Nevertheless, fractional derivatives often lead to singularities that are impractical for modeling dynamic systems. To address this issue, the Caputo-Fabrizio (CF) operator was introduced as a novel fractional derivative (Caputo & Fabrizio, 2015). Despite its advantages, the Caputo-Fabrizio operator presents challenges, including issues related to kernel locality. Atangana & Baleanu (2016) proposed an innovative fractional derivative to resolve these issues, incorporating the generalized Mittag-Leffler function (MLF) derived from the power series analysis of the complex number system as a non-local and non-singular kernel. Gao et al. (2021) introduced a new mathematical model for hepatitis B virus (HBV) incorporating the Caputo-Fabrizio fractional derivative with immune delay. The existence and uniqueness of solutions for this model were established using Laplace transforms and fixed point theorems. Building on this work, Sun et al. (2022) expanded the model to include cytotoxic T lymphocytes (CTL) and alanine aminotransferase (ALT) levels, which are indicative of liver damage. They highlighted the absence of studies analyzing HBV dynamics that integrate logistic proliferation, time delays, and CTL and ALT factors using fractional differential equations.

The non-local nature of fractional differential equations (FDEs) encompasses not only the current state but also historical states. Given that the differentiation order, φ, is unique and can vary significantly based on model outcomes, converting models governed by integer differential equations (IDEs) to FDEs requires precision. IDEs are limited in their capacity to model certain phenomena, whereas FDEs offer a more comprehensive approach. Due to their relevance in modeling mem-

ory and inherited traits, biological systems are predominantly modeled using FDEs. The use of fractional-order derivatives captures various issues, including historical and non-local effects, and has been applied to numerous physical process modeling scenarios. Ahmad et al. (2020) investigated a fractional-order model involving interactions between two immune effectors and cancer cells. Their study incorporated a comprehensive immune system model, considering multi-functional pathways and immune system cross-reactivity.

The (AB) operator has been employed to investigate the tumor immune vitamins model as documented by (Ahmad et al., 2020). A non-singular operator has been utilized to analyze the time-fractional Klein-Gordon equation, encompassing solitary and shock wave solutions (Saifullah et al., 2021). Leveraging a fractional-order operator, Alzahrani et al. (2021) developed a mathematical framework for Covid-19, incorporating effects such as isolation and quarantine. (Ahmed et al., 2012) examined a fractional-order model involving two immune effectors interacting with cancer cells. A novel mathematical paradigm was introduced by (Akman Yıldız et al., 2018) to elucidate the impact of obesity on malignant tumor growth following both immunotherapy and chemotherapy. They addressed an optimal control problem aimed at eradicating the tumor population and optimizing drug dosage over a finite time horizon. The model, incorporating Caputo time fractional derivatives, includes variables such as tumor cells, immune cells, adipose cells, and drug concentrations for both chemotherapy and immunotherapy. Analytical investigations were conducted to ascertain the stability and existence of equilibrium points, including coexisting and tumor-free equilibria. Additionally, they meticulously analyzed the correlation between the cost functional value, the differentiation order α, and the decay rate of chemotherapeutic agents. Their findings suggest that employing a fractional derivative with a nonsingular kernel, in conjunction with an optimal treatment strategy, is beneficial for devising the most effective immunotherapy and chemotherapy regimen.

To the best of the existing knowledge of the subject matter, although extensive research has been conducted to address hepatitis B virus and liver cancer, no

mathematical modeling has been undertaken to explore the co-existence dynamics of these two diseases. This entails the assimilation of both fractional-order and classical-order models, which would enable the incorporation of the immune system's function and the implementation of control strategies for addressing infected cells. Consequently, a convergence of this research with the aforementioned mathematical frameworks related to the transmission dynamics of hepatitis B virus and hepatocellular carcinoma is expected to yield profound insights and bolster initiatives aimed at the eradication of these widespread global maladies.

Chapter Summary

This chapter has encapsulated an exhaustive examination of various mathematical paradigms employed to elucidate the intricacies and mechanisms governing the propagation of the hepatitis B virus and hepatocellular carcinoma, along with the essential role of the immune system in regulating these infectious processes. Furthermore, a historical overview of the implementation of both fractional-order and classical-order mathematical models for the investigation and control of infectious diseases was presented. These models were devised with a meticulous consideration of the properties of the hepatitis B virus, the transmission dynamics of liver cancer, and the immunological responses provoked by these pathogens.

Scholarly endeavors have concentrated on the conventional SIR model to represent the dynamics of hepatitis B virus and liver cancer, while other research has employed modified versions of the SIR framework to explore the transmission dynamics of these conditions and incorporate the immune system's reaction. To determine whether hepatitis B virus and liver cancer could establish endemicity within a population, the basic reproduction number, $\mathbb{R}_0$, was calculated for both classes of models. Consequently, this study adapted the classical SIR model initially introduced by (Kermack & McKendrick, 1927), utilizing both fractional-order and classical-order deterministic models to rigorously investigate the dynamics of hepatitis B virus and liver cancer dissemination.

CHAPTER THREE

RESEARCH METHODS

Introduction

In order to fulfill the goals set in Chapter one, a classical and fractional order mathematical models were developed in this chapter that uses a deterministic method to study the immune system's role in combating the co-existence dynamics of hepatic carcinoma and the hepatitis B virus (HBV). The model's predictive value $(\mathbb{R}_0)$ was assessed based on how well it reflected the biological systems of the two infections. The transition period between acute and chronic infection was also determined.

Classical-order Model

Classical calculus is used to model infectious diseases by employing differential equations to characterize the dynamics of variation within population strata, such as Susceptible (S), Infected (I), and Recovered (R), in models akin to the SIR paradigm. These equations capture how individuals transition between compartments based on factors like infection and recovery rates. For instance, the velocity at which susceptible individuals transition to infected states is frequently represented as commensurate with the number of prevailing infections. Solving these equations allows researchers to predict disease spread, estimate key thresholds such as the basic reproduction number $(\mathbb{R}_0)$, and assess the impact of control measures. This approach provides a mathematical framework to understand and predict the dynamics of disease transmission over time.

Model Formulation

A compartmental mathematical model was developed to explore the complex interactions between hepatitis B pathogen and hepatic malignancy infections. This model relies on recent scientific insights into the core characteristics of HBV infections and hepatic carcinoma, as well as on theoretical constructs and empirical research conducted by other scholars (Nowak et al., 1996; Perelson et al., 1996; Ciupe, Ribeiro, Nelson, & Perelson, 2007; Long & Qi, 2009; Chenar et al., 2018;

Fatehi et al., 2022). The impact of HBV infection and the transition from acute infections to hepatic carcinoma is profoundly impacted by the functions of antibodies, cell-mediated immunity, innate immune mechanisms, and cytokines.

Macrophages exposed to HBV infection exhibit dual functionality; they can act as both targets and defenders (Opoku & Mazandu, 2020). We modeled macrophages (Kupffer cells) as the target cells in our mathematical model, rather than hepatocytes because of their central role in mediating immune responses and inflammation in HBV infection and liver cancer progression. Although hepatocytes are the direct target of HBV, macrophages are critical in detecting HBV, releasing pro-inflammatory cytokines, and contributing to liver damage, fibrosis, and tumor progression Tacke (2017); Wan et al. (2014).

Upon activation, these macrophages are capable of eradicating intracellular pathogens and participating in Type 1 and Type 2 T helper cell-mediated responses. Human hepatic cells (hepatocytes) are categorized into two discrete groups: uninfected macrophages free from malignancy, labeled as M_0, and macrophages compromised by cancer, labeled as M_1. These macrophages, whether or not they harbor cancer, are mobilized from the circulatory system to the locus of infection in reaction to the presence of HBV. Upon encountering the virus, these macrophages engage in phagocytosis, subsequently becoming contaminated at a specific moment t (Long & Qi, 2009; Chenar et al., 2018; Fatehi et al., 2022). The resultant macrophages harboring infection are labeled as I_M.

This phenomenon engenders the contamination of macrophages via interactions with HBV. It is conjectured that uninfected macrophages are synthesized at consistent rates Λ_{M_0} and Λ_{M_1}, while they undergo depletion at rates μ_{M_0} and μ_{M_1}, respectively. In our model, uninfected (cancer-affected) macrophages, M_1, are synthesized at a constant rate Λ_{M_1}, reflecting the steady progression of liver cancer due to external factors like excessive alcohol consumption and smoking. These factors are independent of viral infection but contribute to the overall cancer burden. HBV entities infiltrate macrophages at a rate commensurate with the product of M_0, M_1, and V (specifically, $\beta_1 V M_0$ and $\beta_2 V M_1$), with proportionality coefficients β_1

and β_2 (Long & Qi, 2009; Chenar et al., 2018; Fatehi et al., 2022). Contaminated macrophages are eradicated at a constant rate of μ_{I_M} per cell. Among the infected macrophages, some progress to cirrhosis and subsequently to hepatic carcinoma macrophages at a rate ζ (Bhadauria, 2011). Hepatic carcinoma macrophages may contract hepatitis through tainted blood transfusions or sexual contact with infected individuals. HBV particles V are generated at a rate Λ_V, while infected macrophages produce additional free virions at a rate ω (Chenar et al., 2018; Fatehi et al., 2022). Virions undergo degradation at a constant rate μ_V within each cell. Figure 1 delineates the interactions among diverse cell types within the human liver.

A primary role of the innate immune response is to promptly arrest the spread of the virus to adjacent cells following its entry into the liver cell (Laing, 2022). Innate immune cells are equipped to manage mild HBV infections without inducing severe inflammation once the pathogen is endocytosed and processed. However, in cases of severe infection, an adaptive immune response, characterized by pro-inflammatory macrophages and T cells, becomes essential. The adaptive immune response involves HBV-specific T lymphocytes, referred to as naive T cells T_0, and HBsAg-specific antibodies A that target and neutralize virions (Laing, 2022; Howard et al., 2022).

Pathogen incursion is specifically mitigated by antibodies, which bind to and neutralize the pathogens. During HBV infections, cells compromised by the virus generate surplus sub-viral particles (SVPs) in quantities ranging from one thousand to one million times the number of infectious viral particles. These SVPs may profoundly impact the host's immunological response to HBV infection. As elucidated by Ciupe et al. (2014); J. Hu & Liu (2017), SVPs function as subterfuges, diverting antiviral immunoglobulins away from targeting the hepatitis B virus. Furthermore, they may contribute to immunological tolerance during neonatal contamination, thereby postponing the production of neutralizing antibodies and allowing HBV to circumvent immune surveillance. The response is orchestrated through the generation of macrophages, T lymphocytes, and cytokines. In the absence of infection, HBsAg-specific antibodies (A) are synthesized at a steady rate Λ_A and undergo

degradation at a per capita rate μ_A. During infection, antibodies are produced at a pace ψ, which correlates with the viral burden, and they neutralize viral particles at a pace δ_4 (Ciupe et al., 2014; Chenar et al., 2018; Fatehi et al., 2022).

Macrophage T cells are produced at a pace Λ_{T_0} and experience mortality at a uniform velocity μ_{T_0} (Long & Qi, 2009; Chenar et al., 2018; Fatehi et al., 2022). Following uptake by macrophages compromised by infection, the pathogen continues to proliferate by evading intracellular elimination mechanisms, initially sustaining a latency phase during which pathogen replication remains minimal. This ongoing intracellular replication within infected macrophages leads to an increase in the viral population within the host liver cells. Virus replication within infected macrophages triggers the induction, activation, and differentiation of naive T cells originating from the hematopoietic tissue in the bone marrow into either T helper 1 (T_1) or T helper 2 (T_2) cells (Howard et al., 2022; Beňová et al., 2020; Mueller & Rouse, 2009). The cellular immune responses of T_1 and T_2 cells to HBV infection are influenced by the density of infected macrophages and the quantity of the virus. T helper 1 lymphocytes (T_1) mature at a velocity ρ_1 and undergo apoptosis at a uniform velocity μ_{T_1}, specializing in orchestrated immune responses, whereas T helper 2 lymphocytes (T_2) mature at a rate ρ_2 and undergo apoptosis at a uniform velocity μ_{T_2} (Howard et al., 2022; Beňová et al., 2020). T helper 1 lymphocytes (T_1) induce infected macrophages to secrete cytokines at a velocity π, whereas cytotoxic T lymphocytes primarily target and annihilate the pathogen through the discharge of cytotoxic granules, operating at a steady velocity of δ_3 (Chenar et al., 2018).

Naive T lymphocytes undergo further maturation into controlling T lymphocytes, which orchestrate the modulation of T_1 and T_2 lymphocyte production (Opoku & Mazandu, 2020; Howard et al., 2022; Beňová et al., 2020; Mueller & Rouse, 2009). It has been documented that the genesis of controlling T lymphocytes, which execute cytolytic functions to synthesize interleukin-10 (I_{10}), is delayed due to the pathogen's propensity to exhibit transient quiescence during the acute phase within infected macrophages (Hassuneh et al., 2013). Interleukin-10 is a cytokine endowed with chiefly anti-inflammatory attributes that impacts both T_1 and T_2 adaptive im-

mune paradigms. During HBV infections, it also orchestrates the innate immune system, immunoglobulins, and effector B lymphocytes. Naive T lymphocytes secrete I_{10} at a rate ρ_3, and it undergoes catabolism at a steady velocity $\mu_{I_{10}}$. I_{10} modulates the differentiation of T_1 and T_2 lymphocytes, with its inhibitory effects on antigen-presenting cells (APCs) obstructing the synthesis of pro-inflammatory cytokines such as I_{12}, and attenuating molecules entangled in antigenic presentation and lymphocyte mobilization (Wiah et al., 2011). Although predominantly suppressive, these cytokines also exhibit immune-enhancing properties, such as promoting the proliferation of cytotoxic T lymphocytes, alternatively known as T helper 2 cells. The plus sign signifies cytokine up-regulation, while the minus sign denotes down-regulation (Opoku & Mazandu, 2020).

An additional mechanism through which the immune system ameliorates and precludes the advancement of HBV infection into hepatic neoplasia involves effector B lymphocytes, also known as plasmacytes (Wiah et al., 2011; Laing, 2022). These specialized entities secrete immunoglobulins, facilitate the recuperation of pathogen-invaded cells, and prime T lymphocytes both cytotoxic T lymphocytes and T helper 1 lymphocytes thereby instigating cell-mediated immune reactions (Wiah et al., 2011; Howard et al., 2022; Beňová et al., 2020; Mueller & Rouse, 2009). Effector B lymphocyte populations are maintained at a stable homeostatic equilibrium post-viral eradication due to the persistence of enduring plasma and memory B cells (DeVico & Gallo, 2004). When viral peptide-major histocompatibility complex (MHC) class I molecules, which present viral antigens, are exhibited on the cellular membrane, effector B lymphocytes identify these cells as infected. In the absence of infection, effector B lymphocytes are posited to proliferate at a rate Λ_E and undergo attrition at a steady velocity μ_E per cell (Chenar et al., 2018; Fatehi et al., 2022). During HBV infection, effector B lymphocytes are adept at both eradicating and rehabilitating infected macrophage cells. We represent these dual functions (elimination and restoration) within a singular reaction wherein effector B lymphocytes engage in the destruction and repair of infected macrophages at a rate δ_2. It has been documented that cured cells exhibit a gradual diminution of resistance to productive infection,

with a rate on the order of 10^5 per day, while effector cells concurrently eliminate infected macrophage cells. During an infection, the population of effector cells expands by a factor of $\sigma I_M E$, where σ denotes the maximum proliferation rate. This expansion occurs in a manner contingent upon the antigen density within contaminated cellular populations (Chenar et al., 2018; Fatehi et al., 2022).

The hepatitis B virus demonstrates extraordinary adaptability by utilizing mechanisms to obstruct the translocation of MHC molecules to the cellular membrane, thereby impeding the presentation of viral peptides and evading T cell surveillance. In such scenarios, T lymphocytes may be incapacitated in recognizing the viral presence within the infected cell. Nonetheless, natural killer (NK) cells, also designated as N_K cells, are proficient in targeting cells exhibiting attenuated MHC class I molecule expression (Laing, 2022; Howard et al., 2022; Beňová et al., 2020; Mueller & Rouse, 2009). Upon identifying cells with diminished MHC expression, N_K cells secrete cytotoxic agents, analogous to cytotoxic T lymphocytes, to eradicate the virally compromised cells. In the absence of infection, natural killer N_K cells, which function as the primary line of defense against exogenous pathogens, are conjectured to proliferate at a rate Λ_{N_K} and undergo programmed cell death at a constant per capita rate μ_{N_K}.

In evaluating the immune response dynamics to HBV and hepatic malignancy co-infection, the role of cytokines is crucial (Wiah et al., 2011; Chenar et al., 2018). Interferons, a category of diminutive proteins synthesized and secreted by virally compromised macrophages, are vital for the immunological defense against HBV. Interferons inhibit viral replication within infected macrophages. Type-1 interferon ($IFN_{\alpha/\beta}$), denoted as F_1, is generated by infected macrophages at a rate ε and undergoes degradation at a per-cell rate μ_{F_1} (Guidotti & Chisari, 2001; Busca & Kumar, 2014; Wiah et al., 2011; Chenar et al., 2018). Conversely, Type-2 interferon (IFN_γ), represented by F_2, is also produced by natural killer cells N_K (DeVico & Gallo, 2004; Guidotti et al., 1994; Herbein & O'brien, 2000; Wiah et al., 2011; Chenar et al., 2018) at a rate η and is lost at a per capita rate μ_{F_2}.

IFN_γ instigates the synthesis of protein-10, which augments and recruits N_K

cells (Herbein & O'brien, 2000; Chenar et al., 2018), whereas $IFN_{\alpha/\beta}$ activates natural killer N_K cells during viral invasion (Pawelek et al., 2012; Chenar et al., 2018). Consequently, it is conjectured that the synergistic impact of interferons on the stimulation of N_K cells manifests at a rate of $\theta_1 N_K F_1 + \theta_2 N_K F_2$, where θ_1 denotes the activation rate of N_K cells by Type-1 interferon and θ_2 signifies the activation rate by Type-2 interferon. In addition to augmenting the proliferation of nascent N_K cells, $IFN_{\alpha/\beta}$ and IFN_{γ} elevate the cytotoxicity of N_K cells and effector B cells, respectively (Abbas et al., 2014; Chenar et al., 2018). Therefore, it is postulated that natural killer cells and effector B cells eradicate infected macrophages at rates $\delta_1 (1 + \chi_1 F_1) I_M N_K$ and $\delta_2 (1 + \chi_2 F_2) I_M E$, respectively (Chenar et al., 2018). Here, χ_1 represents the factor by which Type-1 interferon enhances the cytotoxicity of N_K cells, while χ_2 denotes the factor by which Type-2 interferon amplifies the cytotoxicity of effector B cells.

Basic model assumptions

In addition to the assumptions previously outlined, we make the following supplementary assumptions:

(H1) It is hypothesized that a subset of hepatic cells has acquired neoplasms as a result of exogenous influences such as excessive ethanol intake and tobacco use. The work subsequently implement hepatitis B virus (HBV) infection to investigate the ensuing co-occurrence dynamics.

(H2) Temporal lags in the replication mechanisms of discrete cellular constituents are not factored into the model.

(H3) The populations of phagocytic cells and the pathogen are presumed to be uniformly dispersed throughout the system at all times.

(H4) The study incorporate intermediary stages, including T helper-1 (Th1) cells, T helper-2 (Th2) cells, and memory B cells, as part of the progression towards the formation of effector cells and plasma cells.

(H5) The model utilizes the principle of mass action, which asserts that the velocity of viral infections is proportional to the product of the quantities of non-infected phagocytes and infected phagocytes.

The overarching framework of the model, including its state variables and parameters, is elucidated in Figure 1 and detailed in Tables 1, 2, and 3, respectively.

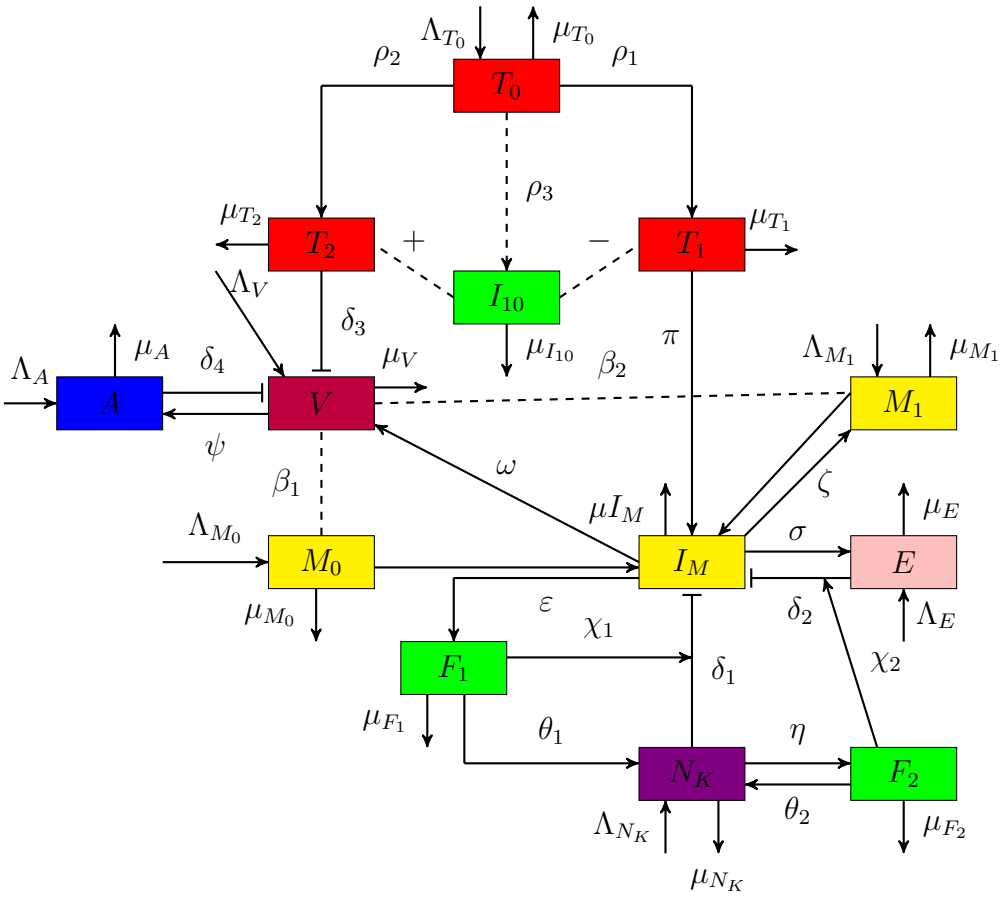

Figure 1: Illustrate the Schematic Representation of the Immunological Reaction to the Concurrent Presence of HBV and Hepatic Carcinoma (Author's construct, 2022)

In Figure 1, yellow rectangles signify the hepatic cellular populations of the host, encompassing uninfected macrophages (both with and without malignancy) as well as infected macrophages. Red rectangles represent the T cell populations, while blue rectangles signify the antibody populations. Pink rectangles illustrate the effector B cells populations. Green rectangles are used to depict cytokines, such as type-1 and type-2 interferons and interleukin-10. The violet rectangle corresponds

to the innate immune cells (N_K cells), and the purple rectangle denotes the virus particle (virion) population. Thick lines with arrowheads indicate direct interactions, thick lines with bar heads signify clearance or destruction, and dashed lines represent various forms of interactions.

Table 1: Model State Variables and their Description

State variable	Description
T_0	Naive T cells
T_1	T helper 1 cells
T_2	T helper 2 (cytotoxic T cells)
M_0	Uninfected macrophages cells without cancer
M_1	Uninfected macrophages cells with cancer
I_M	Infected macrophages cells
V	Virus
A	Antibodies
E	Effector B (Plasma) cells
N_K	Natural killer cells
I_{10}	Interleukin-10 cytokines
F_1	Type-1 interferon (alpha-beta) cytokines
F_2	Type-2 interferon (gamma) cytokines

Source: Author's construct (2022)

Table 2: Parameters of Model and their Description

Parameter	Description
Λ_{T_0}	Supply rate of naïve T cells
Λ_{M_0}	Supply rate of uninfected macrophages without cancer
Λ_{M_1}	Supply rate of uninfected macrophages with cancer
Λ_V	Virus recruitment rate
Λ_A	Antibody growth rate without infection
Λ_E	Effector B cell growth rate without infection
Λ_{N_K}	Natural killer cell growth rate without infection
μ_{T_0}	Naive T cells decay rate
μ_{T_1}	T helper 1 cells decay rate
μ_{T_2}	T helper 2 decay rate
μ_{M_0}	Decay rate of uninfected, neoplasia-free macrophages
μ_{M_1}	Decay rate of malignant uninfected macrophages
μ_{I_M}	Infected macrophages decay rate
μ_V	Virus decay rate
μ_A	Antibodies decay rate
μ_E	Effector B cells decay rate
μ_{N_K}	Natural killer cells decay rate
$\mu_{I_{10}}$	Interleukin-10 cytokines decay rate
μ_{F_1}	Type-1 interferon (α/β) decay rate
μ_{F_2}	Type-2 interferon (γ) decay rate

Source: Author's construct (2022)

Table 3: Parameters of Model and their Description

Parameter	Description
ρ_1	Differentiation rate of T_0 to T_1 induced by cytokines
ρ_2	Differentiation rate of T_0 to T_2 induced by cytokines
ρ_3	Differentiation rate of T_0 to I_{10} induced by cytokines
δ_1	Rate at which NK cells clear and cure infected cells
δ_2	Rate at which effector B cells clear and cure infected cells
δ_3	Rate at which cytotoxic T cells clear the virus
δ_4	Rate at which antibodies bind and neutralized the virus
θ_1	Rate at which $IFN_{\alpha/\beta}$ activates N_K cells
θ_2	Rate at which IFN_{γ} activates N_K cells
χ_1	Rate at which $IFN_{\alpha/\beta}$ enhances the cytotoxicity of NK cells
χ_2	Rate at which IFN_{γ} enhances the cytotoxicity of E cells
β_1	Interaction rate between V and M_0
β_2	Interaction rate between V and M_1
τ_1	IL-10 to T helper 1 differentiation inhibition rate
ψ	Virus (V) lytic effect rate to release antibodies (A)
σ	Lytic effect rate of infected macrophages to release plasma cells
ω	New infectious virions replication rate
ε	(I_M) lytic effect rate to release F_1 cytokines
η	(N_K) lytic effect rate to release F_2 cytokines
π	Lytic effect rate of T_1 cells to activate I_M for cytokine production
ζ	Rate at which I_M cells develop into liver cancer

Source: Author's construct (2022)

Equations of the Model

The ensuing system of differential equations of classical order illustrates the immune response to the concomitance of hepatitis B virus and hepatic carcinoma, based on the previously mentioned postulates. The model framework is supported by tenets of clonal selection theory, mass-action kinetics, and the balance between cellular and molecular population dynamics, including proliferation and attrition.

$$
\left.
\begin{aligned}
\frac{dT_0}{dt} &= \Lambda_{T_0} - \rho_1 I_M T_0 I_{10} - \rho_2 V T_0 I_{10} - \rho_3 T_0 I_M \left(\frac{1}{1+\tau_1 I_{10}}\right) - \mu_{T_0} T_0,\\
\frac{dT_1}{dt} &= \rho_1 I_M T_0 I_{10} - \pi I_M T_1 - \mu_{T_1} T_1,\\
\frac{dT_2}{dt} &= \rho_2 V T_0 I_{10} - \delta_3 T_2 V - \mu_{T_2} T_2,\\
\frac{dM_0}{dt} &= \Lambda_{M_0} - \beta_1 V M_0 - \mu_{M_0} M_0,\\
\frac{dM_1}{dt} &= \Lambda_{M_1} - \beta_2 V M_1 + \zeta I_M - \mu_{M_1} M_1,\\
\frac{dI_M}{dt} &= \beta_1 V M_0 + \beta_2 V M_1 + \pi I_M T_1 - \delta_1 \left(1+\chi_1 F_1\right) I_M N_K\\
&\quad - \delta_2 \left(1+\chi_2 F_2\right) I_M E - \sigma I_M E - \left(\omega + \varepsilon + \zeta + \mu_{I_M}\right) I_M,\\
\frac{dV}{dt} &= \Lambda_V + \omega I_M - \delta_3 T_2 V - \delta_4 A V - \left(\psi + \mu_V\right) V,\\
\frac{dA}{dt} &= \Lambda_A + \psi V - \delta_4 A V - \mu_A A,\\
\frac{dE}{dt} &= \Lambda_E - \delta_2 \left(1+\chi_2 F_2\right) I_M E + \sigma I_M E - \mu_E E,\\
\frac{dN_K}{dt} &= \Lambda_{N_K} - \delta_1 \left(1+\chi_1 F_1\right) I_M N_K + \theta_1 F_1 + \theta_2 F_2 - \left(\eta + \mu_{N_K}\right) N_K,\\
\frac{dI_{10}}{dt} &= \rho_3 I_M T_0 \left(\frac{1}{1+\tau_1 I_{10}}\right) - \mu_{I_{10}} I_{10},\\
\frac{dF_1}{dt} &= \varepsilon I_M - \left(\theta_1 + \mu_{F_1}\right) F_1,\\
\frac{dF_2}{dt} &= \eta N_K - \left(\theta_2 + \mu_{F_2}\right) F_2.
\end{aligned}
\right\} \tag{5}
$$

The system delineated in reference 5 is not adimensional. The term "nondimensional" signifies that, in the absence of precise information about the actual magnitudes of the variables, we assume these magnitudes to be proportional.

Basic Model Properties

This section expounds upon the attributes of positivity, boundedness, existence, and uniqueness of solutions for the model framework.

Positivity of Solutions

To affirm the mathematical and epidemiological robustness of model framework 5, it is imperative to ensure that solutions commencing from positive initial states continue to be positive for all $t > 0$. Hence, it is essential to validate that each state variable remains non-negative, as negative cellular population densities are illogical. This assertion is reinforced by the ensuing lemma.

Lemma 3

If $T_0(0) > 0$, $T_1(0) > 0$, $T_2(0) > 0$, $M_0(0) > 0$, $M_1(0) > 0$, $I_M(0) > 0$, $V(0) > 0$, $A(0) > 0$, $E(0) > 0$, $N_K(0) > 0$, $I_{10}(0) > 0$, $F_1(0) > 0$ and $F_2(0) > 0$, then the solutions $T_0(t) > 0$, $T_1(t) > 0$, $T_2(t) > 0$, $M_0(t) > 0$, $M_1(t) > 0$, $I_M(t) > 0$, $V(t) > 0$, $A(t) > 0$, $E(t) > 0$, $N_K(t) > 0$, $I_{10}(t) > 0$, $F_1(t) > 0$ and $F_2(t) > 0$ of model 5 are positive for all $t \geq 0$.

Proof. We define

$$\begin{aligned}\tau \quad = \quad & \sup\Big\{t > 0 : T_0(t) > 0, M_0(t) > 0, M_1(t) > 0, \text{ and } \quad V(t) \geq 0, \\ & A(t) \geq 0, E(t) \geq 0, N_K(t) \geq 0, T_1(t) \geq 0, T_2(t) \geq 0, I_M(t) \geq 0, \\ & I_{10}(t) \geq 0, F_1(t) \geq 0, F_2(t) \geq 0\Big\}.\end{aligned}$$

This implies that

$$\begin{aligned}& T_0(t) > 0, M_0(t) > 0, M_1(t) > 0, \text{ and } \quad V(t) \geq 0, A(t) \geq 0, E(t) \geq 0, \\ & N_K(t) \geq 0, T_1(t) \geq 0, T_2(t) \geq 0, I_M(t) \geq 0, I_{10}(t) \geq 0, F_1(t) \geq 0, \\ & F_2(t) \geq 0 \quad \forall \quad t \in [0, \tau).\end{aligned}$$

Considering the first equation in system 5, we have

$$\frac{dT_0}{dt} = \Lambda_{T_0} - \rho_1 I_M T_0 I_{10} - \rho_2 V T_0 I_{10} - \rho_3 T_0 I_M \left(\frac{1}{1+\tau_1 I_{10}}\right) - \mu_{T_0} T_0.$$

It follows that

$$\frac{dT_0}{dt} = \Lambda_{T_0} - \rho_1 I_M T_0 I_{10} - \rho_2 V T_0 I_{10} - \rho_3 T_0 I_M - \mu_{T_0} T_0,$$

since $\rho_3 T_0 I_M \left(\frac{1}{1+\tau_1 I_{10}}\right) < \rho_3 T_0 I_M$. Hence,

$$\frac{dT_0}{dt} \geq -\mu_{T_0} T_0 \quad \forall \quad t \in [0, \tau). \tag{6}$$

Seperating variables and integrating both sides of Eq. (6) from 0 to τ gives

$$T_0(\tau) \geq T_0(0) \exp\left[-\mu_{T_0}\tau\right] > 0.$$

For the second equation in system 5, we have

$$\frac{dT_1}{dt} = \rho_1 I_M T_0 I_{10} - \pi I_M T_1 - \mu_{T_1} T_1.$$

It follows that

$$\frac{dT_1}{dt} \geq -\left(\pi I_M + \mu_{T_1}\right) T_1 \quad \forall \quad t \in [0, \tau). \tag{7}$$

Seperating variables and integrating both sides of Eq. (7) from 0 to τ produces

$$T_1(\tau) \geq T_1(0) \exp\left[-\mu_{T_1}\tau - \pi \int_0^\tau I_M(t)dt\right] \geq 0.$$

For the third equation in system 5, we have

$$\frac{dT_2}{dt} = \rho_2 V T_0 I_{10} - \delta_3 T_2 V - \mu_{T_2} T_2.$$

It follows that

$$\frac{dT_2}{dt} \geq -\left(\delta_3 V + \mu_{T_2}\right) T_2 \quad \forall \quad t \in [0, \tau)\,. \tag{8}$$

Seperating variables and integrating both sides of Eq. (8) from 0 to τ results in

$$T_2(\tau) \geq T_2(0) \exp\left[-\mu_{T_2}\tau - \delta_3 \int_0^\tau V(t)dt\right] \geq 0.$$

For the fourth equation in system 5, we obtain

$$\frac{dM_0}{dt} = \Lambda_{M_0} - \beta_1 V M_0 - \mu_{M_0} M_0.$$

It follows that

$$\frac{dM_0}{dt} \geq -\left(\beta_1 V - \mu_{M_0}\right) M_0 \quad \forall \quad t \in [0, \tau)\,. \tag{9}$$

By seperation of variables and integrating both sides of Eq. (9) from 0 to τ, we obtain

$$M_0(\tau) \geq M_0(0) \exp\left[-\mu_{M_0}\tau - \beta_1 \int_0^\tau V(t)dt\right] > 0.$$

For the fifth equation in system 5, we obtain

$$\frac{dM_1}{dt} = \Lambda_{M_1} - \beta_2 V M_1 + \zeta I_M - \mu_{M_1} M_1.$$

It follows that

$$\frac{dM_1}{dt} \geq -\left(\beta_2 V - \mu_{M_1}\right) M_1 \quad \forall \quad t \in [0, \tau)\,. \tag{10}$$

By seperation of variables and integrating both sides of Eq. (10) from 0 to τ, we obtain

$$M_1(\tau) \geq M_1(0) \exp\left[-\mu_{M_1}\tau - \beta_2 \int_0^\tau V(t)dt\right] > 0.$$

For the sixth equation in system 5, we have

$$\begin{aligned}\frac{dI_M}{dt} &= \beta_1 V M_0 + \beta_2 V M_1 + \pi I_M T_1 - \delta_1 (1 + \chi_1 F_1) I_M N_K \\ &\quad -\delta_2 (1 + \chi_2 F_2) I_M E - \sigma I_M E - (\omega + \varepsilon + \zeta + \mu_{I_M}) I_M.\end{aligned}$$

It follows that

$$\frac{dI_M}{dt} \geq -(\omega + \varepsilon + \zeta + \mu_{I_M}) I_M \quad \forall \quad t \in [0, \tau). \tag{11}$$

Seperating variables and integrating both sides of Eq. (11) from 0 to τ gives

$$I_M(\tau) \geq I_M(0) \exp\left[-(\omega + \varepsilon + \zeta + \mu_{I_M})\tau\right] \geq 0.$$

Similarly, for the seventh equation in system 5, we have

$$\frac{dV}{dt} = \Lambda_V + \omega I_M - \delta_3 T_2 V - \delta_4 A V - (\psi + \mu_V) V.$$

It follows that

$$\frac{dV}{dt} \geq -\left[\delta_3 T_2 + \delta_4 A + (\psi + \mu_V)\right] V \quad \forall \quad t \in [0, \tau). \tag{12}$$

Seperating variables and integrating both sides of Eq. (12) from 0 to τ gives

$$V(\tau) \geq V(0) \exp\left[-(\psi + \mu_V)\tau - \delta_3 \int_0^\tau T_2(t)dt - \delta_4 \int_0^\tau A(t)dt\right] > 0.$$

For the eighth equation in system 5, we have

$$\frac{dA}{dt} = \Lambda_A + \psi V - \delta_4 A V - \mu_A A.$$

It follows that

$$\frac{dA}{dt} \geq -(\mu_A + \delta_4 V) A \quad \forall \quad t \in [0, \tau). \tag{13}$$

Seperating variables and integrating both sides of Eq. (13) from 0 to τ gives

$$A(\tau) \geq A(0)\exp\left[-\mu_A\tau - \delta_4\int_0^\tau V(t)dt\right] > 0.$$

For the ninth equation in system 5, we have

$$\frac{dE}{dt} = \Lambda_E - \delta_2\left(1+\chi_2 F_2\right) I_M E + \sigma I_M E - \mu_E E.$$

It follows that

$$\frac{dE}{dt} \geq -\mu_E E \quad \forall \quad t \in [0,\tau). \tag{14}$$

Seperating variables and integrating both sides of Eq. (14) from 0 to τ gives

$$E(\tau) \geq E(0)\exp\left[-\mu_E\tau\right] > 0.$$

For the tenth equation in system 5, we have

$$\frac{dN_K}{dt} = \Lambda_{N_K} - \delta_1\left(1+\chi_1 F_1\right) I_M N_K + \theta_1 F_1 + \theta_2 F_2 - \left(\eta+\mu_{N_K}\right) N_K.$$

It follows that

$$\frac{dN_K}{dt} \geq -\left(\eta+\mu_{N_K}\right) N_K \quad \forall \quad t \in [0,\tau). \tag{15}$$

Seperating variables and integrating both sides of Eq. (15) from 0 to τ gives

$$N_K(\tau) \geq N_K(0)\exp\left[-\left(\eta+\mu_{N_K}\right)\tau\right] > 0.$$

For the eleventh equation in system 5, we have

$$\frac{dI_{10}}{dt} = \rho_3 I_M T_0\left(\frac{1}{1+\tau_1 I_{10}}\right) - \mu_{I_{10}} I_{10}$$

It follows that

$$\frac{dI_{10}}{dt} \geq -\mu_{I_{10}} I_{10} \quad \forall \quad t \in [0, \tau). \tag{16}$$

Seperating variables and integrating both sides of Eq. (16) from 0 to τ gives

$$I_{10}(\tau) \geq I_{10}(0) \exp\left[-\mu_{I_{10}} \tau\right] \geq 0.$$

For the twelveth equation in system 5, we obtain

$$\frac{dF_1}{dt} = \varepsilon I_M - (\theta_1 + \mu_{F_1}) F_1.$$

It follows that

$$\frac{dF_1}{dt} \geq -(\theta_1 + \mu_{F_1}) F_1 \quad \forall \quad t \in [0, \tau). \tag{17}$$

Seperating variables and integrating both sides of Eq. (17) from 0 to τ gives

$$F_1(\tau) \geq F_1(0) \exp\left[-(\theta_1 + \mu_{F_1}) \tau\right] \geq 0.$$

For the thirteenth equation in system 5, we obtain

$$\frac{dF_2}{dt} = \eta N_K - (\theta_2 + \mu_{F_2}) F_2.$$

It follows that

$$\frac{dF_2}{dt} \geq -(\theta_2 + \mu_{F_2}) F_2 \quad \forall \quad t \in [0, \tau). \tag{18}$$

Seperating variables and integrating both sides of Eq. (18) from 0 to τ gives

$$F_2(\tau) \geq F_2(0) \exp\left[-(\theta_2 + \mu_{F_2}) \tau\right] \geq 0.$$

Thus, we have demonstrated that the solutions $T_0(t) > 0$, $M_0(t) > 0$, $M_1(t) > 0$,

$V(t) \geq 0$, $A(t) \geq 0$, $E(t) \geq 0$, $N_K(t) \geq 0$, $T_1(t) \geq 0$, $T_2(t) \geq 0$, $I_M(t) \geq 0$, $I_{10}(t) \geq 0$, $F_1(t) \geq 0$, and $F_2(t) \geq 0$ of system 5 remain positive for all $t \geq 0$, given that $T_0(0) > 0$, $T_1(0) \geq 0$, $T_2(0) \geq 0$, $M_0(0) > 0$, $M_1(0) > 0$, $I_M(0) \geq 0$, $V(0) \geq 0$, $A(0) \geq 0$, $E(0) \geq 0$, $N_K(0) \geq 0$, $I_{10}(0) \geq 0$, $F_1(0) \geq 0$, and $F_2(0) \geq 0$.

Boundedness of Solutions

The fluctuations in model population variables and parameters within framework 5 were scrupulously examined under prescribed conditions. By verifying that all variables and parameters in the model framework are positive for all time instances $t \geq 0$, we establish that all conceivable solutions remain consistently constrained.

Lemma 4

The solutions of the framework with any non-negative initial conditions are constrained for all $t \geq 0$ within the biologically plausible domain delineated by the set

$$\begin{aligned}\Omega_0 \quad = \quad & \Big\{ (T_0, T_1, T_2, M_0, M_1, I_M, V, A, E, N_K, I_{10}, F_1, F_2) \in \mathbb{R}_+^{13} : \\ & T \leq \Gamma_1, M \leq \Gamma_2, V \leq \Gamma_3, A \leq \Gamma_4, E \leq \Gamma_5, N_K \leq \Gamma_6, I_{10} \leq \Gamma_7, \\ & F_2 \leq \Gamma_8, F_2 \leq \Gamma_9 \Big\}.\end{aligned}$$

Proof. Considering the various T cells (i.e T_0, T_1 and T_2) and summing them to obtain the total T cells population, we have

$$\begin{aligned}\frac{d(T_0 + T_1 + T_2)}{dt} \quad = \quad & \Lambda_{T_0} - \mu_{T_0} T_0 - \mu_{T_1} T_1 - \mu_{T_2} T_2 - \rho_3 I_M T_0 \left(\frac{1}{1 + \tau_1 I_{10}} \right) \\ & - \pi I_M T_1 - \delta_3 T_2 V.\end{aligned}$$

It follows that

$$\frac{dT}{dt} \quad \leq \quad \Lambda_{T_0} - \mu T, \quad \text{where} \quad \mu = \min\{\mu_{T_0}, \mu_{T_1}, \mu_{T_2}\}. \tag{19}$$

Integrating Eq. (19) from 0 to t, we obtain

$$T(t) = \frac{\Lambda_{T_0}}{\mu} + \left(T(0) - \frac{\Lambda_{T_0}}{\mu}\right) \exp\left[-\mu t\right].$$

Taking the limit of T at $t \to \infty$ such that

$$\begin{aligned} \lim_{t\to\infty} T(t) &\leq \frac{\Lambda_{T_0}}{\mu} = \Gamma_1, \quad \text{which implies that} \\ & T_0 \leq \frac{\Lambda_{T_0}}{\mu}, T_1 \leq \frac{\Lambda_{T_0}}{\mu}, T_2 \leq \frac{\Lambda_{T_0}}{\mu}. \end{aligned}$$

Hence, the T cells population is bounded. That is

$$T_0 \leq \frac{\Lambda_{T_0}}{\mu}, \quad T_1 \leq \frac{\Lambda_{T_0}}{\mu}, \quad T_2 \leq \frac{\Lambda_{T_0}}{\mu} = \Gamma_1.$$

Taking the macrophages population into consideration and summing them to obtain the total macrophages population leads to

$$\begin{aligned} \frac{d(M_0 + M_1 + I_M)}{dt} &= \Lambda_{M_0} + \Lambda_{M_1} - \mu_{M_0} M_0 - \mu_{M_1} M_1 \\ & -\delta_1 \left(1 + \chi_1 F_1\right) I_M N_K - \delta_2 \left(1 + \chi_2 F_2\right) I_M E \\ & -\sigma I_M E - \left(\omega + \varepsilon + \mu_{I_M}\right) I_M + \pi T_1 I_M. \end{aligned}$$

It follows that

$$\frac{dM}{dt} \leq \Lambda_{M_0} + \Lambda_{M_1} - \mu_{M_0} M_0 - \mu_{M_1} M_1 - \mu_{I_M} I_M + \pi I_M \Gamma_1.$$

But $\Gamma_1 = \frac{\Lambda_{T_0}}{\mu} = T_1$. Hence,

$$\begin{aligned} \frac{dM}{dt} &\leq \Lambda - \mu M \quad \text{where} \quad \mu = \min\{\mu_{M_0}, \mu_{M_1}, \mu_{I_M}\} \\ & \text{and} \quad \Lambda = \min\{\mu_{M_1}, \Lambda_{M_1}\}. \end{aligned} \tag{20}$$

Integrating Eq. (20) from 0 to t gives

$$M(t) = \frac{\Lambda}{\mu} + \left(M(0) - \frac{\Lambda}{\mu}\right) \exp\left[-\mu t\right].$$

Taking the limit of M as $t \to \infty$ such that

$$\lim_{t\to\infty} M(t) \leq \frac{\Lambda}{\mu} = \Gamma_2, \quad \text{which implies that} \quad M_0 \leq \frac{\Lambda}{\mu}, M_1 \leq \frac{\Lambda}{\mu}, I_M \leq \frac{\Lambda}{\mu} = \Gamma_2.$$

So, the macrophages population is bounded. That is

$$M_0 \leq \frac{\Lambda}{\mu}, M_1 \leq \frac{\Lambda}{\mu}, I_M \leq \frac{\Lambda}{\mu}.$$

Taking the virus population into consideration, we have

$$\frac{dV}{dt} = \Lambda_V + \omega I_M - \delta_3 T_2 V - \delta_4 A V - (\psi + \mu_V) V.$$

It follows that

$$\frac{dV}{dt} \leq \Lambda_V - \mu_V V + \omega \Gamma_2.$$

But $\Gamma_2 = \frac{\Lambda}{\mu} = I_M$. Therefore,

$$\frac{dV}{dt} \leq \Lambda_V - \mu_V V. \tag{21}$$

Integrating Eq. (21) from 0 to t gives

$$V(t) = \frac{\Lambda_V}{\mu_V} + \left(V(0) - \frac{\Lambda_V}{\mu_V}\right) \exp\left[-\mu_V t\right].$$

Taking the limit of V as $t \to \infty$ such that

$$\lim_{t\to\infty} V(t) \leq \frac{\Lambda_V}{\mu_V} = \Gamma_3.$$

Hence, the virus population is bounded. That is

$$V \leq \frac{\Lambda_V}{\mu_V}.$$

Considering the antibodies population, we have

$$\frac{dA}{dt} = \Lambda_A + \psi V - \delta_4 AV - \mu_A A.$$

It follows that

$$\frac{dA}{dt} \leq \Lambda_A + \psi\Gamma_3 - \mu_A A,$$

where $\Gamma_3 = \frac{\Lambda_V}{\mu_V} = V$. Hence,

$$\frac{dA}{dt} \leq \Lambda_A - \mu_A A. \tag{22}$$

Integrating Eq. (22) from 0 to t gives

$$A(t) = \frac{\Lambda_A}{\mu_A} + \left(A(0) - \frac{\Lambda_A}{\mu_A}\right) \exp\left[-\mu_A t\right].$$

Taking the limit of A as $t \to \infty$ such that

$$\lim_{t\to\infty} A(t) \leq \frac{\Lambda_A}{\mu_A} = \Gamma_4.$$

Hence, the antibodies population is bounded. That is

$$A \leq \frac{\Lambda_A}{\mu_A}.$$

Taking the effector B cells population into consideration, we have

$$\frac{dE}{dt} = \Lambda_E - \delta_2 \left(1 + \chi_2 F_2\right) I_M E + \sigma I_M E - \mu_E E.$$

It follows that

$$\frac{dE}{dt} \leq \Lambda_E - \mu_E E + \sigma \Gamma_2 E.$$

But $\Gamma_2 = \frac{\Lambda}{\mu} = I_M$. Therefore,

$$\frac{dE}{dt} \leq \Lambda_E - \mu_E E. \tag{23}$$

Integrating Eq. (23) from 0 to t gives

$$E(t) = \frac{\Lambda_E}{\mu_E} + \left(E(0) - \frac{\Lambda_E}{\mu_E}\right) \exp\left[-\mu_E t\right].$$

Taking the limit of E as $t \to \infty$ such that

$$\lim_{t\to\infty} E(t) \leq \frac{\Lambda_E}{\mu_E} = \Gamma_5.$$

Hence, the effector B cells population is bounded. That is

$$E \leq \frac{\Lambda_E}{\mu_E}.$$

Considering the natural killer cells population, we have

$$\frac{dN_K}{dt} = \Lambda_{N_K} - \delta_1 \left(1 + \chi_1 F_1\right) I_M N_K + \theta_1 F_1 + \theta_2 F_2 - \left(\eta + \mu_{N_K}\right) N_K.$$

It follows

$$\frac{dN_K}{dt} \leq \Lambda_{N_K} - \mu_{N_K} N_K + \theta_1 \Gamma_8 + \theta_2 \Gamma_9.$$

But $\Gamma_8 = \dfrac{\varepsilon}{\mu_{F_1}} = F_1$ and $\Gamma_9 = \dfrac{\eta}{\mu_{F_2}} = F_2$. It follows that

$$\frac{dN_K}{dt} \leq \Lambda_{N_K} - \mu_{N_K} N_K. \tag{24}$$

Integrating Eq. (24) from 0 to t gives

$$N_K(t) = \frac{\Lambda_{N_K}}{\mu_{N_K}} + \left(N_K(0) - \frac{\Lambda_{N_K}}{\mu_{N_K}} \right) \exp\left[-\mu_{N_K} t \right].$$

Taking the limit of N_K as $t \to \infty$ such that

$$\lim_{t\to\infty} N_K(t) \leq \frac{\Lambda_{N_K}}{\mu_{N_K}} = \Gamma_6.$$

Hence, the natural killer cells population is bounded. That is

$$N_K \leq \frac{\Lambda_{N_K}}{\mu_{N_K}}.$$

Taking the anti-inflammatory cytokines population into considering, we have

$$\frac{dI_{10}}{dt} = \rho_3 I_M T_0 \left(\frac{1}{1 + \tau_1 I_{10}} \right) - \mu_{I_{10}} I_{10}.$$

It follows that

$$\frac{dI_{10}}{dt} \leq \rho_3 \Gamma_1 \Gamma_2 \left(\frac{1}{1 + \tau_1 I_{10}} \right) - \mu_{I_{10}} I_{10}. \tag{25}$$

Integrating Eq. (25) from 0 to t results to

$$I_{10}(t) = \frac{\rho_3}{\mu_{I_{10}}} + \left(I_{10}(0) - \frac{\rho_3}{\mu_{I_{10}}} \right) \exp\left[-\mu_{I_{10}} t \right].$$

Taking the limit of I_{10} as $t \to \infty$ such that

$$\lim_{t\to\infty} I_{10}(t) \leq \frac{\rho_3}{\mu_{I_{10}}} = \Gamma_7.$$

Hence, the anti-inflammatory cytokines population is bounded. That is

$$I_{10} \leq \frac{\rho_3}{\mu_{I_{10}}}.$$

Considering the type-1 interferon population, we have

$$\frac{dF_1}{dt} = \varepsilon I_M - (\theta_1 + \mu_{F_1}) F_1.$$

It follows that

$$\frac{dF_1}{dt} = \varepsilon \Gamma_2 - \mu_{F_1} F_1. \tag{26}$$

Integrating Eq. (26) from 0 to t gives

$$F_1(t) = \frac{\varepsilon}{\mu_{F_1}} + \left(F_1(0) - \frac{\varepsilon}{\mu_{F_1}} \right) \exp\left[-\mu_{F_1} t \right].$$

Taking the limit of F_1 as $t \to \infty$ such that

$$\lim_{t \to \infty} F_1(t) \leq \frac{\varepsilon}{\mu_{F_1}} = \Gamma_8.$$

Hence, the type-1 interferon population is bounded. That is

$$F_1 \leq \frac{\varepsilon}{\mu_{F_1}}.$$

Considering the type-2 interferon population, we have

$$\frac{dF_2}{dt} = \eta N_K - (\theta_2 + \mu_{F_2}) F_2.$$

It follows that

$$\frac{dF_1}{dt} \leq \eta \Gamma_6 - \mu_{F_2} F_2. \tag{27}$$

Integrating Eq. (27) from 0 to t gives

$$F_2(t) = \frac{\eta}{\mu_{F_2}} + \left(F_2(0) - \frac{\eta}{\mu_{F_2}}\right) \exp\left[-\mu_{F_2} t\right].$$

Taking the limit of F_2 as $t \to \infty$ such that

$$\lim_{t\to\infty} F_2(t) \leq \frac{\eta}{\mu_{F_2}} = \Gamma_9.$$

Hence, the type-2 interferon population is bounded. That is

$$F_2 \leq \frac{\eta}{\mu_{F_2}}.$$

Consequently, we can assert that for $t > 0$, every trajectory of the system remains confined within the bounded domain Ω_0. Consequently, it is essential to scrutinize the dynamics and interrelations of T lymphocytes, macrophages, viral entities, antibodies, effector B lymphocytes, natural killer lymphocytes, and cytokines as outlined by the model within the invariant set Ω_0.

Model Analysis

In this section, we demonstrate the existence and uniqueness of solutions for the model framework and elucidate the criteria under which both pathogen-free and persistent-infection equilibria arise.

Existence and Uniqueness of Solutions

The study begins the model analysis by showing that the model system in Eq. (5) possesses a unique solution.

Given the general first-order ODE with initial condition of the form

$$\frac{dz}{dy} = f(t, y), \quad y(t_0) = y_0, \tag{28}$$

the following questions may be of interest.:

1. under what conditions can the solution of Eq. (28) be said to exist?

2. under what conditions can the existing solution in Eq. (28) be considered unique?

To answer these questions, let:

$$
\begin{aligned}
f_1 &= \Lambda_{T_0} - \rho_1 I_M T_0 I_{10} - \rho_2 V T_0 I_{10} - \rho_3 T_0 I_M \left(\frac{1}{1+\tau_1 I_{10}}\right) - \mu_{T_0} T_0, \\
f_2 &= \rho_1 I_M T_0 I_{10} - \pi I_M T_1 - \mu_{T_1} T_1, \\
f_3 &= \rho_2 V T_0 I_{10} - \delta_3 T_2 V - \mu_{T_2} T_2, \\
f_4 &= \Lambda_{M_0} - \beta_1 V M_0 - \mu_{M_0} M_0, \\
f_5 &= \Lambda_{M_1} - \beta_2 V M_1 + \zeta I_M - \mu_{M_1} M_1, \\
f_6 &= \beta_1 V M_0 + \beta_2 V M_1 + \pi I_M T_1 - \delta_1 \left(1+\chi_1 F_1\right) I_M N_K \\
&\quad -\delta_2 \left(1+\chi_2 F_2\right) I_M E - \sigma I_M E - \left(\omega + \varepsilon + \zeta + \mu_{I_M}\right) I_M, \\
f_7 &= \Lambda_V + \omega I_M - \delta_3 T_2 V - \delta_4 A V - \left(\psi + \mu_V\right) V, \\
f_8 &= \Lambda_A + \psi V - \delta_4 A V - \mu_A A, \\
f_9 &= \Lambda_E - \delta_2 \left(1+\chi_2 F_2\right) I_M E + \sigma I_M E - \mu_E E, \\
f_{10} &= \Lambda_{N_K} - \delta_1 \left(1+\chi_1 F_1\right) I_M N_K + \theta_1 F_1 + \theta_2 F_2 - \left(\eta + \mu_{N_K}\right) N_K, \\
f_{11} &= \rho_3 I_M T_0 \left(\frac{1}{1+\tau_1 I_{10}}\right) - \mu_{I_{10}} I_{10}, \\
f_{12} &= \varepsilon I_M - \left(\theta_1 + \mu_{F_1}\right) F_1, \\
f_{13} &= \eta N_K - \left(\theta_2 + \mu_{F_2}\right) F_2.
\end{aligned}
$$

The following is used to establish the existence and uniqueness of the solution for the hepatitis B virus and liver cancer model.

Theorem 3

Uniqueness of Solutions: *Let D be the domain*

$$
\left.
\begin{aligned}
|t - t_0| \leq a, \quad ||y - y_0|| \leq b, \\
y = (y_1, y_2, \cdots, y_n), \quad y_0 = (y_{10}, y_{20}, \cdots, y_{n0})
\end{aligned}
\right\} \tag{29}
$$

and suppose that $f(t, y)$ *satisfies the Lipschitz condition*

$$||f(t, y_1) - f(t, y_2)|| \leq k||y_1 - y_2||, \tag{30}$$

whenever the pairs (t, y_1) *and* (t, y_2) *belong to the domain* D*, where* k *is used to represent a positive constant. Then there exists a constant* $\delta > 0$ *such that there exist a unique (exactly) one continuous vector solution* $y(t)$ *of system 28 in the interval* $|t - t_0| \leq \delta$*. It is important to note that the condition in Eq.* (30) *is satisfied by the requirement that*

$$\left\{ \frac{\partial f_i}{\partial y_j}, \quad i, j = 1, 2, 3, \cdots, n \right.$$

be continuous and bounded in the domain D*.*

Lemma 5

If $f(y, t)$ has a continuous derivative $\dfrac{\partial f_i}{\partial y_j}$ on a bounded closed convex domain $\mathbb{R}$ (i.e convex set of real numbers), where $\mathbb{R}$ is used to denotes real numbers, then it satisfies a Lipschitz condition in $\mathbb{R}$. The target here is in the domain.

$$1 \leq \epsilon \leq \mathbb{R}. \tag{31}$$

So, a bounded solution of the form

$$1 < \mathbb{R} < \infty$$

is sought. The following existence theorem is now proven.

Theorem 4

Existence of solution: *Let* D *denote the domain in Eq.* (29) *such that Eq.* (30) *and Eq.* (31) *hold. Then there exist a solution of model system 5 which is bounded in the domain* D*.*

Proof. Let

$$\begin{aligned}
f_1 &= \Lambda_{T_0} - \rho_1 I_M T_0 I_{10} - \rho_2 V T_0 I_{10} - \rho_3 T_0 I_M \left(\frac{1}{1+\tau_1 I_{10}}\right) - \mu_{T_0} T_0,\\
f_2 &= \rho_1 I_M T_0 I_{10} - \pi I_M T_1 - \mu_{T_1} T_1,\\
f_3 &= \rho_2 V T_0 I_{10} - \delta_3 T_2 V - \mu_{T_2} T_2,\\
f_4 &= \Lambda_{M_0} - \beta_1 V M_0 - \mu_{M_0} M_0,\\
f_5 &= \Lambda_{M_1} - \beta_2 V M_1 + \zeta I_M - \mu_{M_1} M_1,\\
f_6 &= \beta_1 V M_0 + \beta_2 V M_1 + \pi I_M T_1 - \delta_1 (1+\chi_1 F_1) I_M N_K\\
&\quad -\delta_2 (1+\chi_2 F_2) I_M E - \sigma I_M E - (\omega + \varepsilon + \zeta + \mu_{I_M}) I_M,\\
f_7 &= \Lambda_V + \omega I_M - \delta_3 T_2 V - \delta_4 A V - (\psi + \mu_V) V,\\
f_8 &= \Lambda_A + \psi V - \delta_4 A V - \mu_A A,\\
f_9 &= \Lambda_E - \delta_2 (1+\chi_2 F_2) I_M E + \sigma I_M E - \mu_E E,\\
f_{10} &= \Lambda_{N_K} - \delta_1 (1+\chi_1 F_1) I_M N_K + \theta_1 F_1 + \theta_2 F_2 - (\eta + \mu_{N_K}) N_K,\\
f_{11} &= \rho_3 I_M T_0 \left(\frac{1}{1+\tau_1 I_{10}}\right) - \mu_{I_{10}} I_{10},\\
f_{12} &= \varepsilon I_M - (\theta_1 + \mu_{F_1}) F_1,\\
f_{13} &= \eta N_K - (\theta_2 + \mu_{F_2}) F_2.
\end{aligned}$$

It is shown that

$$\frac{\partial f_i}{\partial y_j}, \quad i,j = 1,2,3,\cdots,13$$

are continuous and bounded. That is the partial derivatives are continuous and bounded. Hence, the following partial derivatives are explored for all the model equations.

From the first equation, the following partial derivatives are obtained

$$\begin{aligned}
\frac{\partial f_1}{\partial T_0} &= -\rho_1 I_M I_{10} - \rho_2 V I_{10} - \frac{\rho_3 I_{10}}{1+\tau_1 I_{10}} - \mu_{T_0},\\
&\left|\frac{\partial f_1}{\partial T_0}\right| = \left|-\rho_1 I_M I_{10} - \rho_2 V I_{10} - \frac{\rho_3 I_{10}}{1+\tau_1 I_{10}} - \mu_{T_0}\right| < \infty,
\end{aligned}$$

$$\frac{\partial f_1}{\partial I_M} = -\rho_1 T_0 I_{10}, \quad \left|\frac{\partial f_1}{\partial I_M}\right| = |-\rho_1 T_0 I_{10}| < \infty,$$

$$\frac{\partial f_1}{\partial V} = -\rho_2 T_0 I_{10}, \quad \left|\frac{\partial f_1}{\partial V}\right| = |-\rho_2 T_0 I_{10}| < \infty,$$

$$\frac{\partial f_1}{\partial I_{10}} = -\rho_1 T_0 I_M - \rho_2 T_0 V - \frac{\rho_3 T_0}{(1+\tau_1 I_{10})^2},$$
$$\left|\frac{\partial f_1}{\partial I_{10}}\right| = \left|-\rho_1 T_0 I_M - \rho_2 T_0 V - \frac{\rho_3 T_0}{(1+\tau_1 I_{10})^2}\right| < \infty.$$

From the second equation, the following partial derivatives are obtained

$$\frac{\partial f_2}{\partial T_1} = -\pi I_M - \mu_{T_1}, \quad \left|\frac{\partial f_2}{\partial T_1}\right| = |-\pi I_M - \mu_{T_1}| < \infty,$$

$$\frac{\partial f_2}{\partial I_M} = \rho_1 T_0 I_{10} - \pi T_1, \quad \left|\frac{\partial f_2}{\partial I_M}\right| = |\rho_1 T_0 I_{10} - \pi T_1| < \infty,$$

$$\frac{\partial f_2}{\partial T_0} = \rho_1 I_M I_{10}, \quad \left|\frac{\partial f_2}{\partial T_0}\right| = |\rho_1 I_M I_{10}| < \infty,$$

$$\frac{\partial f_2}{\partial I_{10}} = \rho_1 T_0 I_M, \quad \left|\frac{\partial f_2}{\partial I_{10}}\right| = |\rho_1 T_0 I_M| < \infty.$$

From the third equation, the following partial derivatives are obtained

$$\frac{\partial f_3}{\partial T_2} = -\delta_3 V - \mu_{T_2}, \quad \left|\frac{\partial f_3}{\partial I_{10}}\right| = |-\delta_3 V - \mu_{T_2}| < \infty,$$

$$\frac{\partial f_3}{\partial I_{10}} = \rho_2 V T_0, \quad \left|\frac{\partial f_3}{\partial I_{10}}\right| = |\rho_2 V T_0| < \infty,$$

$$\frac{\partial f_3}{\partial V} = \rho_2 T_0 I_{10}, \quad \left|\frac{\partial f_3}{\partial V}\right| = |\rho_2 T_0 I_{10}| < \infty,$$

$$\frac{\partial f_3}{\partial T_0} = \rho_2 I_{10} V, \quad \left|\frac{\partial f_3}{\partial T_0}\right| = |\rho_2 I_{10} V| < \infty.$$

From the fourth equation, the following partial derivatives are obtained

$$\frac{\partial f_4}{\partial M_0} = -\beta_1 V - \mu_{M_0}, \quad \left|\frac{\partial f_4}{\partial M_0}\right| = |-\beta_1 V - \mu_{M_0}| < \infty,$$

$$\frac{\partial f_4}{\partial V} = -\beta_1 M_0, \quad \left|\frac{\partial f_4}{\partial V}\right| = |-\beta_1 M_0| < \infty.$$

From the fifth equation, the following partial derivatives are obtained

$$\frac{\partial f_5}{\partial M_1} = -\beta_2 V - \mu_{M_1}, \quad \left|\frac{\partial f_5}{\partial M_1}\right| = |-\beta_2 V - \mu_{M_1}| < \infty,$$

$$\frac{\partial f_5}{\partial V} = -\beta_2 M_1, \quad \left|\frac{\partial f_5}{\partial V}\right| = |-\beta_2 M_1| < \infty.$$

$$\frac{\partial f_5}{\partial I_M} = \zeta, \quad \left|\frac{\partial f_5}{\partial I_M}\right| = |\zeta| < \infty.$$

From the sixth equation, the following partial derivatives are obtained

$$\frac{\partial f_6}{\partial M_0} = \beta_1 V, \quad \left|\frac{\partial f_6}{\partial M_0}\right| = |\beta_1 V| < \infty,$$

$$\frac{\partial f_6}{\partial M_1} = \beta_2 V, \quad \left|\frac{\partial f_6}{\partial M_1}\right| = |\beta_2 V| < \infty,$$

$$\frac{\partial f_6}{\partial V} = \beta_1 M_0 + \beta_2 M_1, \quad \left|\frac{\partial f_6}{\partial V}\right| = |\beta_1 M_0 + \beta_2 M_1| < \infty,$$

$$\begin{aligned}\frac{\partial f_6}{\partial I_M} &= -\delta_1\left(1+\chi F_1\right)N_K - \delta_2\left(1+\chi_2 F_2\right)E - \sigma E \\ &\quad -\left(\omega+\varepsilon+\zeta+\mu_{I_M}\right)+\pi T_1, \\ \left|\frac{\partial f_6}{\partial I_M}\right| &= |-\delta_1\left(1+\chi F_1\right)N_K - \delta_2\left(1+\chi_2 F_2\right)E - \sigma E \\ &\quad -\left(\omega+\varepsilon+\zeta+\mu_{I_M}\right)+\pi T_1| < \infty,\end{aligned}$$

$$\frac{\partial f_6}{\partial N_K} = -\delta_1\left(1+\chi_1 F_1\right)I_M, \quad \left|\frac{\partial f_6}{\partial N_K}\right| = |-\delta_1\left(1+\chi_1 F_1\right)I_M| < \infty,$$

$$\begin{aligned}\frac{\partial f_6}{\partial E} &= -\delta_2\left(1+\chi_2 F_2\right)I_M - \sigma I_M, \\ &\quad \left|\frac{\partial f_6}{\partial E}\right| = |-\delta_2\left(1+\chi_2 F_2\right)I_M - \sigma I_M| < \infty,\end{aligned}$$

$$\frac{\partial f_6}{\partial T_1} = \pi I_M, \quad \left|\frac{\partial f_6}{\partial E}\right| = |\pi I_M| < \infty,$$

$$\frac{\partial f_6}{\partial F_1} = -\delta_1\chi_1 N_K I_M, \quad \left|\frac{\partial f_6}{\partial F_1}\right| = |-\delta_1\chi_1 I_M N_K| < \infty,$$

$$\frac{\partial f_6}{\partial F_2} = -\delta_2\chi_2 I_M E, \quad \left|\frac{\partial f_6}{\partial F_2}\right| = |-\delta_2\chi_2 I_M E| < \infty.$$

From the seventh equation, the following partial derivatives are obtained

$$\begin{aligned}\frac{\partial f_7}{\partial V} &= -\delta_3 T_2 - \delta_4 A - \left(\psi+\mu_V\right), \\ &\quad \left|\frac{\partial f_7}{\partial V}\right| = |-\delta_3 T_2 - \delta_4 A - \left(\psi+\mu_V\right)| < \infty,\end{aligned}$$

$$\frac{\partial f_7}{\partial A} = -\delta_4 V, \quad \left|\frac{\partial f_7}{\partial A}\right| = |-\delta_4 V| < \infty,$$

$$\frac{\partial f_7}{\partial T_2} = -\delta_3 V, \quad \left|\frac{\partial f_7}{\partial T_2}\right| = |-\delta_3 V| < \infty,$$

$$\frac{\partial f_7}{\partial I_M} = \omega, \quad \left|\frac{\partial f_7}{\partial I_M}\right| = |\omega| < \infty.$$

From the eighth equation, the following partial derivatives are obtained

$$\frac{\partial f_8}{\partial A} = -\delta_4 V - \mu_A, \quad \left|\frac{\partial f_8}{\partial A}\right| = |-\delta_4 V - \mu_A| < \infty,$$

$$\frac{\partial f_8}{\partial V} = \psi, \quad \left|\frac{\partial f_8}{\partial A}\right| = |\psi| < \infty.$$

From the ninth equation, the following partial derivatives are obtained

$$\begin{aligned}\frac{\partial f_9}{\partial I_M} &= -\delta_2 \left(1 + \chi_2 F_2\right) E + \sigma E, \quad \left|\frac{\partial f_9}{\partial I_M}\right| \\ &= |-\delta_2 \left(1 + \chi_2 F_2\right) E + \sigma E| < \infty,\end{aligned}$$

$$\begin{aligned}\frac{\partial f_9}{\partial E} &= -\delta_2 \left(1 + \chi_2 F_2\right) I_M + \sigma I_M - \mu_E, \\ &\left|\frac{\partial f_9}{\partial E}\right| = |-\delta_2 \left(1 + \chi_2 F_2\right) I_M + \sigma I_M - \mu_E| < \infty,\end{aligned}$$

$$\frac{\partial f_9}{\partial F_2} = -\delta_2 \chi_2 I_M E, \quad \left|\frac{\partial f_9}{\partial F_2}\right| = |-\delta_2 \chi_2 I_M E| < \infty.$$

From the tenth equation, the following partial derivatives are obtained

$$\begin{aligned}\frac{\partial f_{10}}{\partial N_K} &= -\delta_1 \left(1 + \chi_1 F_1\right) I_M - \left(\eta + \mu_{N_K}\right), \\ &\left|\frac{\partial f_{10}}{\partial N_K}\right| = |-\delta_1 \left(1 + \chi_1 F_1\right) I_M - \left(\eta + \mu_{N_K}\right)| < \infty,\end{aligned}$$

$$\frac{\partial f_{10}}{\partial I_M} = -\delta_1 \left(1 + \chi_1 F_1\right) N_K, \quad \left|\frac{\partial f_{10}}{\partial I_M}\right| = |-\delta_1 \left(1 + \chi_1 F_1\right) N_K| < \infty,$$

$$\frac{\partial f_{10}}{\partial F_1} = -\delta_1\chi_1 I_M N_K + \theta_1, \quad \left|\frac{\partial f_{10}}{\partial F_1}\right| = |-\delta_1\chi_1 I_M N_K + \theta_1| < \infty,$$

$$\frac{\partial f_{10}}{\partial F_2} = \theta_2, \quad \left|\frac{\partial f_{10}}{\partial F_2}\right| = |\theta_2| < \infty.$$

From the eleventh equation, the following partial derivatives are obtained

$$\frac{\partial f_{11}}{\partial T_0} = \frac{\rho_3 I_M}{1+\tau_1 I_{10}}, \quad \left|\frac{\partial f_{11}}{\partial T_0}\right| = \left|\frac{\rho_3 I_M}{1+\tau_1 I_{10}}\right| < \infty,$$

$$\frac{\partial f_{11}}{\partial I_M} = \frac{\rho_3 T_0}{1+\tau_1 I_{10}}, \quad \left|\frac{\partial f_{11}}{\partial I_M}\right| = \left|\frac{\rho_3 T_0}{(1+\tau_1 I_{10})}\right| < \infty,$$

$$\frac{\partial f_{11}}{\partial I_{10}} = \frac{\rho_3 T_0}{(1+\tau_1 I_{10})^2}, \quad \left|\frac{\partial f_{11}}{\partial I_{10}}\right| = \left|\frac{\rho_3 T_0}{(1+\tau_1 I_{10})^2}\right| < \infty.$$

From the Twelfth equation, the following partial derivatives are obtained

$$\frac{\partial f_{12}}{\partial F_1} = -\left(\theta_1 + \mu_{F_1}\right), \quad \left|\frac{\partial f_{12}}{\partial F_1}\right| = |-\left(\theta_1 + \mu_{F_1}\right)| < \infty,$$

$$\frac{\partial f_{12}}{\partial I_M} = \varepsilon, \quad \left|\frac{\partial f_{12}}{\partial I_M}\right| = |\varepsilon| < \infty.$$

From the thirteenth equation, the following partial derivatives are obtained

$$\frac{\partial f_{13}}{\partial F_2} = -\left(\theta_2 + \mu_{F_2}\right), \quad \left|\frac{\partial f_{13}}{\partial F_2}\right| = |-\left(\theta_2 + \mu_{F_2}\right)| < \infty,$$

$$\frac{\partial f_{13}}{\partial N_K} = \eta, \quad \left|\frac{\partial f_{13}}{\partial N_K}\right| = |\eta| < \infty.$$

It has been established that all the partial derivatives are continuous and bounded; hence, by Theorem 4, the existence of a unique solution for the model system 5 in

the region D can be concluded.

Virus-free Equilibrium State (VFE)

Certain hepatocytes are hypothesized to have undergone malignant transformation due to external etiological factors such as chronic alcohol abuse and tobacco use. A hepatitis B virus (HBV) infection has subsequently been incorporated into the model, and the resultant coexistence dynamics have been analyzed. Thus, at the virus-free equilibrium state, the absence of HBV implies the nonexistence of infected macrophages. In this state, both uninfected macrophages (whether cancerous or non-cancerous) are devoid of viral particles to internalize and become infected. Consequently, $V^\star = 0$, which directly leads to $I_M^\star = 0$ and $F_1^\star = 0$. It follows that $A^\star = 0$, $E^\star = 0$, $N_K^\star = 0$ and $F_2^\star = 0$. The absence of infected macrophages signifies that HBV transmission is non-existent, and as a result, naive T cells will not engage in any cytotoxic activity.

When naïve T cells do not perform lytic activity, they fail to eliminate infected cells and control the HBV infection. This results in a situation where the immune system is unable to effectively clear the virus. Consequently, the system may reach a virus-free equilibrium (ε_0), a theoretical state where viral replication is minimal or absent, even though the virus is not completely eradicated. This equilibrium indicates that the virus is controlled but not entirely cleared, due to the lack of an effective immune response. Thus, at the pathogen-free equilibrium, the populations of all immune-responsive cellular types are denoted by

$$\varepsilon_0^\star = (T_0^\star, T_1^\star, T_2^\star, M_0^\star, M_1^\star, I_M^\star, V^\star, A^\star, E^\star, N_K^\star, I_{10}^\star, F_1^\star, F_2^\star)\,.$$

Hence, at the virus-free equilibrium, the following equations are satisfied

$$\left.\begin{aligned} \Lambda_{T_0} - \mu_{T_0} T_0^\star &= 0, \\ -\mu_{T_1} T_1^\star &= 0, \\ -\mu_{T_2} T_2^\star &= 0, \\ \Lambda_{M_0} - \mu_{M_0} M_0^\star &= 0, \\ \Lambda_{M_0} - \mu_{M_0} M_0^\star &= 0, \\ -\mu_{I_{10}} I_{10}^\star &= 0. \end{aligned}\right\} \tag{32}$$

Following Eq. (32), the virus-free equilibrium is obtained to be

$$\varepsilon_0^\star = \left(\frac{\Lambda_{T_0}}{\mu_{T_0}}, 0, 0, \frac{\Lambda_{M_0}}{\mu_{M_0}}, \frac{\Lambda_{M_1}}{\mu_{M_1}}, 0, 0, 0, 0, 0, 0, 0, 0, 0 \right).$$

Basic Reproduction Number; $\mathbb{R}_0$

Subsequently, the Next Generation Matrix methodology, as articulated by Diekmann & Heesterbeek (2000) and utilized in (Chataa et al., 2021), was employed to compute the basic reproduction number of the model system. The basic reproduction number, denoted as $\mathbb{R}_0$, quantifies the expected number of secondary HBV infections initiated by a single infected macrophage introduced into a completely susceptible liver cell population. In other terms, $\mathbb{R}_0$ reflects the average number of new infections generated by one infected macrophage cell when the liver cell population is entirely uninfected. The analysis begins with examining the system's differential equations governing the emergence of newly infected macrophages and the alterations in their states. The derivation of these equations is provided by

$$\left.\begin{aligned} \frac{dI_M}{dt} &= \beta_1 V M_0 + \beta_2 V M_1 + \pi I_M T_1 - \delta_1 \left(1 + \chi_1 F_1\right) I_M N_K \\ &\quad - \delta_2 \left(1 + \chi_2 F_2\right) I_M E - \sigma I_M E - \left(\omega + \varepsilon + \zeta + \mu_{I_M}\right) I_M, \\ \frac{dV}{dt} &= \Lambda_V + \omega I_M - \delta_3 T_2 V - \delta_4 A V - \left(\psi + \mu_V\right) V. \end{aligned}\right\} \tag{33}$$

The ensemble of these equations within framework 33 is designated as the infected subsystem. Linearizing the infected subsystem about the pathogen-free steady state

represents the initial phase, according to prevailing guidelines. When setting

$$\mathbb{X} = (T_0, T_1, T_2, M_0, M_1, I_M, V, A, E, N_K, I_{10}, F_1, F_2)^T ;$$

where T denotes the transpose, the infected subsystem can then be written in the form:

$$\frac{d\mathbb{X}}{dt} = \mathbb{F}(\mathbb{X}) - \mathbb{V}(\mathbb{X}),$$

where

$$\mathbb{F}(\mathbb{X}) = \begin{pmatrix} \beta_1 V M_0 + \beta_2 V M_1 + \pi I_M T_1 \\ 0 \end{pmatrix} \quad \text{and}$$

$$\mathbb{V}(\mathbb{X}) = \begin{pmatrix} \delta_1 (1 + \chi_1 F_1) I_M N_K + \delta_2 (1 + \chi_2 F_2) I_M E + \sigma I_M E + \mathfrak{B} I_M \\ -\Lambda_V - \omega I_M + \delta_3 T_2 V + \delta_4 A V + (\psi + \mu_V) V \end{pmatrix},$$

where $\mathfrak{B} = (\omega + \varepsilon + \zeta + \mu_{I_M})$.

Taking the Jacobian of $\mathbb{F}(\mathbb{X})$ at the virus-free equilibrium state gives

$$\frac{\partial F(\varepsilon_0)}{\partial F_i} = \begin{pmatrix} \frac{\partial F_1(\varepsilon_0)}{\partial I_M} & \frac{\partial F_1(\varepsilon_0)}{\partial V} \\ \frac{\partial F_2(\varepsilon_0)}{\partial I_M} & \frac{\partial F_2(\varepsilon_0)}{\partial V} \end{pmatrix} = \begin{pmatrix} 0 & \beta_1 M_0^\star + \beta_2 M_1^\star \\ 0 & 0 \end{pmatrix}$$

It follows that

$$F = \begin{pmatrix} 0 & \frac{\beta_1 \Lambda_{M_0}}{\mu_{M_0}} + \frac{\beta_2 \Lambda_{M_1}}{\mu_{M_1}} \\ 0 & 0 \end{pmatrix}.$$

Also taking the Jacobian of $\mathbb{V}(\mathbb{X})$ at the virus-free equilibrium gives

$$\begin{aligned}\frac{\partial V(\varepsilon_0)}{\partial V_i} &= \begin{pmatrix} \frac{\partial V_1(\varepsilon_0)}{\partial I_M} & \frac{\partial V_1(\varepsilon_0)}{\partial V} \\ \frac{\partial V_2(\varepsilon_0)}{\partial I_M} & \frac{\partial V_2(\varepsilon_0)}{\partial V} \end{pmatrix} \\ &= \begin{pmatrix} (\omega+\varepsilon+\zeta+\mu_{I_M}) & 0 \\ -\omega & (\psi+\mu_V) \end{pmatrix},\end{aligned}$$

It follows that

$$V = \begin{pmatrix} A & 0 \\ -\omega & B \end{pmatrix},$$

where

$$\begin{aligned} A &= (\omega+\varepsilon+\zeta+\mu_{I_M}), \\ B &= (\psi+\mu_V). \end{aligned}$$

Hence,

$$V^{-1} = \begin{pmatrix} \frac{1}{A} & 0 \\ \frac{\omega}{AB} & \frac{1}{B} \end{pmatrix}.$$

Thus, the ensuing transmission matrix, which quantifies the number of subsequent infections instigated by an individual infected macrophage cell when all hepatic cells are pathogen-free, is articulated as

$$\begin{aligned} FV^{-1} &= \begin{pmatrix} 0 & \beta_1 M_0^\star + \beta_2 M_1^\star \\ 0 & 0 \end{pmatrix} \begin{pmatrix} \frac{1}{A} & 0 \\ \frac{\omega}{AB} & \frac{1}{B} \end{pmatrix} \\ &= \begin{pmatrix} \frac{\omega}{AB}\left[\frac{\beta_1\Lambda_{M_0}}{\mu_{M_0}} + \frac{\beta_2\Lambda_{M_1}}{\mu_{M_1}}\right] & \frac{1}{B}\left[\frac{\beta_1\Lambda_{M_0}}{\mu_{M_0}} + \frac{\beta_2\Lambda_{M_1}}{\mu_{M_1}}\right] \\ 0 & 0 \end{pmatrix}. \end{aligned}$$

Since the matrix FV^{-1} is an upper triangular matrix, it follows that the eigenvalues

are the entries on the principal diagonal. Consequently,

$$\varrho_1 = \frac{\omega}{AB}\left[\frac{\beta_1\Lambda_{M_0}}{\mu_{M_0}} + \frac{\beta_2\Lambda_{M_1}}{\mu_{M_1}}\right] \quad \varrho_2 = 0.$$

But since $\mathbb{R}_0 = \max\left[|\varrho_1||\varrho_2|\right]$ is the largest spectral radius of FV^{-1}, at the virus-free equilibrium, the following holds:

$$\mathbb{R}_0 = \frac{\omega}{AB}\left[\frac{\beta_1\Lambda_{M_0}}{\mu_{M_0}} + \frac{\beta_2\Lambda_{M_1}}{\mu_{M_1}}\right].$$

By substitution, the $\mathbb{R}_0$ was obtain to be

$$\mathbb{R}_0 = \mathbb{R}_1 + \mathbb{R}_2,$$

where

$$\mathbb{R}_1 = \frac{\beta_1\omega\Lambda_{M_0}}{\mu_{M_0}\left(\omega+\varepsilon+\zeta+\mu_{I_M}\right)\left(\psi+\mu_V\right)},$$

$$\mathbb{R}_1 = \frac{\beta_2\omega\Lambda_{M_1}}{\mu_{M_1}\left(\omega+\varepsilon+\zeta+\mu_{I_M}\right)\left(\psi+\mu_V\right)}.$$

Analytical interpretation of $\mathbb{R}_0$

- The basic reproduction number, $\mathbb{R}_0$, is identified as the aggregate of the reproduction numbers associated with the two distinct compartments of uninfected macrophages.
- Consequently, $\mathbb{R}_1$ represents the expected number of secondary infections resulting from the interaction between the virus and uninfected macrophages devoid of cancer cells.
- In a similar fashion, $\mathbb{R}_2$ denotes the expected number of secondary infections arising from the interaction between the virus and uninfected macrophages that are associated with cancer cells.
- The expression $\frac{\Lambda_{M_0}}{\mu_{M_0}}$ signifies the carrying capacity of uninfected macrophages

without cancer within the cellular environment.

- The expression $\frac{\Lambda_{M_1}}{\mu_{M_1}}$ indicates the carrying capacity of uninfected macrophages with cancer within the cellular milieu.

- It is observed that an increase in the new virion replication rate ω leads to a corresponding rise in the production of new virions, which drives the model system towards the virus-persistence equilibrium.

Stability Analysis of Virus-free Equilibrium

In this section, both the local and global stability of the virus-free equilibrium point, ε_0, were rigorously analyzed.

Local Stability of the Virus-free Equilibrium

By evaluating the eigenvalues of the linearized Jacobian matrix at the pathogen-free equilibrium, the local stability of this equilibrium against minor disturbances can be ascertained. Specifically, when a small contingent of infected cells is introduced into the population of susceptible hepatic cells, the stability of the pathogen-free equilibrium ensures that the viral infection can be eradicated from the hepatic cells, provided that $\mathbb{R}_0 < 1$.

Theorem 5

The virus-free equilibrium $\varepsilon_0^\star$ of system 5 is locally asymptotically stable if $\mathbb{R}_0 < 1$ and unstable if $\mathbb{R}_0 > 1$.

Proof. The validation of Theorem 5 is scrutinized through a linearization methodology. The Jacobian matrix pertinent to the model framework 5 at the pathogen-free equilibrium is leveraged to ascertain

$$J_0(\varepsilon_0)^\star = \begin{pmatrix}
-\mu_{T_0} & 0 & 0 & 0 & 0 & -\mathfrak{S}_1 & 0 & 0 & 0 & 0 & 0 & 0 & 0 \\
0 & -\mu_{T_1} & 0 & 0 & 0 & 0 & 0 & 0 & 0 & 0 & 0 & 0 & 0 \\
0 & 0 & -\kappa_1 & 0 & 0 & 0 & 0 & 0 & 0 & 0 & 0 & 0 & 0 \\
0 & 0 & 0 & -\kappa_2 & 0 & 0 & -\mathfrak{S}_2 & 0 & 0 & 0 & 0 & 0 & 0 \\
0 & 0 & 0 & 0 & -\kappa_3 & \zeta & -\mathfrak{S}_3 & 0 & 0 & 0 & 0 & 0 & 0 \\
0 & 0 & 0 & 0 & 0 & -\kappa_4 & \kappa_{11} & 0 & 0 & 0 & 0 & 0 & 0 \\
0 & 0 & 0 & 0 & 0 & \omega & -\kappa_5 & 0 & 0 & 0 & 0 & 0 & 0 \\
0 & 0 & 0 & 0 & 0 & 0 & \kappa_6 & -\kappa_7 & 0 & 0 & 0 & 0 & 0 \\
0 & 0 & 0 & 0 & 0 & 0 & 0 & 0 & -\mu_E & 0 & 0 & 0 & 0 \\
0 & 0 & 0 & 0 & 0 & 0 & 0 & 0 & 0 & -\kappa_8 & 0 & \theta_1 & \theta_2 \\
0 & 0 & 0 & 0 & 0 & \mathfrak{S}_4 & 0 & 0 & 0 & 0 & -\mu_{I_{10}} & 0 & 0 \\
0 & 0 & 0 & 0 & 0 & \varepsilon & 0 & 0 & 0 & 0 & 0 & -\kappa_9 & 0 \\
0 & 0 & 0 & 0 & 0 & 0 & 0 & 0 & 0 & \eta & 0 & 0 & -\kappa_{10}
\end{pmatrix},$$

where

$\kappa_1 = \mu_{T_2}$, $\kappa_2 = \mu_{M_0}$, $\kappa_3 = \mu_{M_1}$,

$\kappa_4 = (\omega + \varepsilon + \zeta + \mu_{I_M})$, $\kappa_5 = (\psi + \mu_V)$, $\kappa_6 = \psi$,

$\kappa_7 = \mu_A$, $\kappa_8 = (\eta + \mu_{N_K})$, $\kappa_9 = (\theta_1 + \mu_{F_1})$,

$\kappa_{10} = (\theta_2 + \mu_{F_2})$, $\kappa_{11} = \beta_1 M_0^\star + \beta_2 M_1^\star$, $\mathfrak{S}_1 = \rho_3 T_0^\star$,

$\mathfrak{S}_2 = \beta_1 M_0^\star$, $\mathfrak{S}_3 = \beta_2 M_1^\star$, $\mathfrak{S}_4 = \mathfrak{S}_1$.

Considering columns 1, 2, 3, 4, 5, 8, 9, and 11, we notice that the eigenvalues are $\lambda_1 = -\mu_{T_0}$, $\lambda_2 = -\mu_{T_1}$, $\lambda_3 = -\mu_{T_2}$, $\lambda_4 = -\mu_{M_0}$, $\lambda_5 = -\mu_{M_1}$, $\lambda_6 = -\mu_A$, $\lambda_7 = -\mu_E$, and $\lambda_8 = -\mu_{I_{10}}$. The remaining five eigenvalues are the eigenvalues of the 5×5 matrix given by

$$J_1\left(\varepsilon_0^\star\right) = \begin{pmatrix} -\kappa_4 & \kappa_{11} & 0 & 0 & 0 \\ \omega & -\kappa_5 & 0 & 0 & 0 \\ 0 & 0 & -\kappa_8 & \theta_1 & \theta_2 \\ \varepsilon & 0 & 0 & -\kappa_9 & 0 \\ 0 & 0 & \eta & 0 & -\kappa_{10} \end{pmatrix}.$$

The row echelon method was used to determine the remaining eigenvalues. Consider $\frac{\eta}{\kappa_8} R_3 + R_5 \to R_5$. It follows that the Jacobian matrix $J_1(\varepsilon_0^\star)$ becomes

$$J_1\left(\varepsilon_0^\star\right) = \begin{pmatrix} -\kappa_4 & \kappa_{11} & 0 & 0 & 0 \\ \omega & -\kappa_5 & 0 & 0 & 0 \\ 0 & 0 & -\kappa_8 & \theta_1 & \theta_2 \\ \varepsilon & 0 & 0 & -\kappa_9 & 0 \\ 0 & 0 & 0 & 0 & -\kappa_{10} \end{pmatrix}.$$

By considering column 3, λ_9 is obtained as $\lambda_9 = -\kappa_8 = -\left(\eta + \mu_{N_K}\right)$. The remaining four eigenvalues are the eigenvalues of the 4×4 matrix given by

$$J_2\left(\varepsilon_0^\star\right) = \begin{pmatrix} -\kappa_4 & \kappa_{11} & 0 & 0 \\ \omega & -\kappa_5 & 0 & 0 \\ \varepsilon & 0 & -\kappa_9 & 0 \\ 0 & 0 & 0 & -\kappa_{10} \end{pmatrix}.$$

By considering columns 3 and 4, λ_{10} and λ_{11} are obtained to be $\lambda_{10} = -\kappa_9 = -\left(\theta_1 + \mu_{F_1}\right)$ and $\lambda_{11} = -\kappa_{10} = -\left(\theta_2 + \mu_{F_2}\right)$, respectively. The remaining two

eigenvalues are the eigenvalues of the 2×2 matrix given by

$$J_3\left(\varepsilon_0^\star\right) = \begin{pmatrix} -\kappa_4 & \kappa_{11} \\ \omega & -\kappa_5 \end{pmatrix}.$$

The characteristics polynomial of the Jacobian matrix $J_3\left(\varepsilon_0^\star\right)$ is given by

$$\lambda^2 + \lambda\left[(\omega + \varepsilon + \zeta + \mu_{I_M}) + (\psi + \mu_V)\right] + 1 - \mathbb{R}_0 = 0. \tag{34}$$

Since all coefficients of the characteristic polynomial in Eq. (34) are positive when $\mathbb{R}_0 < 1$, the Routh-Hurwitz criterion implies that the roots of the characteristic polynomial have negative real parts. Consequently, all eigenvalues of the Jacobian matrix $J_0(\varepsilon_0^\star)$ exhibit negative real components when $\mathbb{R}_0 < 1$. Therefore, by applying the Routh-Hurwitz criterion, it is established that the virus-free equilibrium $\varepsilon_0^\star$ of system 5 is locally asymptotically stable.

Global Stability of Virus-free Equilibrium

From model framework 5, the pathogen-free equilibrium

$$\varepsilon_0 = (T_0^\star, T_1^\star, T_2^\star, M_0^\star, M_1^\star, I_M^\star, V^\star, A^\star, E^\star, N_K^\star, I_{10}^\star, F_1^\star, F_2^\star)$$

is globally asymptotically stable if $\mathbb{R}_0 < 1$ and conditions (G_1) and (G_2) are satisfied. Techniques from Castillo-Chavez & Song (2004) are employed to validate the global stability of the pathogen-free equilibrium.

Theorem 6

If a model framework can be formulated as:

$$\frac{dX}{dt} = F(X, 0), \quad \frac{dI}{dt} = G(X, I), \quad G(X, 0) = 0,$$

where $X \in \mathbb{R}^m$ signifies the count of uninfected macrophage cells and $I \in \mathbb{R}^n$ denotes the count of infected macrophage cells, encompassing latent, acute, and exposed cells. $U\left(X^\star, 0\right)$ represents the pathogen-free equilibrium of the model frame-

work. To ensure local asymptotic stability, the criteria (G_1) *and* (G_2) *must be fulfilled.*

G_1 : *For* $\frac{dX}{dt} = F(X, 0)$, $X^\star$ *is globally asymptotically stable.*

G_2 : $G(X, I) = AI - \hat{G}(X, 0) \geq 0$ *for* $(X, I) \in \Omega$, *where* $A = D_i G(X^\star, 0)$ *is a Metzler matrix (with non-negative off-diagonal elements) and* Ω *denotes the domain where the model is biologically plausible and mathematically sound. Hence, the fixed point* $U_0 = (X^\star, 0)$ *is a globally asymptotically stable equilibrium of the immune response to hepatitis B virus and liver carcinoma infection model framework 5, provided that* $\mathbb{R}_0 < 1$.

Proof. From the model system in 5, we have

$$X \in \mathbb{R}^{11} = (T_0^\star, T_1^\star, T_2^\star, M_0^\star, M_1^\star, A^\star, E^\star, N_K^\star, I_{10}^\star, F_1^\star, F_2^\star)$$

and $I \in \mathbb{R}^2 = (I_M^\star, V^\star)$. Hence, for condition (G_1), we have

$$\frac{dX}{dt} = \begin{pmatrix} \Lambda_{T_0} - \rho_1 I_M T_0 I_{10} - \rho_2 V T_0 I_{10} - \rho_3 T_0 I_M \left(\frac{1}{1+\tau_1 I_{10}}\right) - \mu_{T_0} T_0 \\ \rho_1 I_M T_0 I_{10} - \pi I_M T_1 - \mu_{T_1} T_1 \\ \rho_2 V T_0 I_{10} - \delta_3 T_2 V - \mu_{T_2} T_2 \\ \Lambda_{M_0} - \beta_1 V M_0 - \mu_{M_0} M_0 \\ \Lambda_{M_1} - \beta_2 V M_1 + \zeta I_M - \mu_{M_1} M_1 \\ \Lambda_A + \psi V - \delta_4 A V - \mu_A A \\ \Lambda_E - \delta_2 \left(1 + \chi_2 F_2\right) I_M E + \sigma I_M E - \mu_E E \\ \Lambda_{N_K} - \delta_1 \left(1 + \chi_1 F_1\right) I_M N_K + \theta_1 F_1 + \theta_2 F_2 - \left(\eta + \mu_{N_K}\right) N_K \\ \rho_3 I_M T_0 \left(\frac{1}{1+\tau_1 I_{10}}\right) - \mu_{I_{10}} I_{10} \\ \varepsilon I_M - \left(\theta_1 + \mu_{F_1}\right) F_1 \\ \eta N_K - \left(\theta_2 + \mu_{F_2}\right) F_2 \end{pmatrix} \tag{35}$$

and

$$\begin{aligned}\frac{dI}{dt} &= G(X,I)\\ &= \begin{pmatrix}\beta_1 V M_0 + \beta_2 V M_1 + \pi I_M T_1 - \delta_1 (1+\chi_1 F_1) I_M N_K - \clubsuit\\ \Lambda_V + \omega I_M - \delta_3 T_2 V - \delta_4 A V - (\psi + \mu_V) V,\end{pmatrix} \qquad (36)\\ &\text{where} \quad \clubsuit = \delta_2 (1+\chi_2 F_2) I_M E + \sigma I_M E + (\omega + \varepsilon + \zeta + \mu_{I_M}) I_M.\end{aligned}$$

It follows from Eq. (35) that

$$F(X,0) = \begin{pmatrix}
-\mu_{T_0} & 0 & 0 & 0 & 0 & 0 & 0 & 0 & 0 & 0 & 0\\
0 & -\mu_{T_1} & 0 & 0 & 0 & 0 & 0 & 0 & 0 & 0 & 0\\
0 & 0 & -\nu_1 & 0 & 0 & 0 & 0 & 0 & 0 & 0 & 0\\
0 & 0 & 0 & -\nu_2 & 0 & 0 & 0 & 0 & 0 & 0 & 0\\
0 & 0 & 0 & 0 & -\nu_3 & 0 & 0 & 0 & 0 & 0 & 0\\
0 & 0 & 0 & 0 & 0 & -\nu_4 & 0 & 0 & 0 & 0 & 0\\
0 & 0 & 0 & 0 & 0 & 0 & -\mu_E & 0 & 0 & 0 & 0\\
0 & 0 & 0 & 0 & 0 & 0 & 0 & -\nu_5 & 0 & \theta_1 & \theta_2\\
0 & 0 & 0 & 0 & 0 & 0 & 0 & 0 & -\mathfrak{X} & 0 & 0\\
0 & 0 & 0 & 0 & 0 & 0 & 0 & 0 & 0 & -\nu_6 & 0\\
0 & 0 & 0 & 0 & 0 & 0 & 0 & \eta & 0 & 0 & -\nu_7
\end{pmatrix},$$

where

$$\begin{aligned}
&\nu_1 = \mu_{T_2}, && \nu_2 = \mu_{M_0}, && \nu_3 = \mu_{M_1},\\
&\nu_4 = \mu_A, && \nu_5 = (\eta + \mu_{N_K}), && \nu_6 = (\theta_1 + \mu_{F_1}),\\
&\nu_7 = (\theta_2 + \mu_{F_2}), && \mathfrak{X} = \mu_{I_{10}}.
\end{aligned}$$

The eigenvaules from the matrix $F(X,0)$ are obtained to be

$$\begin{aligned}
&\lambda_1 = -\mu_{T_0}, && \lambda_2 = -\mu_{T_1}, && \lambda_3 = -\mu_{T_2},\\
&\lambda_4 = -\mu_{M_0}, && \lambda_5 = -\mu_{M_1}, && \lambda_6 = -\mu_A,\\
&\lambda_7 = -\mu_E, && \lambda_8 = -(\eta + \mu_{N_K}), && \lambda_9 = -\mu_{I_{10}},\\
&\lambda_{10} = -(\theta_1 + \mu_{F_1}), && \lambda_{11} = -\frac{\mu_{F_2}(\eta + \theta_2 + \mu_{N_K})}{\eta + \mu_{N_K}}.
\end{aligned}$$

Given that all eigenvalues are real and negative, it consequently follows that $X^\star$ is perpetually globally asymptotically stable. Furthermore, employing Theorem 6 to the immunological response model framework 5 yields

$$\begin{aligned}\hat{G}(X,I) &= AI - G(X,I)\\ &= \begin{pmatrix} -(\omega+\varepsilon+\zeta+\mu_{I_M}) & \beta_1 M_0^\star + \beta_2 M_1^\star \\ \omega & -(\psi+\mu_V)\end{pmatrix}\begin{pmatrix} I_M \\ V\end{pmatrix}\\ &\quad - \begin{pmatrix} \beta_1 V M_0 + \beta_2 V M_1 + \pi I_M T_1 - \delta_1(1+\chi_1 F_1) I_M N_K - \clubsuit \\ \Lambda_V + \omega I_M - \delta_3 T_2 V - \delta_4 A V - (\psi+\mu_V) V\end{pmatrix},\end{aligned}$$

where

$$\clubsuit = \delta_2(1+\chi_2 F_2) I_M E + \sigma I_M E + (\omega+\varepsilon+\zeta+\mu_{I_M}) I_M.$$

Hence,

$$\begin{aligned}\hat{G}(X,I) &= \begin{pmatrix} -(\omega+\varepsilon+\zeta+\mu_{I_M}) I_M + \beta_1 M_0^\star V^\star + \beta_2 M_1^\star V^\star \\ \omega I_M - \psi V - \mu_V V\end{pmatrix}\\ &\quad - \begin{pmatrix} \beta_1 V M_0 + \beta_2 V M_1 + \pi I_M T_1 - \delta_1(1+\chi_1 F_1) I_M N_K - \clubsuit \\ \Lambda_V + \omega I_M - \delta_3 T_2 V - \delta_4 A V - (\psi+\mu_V) V\end{pmatrix},\end{aligned}$$

where

$$\clubsuit = \delta_2(1+\chi_2 F_2) I_M E + \sigma I_M E + (\omega+\varepsilon+\zeta+\mu_{I_M}) I_M.$$

Therefore,

$$\hat{G}(X,I) = \begin{pmatrix} [\beta_1 M_0^\star V^\star - \beta_1 V M_0] + [\beta_2 M_1^\star V^\star - \beta_2 V M_1] + \clubsuit_\kappa - \pi I_M T_1 \\ -\Lambda_V + \delta_3 T_2 V + \delta_4 A V\end{pmatrix},$$

where

$$\clubsuit_\kappa = \delta_1(1+\chi_1 F_1) I_M N_K + \delta_2(1+\chi_2 F_2) I_M E + \sigma I_M E.$$

Here, $(\sigma I_M E + \delta_1(1+\chi_1 F_1) I_M N_K + \delta_2(1+\chi_2 F_2) I_M E) \geq \pi I_M T_1$, and $(\delta_3 T_2 V + \delta_4 A V) > \Lambda_V$. Since our interest lies in the infectious compartments, all other com-

pound terms are ignored. It follows that

$$\hat{G}(X,I) = \begin{pmatrix} [\beta_1 M_0^\star V^\star - \beta_1 V M_0] + [\beta_2 M_1^\star V^\star - \beta_2 V M_1] \\ 0 \end{pmatrix}.$$

In addition, since all off-diagonal elements of the matrix A are non-negative, A is an M-matrix. It is observed that

$$\hat{G}(X,I) = \begin{pmatrix} [\beta_1 M_0^\star V^\star - \beta_1 V M_0] + [\beta_2 M_1^\star V^\star - \beta_2 V M_1] \\ 0 \end{pmatrix} \geq 0,$$

because $[V^\star M_0^\star - V M_0] + [V^\star M_1^\star - V^\star M_1] \geq 0$. That is in the absence of infection, the proportional product of the macrophages with and without cancer at the virus-free equilibrium are obtained to be $V^\star M_1^\star$ and $V^\star M_0^\star$ respectively while $V M_1$ and $V M_0$ represent the proportion to the product of macrophages with and without cancer in the population. By definition, $V^\star M_0^\star$ and $V^\star M_1^\star$ are either greater than or equal to $V M_0$ and $V M_1$, ensuring the inequality holds. Therefore, the virus-free equilibrium ε_0 is globally asymptotically stable.

Virus-persistence Equilibrium (VPE) and Stability Analysis

In this segment, we ascertain the viral-persistence equilibrium points by concurrently resolving model framework 5 for the state variables $T_0^\star$, $T_1^\star$, $T_2^\star$, $M_0^\star$, $I_M^\star$, $V^\star$, $A^\star$, $E^\star$, $N_K^\star$, $I_{10}^\star$, $F_1^\star$, and $F_2^\star$. The viral-persistence equilibrium points signify steady-state solutions wherein the hepatitis B virus and hepatic carcinoma persist within the cellular framework, indicating that complete eradication of the infections remains unaccomplished, and the pathogens continue to influence the overall cell populations. It is posited that a subset of hepatic cells might have undergone neoplastic transformation due to extrinsic factors such as chronic ethanol ingestion or tobacco use. Consequently, the integration of HBV infection into this context necessitates an exploration of the novel co-existence dynamics. For the hepatitis B virus to endure within the host hepatic cells, the viral reservoir must remain non-zero. Thus, the system's behavior is contingent upon all state variables. At the

viral-persistence equilibrium, previously uninfected macrophages become infected, leading to the activation of these infected macrophages through cytokine-mediated signaling. Accordingly, at this equilibrium, the following equations are satisfied:

$$
\left.
\begin{aligned}
0 &= \Lambda_{T_0} - \rho_1 I_M^\star T_0^\star I_{10}^\star - \rho_2 V^\star T_0^\star I_{10}^\star - \rho_3 T_0^\star I_M^\star \left(\frac{1}{1+\tau_1 I_{10}^\star}\right) - \mu_{T_0} T_0^\star, \\
0 &= \rho_1 I_M^\star T_0^\star I_{10}^\star - \pi I_M^\star T_1^\star - \mu_{T_1} T_1^\star, \\
0 &= \rho_2 V^\star T_0^\star I_{10}^\star - \delta_3 T_2^\star V^\star - \mu_{T_2} T_2^\star, \\
0 &= \Lambda_{M_0} - \beta_1 V^\star M_0^\star - \mu_{M_0} M_0^\star, \\
0 &= \Lambda_{M_1} - \beta_2 V^\star M_1^\star + \zeta I_M^\star - \mu_{M_1} M_1^\star, \\
0 &= \beta_1 V^\star M_0^\star + \beta_2 V^\star M_1^\star + \pi I_M^\star T_1^\star - \delta_1 \left(1+\chi_1 F_1^\star\right) I_M^\star N_K^\star \\
&\quad - \delta_2 \left(1+\chi_2 F_2^\star\right) I_M^\star E^\star - \sigma I_M^\star E^\star - \left(\omega+\varepsilon+\zeta+\mu_{I_M}\right) I_M^\star, \\
0 &= \Lambda_V + \omega I_M^\star - \delta_3 T_2^\star V^\star - \delta_4 A^\star V^\star - \left(\psi+\mu_V\right) V^\star, \\
0 &= \Lambda_A + \psi V^\star - \delta_4 A^\star V^\star - \mu_A A^\star, \\
0 &= \Lambda_E - \delta_2 \left(1+\chi_2 F_2^\star\right) I_M^\star E^\star + \sigma I_M^\star E^\star - \mu_E E^\star, \\
0 &= \Lambda_{N_K} - \delta_1 \left(1+\chi_1 F_1^\star\right) I_M^\star N_K^\star + \theta_1 F_1^\star + \theta_2 F_2^\star - \left(\eta+\mu_{N_K}\right) N_K^\star, \\
0 &= \rho_3 I_M^\star T_0^\star \left(\frac{1}{1+\tau_1 I_{10}^\star}\right) - \mu_{I_{10}} I_{10}^\star, \\
0 &= \varepsilon I_M^\star - \left(\theta_1+\mu_{F_1}\right) F_1^\star, \\
0 &= \eta N_K^\star - \left(\theta_2+\mu_{F_2}\right) F_2^\star.
\end{aligned}
\right\}
$$

Given the intricacy of model framework 5, it is judicious to investigate a comprehensive array of potential boundary equilibrium states. To systematically identify and examine these equilibrium states, the focus begins with those characterized by the presence of hepatitis B virus particles (i.e., $V^\star \neq 0$). Various permutations of the following conditions are evaluated: $T_0^\star = 0$ or $T_0^\star \neq 0$, $E^\star = 0$ or $E^\star \neq 0$, and $N_K^\star = 0$ or $N_K^\star \neq 0$.

Case I: For the initial scenario in which $V^\star \neq 0$, $T_0^\star \neq 0$, $E^\star \neq 0$, and $N_K^\star \neq 0$, a

boundary equilibrium state was derived in the following configuration:

$$\varepsilon_1^\star = \left\{ \frac{\Lambda_{T_0}}{\rho_1 I_M^\star I_{10}^\star + \rho_2 V^\star I_{10}^\star + \frac{\rho_3 I_M^\star}{1+\tau_1 I_{10}^\star} + \mu_{T_0}}, \frac{\rho_1 I_M^\star T_0^\star I_{10}^\star}{\pi I_M^\star + \mu_{T_1}}, \frac{\rho_2 V^\star T_0^\star I_{10}^\star}{\delta_3 V^\star + \mu_{T_2}}, \right.$$
$$\frac{\Lambda_{M_0}}{\beta_1 V^\star + \mu_{M_0}}, \frac{\Lambda_{M_1} + \zeta I_M^\star}{\beta_2 V^\star + \mu_{M_1}}, I_M^\star, \frac{\Lambda_V + \omega I_M^\star}{\delta_3 T_2^\star + \delta_4 A^\star + (\psi + \mu_V)},$$
$$\frac{\Lambda_A + \psi V^\star}{\delta_4 V^\star + \mu_A}, \frac{\Lambda_E}{\delta_2 \left(1 + \chi_2 F_2^\star\right) I_M^\star + \mu_E - \sigma I_M^\star},$$
$$\frac{\Lambda_{N_K} + \theta_1 F_1^\star + \theta_2 F_2^\star}{\delta_1 \left(1 + \chi_1 F_1^\star\right) I_M^\star + (\eta + \mu_{N_K})},$$
$$\left. \frac{-\mu_{I_{10}} + \sqrt{\mu_{I_{10}}^2 + 4\mu_{I_{10}} \tau_1 \rho_3 I_M^\star T_0^\star}}{2\mu_{I_{10}} \tau_1}, \frac{\varepsilon I_M^\star}{(\theta_1 + \mu_{F_1})}, \frac{\eta N_K^\star}{\theta_2 + \mu_{F_2}} \right\},$$

where $I_M^\star = \frac{\beta_1 V^\star M_0^\star + \beta_2 V^\star M_1^\star}{\left[\delta_1 \left(1+\chi_1 F_1^\star\right) N_K^\star + \delta_2 \left(1+\chi_2 F_2^\star\right) E^\star + \sigma E^\star + \mathfrak{B} - \pi T_1^\star\right]}$

and $\mathfrak{B} = (\omega + \varepsilon + \zeta + \mu_{I_M})$.

This equilibrium state $\varepsilon_1^\star$ exists when $\delta_2 \left(1 + \chi_2 F_2^\star\right) I_M^\star + \mu_E > \sigma I_M^\star$,

and $\delta_1 \left(1 + \chi_1 F_1^\star\right) N_K^\star + \delta_2 \left(1 + \chi_2 F_2^\star\right) E^\star + \sigma E^\star + \mathfrak{B} > \pi T_1^\star$.

Given initial conditions for the state variables

$$T_0(0) = 5 \times 10^5, \quad T_1(0) = 0, \quad T_2(0) = 0,$$
$$M_0(0) = 4 \times 10^5, \quad M_1(0) = 4 \times 10^5, \quad I_M(0) = 0,$$
$$V(0) = 300, \quad A(0) = 0, \quad E(0) = 0,$$
$$N_K(0) = 0, \quad I_{10}(0) = 0, \quad F_1(0) = 0,$$
$$F_2(0).$$

and parameter values in Tables 5 and 6 the components of $\varepsilon_1^\star$ are obtain as follows:

First component:

$$\varepsilon_{1,1}^\star = \frac{\Lambda_{T_0}}{\rho_1 I_M^\star I_{10}^\star + \rho_2 V^\star I_{10}^\star + \frac{\rho_3 I_M^\star}{1+\tau_1 I_{10}^\star} + \mu_{T_0}}$$

Substitute $\Lambda_{T_0} = 0.99$, $\rho_1 = 3.7523$, $I_M^\star = 0$, $I_{10}^\star = 0$, $\rho_2 = 3.0210$, $V^\star = 300$, $\rho_3 = 0.6697$, $\tau_1 = 0.1642$, $\mu_{T_0} = 6.7 \times 10^{-7}$:

$$\varepsilon_{1,1}^\star = \frac{0.99}{3.7523 \cdot 0 \cdot 0 + 3.0210 \cdot 300 \cdot 0 + \frac{0.6697 \cdot 0}{1+0.1642 \cdot 0} + 6.7 \times 10^{-7}}$$

$$\approx 1,477611.94$$

Second component:

$$\varepsilon_{1,2}^\star = \frac{\rho_1 I_M^\star T_0^\star I_{10}^\star}{\pi I_M^\star + \mu_{T_1}}$$

Substitute $\rho_1 = 3.7523$, $I_M^\star = 0$, $T_0^\star = 5 \times 10^5$, $I_{10}^\star = 0$, $\pi = 0.3359$, $\mu_{T_1} = 0.3333$:

$$\varepsilon_{1,2}^\star = \frac{3.7523 \cdot 0 \cdot 5 \times 10^5 \cdot 0}{0.3359 \cdot 0 + 0.3333} = 0$$

Third component:

$$\varepsilon_{1,3}^\star = \frac{\rho_2 V^\star T_0^\star I_{10}^\star}{\delta_3 V^\star + \mu_{T_2}}$$

Substitute $\rho_2 = 3.0210$, $V^\star = 300$, $T_0^\star = 5 \times 10^5$, $I_{10}^\star = 0$, $\delta_3 = 1.3114$, $\mu_{T_2} = 0.3333$:

$$\varepsilon_{1,3}^\star = \frac{3.0210 \cdot 300 \cdot 5 \times 10^5 \cdot 0}{1.3114 \cdot 300 + 0.3333} = 0$$

Fourth component:

$$\varepsilon_{1,4}^\star = \frac{\Lambda_{M_0}}{\beta_1 V^\star + \mu_{M_0}}$$

Substitute $\Lambda_{M_0} = 4 \times 10^5$, $\beta_1 = 0.8903$, $V^\star = 300$, $\mu_{M_0} = 0.011$:

$$\varepsilon_{1,4}^\star = \frac{4 \times 10^5}{0.8903 \cdot 300 + 0.011} \approx 136147.50$$

Fifth component:

$$\varepsilon_{1,5}^\star = \frac{\Lambda_{M_1} + \zeta I_M^\star}{\beta_2 V^\star + \mu_{M_1}}$$

Substitute $\Lambda_{M_1} = 0.015$, $\zeta = 1.0014$, $I_M^\star = 0$, $\beta_2 = 0.9157$, $V^\star = 300$, $\mu_{M_1} = 0.01$:

$$\varepsilon_{1,5}^\star = \frac{0.015 + 1.0014 \cdot 0}{0.9157 \cdot 300 + 0.01} \approx 0.000054$$

Sixth component:

$$\begin{aligned}\varepsilon_{1,6}^{\star} &= I_M^{\star} = \frac{\beta_1 V^{\star} M_0^{\star} + \beta_2 V^{\star} M_1^{\star}}{\left[\delta_1\left(1+\chi_1 F_1^{\star}\right) N_K^{\star} + \delta_2\left(1+\chi F_2^{\star}\right) E^{\star} + \sigma E^{\star} + \mathfrak{B} - \pi T_1^{\star}\right]},\\ \mathfrak{B} &= \left(\omega + \varepsilon + \zeta + \mu_{I_M}\right).\end{aligned}$$

Substitute $\beta_1 = 0.8903$, $\beta_2 = 0.9157$, $\omega = 20.0342$, $\delta_1 = 0.7$, $\delta_2 = 0.9308$, $\pi = 0.3359$, $\sigma = 0.5$, $\varepsilon = 1$, $\zeta = 1.0014$, $\chi_1 = 1.5$, $\chi_2 = 2.0$, $\mu_{I_M} = 0.5636$, $M_0^{\star} = 4 \times 10^5$, $M_1^{\star} = 4 \times 10^5$, $V^{\star} = 300$, $E^{\star} = 0$, $N_K^{\star} = 0$, $T_1^{\star} = 0$, $F_1^{\star} = 0$, $F_2^{\star} = 0$:

$$\varepsilon_{1,6}^{\star} = \frac{26709000 + 27471000}{22.5992} \approx 2397430.00$$

Seventh component:

$$\varepsilon_{1,7}^{\star} = \frac{\Lambda_V + \omega I_M^{\star}}{\delta_4 A^{\star} + \psi + \mu_V}$$

Substitute $\Lambda_V = 0.3$, $\omega = 20.0342$, $I_M^{\star} = 0$, $\delta_4 = 0.7$, $A^{\star} = 0$, $\psi = 5.0003$, $\mu_V = 0.67$:

$$\varepsilon_{8,7}^{\star} = \frac{0.3 + 20.0342 \cdot 0}{0.7 \cdot 0 + 5.0003 + 0.67} \approx 0.05291$$

Eighth component:

$$\varepsilon_{1,8}^{\star} = \frac{\Lambda_A + \psi V^{\star}}{\delta_4 A^{\star} + \mu_A}$$

Substitute $\Lambda_A = 3.4 \times 10^{12}$, $\psi = 5.0003$, $V^{\star} = 300$, $\delta_4 = 0.7$, $A^{\star} = 0$, $\mu_A = 0.332$:

$$\varepsilon_{1,8}^{\star} = \frac{3.4 \times 10^{12} + 5.0003 \cdot 300}{0.7 \cdot 0 + 0.332} \approx 1.0241 \times 10^{13}$$

Ninth component:

$$\varepsilon_{1,9}^{\star} = \frac{\Lambda_E}{\delta_2\left(1+\chi_2 F_2^{\star}\right) I_M^{\star} + \mu_E - \sigma I_M^{\star}}$$

Substitute $\Lambda_E = 10$, $\delta_2 = 0.9308$, $\chi_2 = 2.0$, $F_2^{\star} = 0$, $I_M^{\star} = 0$, $\mu_E = 0.5$,

$\sigma = 0.5$:

$$\varepsilon^{\star}_{1,9} = \frac{10}{0.9308 \cdot (1 + 2.0 \cdot 0) \cdot 0 + 0.5 - 0.5 \cdot 0} \approx 20$$

Tenth component:

$$\varepsilon^{\star}_{1,10} = \frac{\Lambda_{N_K} + \theta_1 F^{\star}_1 + \theta_2 F^{\star}_2}{\delta_1 \left(1 + \chi_1 F^{\star}_1\right) I^{\star}_M + \eta + \mu_{N_K}}$$

Substitute $\Lambda_{N_K} = 0.057$, $\theta_1 = 0.8$, $F^{\star}_1 = 0$, $\theta_2 = 0.6$, $F^{\star}_2 = 0$, $\delta_1 = 0.7$, $\chi_1 = 1.5$, $I^{\star}_M = 0$, $\eta = 0.057$, $\mu_{N_K} = 0.42$:

$$\varepsilon^{\star}_{1,10} = \frac{0.057 + 0.8 \cdot 0 + 0.6 \cdot 0}{0.7 \cdot (1 + 1.5 \cdot 0) \cdot 0 + 0.057 + 0.42} \approx 0.1195$$

Eleventh component:

$$\varepsilon^{\star}_{1,11} = \frac{-\mu_{I_{10}} \pm \sqrt{\mu^2_{I_{10}} + 4\mu_{I_{10}} \tau_1 \rho_3 I^{\star}_M T^{\star}_0}}{2\mu_{I_{10}} \tau_1} \tag{37}$$

Substitute the values:

$$\mu_{I_{10}} = 3.70 \times 10^{-2}, \quad \tau_1 = 0.1642, \quad \rho_3 = 0.6697,$$
$$I^{\star}_M = 0, \quad T^{\star}_0 = 5 \times 10^5$$

Calculate the discriminant:

$$\Delta = \mu^2_{I_{10}} + 4\mu_{I_{10}} \tau_1 \rho_3 I^{\star}_M T^{\star}_0 \tag{38}$$
$$= (3.70 \times 10^{-2})^2 + 4 \cdot 3.70 \times 10^{-2} \cdot 0.1642 \cdot 0.6697 \cdot 0 \cdot 5 \times 10^5.$$

It follows from Eq. (38) that

$$\Delta = (1.369 \times 10^{-3}) + 0$$

Calculate the square root of the discriminant:

$$\sqrt{\Delta} = \sqrt{1.369 \times 10^{-3}} = 0.037$$

Now, substitute back into Eq. (37) gives

$$\varepsilon^{\star}_{1,11} = \frac{-0.037 \pm 0.037}{2 \cdot 0.037 \cdot 0.1642}$$

Calculate the two roots:

$$\varepsilon^{\star}_{1,11} = \frac{-0.037 + 0.037}{2 \cdot 0.037 \cdot 0.1642} = 0, \quad \varepsilon^{\star}_{1,11} = \frac{-0.037 - 0.037}{2 \cdot 0.037 \cdot 0.1642} \approx -6.0901$$

Therefore, the solutions are:

$$\varepsilon^{\star}_{1,11} = 0 \quad \text{and} \quad \varepsilon^{\star}_{8,11} \approx -6.0901.$$

Since the interleukin-10 population is non-negative, its equilibrium value is

$$\varepsilon^{\star}_{1,11} = 0.$$

Twelfth component:

$$\varepsilon^{\star}_{1,12} = \frac{\varepsilon I^{\star}_{M}}{\theta_1 + \mu_{F_1}}$$

Substitute $\varepsilon = 1$, $I^{\star}_{M} = 0$, $\theta_1 = 0.8$, $\mu_{F_1} = 4.9$:

$$\varepsilon^{\star}_{1,11} = \frac{1 \cdot 0}{0.8 + 4.9} = 0$$

Thirteenth component:

$$\varepsilon^{\star}_{1,13} = \frac{\eta N^{\star}_{K}}{\theta_2 + \mu_{F_2}}$$

Substitute $\eta = 0.057$, $N^{\star}_{K} = 0$, $\theta_2 = 0.6$, $\mu_{F_2} = 5.16$:

$$\varepsilon^{\star}_{1,13} = \frac{0.057 \cdot 0}{0.6 + 5.16} = 0.$$

Combining all components gives

$$\varepsilon_1^\star = \Big\{1477611.94, 0, 0, 136147.50, 0.000054, 2397430, 0.05291, 1.0241 \times 10^{13}, 20, 0.1195, 0, 0, 0\Big\}$$

Upon linearizing the model framework 5 around the equilibrium state $\varepsilon_1^\star$, a Jacobian matrix was derived in the following configuration:

$$J_{\varepsilon_1^\star} = \begin{pmatrix}
-\varpi_1 & 0 & 0 & 0 & 0 & -\varpi_2 & 0 & 0 & 0 & 0 & \varpi_3 & 0 & 0 \\
0 & -\varpi_4 & 0 & 0 & 0 & 0 & 0 & 0 & 0 & 0 & \varpi_5 & 0 & 0 \\
0 & 0 & -\varpi_6 & 0 & 0 & 0 & 0 & 0 & 0 & 0 & \varpi_7 & 0 & 0 \\
0 & 0 & 0 & -\varpi_8 & 0 & 0 & -\varpi_9 & 0 & 0 & 0 & 0 & 0 & 0 \\
0 & 0 & 0 & 0 & -\varpi_{10} & \varpi_{11} & -\varpi_{12} & 0 & 0 & 0 & 0 & 0 & 0 \\
0 & \varpi_{13} & 0 & \varpi_9 & \varpi_{12} & -\varpi_{14} & \varpi_{15} & 0 & -\varpi_{16} & -\varpi_{17} & 0 & -\varpi_{18} & -\varpi_{19} \\
0 & 0 & -\varpi_{20} & 0 & 0 & \varpi_{21} & -\varpi_{22} & -\varpi_{23} & 0 & 0 & 0 & 0 & 0 \\
0 & 0 & 0 & 0 & 0 & 0 & -\varpi_{24} & -\varpi_{25} & 0 & 0 & 0 & 0 & 0 \\
0 & 0 & 0 & 0 & 0 & -\varpi_{26} & 0 & 0 & -\varpi_{27} & 0 & 0 & 0 & -\varpi_{28} \\
0 & 0 & 0 & 0 & 0 & -\varpi_{29} & 0 & 0 & 0 & -\varpi_{30} & 0 & -\varpi_{31} & \varpi_{32} \\
\varpi_{33} & 0 & 0 & 0 & 0 & \varpi_2 & 0 & 0 & 0 & 0 & -\varpi_{34} & 0 & 0 \\
0 & 0 & 0 & 0 & 0 & \varpi_{35} & 0 & 0 & 0 & 0 & 0 & -\varpi_{36} & 0 \\
0 & 0 & 0 & 0 & 0 & 0 & 0 & 0 & 0 & \varpi_{37} & 0 & 0 & -\varpi_{38}
\end{pmatrix},$$

where

$$\varpi_1 = 1605558.8710, \qquad \varpi_2 = 989566.7162,$$

$$\varpi_3 = 389546923730.2857, \qquad \varpi_4 = 805297.0703,$$

$$\varpi_5 = 13292414658672.8, \qquad \varpi_6 = 0.4027,$$

$$\varpi_7 = 236183.1326, \qquad \varpi_8 = 0.0581,$$

$$\varpi_9 = 121212.1193, \qquad \varpi_{10} = 0.0584,$$

$$\varpi_{11} = 1.0014, \qquad \varpi_{12} = 0.00004945,$$

$$\varpi 13 = 79752.737, \qquad \varpi_{14} = 51.2989,$$

$$\varpi_{15} = 121212.1193, \qquad \varpi_{16} = 4342704.702,$$
$$\varpi_{17} = 1678201, \qquad \varpi_{18} = 429739.3275,$$
$$\varpi_{19} = 89261113.76, \qquad \varpi_{20} = 0.0694,$$
$$\varpi_{21} = 20.0342, \qquad \varpi_{22} = 7168700000005.67,$$
$$\varpi_{23} = 0.0370, \qquad \varpi_{24} = 4.9633,$$
$$\varpi_{25} = 0.3690, \qquad \varpi_{26} = 8.616,$$
$$\varpi_{27} = 1945275.202, \qquad \varpi_{28} = 89261113.76,$$
$$\varpi_{29} = 0.08365, \qquad \varpi_{30} = 1678202.32,$$
$$\varpi_{31} = 300816.7293, \qquad \varpi_{32} = 0.6,$$
$$\varpi_{33} = 1605558.871, \qquad \varpi_{34} = 389546923730.2487,$$
$$\varpi_{35} = 1, \qquad \varpi_{36} = 5.7,$$
$$\varpi_{37} = 0.9, \qquad \varpi_{38} = 5.76.$$

The eigenvalues associated with the coexisting equilibrium point $J_{\varepsilon_1^\star}$ are:

$$\lambda_1 = -7.1687 \times 10^{12}, \qquad \lambda_2 = -3.89549 \times 10^{11},$$
$$\lambda_3 = -2.10506 \times 10^{6}, \qquad \lambda_4 = -1.94521 \times 10^{6},$$
$$\lambda_5 = -1.66852 \times 10^{6}, \qquad \lambda_6 = 1.28996 \times 10^{6},$$
$$\lambda_7 = -7.93942, \qquad \lambda_8 = -3.33513,$$
$$\lambda_9 = -0.4027, \qquad \lambda_{10} = -0.369,$$
$$\lambda_{11} = -0.0584, \qquad \lambda_{12} = -0.0581,$$
$$\lambda_{13} = 0.000219653.$$

These eigenvalues suggest that $J_{\varepsilon_1^\star}$ is defined by a perturbed equilibrium point. The presence of antibodies, effector B lymphocytes, naive T lymphocytes, and natural killer cells renders the virus-persistence equilibrium state inconsequential. Consequently, the virus-free equilibrium attains stability, facilitating the

potential for viral eradication.

Case II: For the subsequent scenario in which $V \neq 0$, $T_0^\star = 0$, $E^\star = 0$, and $N_K^\star = 0$, a boundary equilibrium state was derived, characterized by:

$$\varepsilon_2^\star = \left\{0, 0, 0, \frac{\Lambda_{M_0}}{\beta_1 V^\star + \mu_{M_0}}, \frac{\Lambda_{M_1} + \zeta I_M^\star}{\beta_2 V^\star + \mu_{M_1}}, \frac{\beta_1 V^\star M_0^\star + \beta_2 V^\star M_1^\star}{(\omega + \varepsilon + \zeta + \mu_{I_M})}, \frac{\Lambda_V + \omega I_M^\star}{\delta_3 T_2^\star + \delta_4 A^\star + (\psi + \mu_V)}, \frac{\Lambda_A + \psi V^\star}{\delta_4 V^\star + \mu_A}, 0, 0, 0, \frac{\varepsilon I_M^\star}{(\theta_1 + \mu_{F_1})}, 0\right\},$$

Considering the initial conditions for the state variables and parameter values in Tables 5 and 6, the following was obtained:

$$\varepsilon_2^\star = \left\{0, 0, 0, 136147.50, 0.000054, 2397430, 0.05291, 1.0241 \times 10^{13}, 0, 0, 0, 0, 0\right\}$$

Linearizing system 5 about the equilibrium state $\varepsilon_2^\star$ results in a Jacobian matrix of the following form:

$$J_{\varepsilon_2^\star} = \begin{pmatrix}
-\varpi_1 & 0 & 0 & 0 & 0 & 0 & 0 & 0 & 0 & 0 & 0 & 0 & 0 \\
0 & -\varpi_4 & 0 & 0 & 0 & 0 & 0 & 0 & 0 & 0 & 0 & 0 & 0 \\
0 & 0 & -\varpi_6 & 0 & 0 & 0 & 0 & 0 & 0 & 0 & 0 & 0 & 0 \\
0 & 0 & 0 & -\varpi_8 & 0 & 0 & -\varpi_9 & 0 & 0 & 0 & 0 & 0 & 0 \\
0 & 0 & 0 & 0 & -\varpi_{10} & \varpi_{11} & -\varpi_{12} & 0 & 0 & 0 & 0 & 0 & 0 \\
0 & \varpi_{13} & 0 & \varpi_9 & \varpi_{12} & -\varpi_{39} & \varpi_{15} & 0 & -\varpi_{16} & -\varpi_{17} & 0 & 0 & 0 \\
0 & 0 & -\varpi_{20} & 0 & 0 & \varpi_{21} & -\varpi_{22} & -\varpi_{23} & 0 & 0 & 0 & 0 & 0 \\
0 & 0 & 0 & 0 & 0 & 0 & -\varpi_{24} & -\varpi_{25} & 0 & 0 & 0 & 0 & 0 \\
0 & 0 & 0 & 0 & 0 & 0 & 0 & 0 & -\varpi_{27} & 0 & 0 & 0 & 0 \\
0 & 0 & 0 & 0 & 0 & 0 & 0 & 0 & 0 & -\varpi_{30} & 0 & \varpi_{40} & \varpi_{32} \\
\varpi_{33} & 0 & 0 & 0 & 0 & 0 & 0 & 0 & 0 & 0 & -\varpi_{41} & 0 & 0 \\
0 & 0 & 0 & 0 & 0 & \varpi_{35} & 0 & 0 & 0 & 0 & 0 & -\varpi_{36} & 0 \\
0 & 0 & 0 & 0 & 0 & 0 & 0 & 0 & 0 & \varpi_{37} & 0 & 0 & -\varpi_{38}
\end{pmatrix},$$

where

$$\varpi_{39} = 22.5992, \qquad \varpi_{40} = 0.8, \qquad \varpi_{41} = 0.0370.$$

The eigenvalues corresponding to the equilibrium point $\varepsilon_2^\star$ are:

$$\begin{aligned}
&\zeta_1 = -7.1687 \times 10^{12}, && \zeta_2 = -1.94528 \times 10^{6},\\
&\zeta_3 = -1.6782 \times 10^{6}, && \zeta_4 = -1.60556 \times 10^{6},\\
&\zeta_5 = -22.5499, && \zeta_6 = -805297,\\
&\zeta_7 = -5.76, && \zeta_8 = -5.74748,\\
&\zeta_9 = -0.4027, && \zeta_{10} = -0.369,\\
&\zeta_{11} = -0.0599221, && \zeta_{12} = -0.0584013,\\
&\zeta_{13} = -0.037.
\end{aligned}$$

The eigenvalue spectrum indicates that $\varepsilon_2^\star$ is a saddle point. Thus, the system exhibits local stability around this equilibrium. This equilibrium is categorized as a chronic state due to the absence of T cells, natural killer cells, effector B cells, and cytokines with the capacity to eliminate the virus. Consequently, the mere presence of antibodies is insufficient to achieve viral clearance.

Case III: For the third case in which $V^\star \neq 0$, $T_0^\star = 0$, $E^\star = 0$, and $N_K^\star \neq 0$, a boundary equilibrium state was derived in the following configuration:

$$\begin{aligned}
\varepsilon_3^\star \;=\; \Bigg\{ & 0, 0, 0, \frac{\Lambda_{M_0}}{\beta_1 V^\star + \mu_{M_0}}, \frac{\Lambda_{M_1} + \zeta I_M^\star}{\beta_2 V^\star + \mu_{M_1}},\\
& \frac{\beta_1 V^\star M_0^\star + \beta_2 V^\star M_1^\star}{\delta_1 \left(1 + \chi_1 F_1^\star\right) N_K^\star + \left(\omega + \varepsilon + \zeta + \mu_{I_M}\right)}, \frac{\Lambda_V + \omega I_M^\star}{\delta_3 T_2^\star + \delta_4 A^\star + \mu_V},\\
& \frac{\Lambda_A + \psi V^\star}{\delta_4 V^\star + \mu_A}, 0, \frac{\Lambda_{N_K} + \theta_1 F_1^\star + \theta_2 F_2^\star}{\delta_1 \left(1 + \chi_1 F_1^\star\right) I_M^\star + \eta + \mu_{N_K}}, 0,\\
& \frac{\varepsilon I_M^\star}{\left(\theta_1 + \mu_{F_1}\right)}, \frac{\eta N_K^\star}{\left(\theta_2 + \mu_{F_2}\right)} \Bigg\},
\end{aligned}$$

Considering the preliminary conditions for the state variables and parameter

values as delineated in Tables 5 and 6, the following was ascertained:

$$\varepsilon_3^\star = \Big\{0, 0, 0, 136147.50, 0.000054, 2397430, 0.05291, 1.0241 \times 10^{13}, 0, 0.1195, 0, 0, 0\Big\}$$

Linearizing system 5 about the equilibrium state $\varepsilon_3^\star$, a Jacobian matrix of the following form was obtained:

$$\varepsilon_3^\star = \begin{pmatrix}
-\varpi_1 & 0 & 0 & 0 & 0 & 0 & 0 & 0 & 0 & 0 & 0 & 0 & 0 \\
0 & -\varpi_4 & 0 & 0 & 0 & 0 & 0 & 0 & 0 & 0 & 0 & 0 & 0 \\
0 & 0 & -\varpi_6 & 0 & 0 & 0 & 0 & 0 & 0 & 0 & 0 & 0 & 0 \\
0 & 0 & 0 & -\varpi_8 & 0 & 0 & -\varpi_9 & 0 & 0 & 0 & 0 & 0 & 0 \\
0 & 0 & 0 & 0 & -\varpi_{10} & \varpi_{11} & -\varpi_{12} & 0 & 0 & 0 & 0 & 0 & 0 \\
0 & \varpi_{13} & 0 & \varpi_9 & \varpi_{12} & -\varpi_{42} & \varpi_{15} & 0 & -\varpi_{16} & -\varpi_{17} & 0 & -\varpi_{18} & 0 \\
0 & 0 & -\varpi_{20} & 0 & 0 & \varpi_{21} & -\varpi_{22} & -\varpi_{23} & 0 & 0 & 0 & 0 & 0 \\
0 & 0 & 0 & 0 & 0 & 0 & -\varpi_{24} & -\varpi_{25} & 0 & 0 & 0 & 0 & 0 \\
0 & 0 & 0 & 0 & 0 & 0 & 0 & 0 & -\varpi_{27} & 0 & 0 & 0 & 0 \\
0 & 0 & 0 & 0 & 0 & -\varpi_{29} & 0 & 0 & 0 & -\varpi_{30} & 0 & -\varpi_{31} & \varpi_{32} \\
\varpi_{33} & 0 & 0 & 0 & 0 & 0 & 0 & 0 & 0 & 0 & -\varpi_{41} & 0 & 0 \\
0 & 0 & 0 & 0 & 0 & \varpi_{35} & 0 & 0 & 0 & 0 & 0 & -\varpi_{36} & 0 \\
0 & 0 & 0 & 0 & 0 & 0 & 0 & 0 & 0 & \varpi_{37} & 0 & 0 & -\varpi_{38}
\end{pmatrix},$$

where

$$\varpi_{42} = 22.6829.$$

The eigenvalues associated with the equilibrium point $\varepsilon_3^\star$ are:

$$\varrho_1 = -7.1687 \times 10^{12}, \qquad \varrho_2 = -1.94528 \times 10^6,$$
$$\varrho_3 = -1.6782 \times 10^6, \qquad \varrho_4 = -1.60556 \times 10^6,$$
$$\varrho_5 = -805297, \qquad \varrho_6 = -14.3615 + 358.959i,$$

$$\varrho_7 = -14.3615 - 358.959i, \qquad \varrho_8 = -5.76,$$

$$\varrho_9 = -0.4027, \qquad \varrho_{10} = -0.369,$$

$$\varrho_{11} = 0.186273, \qquad \varrho_{12} = -0.0584,$$

$$\varrho_{13} = -0.037.$$

The eigenvalue analysis indicates that $\varepsilon_3^\star$ is a saddle spiral point, suggesting that the system is locally unstable around this equilibrium. Despite the lack of T lymphocytes, effector B lymphocytes, and cytokines such as interferon alpha, beta, and gamma at this equilibrium state obstructs the potential for viral eradication, the presence of antibodies and natural killer cells is sufficient to disrupt the virus-persistence equilibrium and accomplish viral abatement.

Case IV: For the fourth case in which $V^\star \neq 0$, $T_0^\star = 0$, $E^\star \neq 0$, and $N_K^\star = 0$, a boundary equilibrium configuration of the following nature is derived:

$$\begin{aligned}\varepsilon_4^\star \;=\; \Bigg\{ & 0, 0, 0, \frac{\Lambda_{M_0}}{\beta_1 V^\star + \mu_{M_0}}, \frac{\Lambda_{M_1} + \zeta I_M^\star}{\beta_2 V^\star + \mu_{M_1}}, \\ & \frac{\beta_1 V^\star M_0^\star + \beta_2 V^\star M_1^\star}{(\delta_2 + \sigma) E^\star + (\omega + \varepsilon + \zeta + \mu_{I_M})}, \frac{\Lambda_V + \omega I_M^\star}{\delta_3 T_2^\star + \delta_4 A^\star + (\psi + \mu_V)}, \\ & \frac{\Lambda_A + \psi V^\star}{\delta_4 V^\star + \mu_A}, \frac{\Lambda_E}{(\delta_2 - \sigma) I_M^\star + \mu_E}, 0, 0, \frac{\varepsilon I_M^\star}{(\theta_1 + \mu_{F_1})}, 0 \Bigg\}.\end{aligned}$$

The equilibrium state $\varepsilon_4^\star$ will exist if $\delta_2 > \sigma$. Considering the preliminary conditions for the state variables and parameter values as delineated in Tables 5 and 6, the following was ascertained:

$$\begin{aligned}\varepsilon_4^\star \;=\; \Bigg\{ & 0, 0, 0, 136147.50, 0.000054, 2397430, 0.05291, \\ & 1.0241 \times 10^{13}, 20, 0, 0, 0, 0 \Bigg\}.\end{aligned}$$

Linearizing system 5 about the equilibrium state $\varepsilon_4^\star$, a Jacobian matrix of the following form was obtained:

$$\varepsilon_4^\star = \begin{pmatrix}
-\varpi_1 & 0 & 0 & 0 & 0 & 0 & 0 & 0 & 0 & 0 & 0 & 0 & 0 \\
0 & -\varpi_4 & 0 & 0 & 0 & 0 & 0 & 0 & 0 & 0 & 0 & 0 & 0 \\
0 & 0 & -\varpi_6 & 0 & 0 & 0 & 0 & 0 & 0 & 0 & 0 & 0 & 0 \\
0 & 0 & 0 & -\varpi_8 & 0 & 0 & -\varpi_9 & 0 & 0 & 0 & 0 & 0 & 0 \\
0 & 0 & 0 & 0 & -\varpi_{10} & \varpi_{11} & -\varpi_{12} & 0 & 0 & 0 & 0 & 0 & 0 \\
0 & \varpi_{13} & 0 & \varpi_9 & \varpi_{12} & -\varpi_{43} & \varpi_{15} & 0 & -\varpi_{16} & -\varpi_{17} & 0 & 0 & -\varpi_{19} \\
0 & 0 & -\varpi_{20} & 0 & 0 & \varpi_{21} & -\varpi_{22} & -\varpi_{23} & 0 & 0 & 0 & 0 & 0 \\
0 & 0 & 0 & 0 & 0 & 0 & -\varpi_{24} & -\varpi_{25} & 0 & 0 & 0 & 0 & 0 \\
0 & 0 & 0 & 0 & 0 & -\varpi_{26} & 0 & 0 & -\varpi_{27} & 0 & 0 & 0 & -\varpi_{28} \\
0 & 0 & 0 & 0 & 0 & 0 & 0 & 0 & 0 & -\varpi_{30} & 0 & \varpi_{40} & \varpi_{32} \\
\varpi_{33} & 0 & 0 & 0 & 0 & 0 & 0 & 0 & 0 & 0 & -\varpi_{41} & 0 & 0 \\
0 & 0 & 0 & 0 & 0 & \varpi_{35} & 0 & 0 & 0 & 0 & 0 & -\varpi_{36} & 0 \\
0 & 0 & 0 & 0 & 0 & 0 & 0 & 0 & 0 & \varpi_{37} & 0 & 0 & -\varpi_{38}
\end{pmatrix},$$

where

$$\varpi_{43} = 51.2152.$$

The eigenvalues corresponding to the equilibrium point $\varepsilon_4^\star$ are:

$$\begin{aligned}
\gamma_1 &= -7.1687 \times 10^{12}, & \gamma_2 &= -1.94529 \times 10^6, \\
\gamma_3 &= -1.6782 \times 10^6, & \gamma_4 &= -1.60556 \times 10^6, \\
\gamma_5 &= -805297, & \gamma_6 &= -31.6025, \\
\gamma_7 &= -7.23622, & \gamma_8 &= -4.51634, \\
\gamma_9 &= -0.4027, & \gamma_{10} &= -0.369, \\
\gamma_{11} &= -0.0590878, & \gamma_{12} &= -0.0583867, \\
\gamma_{13} &= -0.037.
\end{aligned}$$

The eigenvalue analysis reveals that $\varepsilon_4^\star$ is a stable point, indicating that the system is locally stable around this equilibrium. In the absence of T cells, natural killer cells, and cytokines such as interferon alpha, beta, and gamma, there is no mechanism present to facilitate viral clearance. Consequently, the

presence of antibodies and effector B cells alone is insufficient to destabilize the virus-persistence equilibrium and induce viral clearance.

Case V: For the fifth situation where $V^\star \neq 0$, $T_0^\star \neq 0$, $E^\star = 0$, and $N_K^\star = 0$, a boundary equilibrium configuration of the following type was ascertained:

$$\begin{aligned}\varepsilon_5^\star = \Bigg\{ & \frac{\Lambda_{T_0}}{\rho_1 I_M^\star I_{10}^\star + \rho_2 V^\star I_{10}^\star + \frac{\rho_3 I_M^\star}{1+\tau_1 I_{10}^\star} + \mu_{T_0}}, \frac{\rho_1 I_M^\star T_0^\star I_{10}^\star}{\pi I_M^\star + \mu_{T_1}}, \frac{\rho_2 V^\star T_0^\star I_{10}^\star}{\delta_3 V^\star + \mu_{T_2}}, \\ & \frac{\Lambda_{M_0}}{\beta_1 V^\star + \mu_{M_0}}, \frac{\Lambda_{M_1} + \zeta I_M^\star}{\beta_2 V^\star + \mu_{M_1}}, \frac{\beta_1 V^\star M_0^\star + \beta_2 V^\star M_1^\star}{(\omega + \varepsilon + \zeta + \mu_{I_M})}, \\ & \frac{\Lambda_V + \omega I_M^\star}{\delta_3 T_2^\star + \delta_4 A^\star + (\psi + \mu_V)}, \frac{\Lambda_A + \psi V^\star}{\delta_4 V^\star + \mu_A}, 0, 0, \\ & \frac{-\mu_{I_{10}} + \sqrt{\mu_{I_{10}}^2 + 4\mu_{I_{10}}\tau_1\rho_3 I_M^\star T_0^\star}}{2\mu_{I_{10}}\tau_1}, \frac{\varepsilon I_M^\star}{(\theta_1 + \mu_{F_1})}, 0 \Bigg\},\end{aligned}$$

Considering the preliminary conditions for the state variables and parameter values as delineated in Tables 5 and 6, the following was ascertained:

$$\begin{aligned}\varepsilon_5^\star = \Bigg\{ & 1477611.94, 0, 0, 136147.50, 0.000054, 2397430, 0.05291, \\ & 1.0241 \times 10^{13}, 0, 0, 0, 0, 0 \Bigg\}\end{aligned}$$

Linearizing system 5 about the equilibrium state $\varepsilon_5^\star$, a Jacobian matrix of the

following form was obtained:

$$\varepsilon_5^\star = \begin{pmatrix} -\varpi_1 & 0 & 0 & 0 & 0 & -\varpi_2 & 0 & 0 & 0 & 0 & \varpi_3 & 0 & 0 \\ 0 & -\varpi_4 & 0 & 0 & 0 & 0 & 0 & 0 & 0 & 0 & \varpi_5 & 0 & 0 \\ 0 & 0 & -\varpi_6 & 0 & 0 & 0 & 0 & 0 & 0 & 0 & \varpi_7 & 0 & 0 \\ 0 & 0 & 0 & -\varpi_8 & 0 & 0 & -\varpi_9 & 0 & 0 & 0 & 0 & 0 & 0 \\ 0 & 0 & 0 & 0 & -\varpi_{10} & \varpi_{11} & -\varpi_{12} & 0 & 0 & 0 & 0 & 0 & 0 \\ 0 & \varpi_{13} & 0 & \varpi_9 & \varpi_{12} & -\varpi_{39} & \varpi_{15} & 0 & -\varpi_{16} & -\varpi_{17} & 0 & 0 & 0 \\ 0 & 0 & -\varpi_{20} & 0 & 0 & \varpi_{21} & -\varpi_{22} & -\varpi_{23} & 0 & 0 & 0 & 0 & 0 \\ 0 & 0 & 0 & 0 & 0 & 0 & -\varpi_{24} & -\varpi_{25} & 0 & 0 & 0 & 0 & 0 \\ 0 & 0 & 0 & 0 & 0 & 0 & 0 & 0 & -\varpi_{27} & 0 & 0 & 0 & 0 \\ 0 & 0 & 0 & 0 & 0 & 0 & 0 & 0 & 0 & -\varpi_{30} & 0 & \varpi_{40} & \varpi_{32} \\ \varpi_{33} & 0 & 0 & 0 & 0 & \varpi_2 & 0 & 0 & 0 & 0 & -\varpi_{34} & 0 & 0 \\ 0 & 0 & 0 & 0 & 0 & \varpi_{35} & 0 & 0 & 0 & 0 & 0 & -\varpi_{36} & 0 \\ 0 & 0 & 0 & 0 & 0 & 0 & 0 & 0 & 0 & \varpi_{37} & 0 & 0 & -\varpi_{38} \end{pmatrix}.$$

For the equilibrium point $\varepsilon_5^\star$, the eigenvalues are:

$$\begin{aligned} &\xi_1 = -7.1687 \times 10^{12}, && \xi_2 = -3.89549 \times 10^{11}, \\ &\xi_3 = -2.09237 \times 10^{6}, && \xi_4 = -1.94528 \times 10^{6}, \\ &\xi_5 = -1.6782 \times 10^{6}, && \xi_6 = 1.28704 \times 10^{6}, \\ &\xi_7 = -5.76, && \xi_8 = -5.70011, \\ &\xi_9 = -0.4027, && \xi_{10} = -0.369, \\ &\xi_{11} = -0.0584002, && \xi_{12} = -0.0581, \\ &\xi_{13} = 0.0000988964. \end{aligned}$$

The eigenvalue spectrum indicates that the equilibrium point $\varepsilon_5^\star$ is classified as an unstable saddle point. From a biological perspective, augmenting the production of T cells, supported by antibodies, is sufficient to destabilize the virus-persistence equilibrium state. This destabilization facilitates the transition to a stable virus-free equilibrium, effectively leading to viral clearance.

Case VI: For the sixth scenario where $V^\star \neq 0$, $T_0^\star \neq 0$, $E^\star \neq 0$, and $N_K^\star = 0$, a

boundary steady state of the following form was obtained:

$$\begin{aligned}\varepsilon_6^\star = \Bigg\{ & \frac{\Lambda_{T_0}}{\rho_1 I_M^\star I_{10}^\star + \rho_2 V^\star I_{10}^\star + \rho_3 I_M^\star \left(\frac{1}{1+\tau_1 I_{10}^\star}\right) + \mu_{T_0}}, \frac{\rho_1 I_M^\star T_0^\star I_{10}^\star}{\pi I_M^\star + \mu_{T_1}}, \\ & \frac{\rho_2 V^\star T_0^\star I_{10}^\star}{\delta_3 V^\star + \mu_{T_2}}, \frac{\Lambda_{M_0}}{\beta_1 V^\star + \mu_{M_0}}, \frac{\Lambda_{M_1} + \zeta I_M^\star}{\beta_2 V^\star + \mu_{M_1}}, \\ & \frac{\beta_1 V^\star M_0^\star + \beta_2 V^\star M_1^\star}{(\delta_2 + \sigma) E^\star + (\omega + \varepsilon + \zeta + \mu_{I_M})}, \frac{\Lambda_V + \omega I_M^\star}{\delta_3 T_2^\star + \delta_4 A^\star + \psi + \mu_V}, \\ & \frac{\Lambda_A + \psi V^\star}{\delta_4 A^\star + \mu_A}, \frac{\Lambda_E}{(\delta_2 - \sigma) I_M^\star + \mu_E}, 0, \\ & \frac{-\mu_{I_{10}} + \sqrt{\mu_{I_{10}}^2 + 4\mu_{I_{10}}\tau_1\rho_3 I_M^\star T_0^\star}}{2\mu_{I_{10}}\tau_1}, \frac{\varepsilon I_M^\star}{\theta_1 + \mu_{F_1}}, 0 \Bigg\},\end{aligned}$$

The equilibrium state $\varepsilon_6^\star$ would materialize provided that $\delta_2 > \sigma$. Given the initial conditions for the state variables and parameter values specified in Tables 5 and 6, the following was determined:

$$\begin{aligned}\varepsilon_6^\star = \Bigg\{ & 1477611.94, 0, 0, 136147.50, 0.000054, 2397430, 0.05291, \\ & 1.0241 \times 10^{13}, 20, 0, 0, 0, 0 \Bigg\}\end{aligned}$$

Linearizing system 5 around the equilibrium state $\varepsilon_6^\star$, a Jacobian matrix of the following structure was derived:

$$\varepsilon_6^\star = \begin{pmatrix}
-\varpi_1 & 0 & 0 & 0 & 0 & -\varpi_2 & 0 & 0 & 0 & 0 & \varpi_3 & 0 & 0 \\
0 & -\varpi_4 & 0 & 0 & 0 & 0 & 0 & 0 & 0 & 0 & \varpi_5 & 0 & 0 \\
0 & 0 & -\varpi_6 & 0 & 0 & 0 & 0 & 0 & 0 & 0 & \varpi_7 & 0 & 0 \\
0 & 0 & 0 & -\varpi_8 & 0 & 0 & -\varpi_9 & 0 & 0 & 0 & 0 & 0 & 0 \\
0 & 0 & 0 & 0 & -\varpi_{10} & \varpi_{11} & -\varpi_{12} & 0 & 0 & 0 & 0 & 0 & 0 \\
0 & \varpi_{13} & 0 & \varpi_9 & \varpi_{12} & -\varpi_{43} & \varpi_{15} & 0 & -\varpi_{16} & -\varpi_{17} & 0 & 0 & -\varpi_{19} \\
0 & 0 & -\varpi_{20} & 0 & 0 & \varpi_{21} & -\varpi_{22} & -\varpi_{23} & 0 & 0 & 0 & 0 & 0 \\
0 & 0 & 0 & 0 & 0 & 0 & -\varpi_{24} & -\varpi_{25} & 0 & 0 & 0 & 0 & 0 \\
0 & 0 & 0 & 0 & 0 & -\varpi_{26} & 0 & 0 & -\varpi_{27} & 0 & 0 & 0 & -\varpi_{28} \\
0 & 0 & 0 & 0 & 0 & 0 & 0 & 0 & 0 & -\varpi_{23} & 0 & \varpi_{40} & \varpi_{32} \\
\varpi_{33} & 0 & 0 & 0 & 0 & \varpi_2 & 0 & 0 & 0 & 0 & -\varpi_{34} & 0 & 0 \\
0 & 0 & 0 & 0 & 0 & \varpi_{35} & 0 & 0 & 0 & 0 & 0 & -\varpi_{36} & 0 \\
0 & 0 & 0 & 0 & 0 & 0 & 0 & 0 & 0 & \varpi_{37} & 0 & 0 & -\varpi_{38}
\end{pmatrix}.$$

The eigenvalues corresponding to the equilibrium point $\varepsilon_6^\star$ are:

$$\pi_1 = -7.1687 \times 10^{12}, \qquad \pi_2 = -3.89549 \times 10^{11},$$
$$\pi_3 = -2.09247 \times 10^{6}, \qquad \pi_4 = -1.94519 \times 10^{6},$$
$$\pi_5 = -1.6782 \times 10^{6}, \qquad \pi_6 = 1.28703 \times 10^{6},$$
$$\pi_7 = -5.76009, \qquad \pi_8 = -5.69985,$$
$$\pi_9 = 0.4027, \qquad \pi_{10} = -0.369,$$
$$\pi_{11} = -0.0583484, \qquad \pi_{12} = -0.0581,$$
$$\pi_{13} = -0.0000543191.$$

The eigenvalues denote that the equilibrium point $\varepsilon_6^\star$ is categorized as an unstable attractor. The presence of naive T lymphocytes and effector B lymphocytes, in concert with the effector functions of antibodies, is sufficiently potent to perturb the virus-persistence equilibrium, thereby culminating in the resolution of the viral pathology.

Case VII: For the seventh condition where $V^\star \neq 0$, $T_0^\star \neq 0$, $E^\star = 0$, and $N_K^\star \neq 0$, a boundary steady-state configuration of the following form was ascertained:

$$\begin{aligned}
\varepsilon_7^\star \;=\; \Bigg\{ & \frac{\Lambda_{T_0}}{\rho_1 I_M^\star I_{10}^\star + \rho_2 V^\star I_{10}^\star + \rho_3 I_M^\star \left(\frac{1}{1+\tau_1 I_{10}^\star}\right) + \mu_{T_0}}, \frac{\rho_1 I_M^\star T_0^\star I_{10}^\star}{\pi I_M^\star + \mu_{T_1}}, \\
& \frac{\rho_2 V^\star T_0^\star I_{10}^\star}{\delta_3 V^\star + \mu_{T_2}}, \frac{\Lambda_{M_0}}{\beta_1 V^\star + \mu_{M_0}}, \frac{\Lambda_{M_1} + \zeta I_M^\star}{\beta_2 V^\star + \mu_{M_1}}, \\
& \frac{\beta_1 V^\star M_0^\star + \beta_2 V^\star M_1^\star}{\delta_1 \left(1 + \chi_1 F_1^\star\right) N_K^\star + (\omega + \varepsilon + \zeta + \mu_{I_M}) - \pi T_1^\star}, \\
& \frac{\Lambda_V + \omega I_M^\star}{\delta_3 T_2^\star + \delta_4 A^\star + \psi + \mu_V}, \frac{\Lambda_A + \psi V^\star}{\delta_4 A^\star + \mu_A}, 0, \\
& \frac{\Lambda_{N_K} + \theta_1 F_1^\star + \theta_2 F_2^\star}{\delta_1 \left(1 + \chi_1 F_1^\star\right) I_M^\star + (\eta + \mu_{N_K})}, \frac{-\mu_{I_{10}} + \sqrt{\mu_{I_{10}}^2 + 4\mu_{I_{10}} \tau_1 \rho_3 I_M^\star T_0^\star}}{2\mu_{I_{10}} \tau_1}, \\
& \frac{\varepsilon I_M^\star}{\theta_1 + \mu_{F_1}}, \frac{\eta N_K^\star}{\theta_2 + \mu_{F_2}} \Bigg\}.
\end{aligned}$$

The equilibrium $\varepsilon_7^\star$ would be attainable if

$$\delta_1 \left(1 + \chi_1 F_1^\star\right) N_K^\star + \left(\omega + \varepsilon + \zeta + \mu_{I_M}\right) > \pi T_1^\star.$$

Given the initial conditions for the state variables and parameter values delineated in Tables 5 and 6, the following was ascertained:

$$\varepsilon_7^\star = \Big\{1477611.94, 0, 0, 136147.50, 0, 000054, 2397430, 0.05291, 1.0241 \times 10^{13}, 0, 0.1195, 0, 0, 0\Big\}$$

Upon linearizing system 5 at the equilibrium state $\varepsilon_7^\star$, a Jacobian matrix of the following form was obtained:

$$\varepsilon_7^\star = \begin{pmatrix}
-\varpi_1 & 0 & 0 & 0 & 0 & -\varpi_2 & 0 & 0 & 0 & 0 & \varpi_3 & 0 & 0 \\
0 & -\varpi_4 & 0 & 0 & 0 & 0 & 0 & 0 & 0 & 0 & \varpi_5 & 0 & 0 \\
0 & 0 & -\varpi_6 & 0 & 0 & 0 & 0 & 0 & 0 & 0 & \varpi_7 & 0 & 0 \\
0 & 0 & 0 & -\varpi_8 & 0 & 0 & -\varpi_9 & 0 & 0 & 0 & 0 & 0 & 0 \\
0 & 0 & 0 & 0 & -\varpi_{10} & \varpi_{11} & -\varpi_{12} & 0 & 0 & 0 & 0 & 0 & 0 \\
0 & \varpi_{13} & 0 & \varpi_9 & \varpi_{12} & -\varpi_{42} & \varpi_{15} & 0 & -\varpi_{16} & -\varpi_{17} & 0 & -\varpi_{18} & 0 \\
0 & 0 & -\varpi_{20} & 0 & 0 & \varpi_{21} & -\varpi_{22} & -\varpi_{23} & 0 & 0 & 0 & 0 & 0 \\
0 & 0 & 0 & 0 & 0 & 0 & -\varpi_{24} & -\varpi_{25} & 0 & 0 & 0 & 0 & 0 \\
0 & 0 & 0 & 0 & 0 & 0 & 0 & 0 & -\varpi_{27} & 0 & 0 & 0 & 0 \\
0 & 0 & 0 & 0 & 0 & -\varpi_{29} & 0 & 0 & 0 & -\varpi_{30} & 0 & -\varpi_{31} & \varpi_{32} \\
\varpi_{33} & 0 & 0 & 0 & 0 & \varpi_2 & 0 & 0 & 0 & 0 & -\varpi_{34} & 0 & 0 \\
0 & 0 & 0 & 0 & 0 & \varpi_{35} & 0 & 0 & 0 & 0 & 0 & -\varpi_{36} & 0 \\
0 & 0 & 0 & 0 & 0 & 0 & 0 & 0 & 0 & \varpi_{37} & 0 & 0 & -\varpi_{38}
\end{pmatrix}.$$

The eigenvalues associated with the Jacobian matrix at the equilibrium point $\varepsilon_7^\star$ are:

$$\vartheta_1 = -7.1687 \times 10^{12}, \qquad \vartheta_2 = -3.89549 \times 10^{11},$$
$$\vartheta_3 = -2.09237 \times 10^{6}, \qquad \vartheta_4 = -1.94528 \times 10^{6},$$
$$\vartheta_5 = -1.6782 \times 10^{6}, \qquad \vartheta_6 = 1.28704 \times 10^{6},$$

$$\vartheta_7 = -5.76, \qquad \vartheta_8 = -4.574,$$
$$\vartheta_9 = -1.08746, \qquad \vartheta_{10} = 0.4027,$$
$$\vartheta_{11} = -0.369, \qquad \vartheta_{12} = -0.0584481,$$
$$\vartheta_{13} = -0.0581014.$$

These eigenvalues elucidate that the equilibrium state $\varepsilon_7^\star$ is typified as an unstable singularity. The simultaneous presence of naive T lymphocytes and natural killer cells, coupled with the action of antibodies, is adequate to perturb the virus-persistence equilibrium and ultimately engender viral eradication.

Case VIII: In the eighth scenario, where $V^\star \neq 0$, $T_0^\star = 0$, $E^\star \neq 0$, and $N_K^\star \neq 0$, a boundary steady-state arrangement of the following nature was ascertained:

$$\varepsilon_8^\star = \left\{0, 0, 0, \frac{\Lambda_{M_0}}{\beta_1 V^\star + \mu_{M_0}}, \frac{\Lambda_{M_1} + \zeta I_M^\star}{\beta_2 V^\star + \mu_{M_1}}, I_M^\star, \frac{\Lambda_V + \omega I_M^\star}{\delta_3 T_2^\star + \delta_4 A^\star + \psi + \mu_V}, \right.$$
$$\frac{\Lambda_A + \psi V^\star}{\delta_4 A^\star + \mu_A}, \frac{\Lambda_E}{\delta_2\left(1 + \frac{\chi_2 \eta N_K^\star}{\theta_2 + \mu_{F_2}}\right) I_M^\star + \mu_E - \sigma I_M^\star},$$
$$\left. \frac{\frac{\theta_1 \varepsilon I_M^\star}{\theta_1 + \mu_{F_1}} + \frac{\theta_2 \eta N_K^\star}{\theta_2 + \mu_{F_2}}}{\delta_1\left(1 + \frac{\chi_1 \varepsilon I_M^\star}{\theta_1 + \mu_{F_1}}\right) I_M^\star + \eta + \mu_{N_K} - \Lambda_{N_K}}, 0, \frac{\varepsilon I_M^\star}{\theta_1 + \mu_{F_1}}, \frac{\eta N_K^\star}{\theta_2 + \mu_{F_2}} \right\},$$

where $I_M^\star = \frac{\beta_1 V^\star M_0^\star + \beta_2 V^\star M_1^\star}{\left[\delta_1\left(1+\chi_1 F_1^\star\right) N_K^\star + \delta_2\left(1+\chi_2 F_2^\star\right) E^\star + \sigma E^\star + \mathfrak{B} - \pi T_1^\star\right]}$,

and $\mathfrak{B} = (\omega + \varepsilon + \zeta + \mu_{I_M})$.

The equilibrium state $\varepsilon_8^\star$ would be viable if:

$$\delta_2\left(1 + \frac{\chi_2 \eta N_K^\star}{\theta_2 + \mu_{F_2}}\right) I_M^\star + \mu_E > \sigma I_M^\star,$$

$$\delta_1\left(1 + \frac{\chi_1 \varepsilon I_M^\star}{\theta_1 + \mu_{F_1}}\right) I_M^\star + \eta + \mu_{N_K} > \Lambda_{N_K},$$

and

$$\delta_1 \left(1 + \chi_1 F_1^\star\right) N_K^\star + \delta_2 \left(1 + \chi_2 F_2^\star\right) E^\star + \sigma E^\star + \mathfrak{B} > \pi T_1^\star.$$

Given the initial conditions for the state variables and parameter values in Tables 5 and 6, the following was derived:

$$\begin{aligned} \varepsilon_8^\star &= \Big\{0, 0, 0, 136147.50, 0.000054, 2397430, 0.05291, \\ &\qquad 1.0241 \times 10^{13}, 20, 0, 0, 0, 0\Big\}. \end{aligned}$$

Upon linearizing the model framework 5 around the equilibrium state $\varepsilon_8^\star$, a Jacobian matrix of the following structure was derived:

$$\varepsilon_8^\star = \begin{pmatrix} -\varpi_1 & 0 & 0 & 0 & 0 & 0 & 0 & 0 & 0 & 0 & 0 & 0 & 0 \\ 0 & -\varpi_4 & 0 & 0 & 0 & 0 & 0 & 0 & 0 & 0 & 0 & 0 & 0 \\ 0 & 0 & -\varpi_6 & 0 & 0 & 0 & 0 & 0 & 0 & 0 & 0 & 0 & 0 \\ 0 & 0 & 0 & -\varpi_8 & 0 & 0 & -\varpi_9 & 0 & 0 & 0 & 0 & 0 & 0 \\ 0 & 0 & 0 & 0 & -\varpi_{10} & \varpi_{11} & -\varpi_{12} & 0 & 0 & 0 & 0 & 0 & 0 \\ 0 & \varpi_{13} & 0 & \varpi_9 & \varpi_{12} & -\varpi_{14} & \varpi_{15} & 0 & -\varpi_{16} & -\varpi_{17} & 0 & -\varpi_{18} & -\varpi_{19} \\ 0 & 0 & -\varpi_{20} & 0 & 0 & \varpi_{21} & -\varpi_{22} & -\varpi_{23} & 0 & 0 & 0 & 0 & 0 \\ 0 & 0 & 0 & 0 & 0 & 0 & -\varpi_{24} & -\varpi_{25} & 0 & 0 & 0 & 0 & 0 \\ 0 & 0 & 0 & 0 & 0 & -\varpi_{26} & 0 & 0 & -\varpi_{27} & 0 & 0 & 0 & -\varpi_{28} \\ 0 & 0 & 0 & 0 & 0 & -\varpi_{29} & 0 & 0 & 0 & -\varpi_{30} & 0 & -\varpi_{31} & \varpi_{32} \\ \varpi_{33} & 0 & 0 & 0 & 0 & 0 & 0 & 0 & 0 & 0 & -\varpi_{41} & 0 & 0 \\ 0 & 0 & 0 & 0 & 0 & \varpi_{35} & 0 & 0 & 0 & 0 & 0 & -\varpi 36 & 0 \\ 0 & 0 & 0 & 0 & 0 & 0 & 0 & 0 & 0 & \varpi_{37} & 0 & 0 & -\varpi_{38} \end{pmatrix}.$$

The equilibrium point $\varepsilon_8^\star$ exhibits the following eigenvalues:

$$\begin{aligned} \varkappa_1 &= -7.1687 \times 10^{12}, & \varkappa_2 &= -1.94529 \times 10^6, \\ \varkappa_3 &= -1.6782 \times 10^6, & \varkappa_4 &= -1.60556 \times 10^6, \\ \varkappa_5 &= -805297, & \varkappa_6 &= -46.0454 + 362.858i, \\ \varkappa_7 &= -46.0454 - 362.858i, & \varkappa_8 &= 48.4958, \end{aligned}$$

$$\varkappa_9 = -0.4027, \qquad \varkappa_{10} = -0.369,$$

$$\varkappa_{11} = -0.083031, \qquad \varkappa_{12} = -0.0584,$$

$$\varkappa_{13} = -0.037.$$

These eigenvalues delineate that the equilibrium state $\varepsilon_8^\star$ is characterized as an unstable saddle-node. The absence of naive T lymphocytes fails to contribute to the equilibrium stability of the persistent viral infection. The synthesis of antibodies and the elevation of effector B cell counts are sufficiently potent to destabilize the virus-persistence equilibrium. This accentuates the fundamental significance of the synergistic contribution of both antibodies and effector B cells in the eradication of hepatitis B virus infection.

Fractional-order Model

Fractional calculus has garnered significant attention from numerous scholars and has found utility across various disciplines. Researchers have engineered mathematical frameworks for a wide spectrum of infectious diseases, leveraging contemporary calculus techniques. The preponderance of mathematical modeling methodologies is predicated upon classical ordinary integral and differential equations, or systems of linear and nonlinear differential equations. Nevertheless, over the last three decades, in order to address real-world complexities with superior precision and exactitude, arbitrary-order fractional integral and differential equations (FDEs) have been increasingly adopted (X. Liu et al., 2022).

The conventional mathematical model of integer order often proves inadequate in certain scenarios. For instance, virus propagation typically exhibits discontinuous behavior, a nuance classical differential models struggle to capture effectively. In contrast, fractional systems naturally accommodate such discontinuities (L. Zhang et al., 2021). Consequently, fractional calculus has made substantial contributions to the fields of mechanics, chemistry, biology, and image processing. Several physical problems have been successfully addressed through the application of fractional calculus. Since the fractional order can assume any positive real value, denoted as φ,

researchers can select the value that best fits the available data (Nisar et al., 2022). Thus, models can be tailored to real-world data, enhancing our ability to predict the future evolution of diseases by considering their past and present states (L. Zhang et al., 2021).

To incorporate the memory effect of hepatitis B virus and liver cancer on host liver cells, we introduce the Atangana-Baleanu fractional differential operator into the proposed model. This decision stems from the fact that human body cells, including liver cells, are susceptible to various viral infections, necessitating the use of fractional differential operators to understand how liver cells respond to these infections based on their prior experiences with other pathogens. Additionally, this approach enables the examination of how both infected and uninfected macrophage populations utilize their memory to prevent infections in compartmental models. These considerations have elevated the fractional-order model to prominence in contemporary biological process modeling. Thus, our motivation lies in investigating the dynamics of hepatitis B virus and liver cancer coexistence using Atangana-Baleanu fractional differential and integral operators in Caputo sense.

Immune Response in HBV and Liver Cancer Model via ABC Operator

The proposed model 5 is presently being augmented to correspond with the foundational fractional differential and integral operators, in conjunction with the theorems delineated earlier. In accordance with the authoritative literature on fractional differential equation models, the immune response model 5 can be articulated

within the purview of the Atangana-Baleanu Caputo formulation as follows.

$$
\begin{cases}
{}_{0}^{ABC}\mathbb{D}_{t}^{\varphi}T_0 &= \Lambda_{T_0}^{\varphi} - \rho_1^{\varphi} I_M T_0 I_{10} - \rho_2^{\varphi} V T_0 I_{10} - \rho_3^{\varphi} T_0 I_M \left(\frac{1}{1+\tau_1^{\varphi} I_{10}}\right) \\
&\quad -\mu_{T_0}^{\varphi} T_0, \\
{}_{0}^{ABC}\mathbb{D}_{t}^{\varphi}T_1 &= \rho_1^{\varphi} I_M T_0 I_{10} - \pi^{\varphi} I_M T_1 - \mu_{T_1}^{\varphi} T_1, \\
{}_{0}^{ABC}\mathbb{D}_{t}^{\varphi}T_2 &= \rho_2^{\varphi} V T_0 I_{10} - \delta_3^{\varphi} T_2 V - \mu_{T_2}^{\varphi} T_2, \\
{}_{0}^{ABC}\mathbb{D}_{t}^{\varphi}M_0 &= \Lambda_{M_0}^{\varphi} - \beta_1^{\varphi} V M_0 - \mu_{M_0}^{\varphi} M_0, \\
{}_{0}^{ABC}\mathbb{D}_{t}^{\varphi}M_1 &= \Lambda_{M_1}^{\varphi} - \beta_2^{\varphi} V M_1 + \zeta^{\varphi} I_M - \mu_{M_1}^{\varphi} M_1, \\
{}_{0}^{ABC}\mathbb{D}_{t}^{\varphi}I_M &= \beta_1^{\varphi} V M_0 + \beta_2^{\varphi} V M_1 + \pi^{\varphi} I_M T_1 - \delta_1^{\varphi} \left(1 + \chi_1^{\varphi} F_1\right) I_M N_K \\
&\quad -\delta_2^{\varphi} \left(1 + \chi_2^{\varphi} F_2\right) I_M E - \sigma^{\varphi} I_M E \\
&\quad - \left(\omega^{\varphi} + \varepsilon^{\varphi} + \zeta^{\varphi} + \mu_{I_M}^{\varphi}\right) I_M, \\
{}_{0}^{ABC}\mathbb{D}_{t}^{\varphi}V &= \Lambda_V^{\varphi} + \omega^{\varphi} I_M - \delta_3^{\varphi} T_2 V - \delta_4^{\varphi} A V - \left(\psi^{\varphi} + \mu_V^{\varphi}\right) V, \\
{}_{0}^{ABC}\mathbb{D}_{t}^{\varphi}A &= \Lambda_A^{\varphi} + \psi^{\varphi} V - \delta_4^{\varphi} A V - \mu_A^{\varphi} A, \\
{}_{0}^{ABC}\mathbb{D}_{t}^{\varphi}E &= \Lambda_E^{\varphi} - \delta_2^{\varphi} \left(1 + \chi_2^{\varphi} F_2\right) I_M E + \sigma^{\varphi} I_M E - \mu_E^{\varphi} E, \\
{}_{0}^{ABC}\mathbb{D}_{t}^{\varphi}N_K &= \Lambda_{N_K}^{\varphi} - \delta_1^{\varphi} \left(1 + \chi_1^{\varphi} F_1\right) I_M N_K + \theta_1^{\varphi} F_1 + \theta_2^{\varphi} F_2 \\
&\quad - \left(\eta^{\varphi} + \mu_{N_K}^{\varphi}\right) N_K, \\
{}_{0}^{ABC}\mathbb{D}_{t}^{\varphi}I_{10} &= \rho_3^{\varphi} I_M T_0 \left(\frac{1}{1+\tau_1^{\varphi} I_{10}}\right) - \mu_{I_{10}}^{\varphi} I_{10}, \\
{}_{0}^{ABC}\mathbb{D}_{t}^{\varphi}F_1 &= \varepsilon^{\varphi} I_M - \left(\theta_1^{\varphi} + \mu_{F_1}^{\varphi}\right) F_1, \\
{}_{0}^{ABC}\mathbb{D}_{t}^{\varphi}F_2 &= \eta^{\varphi} N_K - \left(\theta_2^{\varphi} + \mu_{F_2}^{\varphi}\right) F_2.
\end{cases}
\tag{39}
$$

With initial conditions $T_0 = T_{0^\star}$, $T_1 = T_{1^\star}$, $T_2 = T_{2^\star}$, $M_0 = M_{0^\star}$, $M_1 = M_{1^\star}$, $I_M = I_{M^\star}$, $V = V_0$, $A = A_0$, $E = E_0$, $N_K = N_{K^\star}$, $I_{10} = I_{10^\star}$, $F_1 = F_{1^\star}$, $F_2 = F_{2^\star}$.

Basic Model Properties

This section elucidates the non-negativity and boundedness of the solutions, alongside the computation of the reproduction number for the proposed model. Furthermore, the existence and uniqueness of the solutions pertaining to the analyzed

model are examined. Let

$$\begin{aligned}\Delta &= \Big\{(T_0, T_1, T_2, M_0, M_1, I_M, V, A, E, N_K, I_{10}, F_1, F_2) \in \mathbb{R}_+^{13} : \\ &\quad T_0, T_1, T_2, M_0, M_1, I_M, V, A, E, N_K, I_{10}, F_1, F_2 \in \mathbb{R}^+\Big\}\end{aligned}$$

be the required invariant region.

Lemma 6

Let $f(t) \in C[a,b]$ and suppose ${}_0^{ABC}\mathbb{D}_t^{\varphi} f(t) \in C\,[a,b]$ when $0 < \varphi \leq 1$. Then the generalized mean value theorem states that

$$f(t) = f(a) + \frac{1}{\Gamma(\varphi)}\left[{}_0^{ABC}\mathbb{D}_t^{\varphi} f(s)\,(t-a)^{\varphi}\right],$$

where $0 \leq s \leq t$.

Let $\varphi \in (0,1]$, $f(t) \in C\,[0,b]$ and ${}_0^{ABC}\mathbb{D}_t^{\varphi} f(t) \in C\,[0,b]$. It is clear from the Lemma 6 above that ${}_0^{ABC}\mathbb{D}_t^{\varphi} f(t) \geq 0, \forall t \in (0,b]$, then the function $f(t)$ increases while if ${}_0^{ABC}\mathbb{D}_t^{\varphi} f(t) \leq 0, \forall t \in (0,b]$, then the function $f(t)$ decreases.

Theorem 7

Positivity of solutions

The solutions of the model system 39 are non-negative provided all initial conditions are all positive.

Proof. From the considered model system 39, the following expression can be written for any non-negative initial condition:

$$\begin{aligned}{}_0^{ABC}\mathbb{D}_t^{\varphi} T_0(t)|_{T_0=0} &= \Lambda_{T_0}^{\varphi} \geq 0,\\ {}_0^{ABC}\mathbb{D}_t^{\varphi} T_1(t)|_{T_1=0} &= \rho_1^{\varphi} I_M(t) T_0(t) I_{10}(t) \geq 0,\\ {}_0^{ABC}\mathbb{D}_t^{\varphi} T_2(t)|_{T_2=0} &= \rho_2^{\varphi} V(t) T_0(t) I_{10}(t) \geq 0,\\ {}_0^{ABC}\mathbb{D}_t^{\varphi} M_0(t)|_{M_0=0} &= \Lambda_{M_0}^{\varphi} \geq 0,\\ {}_0^{ABC}\mathbb{D}_t^{\varphi} M_1(t)|_{M_1=0} &= \Lambda_{M_1}^{\varphi} + \zeta^{\varphi} I_M(t) \geq 0,\end{aligned}$$

$$
\begin{aligned}
{}_0^{ABC}\mathbb{D}_t^{\varphi} V(t)|_{V=0} &= \Lambda_V^{\varphi} + \omega^{\varphi} I_M(t) \geq 0, \\
{}_0^{ABC}\mathbb{D}_t^{\varphi} I_M(t)|_{I_M=0} &= \beta_1^{\varphi} V(t) M_0(t) + \beta_2^{\varphi} V(t) M_1(t) \geq 0, \\
{}_0^{ABC}\mathbb{D}_t^{\varphi} A(t)|_{A=0} &= \Lambda_A^{\varphi} + \psi^{\varphi} V(t) \geq 0, \\
{}_0^{ABC}\mathbb{D}_t^{\varphi} E(t)|_{E=0} &= \Lambda_E^{\varphi} \geq 0, \\
{}_0^{ABC}\mathbb{D}_t^{\varphi} N_K(t)|_{N_K=0} &= \Lambda_{N_K}^{\varphi} + \theta_1^{\varphi} F_1(t) + \theta_2^{\varphi} F_2(t) \geq 0, \\
{}_0^{ABC}\mathbb{D}_t^{\varphi} T_1(t)|_{T_1=0} &= \rho_3^{\varphi} I_M(t) T_0(t) \geq 0, \\
{}_0^{ABC}\mathbb{D}_t^{\varphi} F_1(t)|_{T_0=0} &= \varepsilon^{\varphi} I_M(t) \geq 0, \\
{}_0^{ABC}\mathbb{D}_t^{\varphi} F_2(t)|_{F_2=0} &= \eta^{\varphi} N_K(t) \geq 0.
\end{aligned}
$$

Thus, from Lemma 6, all solutions of the considered immune response to HBV and liver cancer co-existence model are non-negative given any positive initial conditions for all $t \geq 0$.

Lemma 7

Boundedness of solutions (positively invariant region)

The population variables and parameter fluctuations within system 39 are meticulously scrutinized. Given that the variables and parameters in the model system remain strictly positive for all values of $t \geq 0$, it is substantiated that all possible solutions are uniformly bounded within finite limits.

Let

$$
\begin{aligned}
\Delta = \Bigg\{ & (T_0, T_1, T_2, M_0, M_1, I_M, V, A, E, N_K, I_{10}, F_1, F_2) \in \mathbb{R}_+^{13} : \\
& T \leq \Gamma_1, M \leq \Gamma_2, V \leq \Gamma_3, A \leq \Gamma_4, E \leq \Gamma_5, N_K \leq \Gamma_6, I_{10} \leq \Gamma_7, \\
& F_2 \leq \Gamma_8, F_2 \leq \Gamma_9 \Bigg\}.
\end{aligned}
$$

The solutions of system 39, given any non-negative initial conditions, remain constrained within the biologically viable domain delineated by the set Δ for all $t \geq 0$. Consequently, Δ serves as a positively invariant domain for the model system described in Eq. (39).

Proof. Taking into account the different T cell subsets (i.e., T_0, T_1, and T_2) and

aggregating them to determine the overall T cell population, the following was obtained:

$$\begin{aligned} {}_0^{ABC}\mathbb{D}_t^{\varphi}(T_0+T_1+T_2) &= \Lambda_{T_0}^{\varphi}-\mu_{T_0}^{\varphi}T_0-\mu_{T_1}^{\varphi}T_1-\mu_{T_2}^{\varphi}T_2 \\ &\quad -\rho_3^{\varphi}I_M T_0\left(\frac{1}{1+\tau_1^{\varphi}I_{10}}\right)-\pi^{\varphi}I_M T_1-\delta_3^{\varphi}T_2 V. \end{aligned}$$

It follows that

$$ {}_0^{ABC}\mathbb{D}_t^{\varphi}\left[T(t)\right] \leq \Lambda_{T_0}^{\varphi}-\mu^{\varphi}T, \quad \text{where} \quad \mu^{\varphi}=\min\{\mu_{T_0}^{\varphi},\mu_{T_1}^{\varphi},\mu_{T_2}^{\varphi}\}. \tag{40}$$

By applying the Laplace transform to both sides of Eq. (40), the following was obtained:

$$\begin{aligned} T(t) \leq & \left[\frac{ABC(\varphi)T(0)}{ABC(\varphi)-(1-\varphi)\mu^{\varphi}}+\frac{(1-\varphi)\Lambda_{T_0}^{\varphi}}{ABC(\varphi)-(1-\varphi)\mu^{\varphi}}\right]\times\mathbb{E}_{\varphi,1}\left(-\ell t^{\varphi}\right) \\ & +\frac{\varphi\Lambda_{T_0}^{\varphi}}{ABC(\varphi)-(1-\varphi)\mu^{\varphi}}\times\mathbb{E}_{\varphi,\varphi+1}\left(-\ell t^{\varphi}\right), \end{aligned} \tag{41}$$

where

$$\ell = \frac{\varphi\mu^{\varphi}}{ABC(\varphi)-(1-\varphi)\mu^{\varphi}} \quad \text{and} \quad T(0)=T_0(0)+T_1(0)+T_2(0).$$

Since

$$\mathbb{E}_{\alpha,\beta}(t) = t\mathbb{E}_{\alpha,\alpha+\beta}(t)+\frac{1}{\Gamma(\beta)}, \tag{42}$$

following Eq. (42), the relation in Eq. (41) transform to

$$\begin{aligned} T(t) \leq & \frac{\Lambda_{T_0}^{\varphi}}{\mu^{\varphi}}+\frac{ABC(\varphi)}{ABC(\varphi)-(1-\varphi)\mu^{\varphi}} \\ & \times\left[T(0)-\frac{\Lambda_{T_0}^{\varphi}}{\mu^{\varphi}}\right]\times\mathbb{E}_{\varphi,1}\left(-\ell t^{\varphi}\right). \end{aligned} \tag{43}$$

It follows from Eq. (43) that $T(t) \leq \frac{\Lambda_{T_0}^{\varphi}}{\mu^{\varphi}} = \Gamma_1$ as $t \to \infty$. Thus, the T cells population is bounded. That is $T_0 \leq \frac{\Lambda_{T_0}^{\varphi}}{\mu^{\varphi}}$, $T_1 \leq \frac{\Lambda_{T_0}^{\varphi}}{\mu^{\varphi}}$ and $T_2 \leq \frac{\Lambda_{T_0}^{\varphi}}{\mu^{\varphi}}$.

Taking the macrophage population into consideration (i.e., M_0, M_1, and I_M) and summing them to obtain the total macrophage cell population, the following was obtained:

$$\begin{aligned} {}_0^{ABC}\mathbb{D}_t^{\varphi}(M_0+M_1+I_M) &= \Lambda_{M_0}^{\varphi}+\Lambda_{M_1}^{\varphi}-\mu_{M_0}^{\varphi}M_0-\mu_{M_1}^{\varphi}M_1-\mu_{I_M}^{\varphi}I_M \\ &\quad -\delta_1\left(1+\chi_1F_1\right)I_MN_K-\delta_2\left(1+\chi_2F_2\right)I_ME \\ &\quad -\sigma^{\varphi}I_ME-\left(\omega^{\varphi}+\varepsilon^{\varphi}+\mu_{I_M^{\varphi}}\right)I_M+\pi^{\varphi}I_MT_1. \end{aligned}$$

It follows that

$$\begin{aligned} {}_0^{ABC}\mathbb{D}_t^{\varphi}(M_0+M_1+I_M) &\leq \Lambda_{M_0}^{\varphi}+\Lambda_{M_1}^{\varphi}-\mu_{M_0}^{\varphi}M_0-\mu_{M_1}^{\varphi}M_1-\mu_{I_M}^{\varphi}I_M \\ &\quad +\pi^{\varphi}I_M\Gamma_1. \end{aligned}$$

But $\Gamma_1=\frac{\Lambda_{T_0}^{\varphi}}{\mu^{\varphi}}=T_1$. Hence,

$$ {}_0^{ABC}\mathbb{D}_t^{\varphi}\left[M(t)\right] \leq \Lambda^{\varphi}-\mu^{\varphi}M, \tag{44}$$

where $\Lambda^{\varphi}=\min\{\Lambda_{M_0}^{\varphi},\Lambda_{M_1}^{\varphi}\}$ and $\mu^{\varphi}=\min\{\mu_{M_0}^{\varphi},\mu_{M_1}^{\varphi},\mu_{I_M}^{\varphi}\}$. By applying the Laplace transform to both sides of Eq. (44), the following was obtained:

$$\begin{aligned} M(t) &\leq \left[\frac{ABC(\varphi)M(0)}{ABC(\varphi)-(1-\varphi)\mu^{\varphi}}+\frac{(1-\varphi)\Lambda^{\varphi}}{ABC(\varphi)-(1-\varphi)\mu^{\varphi}}\right]\times\mathbb{E}_{\varphi,1}\left(-\ell t^{\varphi}\right) \\ &\quad +\frac{\varphi\Lambda^{\varphi}}{ABC(\varphi)-(1-\varphi)\mu^{\varphi}}\times\mathbb{E}_{\varphi,\varphi+1}\left(-\ell t^{\varphi}\right), \end{aligned} \tag{45}$$

where

$$\ell = \frac{\varphi\mu^{\varphi}}{ABC(\varphi)-(1-\varphi)\mu^{\varphi}} \quad \text{and} \quad M(0)=M_0(0)+M_1(0)+I_M(0).$$

Since

$$\mathbb{E}_{\alpha,\beta}(t) = t\mathbb{E}_{\beta,\alpha+\beta}(t)+\frac{1}{\Gamma(\beta)}, \tag{46}$$

following Eq. (46), the relation in Eq. (45) convert to

$$\begin{aligned} M(t) &\leq \frac{\Lambda^{\varphi}}{\mu^{\varphi}} + \frac{ABC(\varphi)}{ABC(\varphi) - (1-\varphi)\mu^{\varphi}} \\ &\times \left[M(0) - \frac{\Lambda^{\varphi}}{\mu^{\varphi}} \right] \times \mathbb{E}_{\varphi,1}\left(-\ell t^{\varphi}\right). \end{aligned} \tag{47}$$

It follows from Eq. (47) that $M(t) \leq \frac{\Lambda^{\varphi}}{\mu^{\varphi}} = \Gamma_2$ as $t \to \infty$. Thus, the macrophages cells population is bounded. That is $M_0 \leq \frac{\Lambda^{\varphi}}{\mu^{\varphi}}$, $M_1 \leq \frac{\Lambda^{\varphi}}{\mu^{\varphi}}$ and $I_M \leq \frac{\Lambda^{\varphi}}{\mu^{\varphi}}$.

Considering the virus population, the following is obtained:

$$ {}_0^{ABC}\mathbb{D}_t^{\varphi} V(t) = \Lambda_V^{\varphi} + \omega^{\varphi} I_M - \mu_V^{\varphi} V - \delta_3^{\varphi} T_2 V - \delta_4^{\varphi} A V - \psi^{\varphi} V. $$

It follows that

$$ {}_0^{ABC}\mathbb{D}_t^{\varphi} V(t) \leq \Lambda_V^{\varphi} - \mu_V^{\varphi} V + \omega^{\varphi} \Gamma_2. $$

But $\Gamma_2 = \frac{\Lambda^{\varphi}}{\mu^{\varphi}} = I_M$. Hence,

$$ {}_0^{ABC}\mathbb{D}_t^{\varphi} \left[V(t) \right] \leq \Lambda_V^{\varphi} - \mu_V^{\varphi} V. \tag{48}$$

By applying the Laplace transform to both sides of Eq. (48), the following was obtained:

$$\begin{aligned} V(t) &\leq \left[\frac{ABC(\varphi) V(0)}{ABC(\varphi) - (1-\varphi)\mu_V^{\varphi}} + \frac{(1-\varphi)\Lambda_V^{\varphi}}{ABC(\varphi) - (1-\varphi)\mu_V^{\varphi}} \right] \times \mathbb{E}_{\varphi,1}\left(-\ell t^{\varphi}\right) \\ &+ \frac{\varphi \Lambda_V^{\varphi}}{ABC(\varphi) - (1-\varphi)\mu_V^{\varphi}} \times \mathbb{E}_{\varphi,\varphi+1}\left(-\ell t^{\varphi}\right), \end{aligned} \tag{49}$$

where

$$ \ell = \frac{\varphi \mu_V^{\varphi}}{ABC(\varphi) - (1-\varphi)\mu_V^{\varphi}} \quad \text{and} \quad V(0) = V_0. $$

Since

$$\mathbb{E}_{\alpha,\beta}(t) = t\mathbb{E}_{\alpha,\alpha+\beta}(t) + \frac{1}{\Gamma(\beta)}, \tag{50}$$

following Eq. (50), the expression in Eq. (49) changes to

$$\begin{aligned} V(t) \leq & \frac{\Lambda_V^{\varphi}}{\mu_V^{\varphi}} + \frac{ABC(\varphi)}{ABC(\varphi) - (1-\varphi)\mu_V^{\varphi}} \\ & \times \left[M(0) - \frac{\Lambda_V^{\varphi}}{\mu_V^{\varphi}} \right] \times \mathbb{E}_{\varphi,1}\left(-\ell t^{\varphi}\right). \end{aligned} \tag{51}$$

It follows from Eq. (51) that $V(t) \leq \frac{\Lambda_V^{\varphi}}{\mu_V^{\varphi}} = \Gamma_3$ as $t \to \infty$. Thus, the virus population is bounded.

Considering the humoral immune response (antibodies) population, the following was obtained:

$${}_0^{ABC}\mathbb{D}_t^{\varphi} A(t) = \Lambda_A^{\varphi} + \psi^{\varphi} V - \delta_4^{\varphi} AV - \mu_A^{\varphi} A.$$

It follows that

$${}_0^{ABC}\mathbb{D}_t^{\varphi} A(t) \leq \Lambda_A^{\varphi} + \psi^{\varphi}\Gamma_3 - \mu_A^{\varphi} A$$

But $\Gamma_3 = \frac{\Lambda_V^{\varphi}}{\mu_V^{\varphi}} = V$. Hence,

$${}_0^{ABC}\mathbb{D}_t^{\varphi}\left[A(t)\right] \leq \Lambda_A^{\varphi} - \mu_A^{\varphi} A. \tag{52}$$

By applying the Laplace transform to both sides of Eq. (52), the following was obtained:

$$\begin{aligned} A(t) \leq & \left[\frac{ABC(\varphi)A(0)}{ABC(\varphi) - (1-\varphi)\mu_A^{\varphi}} + \frac{(1-\varphi)\Lambda_A^{\varphi}}{ABC(\varphi) - (1-\varphi)\mu_A^{\varphi}} \right] \times \mathbb{E}_{\varphi,1}\left(-\ell t^{\varphi}\right) \\ & + \frac{\varphi\Lambda_A^{\varphi}}{ABC(\varphi) - (1-\varphi)\mu_A^{\varphi}} \times \mathbb{E}_{\varphi,\varphi+1}\left(-\ell t^{\varphi}\right), \end{aligned} \tag{53}$$

where

$$\ell = \frac{\varphi\mu_A}{ABC(\varphi)-(1-\varphi)\mu_A^{\varphi}} \quad \text{and} \quad A(0)=A_0.$$

Since

$$\mathbb{E}_{\alpha,\beta}(t) = t\mathbb{E}_{\alpha,\alpha+\beta}(t)+\frac{1}{\Gamma(\beta)}, \tag{54}$$

following Eq. (54), the relation in Eq. (53) convert to

$$\begin{aligned} A(t) \leq & \frac{\Lambda_A^{\varphi}}{\mu_A^{\varphi}}+\frac{ABC(\varphi)}{ABC(\varphi)-(1-\varphi)\mu_A^{\varphi}} \\ & \times\left[A(0)-\frac{\Lambda_A^{\varphi}}{\mu_A^{\varphi}}\right]\times\mathbb{E}_{\varphi,1}\left(-\ell t^{\varphi}\right). \end{aligned} \tag{55}$$

It follows from Eq. (55) that $A(t) \leq \frac{\Lambda_A^{\varphi}}{\mu_A^{\varphi}} = \Gamma_4$ as $t \to \infty$. Thus, the antibodies population is bounded.

Considering the effector B cell population, the following was obtained:

$${}_0^{ABC}\mathbb{D}_t^{\varphi}E(t) = \Lambda_E^{\varphi}-\delta_2^{\varphi}\left(1+\chi_2^{\varphi}F_2\right)I_M E+\sigma^{\varphi}I_M E-\mu_E^{\varphi}E.$$

It follows that

$${}_0^{ABC}\mathbb{D}_t^{\varphi}E(t) \leq \Lambda_E^{\varphi}+\sigma^{\varphi}\Gamma_2 E-\mu_E^{\varphi}E.$$

But $\Gamma_2 = \frac{\Lambda^{\varphi}}{\mu^{\varphi}} = I_M$. Hence,

$${}_0^{ABC}\mathbb{D}_t^{\varphi}\left[E(t)\right] \leq \Lambda_E^{\varphi}-\mu_E^{\varphi}E. \tag{56}$$

By applying the Laplace transform to both sides of Eq. (56), the following was

obtained:

$$E(t) \leq \left[\frac{ABC(\varphi)E(0)}{ABC(\varphi)-(1-\varphi)\mu_E^{\varphi}}+\frac{(1-\varphi)\Lambda_E^{\varphi}}{ABC(\varphi)-(1-\varphi)\mu_E^{\varphi}}\right]\times \mathbb{E}_{\varphi,1}\left(-\ell t^{\varphi}\right) + \frac{\varphi\Lambda_E^{\varphi}}{ABC(\varphi)-(1-\varphi)\mu_E^{\varphi}}\times \mathbb{E}_{\varphi,\varphi+1}\left(-\ell t^{\varphi}\right), \tag{57}$$

where

$$\ell = \frac{\varphi\mu_E^{\varphi}}{ABC(\varphi)-(1-\varphi)\mu_E^{\varphi}} \quad \text{and} \quad E(0)=E_0.$$

Since

$$\mathbb{E}_{\alpha,\beta}(g) = t\mathbb{E}_{\alpha,\alpha+\beta}(t)+\frac{1}{\Gamma(\beta)}, \tag{58}$$

following Eq. (58), the relation in Eq. (57) convert to

$$E(t) \leq \frac{\Lambda_E^{\varphi}}{\mu_E^{\varphi}}+\frac{ABC(\varphi)}{ABC(\varphi)-(1-\varphi)\mu_E^{\varphi}} \times\left[E(0)-\frac{\Lambda_E^{\varphi}}{\mu_E^{\varphi}}\right]\times \mathbb{E}_{\varphi,1}\left(-\ell t^{\varphi}\right). \tag{59}$$

It follows from Eq. (59) that

$$E(t)\leq \frac{\Lambda_E^{\varphi}}{\mu_E^{\varphi}} = \Gamma_5,$$

as $t\to\infty$. Thus, the effector B cells population is bounded.

Considering the natural killer cell population, the following was obtained:

$${}_0^{ABC}\mathbb{D}_t^{\varphi}N_K(t) = \Lambda_{N_K}^{\varphi}-\delta_1^{\varphi}\left(1+\chi_1^{\varphi}F_1\right)I_M N_K+\theta_1^{\varphi}F_1+\theta_2^{\varphi}F_2 - \left(\eta^{\varphi}+\mu_{N_K}^{\varphi}\right)N_K.$$

It follows that

$${}_0^{ABC}\mathbb{D}_t^{\varphi}N_K(t) \leq \Lambda_{N_K}^{\varphi}-\mu_{N_K}^{\varphi}N_K+\theta_1^{\varphi}\Gamma_8+\theta_2^{\varphi}\Gamma_9.$$

But $\Gamma_8 = \frac{\varepsilon^{\varphi}}{\mu_{F_1}^{\varphi}}$ and $\Gamma_9 = \frac{\eta^{\varphi}}{\mu_{F_2}^{\varphi}}$. Hence,

$$ {}_0^{ABC}\mathbb{D}_t^{\varphi}\left[N_K(t)\right] \leq \Lambda_{N_K}^{\varphi} - \mu_{N_K}^{\varphi} N_K. \tag{60} $$

By applying the Laplace transform to both sides of Eq. (60), the following was obtained:

$$ \begin{aligned} N_K(t) \leq & \left[\frac{ABC(\varphi)N_K(0)}{ABC(\varphi)-(1-\varphi)\mu_{N_K}^{\varphi}} + \frac{(1-\varphi)\Lambda_{N_K}^{\varphi}}{ABC(\varphi)-(1-\varphi)\mu_{N_K}^{\varphi}}\right] \\ & \times \mathbb{E}_{\varphi,1}\left(-\ell t^{\varphi}\right) + \frac{\varphi\Lambda_{N_K}^{\varphi}}{ABC(\varphi)-(1-\varphi)\mu_{N_K}^{\varphi}} \\ & \times \mathbb{E}_{\varphi,\varphi+1}\left(-\ell t^{\varphi}\right), \end{aligned} \tag{61} $$

where

$$ \ell = \frac{\varphi\mu_{N_K}^{\varphi}}{ABC(\varphi)-(1-\varphi)\mu_{N_K}^{\varphi}} \quad \text{and} \quad N_K(0) = N_{K^{\star}}. $$

Since

$$ \mathbb{E}_{\alpha,\beta}(t) = t\mathbb{E}_{\alpha,\alpha+\beta}(g) + \frac{1}{\Gamma(\beta)}, \tag{62} $$

following Eq. (62), the relation in Eq. (61) convert to

$$ \begin{aligned} E(t) \leq & \frac{\Lambda_{N_K}^{\varphi}}{\mu_{N_K}^{\varphi}} + \frac{ABC(\varphi)}{ABC(\varphi)-(1-\varphi)\mu_{N_K}^{\varphi}} \\ & \times \left[N_K(0) - \frac{\Lambda_{N_K}^{\varphi}}{\mu_{N_K}^{\varphi}}\right] \times \mathbb{E}_{\varphi,1}\left(-\ell t^{\varphi}\right). \end{aligned} \tag{63} $$

It follows from Eq. (63) that $N_K(t) \leq \frac{\Lambda_{N_K}^{\varphi}}{\mu_{N_K}^{\varphi}} = \Gamma_6$ as $t \to \infty$. Thus, natural killer cells population is bounded.

Considering the anti-inflammatory cytokine (i.e., interleukin-10) population, the following was obtained:

$$ {}_0^{ABC}\mathbb{D}_t^{\varphi} I_{10}(t) = \rho_3^{\varphi} I_M T_0 \left(\frac{1}{1+\tau_1^{\varphi} I_{10}}\right) - \mu_{I_{10}}^{\varphi} I_{10}. $$

It follows that

$$ {}_{0}^{ABC}\mathbb{D}_{t}^{\varphi} I_{10}(t) \leq \rho_3^{\varphi}\Gamma_1\Gamma_2\left(\frac{1}{1+\tau_1^{\varphi} I_{10}}\right) - \mu_{I_{10}} I_{10}. \tag{64} $$

But $\Gamma_1 = \frac{\Lambda_{T_0}^{\varphi}}{\mu^{\varphi}} = T_0$ and $\Gamma_2 = \frac{\Lambda^{\varphi}}{\mu^{\varphi}} = I_M$. By applying the Laplace transform to both sides of Eq. (64), the following was obtained:

$$ \begin{aligned} I_{10}(t) \leq & \left[\frac{ABC(\varphi) I_{10}(0)}{ABC(\varphi)-(1-\varphi)\mu_{I_{10}}^{\varphi}} + \frac{(1-\varphi)\rho_3^{\varphi}}{ABC(\varphi)-(1-\varphi)\mu_{I_{10}}^{\varphi}}\right] \times \mathbb{E}_{\varphi,1}\left(-\ell t^{\varphi}\right) \\ & + \frac{\varphi\rho_3^{\varphi}}{ABC(\varphi)-(1-\varphi)\mu_{I_{10}}^{\varphi}} \times \mathbb{E}_{\varphi,\varphi+1}\left(-\ell t^{\varphi}\right), \end{aligned} \tag{65} $$

where

$$ \ell = \frac{\varphi\mu_{I_{10}}^{\varphi}}{ABC(\varphi)-(1-\varphi)\mu_{I_{10}}^{\varphi}} \quad \text{and} \quad I_{10}(0) = I_{10^{\star}}. $$

Since

$$ \mathbb{E}_{\alpha,\beta}(t) = t\mathbb{E}_{\alpha,\alpha+\alpha}(t) + \frac{1}{\Gamma(\beta)}, \tag{66} $$

following Eq. (66), the relation in Eq. (65) convert to

$$ \begin{aligned} I_{10}(t) \leq & \frac{\rho_3^{\varphi}}{\mu_{I_{10}}^{\varphi}} + \frac{ABC(\varphi)}{ABC(\varphi)-(1-\varphi)\mu_{I_{10}}^{\varphi}} \\ & \times \left[I_{10}(0) - \frac{\rho_3^{\varphi}}{\mu_{I_{10}}^{\varphi}}\right] \times \mathbb{E}_{\varphi,1}\left(-\ell t^{\varphi}\right). \end{aligned} \tag{67} $$

It follows from Eq. (67) that $I_{10}(t) \leq \frac{\rho_3^{\varphi}}{\mu_{I_{10}}^{\varphi}} = \Gamma_7$ as $t \to \infty$. Thus, the interleukin-10 population is bounded.

Considering the anti-inflammatory cytokine (i.e., type-1 interferon) population, the following was obtained:

$$ {}_{0}^{ABC}\mathbb{D}_{t}^{\varphi} F_1(t) = \varepsilon^{\varphi} I_M - \left(\theta_1^{\varphi} + \mu_{F_1}^{\varphi}\right) F_1. $$

It follows that

$$ {}_{0}^{ABC}\mathbb{D}_{t}^{\varphi} F_1(t) \leq \varepsilon^{\varphi}\Gamma_2 - \mu_{F_1}^{\varphi} F_1. \tag{68} $$

But $\Gamma_2 = \frac{\Lambda^{\varphi}}{\mu^{\varphi}} = I_M$. By applying the Laplace transform to both sides of Eq. (68), the following was obtained:

$$ \begin{aligned} F_1(t) \leq & \left[\frac{ABC(\varphi)F_1(0)}{ABC(\varphi)-(1-\varphi)\mu_{F_1}^{\varphi}} + \frac{(1-\varphi)\varepsilon^{\varphi}}{ABC(\varphi)-(1-\varphi)\mu_{F_1}^{\varphi}}\right] \times \mathbb{E}_{\varphi,1}\left(-\ell t^{\varphi}\right) \\ & + \frac{\varphi\varepsilon^{\varphi}}{ABC(\varphi)-(1-\varphi)\mu_{F_1}^{\varphi}} \times \mathbb{E}_{\varphi,\varphi+1}\left(-\ell t^{\varphi}\right), \end{aligned} \tag{69} $$

where

$$ \ell = \frac{\varphi\mu_{F_1}^{\varphi}}{ABC(\varphi)-(1-\varphi)\mu_{F_1}^{\varphi}} \quad \text{and} \quad F_1(0) = F_{1^{\star}}. $$

Since

$$ \mathbb{E}_{\alpha,\beta}(t) = t\mathbb{E}_{\alpha,\alpha+\beta}(t) + \frac{1}{\Gamma(\beta)}, \tag{70} $$

following Eq. (70), the relation in Eq. (69) convert to

$$ \begin{aligned} F_1(t) \leq & \frac{\varepsilon^{\varphi}}{\mu_{F_1}^{\varphi}} + \frac{ABC(\varphi)}{ABC(\varphi)-(1-\varphi)\mu_{F_1}^{\varphi}} \\ & \times \left[F_1(0) - \frac{\varepsilon^{\varphi}}{\mu_{F_1}^{\varphi}}\right] \times \mathbb{E}_{\varphi,1}\left(-\ell t^{\varphi}\right). \end{aligned} \tag{71} $$

It follows from Eq. (71) that $F_{10}(t) \leq \frac{\varepsilon^{\varphi}}{\mu_{F_1}^{\varphi}} = \Gamma_8$ as $t \to \infty$. Thus, the type-1 interferon population is bounded.

Finally, considering the type-2 interferon population, the following was obtained:

$$ {}_{0}^{ABC}\mathbb{D}_{t}^{\varphi} F_2(t) = \eta^{\varphi} N_K - \left(\theta_2^{\varphi} + \mu_{F_2}^{\varphi}\right) F_2. $$

It follows that

$$ {}_{0}^{ABC}\mathbb{D}_{t}^{\varphi} F_2(t) \leq \eta^{\varphi}\Gamma_6 - \mu_{F_2} F_2. \tag{72} $$

But $\Gamma_6 = \frac{\Lambda_{N_K}^{\varphi}}{\mu_{N_K}^{\varphi}} = N_K$. By applying the Laplace transform to both sides of Eq. (72), the following was obtained:

$$ \begin{aligned} F_1(t) \leq & \left[\frac{ABC(\varphi)F_2(0)}{ABC(\varphi)-(1-\varphi)\mu_{F_2}^{\varphi}} + \frac{(1-\varphi)\eta^{\varphi}}{ABC(\varphi)-(1-\varphi)\mu_{F_2}^{\varphi}}\right] \times \mathbb{E}_{\varphi,1}\left(-\ell t^{\varphi}\right) \\ & + \frac{\varphi\eta^{\varphi}}{ABC(\varphi)-(1-\varphi)\mu_{F_2}^{\varphi}} \times \mathbb{E}_{\varphi,\varphi+1}\left(-\ell t^{\varphi}\right), \end{aligned} \tag{73} $$

where

$$ \ell = \frac{\varphi\mu_{F_2}^{\varphi}}{ABC(\varphi)-(1-\varphi)\mu_{F_2}^{\varphi}} \quad \text{and} \quad F_2(0) = F_{2^{\star}}. $$

Since

$$ \mathbb{E}_{\alpha,\beta}(t) = t\mathbb{E}_{\alpha,\alpha+\beta}(t) + \frac{1}{\Gamma(\beta)}, \tag{74} $$

following Eq. (74), the relation in Eq. (73) convert to

$$ \begin{aligned} F_2(t) \leq & \frac{\eta^{\varphi}}{\mu_{F_2}^{\varphi}} + \frac{ABC(\varphi)}{ABC(\varphi)-(1-\varphi)\mu_{F_2}^{\varphi}} \\ & \times \left[F_2(0) - \frac{\varepsilon^{\varphi}}{\mu_{F_2}^{\varphi}}\right] \times \mathbb{E}_{\varphi,1}\left(-\ell t^{\varphi}\right). \end{aligned} \tag{75} $$

It follows from Eq. (75) that $F_2(t) \leq \frac{\eta^{\varphi}}{\mu_{F_2}^{\varphi}} = \Gamma_9$ as $t \to \infty$. Thus, the type-1 interferon population is bounded. Thus, all solutions belong to the set Δ. Consequently, the closed set Δ is positively invariant.

Model Analysis

We begin the model analysis by looking at the virus-free equilibrium state.

Virus-free Equilibrium State (VFE)

At the virus-free equilibrium state, the complete absence of the hepatitis B virus signifies the eradication of infected macrophages. This eradication results from the fact that uninfected macrophages have no pathogen to engulf, thus precluding infection. Consequently, $V^\star = 0$ necessitates that $I_M^\star = 0$ and $F_1^\star = 0$. It follows that $A^\star = 0$, $E^\star = 0$, $N_K^\star = 0$ and $F_2^\star = 0$. Thus at the virus-free equilibrium, the following equations are satisfied

$$\left.\begin{aligned} \Lambda_{T_0}^{\varphi} - \mu_{T_0}^{\varphi} T_0^\star &= 0, \\ -\mu_{T_1}^{\varphi} T_1^\star &= 0, \\ -\mu_{T_2}^{\varphi} T_2^\star &= 0, \\ \Lambda_{M_0}^{\varphi} - \mu_{M_0}^{\varphi} M_0^\star &= 0, \\ \Lambda_{M_0}^{\varphi} - \mu_{M_0}^{\varphi} M_0^\star &= 0, \\ -\mu_{I_{10}}^{\varphi} I_{10}^\star &= 0. \end{aligned}\right\} \tag{76}$$

Therefore, at the virus-free equilibrium,

$$\varepsilon_0 = (T_0^\star, T_1^\star, T_2^\star, M_0^\star, M_1^\star, I_M^\star, V^\star, A^\star, E^\star, N_K^\star, I_{10}^\star, F_1^\star, F_2^\star),$$

populations of all species involved in the immune interactions are given by

$$\varepsilon_0 = \left(\frac{\Lambda_{T_0}^{\varphi}}{\mu_{T_0}^{\varphi}}, 0, 0, \frac{\Lambda_{M_0}^{\varphi}}{\mu_{M_0}^{\varphi}}, \frac{\Lambda_{M_1}^{\varphi}}{\mu_{M_1}^{\varphi}}, 0, 0, 0, 0, 0, 0, 0, 0\right).$$

Basic Reproduction Number; $\mathcal{R}_0$

Subsequently, the infection reproduction number of the model system was determined using the Next Generation Matrix methodology, as outlined by (Diekmann & Heesterbeek, 2000) and applied in (Chataa et al., 2021). The process begins with an examination of the equations within the model system that describe the proliferation of newly infected macrophages and the transitions in the infected macrophage

state. These equations are articulated as follows:

$$\left.\begin{aligned} {}_0^{ABC}\mathbb{D}_t^{\varphi} I_M(t) &= \beta_1^{\varphi} V M_0 + \beta_2^{\varphi} V M_1 + \pi^{\varphi} I_M T_1 - \delta_1 \left(1 + \chi_1^{\varphi} F_1\right) I_M N_K \\ &\quad - \delta_2^{\varphi} \left(1 + \chi_2^{\varphi} F_2\right) I_M E - \sigma^{\varphi} I_M E - \mathfrak{E} I_M, \\ {}_0^{ABC}\mathbb{D}_t^{\varphi} V(t) &= \Lambda_V^{\varphi} + \omega^{\varphi} I_M - \delta_3^{\varphi} T_2 V - \delta_4^{\varphi} A V - \left(\psi^{\varphi} + \mu_V^{\varphi}\right) V. \\ \text{where} \quad \mathfrak{E} &= \left(\omega^{\varphi} + \varepsilon^{\varphi} + \zeta^{\varphi} + \mu_{I_M}^{\varphi}\right) \end{aligned}\right\} \tag{77}$$

This ensemble of equations in system 77 is designated as the infected subsystem. Adhering to the established protocol of the Next Generation Matrix methodology, the initial step involves linearizing the infected subsystem around the virus-free steady state. If $\mathbb{X}$ is stipulated as

$$\mathbb{X} = \left(T_0, T_1, T_2, M_0, M_1, I_M, V, A, E, N_K, I_{10}, F_1, F_2\right)^T,$$

where T denotes the transpose, the infected subsystem can subsequently be expressed in the following configuration

$${}_0^{ABC}\mathbb{D}_t^{\varphi}\mathbb{X}(t) = \mathbb{F}(\mathbb{X}) - \mathbb{V}(\mathbb{X}),$$

where

$$\mathbb{F}(\mathbb{X}) = \begin{pmatrix} \beta_1^{\varphi} V M_0 + \beta_2^{\varphi} V M_1 + \pi^{\varphi} I_M T_1 \\ 0 \end{pmatrix} \quad \text{and}$$

$$\mathbb{V}(\mathbb{X}) = \begin{pmatrix} \delta_1^{\varphi} \left(1 + \chi_1^{\varphi} F_1\right) I_M N_K + \delta_2^{\varphi} \left(1 + \chi_2^{\varphi} F_2\right) I_M E + \sigma^{\varphi} I_M E + \mathfrak{E} I_M \\ -\Lambda_V^{\varphi} - \omega^{\varphi} I_M + \delta_3^{\varphi} T_2 V + \delta_4^{\varphi} A V + \left(\psi^{\varphi} + \mu_V^{\varphi}\right) V \end{pmatrix}.$$

Computing the Jacobian matrix of $\mathbb{F}(\mathbb{X})$ at the virus-free equilibrium state gives

$$F = \begin{pmatrix} 0 & \beta_1^{\varphi} M_0^{\star} + \beta_2^{\varphi} M_1^{\star} \\ 0 & 0 \end{pmatrix}$$

By employing substitution, the following expression was derived.

$$F = \begin{pmatrix} 0 & \frac{\beta_1^{\varphi}\Lambda_{M_0}^{\varphi}}{\mu_{M_0}^{\varphi}} + \frac{\beta_2\Lambda_{M_1}^{\varphi}}{\mu_{M_1}^{\varphi}} \\ 0 & 0 \end{pmatrix}.$$

Additionally, by computing the Jacobian matrix of $\mathbb{V}(\mathbb{X})$ at the virus-free equilibrium and performing substitution gives

$$V = \begin{pmatrix} \left(\omega^{\varphi} + \varepsilon^{\varphi} + \zeta^{\varphi} + \mu_{I_M}^{\varphi}\right) & 0 \\ \omega^{\varphi} & \left(\psi^{\varphi} + \mu_V^{\varphi}\right) \end{pmatrix}.$$

It follows that

$$V = \begin{pmatrix} A & 0 \\ -\omega & B \end{pmatrix},$$

where

$$\begin{aligned} A &= \left(\omega^{\varphi} + \varepsilon^{\varphi} + \zeta^{\varphi} + \mu_{I_M}^{\varphi}\right), \\ B &= \left(\psi^{\varphi} + \mu_V^{\varphi}\right). \end{aligned}$$

Hence,

$$V^{-1} = \begin{pmatrix} \frac{1}{A} & 0 \\ \frac{\omega^{\varphi}}{AB} & \frac{1}{B} \end{pmatrix}.$$

Thus, the Next Generation Matrix, which encapsulates the aggregate infectiousness of hepatic cells throughout the entire infection period, is delineated as

$$\begin{aligned} FV^{-1} &= \begin{pmatrix} 0 & \beta_1^{\varphi}M_0^{\star} + \beta_2^{\varphi}M_1^{\star} \\ 0 & 0 \end{pmatrix} \begin{pmatrix} \frac{1}{A} & 0 \\ \frac{\omega^{\varphi}}{AB} & \frac{1}{B} \end{pmatrix} \\ &= \begin{pmatrix} \frac{\omega^{\varphi}}{AB}\left[\frac{\beta_1^{\varphi}\Lambda_{M_0}^{\varphi}}{\mu_{M_0}^{\varphi}} + \frac{\beta_2^{\varphi}\Lambda_{M_1}^{\varphi}}{\mu_{M_1}^{\varphi}}\right] & \frac{1}{B}\left[\frac{\beta_1^{\varphi}\Lambda_{M_0}^{\varphi}}{\mu_{M_0}^{\varphi}} + \frac{\beta_2^{\varphi}\Lambda_{M_1}^{\varphi}}{\mu_{M_1}^{\varphi}}\right] \\ 0 & 0 \end{pmatrix}. \end{aligned}$$

Since the matrix FV^{-1} is an upper triangular matrix, it follows that the eigenvalues correspond to the elements on the principal diagonal. Consequently,

$$\varrho_1 = \frac{\omega^{\varphi}}{AB}\left[\frac{\beta_1^{\varphi}\Lambda_{M_0}^{\varphi}}{\mu_{M_0}^{\varphi}} + \frac{\beta_2^{\varphi}\Lambda_{M_1}^{\varphi}}{\mu_{M_1}^{\varphi}}\right] \quad \varrho_2 = 0.$$

Since $\mathcal{R}_0 = \max\left[|\varrho_1||\varrho_2|\right]$ represents the spectral radius of FV^{-1}, the following holds at the virus-free equilibrium.

$$\mathcal{R}_0 = \frac{\omega^{\varphi}}{AB}\left[\frac{\beta_1^{\varphi}\Lambda_{M_0}^{\varphi}}{\mu_{M_0}^{\varphi}} + \frac{\beta_2^{\varphi}\Lambda_{M_1}^{\varphi}}{\mu_{M_1}^{\varphi}}\right].$$

By substitution, the $\mathbb{R}_0$ was obtain to be

$$\mathcal{R}_0 = \mathcal{R}_{M_0} + \mathcal{R}_{M_1},$$

where

$$\mathcal{R}_{M_0} = \frac{\beta_1^{\varphi}\omega^{\varphi}\Lambda_{M_0}^{\varphi}}{\mu_{M_0}^{\varphi}\left(\omega^{\varphi} + \varepsilon^{\varphi} + \zeta^{\varphi} + \mu_{I_M}^{\varphi}\right)\left(\psi^{\varphi} + \mu_V^{\varphi}\right)},$$

$$\mathcal{R}_{M_1} = \frac{\beta_2^{\varphi}\omega^{\varphi}\Lambda_{M_1}^{\varphi}}{\mu_{M_1}^{\varphi}\left(\omega^{\varphi} + \varepsilon^{\varphi} + \zeta^{\varphi} + \mu_{I_M}^{\varphi}\right)\left(\psi^{\varphi} + \mu_V^{\varphi}\right)}.$$

Existence and Uniqueness of Solutions

This section addresses the existence of solutions for the model under consideration, and if such solutions exist, they are proven to be unique. To establish the existence and uniqueness of solutions, the renowned Banach fixed-point theorem was employed. Let $B(S) = B(S) \times B(S) \times B(S) \times B(S) \times B(S) \times B(S) \times B(S) \times B(S) \times B(S) \times B(S) \times B(S) \times B(S) \times B(S)$ be a set, where $B(S) \in C\left[0, T\right]$ is a Banach space for an interval-defined continuous real-valued function defined on the

interval $S = [0, q]$ with the norm

$$\begin{aligned} & ||T_0, T_1, T_2, M_0, M_1, I_M, V, A, E, N_K, I_{10}, F_1, F_2|| \\ = \; & ||T_0|| + ||T_1|| + ||T_2|| + ||M_0|| + ||M_1|| + ||I_M|| + ||V|| + ||A|| + ||E|| \\ & + ||N_K|| + ||I_{10}|| + ||F_1|| + ||F_2||, \end{aligned}$$

where

$$||T_0|| = \sup_{t \in S} |T_0|, \quad ||T_1|| = \sup_{t \in S} |T_1|, \quad ||T_2|| = \sup_{t \in S} |T_2|,$$

$$||M_0|| = \sup_{t \in S} |M_0|, \quad ||M_1|| = \sup_{t \in S} |M_1|, \quad ||I_M|| = \sup_{t \in S} |I_M|,$$

$$||V|| = \sup_{t \in S} |V| \quad ,||A|| = \sup_{t \in S} |A|, \quad ||E|| = \sup_{t \in S} |E|,$$

$$||N_K|| = \sup_{t \in S} |N_K|, \quad ||I_{10}|| = \sup_{t \in S} |I_{10}|, \quad ||F_1|| = \sup_{t \in S} |F_1|,$$

$$||F_2|| = \sup_{t \in S} |F_2|.$$

The model system 39 can be written in terms of ABC integral operator as

$$\begin{cases} T_0(t)-T_0(0) & =_0^{ABC}\mathbb{I}_t^{\varphi}\Big\{\Lambda_{T_0}^{\varphi}-\rho_1^{\varphi}I_MT_0I_{10}-\rho_2^{\varphi}VT_0I_{10} \\ & \quad -\rho_3^{\varphi}T_0I_M\left(\frac{1}{1+\tau_1^{\varphi}I_{10}}\right)-\mu_{T_0}^{\varphi}T_0\Big\}, \\ T_1(t)-T_1(0) & =_0^{ABC}\mathbb{I}_t^{\varphi}\{\rho_1^{\varphi}I_MT_0I_{10}-\pi^{\varphi}I_MT_1-\mu_{T_1}^{\varphi}T_1\}, \\ T_2(t)-T_1(0) & =_0^{ABC}\mathbb{I}_t^{\varphi}\{\rho_2^{\varphi}VT_0I_{10}-\delta_3^{\varphi}T_2V-\mu_{T_2}^{\varphi}T_2\}, \\ M_0(t)-M_0(0) & =_0^{ABC}\mathbb{I}_t^{\varphi}\{\Lambda_{M_0}^{\varphi}-\beta_1^{\varphi}VM_0-\mu_{M_0}^{\varphi}M_0\}, \\ M_1(t)-M_1(0) & =_0^{ABC}\mathbb{I}_t^{\varphi}\{\Lambda_{M_1}^{\varphi}-\beta_2^{\varphi}VM_1+\zeta^{\varphi}I_M-\mu_{M_1}^{\varphi}M_1\}, \\ I_M(t)-I_M(0) & =_0^{ABC}\mathbb{I}_t^{\varphi}\{\beta_1^{\varphi}VM_0+\beta_2^{\varphi}VM_1+\pi^{\varphi}I_MT_1 \\ & \quad -\delta_1^{\varphi}\left(1+\chi_1^{\varphi}F_1\right)I_MN_K-\delta_2^{\varphi}\left(1+\chi_2^{\varphi}F_2\right)I_ME \\ & \quad -\sigma^{\varphi}I_ME-\left(\omega^{\varphi}+\varepsilon^{\varphi}+\zeta^{\varphi}+\mu_{I_M}^{\varphi}\right)I_M\}, \\ V(t)-V(0) & =_0^{ABC}\mathbb{I}_t^{\varphi}\{\Lambda_V^{\varphi}+\omega^{\varphi}I_M-\delta_3^{\varphi}T_2V-\delta_4^{\varphi}AV \\ & \quad -\left(\psi^{\varphi}+\mu_V^{\varphi}\right)V\}, \\ A(t)-A(0) & =_0^{ABC}\mathbb{I}_t^{\varphi}\{\Lambda_A^{\varphi}+\psi^{\varphi}V-\delta_4^{\varphi}AV-\mu_A^{\varphi}A\}, \\ E(t)-E(0) & =_0^{ABC}\mathbb{I}_t^{\varphi}\{\Lambda_E^{\varphi}-\delta_2^{\varphi}\left(1+\chi_2^{\varphi}F_2\right)I_ME \\ & \quad +\sigma^{\varphi}I_ME-\mu_E^{\varphi}E\}, \\ N_K(t)-N_K(0) & =_0^{ABC}\mathbb{I}_t^{\varphi}\{\Lambda_{N_K}^{\varphi}-\delta_1^{\varphi}\left(1+\chi_1^{\varphi}F_1\right)I_MN_K+\theta_1^{\varphi}F_1 \\ & \quad +\theta_2^{\varphi}F_2-\left(\eta^{\varphi}+\mu_{N_K}^{\varphi}\right)N_K\}, \\ I_{10}(t)-I_{10}(0) & =_0^{ABC}\mathbb{I}_t^{\varphi}\left\{\rho_3^{\varphi}I_MT_0\left(\frac{1}{1+\tau_1^{\varphi}I_{10}}\right)-\mu_{I_{10}}^{\varphi}I_{10}\right\}, \\ F_1(t)-F_1(0) & =_0^{ABC}\mathbb{I}_t^{\varphi}\{\varepsilon^{\varphi}I_M-\left(\theta_1^{\varphi}+\mu_{F_1}^{\varphi}\right)F_1\}, \\ F_2(t)-F_2(0) & =_0^{ABC}\mathbb{I}_t^{\varphi}\{\eta^{\varphi}N_K-\left(\theta_2^{\varphi}+\mu_{F_2}^{\varphi}\right)F_2\}. \end{cases} \tag{78}$$

Applying definition 9 in Eq. (78) yields Eq. (79), Eq. (80), and Eq. (81).

$$
\begin{aligned}
T_0(t) - T_{0^\star} &= \frac{1-\varphi}{\mathbb{N}(\varphi)}\Bigg\{\Lambda_{T_0}^{\varphi} - \rho_1^{\varphi} I_M(t) T_0(t) I_{10}(t) - \rho_2^{\varphi} V(t) T_0(t) I_{10}(t) \\
&\quad -\rho_3^{\varphi} T_0(t) I_M(t)\left(\frac{1}{1+\tau_1^{\varphi} I_{10}}\right) - \mu_{T_0}^{\varphi} T_0(t)\Bigg\} \\
&\quad +\frac{\varphi}{\mathbb{N}(\varphi)\Gamma(\varphi)} \times \int_0^t (t-\nu)^{\varphi-1}\Bigg\{\Lambda_{T_0}^{\varphi} - \rho_1^{\varphi} I_M(\nu) T_0(\nu) I_{10}(\nu) \\
&\quad -\rho_2^{\varphi} V(\nu) T_0(\nu) I_{10}(\nu) - \rho_3^{\varphi} T_0(\nu) I_M(\nu)\left(\frac{1}{1+\tau_1^{\varphi} I_{10}}\right) \\
&\quad -\mu_{T_0}^{\varphi} T_0(\nu)\Bigg\} d\nu, \\
T_1(t) - T_{1^\star} &= \frac{1-\varphi}{\mathbb{N}(\varphi)}\left(\rho_1^{\varphi} I_M(t) T_0(t) I_{10}(t) - \pi^{\varphi} I_M(t) T_1(t) - \mu_{T_1}^{\varphi} T_1(t)\right) \\
&\quad +\frac{\varphi}{\mathbb{N}(\varphi)\Gamma(\varphi)} \times \int_0^t (t-\nu)^{\varphi-1}\left\{\rho_1^{\varphi} I_M(\nu) T_0(\nu) I_{10}(\nu)\right. \\
&\quad \left.-\pi^{\varphi} I_M(\nu) T_1(\nu) - \mu_{T_1}^{\varphi} T_1(\nu)\right\} d\nu, \qquad (79) \\
T_2(t) - T_{2^\star} &= \frac{1-\varphi}{\mathbb{N}(\varphi)}\left(\rho_2^{\varphi} V(t) T_0(t) I_{10}(t) - \delta_3^{\varphi} T_2(t) V(t) - \mu_{T_2}^{\varphi} T_2(t)\right) \\
&\quad +\frac{\varphi}{\mathbb{N}(\varphi)\Gamma(\varphi)} \times \int_0^t (t-\nu)^{\varphi-1}\left\{\rho_2^{\varphi} V(\nu) T_0(\nu) I_{10}(\nu)\right. \\
&\quad \left.-\delta_3^{\varphi} T_2(\nu) V(\nu) - \mu_{T_2}^{\varphi} T_2(\nu)\right\} d\nu, \\
M_0(t) - M_{0^\star} &= \frac{1-\varphi}{\mathbb{N}(\varphi)}\left(\Lambda_{M_0}^{\varphi} - \beta_1^{\varphi} V(t) M_0(t) - \mu_{M_0}^{\varphi} M_0(t)\right) \\
&\quad +\frac{\varphi}{\mathbb{N}(\varphi)\Gamma(\varphi)} \times \int_0^t (t-\nu)^{\varphi-1}\left\{\Lambda_{M_0}^{\varphi} - \beta_1^{\varphi} V(\nu) M_0(\nu)\right. \\
&\quad \left.-\mu_{M_0}^{\varphi} M_0(\nu)\right\} d\nu, \\
M_1(t) - M_{1^\star} &= \frac{1-\varphi}{\mathbb{N}(\varphi)}\left(\Lambda_{M_1}^{\varphi} - \beta_2^{\varphi} V(t) M_1(t) + \zeta^{\varphi} I_M(t) - \mu_{M_1}^{\varphi} M_1(t)\right) \\
&\quad +\frac{\varphi}{\mathbb{N}(\varphi)\Gamma(\varphi)} \times \int_0^t (t-\nu)^{\varphi-1}\left\{\Lambda_{M_1}^{\varphi} - \beta_2^{\varphi} V(\nu) M_1(\nu)\right. \\
&\quad \left.+\zeta^{\varphi} I_M(\nu) - \mu_{M_1}^{\varphi} M_1(\nu)\right\} d\nu,
\end{aligned}
$$

$$
\begin{aligned}
I_M(t)-I_{M^\star} &= \frac{1-\varphi}{\mathbb{N}(\varphi)}\{\beta_1^\varphi V(t)M_0(t)+\beta_2^\varphi V(t)M_1(t)+\pi^\varphi I_M(t)T_1(t)\\
&\quad -\delta_1^\varphi\left(1+\chi_1^\varphi F_1(t)\right)I_M(t)N_K(t)\\
&\quad -\sigma^\varphi I_M(t)E(t)-\left(\omega^\varphi+\varepsilon^\varphi+\zeta^\varphi+\mu_{I_M}^\varphi\right)I_M(t)\}\\
&\quad +\frac{\varphi}{\mathbb{N}(\varphi)\Gamma(\varphi)}\times\int_0^t(t-\nu)^{\varphi-1}\{\beta_1^\varphi V(\nu)M_0(\nu)\\
&\quad +\beta_2^\varphi V(\nu)M_1(\nu)+\pi^\varphi I_M(\nu)T_1(\nu)\\
&\quad -\delta_1^\varphi\left(1+\chi_1^\varphi F_1(\nu)\right)I_M(\nu)N_K(\nu)\\
&\quad -\delta_2^\varphi\left(1+\chi_2^\varphi F_2(\nu)\right)I_M(\nu)E(\nu)-\sigma^\varphi I_M(\nu)E(\nu)\\
&\quad -\left(\omega^\varphi+\varepsilon^\varphi+\zeta^\varphi+\mu_{I_M}^\varphi\right)I_M(\nu)\}d\nu,\\
V(t)-V_0 &= \frac{1-\varphi}{\mathbb{N}(\varphi)}\{\Lambda_V^\varphi+\omega^\varphi I_M(t)-\delta_3^\varphi T_2(t)V(t)-\delta_4^\varphi A(t)V(t)\\
&\quad -\left(\psi^\varphi+\mu_V^\varphi\right)V(t)\}\\
&\quad +\frac{\varphi}{\mathbb{N}(\varphi)\Gamma(\varphi)}\times\int_0^t(t-\nu)^{\varphi-1}\{\Lambda_V^\varphi+\omega^\varphi I_M(\nu)\\
&\quad -\delta_3^\varphi T_2(\nu)V(\nu)-\delta_4^\varphi A(\nu)V(\nu)-\left(\psi^\varphi+\mu_V^\varphi\right)V(\nu)\}d\nu,\\
A(t)-A_0 &= \frac{1-\varphi}{\mathbb{N}(\varphi)}\left(\Lambda_A^\varphi+\psi^\varphi V(t)-\delta_4^\varphi A(t)V(t)-\mu_A^\varphi A(t)\right)\\
&\quad +\frac{\varphi}{\mathbb{N}(\varphi)\Gamma(\varphi)}\times\int_0^t(t-\nu)^{\varphi-1}\{\Lambda_A^\varphi+\psi^\varphi V(\nu)\\
&\quad -\delta_4^\varphi A(\nu)V(\nu)-\mu_A^\varphi A(\nu)\}d\nu,\\
E(t)-E_0 &= \frac{1-\varphi}{\mathbb{N}(\varphi)}\{\Lambda_E^\varphi+\sigma^\varphi I_M(t)E(t)-\delta_2^\varphi\left(1+\chi_2^\varphi F_2(t)\right)I_M(t)E(t)\\
&\quad -\mu_E^\varphi E(t)\}\\
&\quad +\frac{\varphi}{\mathbb{N}(\varphi)\Gamma(\varphi)}\times\int_0^t(t-\nu)^{\varphi-1}\{\Lambda_E^\varphi+\sigma^\varphi I_M(\nu)E(\nu)\\
&\quad -\delta_2^\varphi\left(1+\chi_2^\varphi F_2(\nu)\right)I_M(\nu)E(\nu)-\mu_E^\varphi E(\nu)\}d\nu,\\
N_K(t)-N_{K^\star} &= \frac{1-\varphi}{\mathbb{N}(\varphi)}\{\Lambda_{N_K}^\varphi+\theta_\varphi^\varphi F_1(t)+\theta_2^\varphi F_2(t)\\
&\quad -\delta_1^\varphi\left(1+\chi_1^\varphi F_1(t)\right)I_M(t)N_K(t)-\left(\eta^\varphi+\mu_{N_K}^\varphi\right)N_K(t)\}\\
&\quad +\frac{\varphi}{\mathbb{N}(\varphi)\Gamma(\varphi)}\times\int_0^t(t-\nu)^{\varphi-1}\{\Lambda_{N_K}^\varphi+\theta_1^\varphi F_1(\nu)+\theta_2^\varphi F_2(\nu)\\
&\quad -\delta_1^\varphi\left(1+\chi_1^\varphi F_1(\nu)\right)I_M(\nu)N_K(\nu)-\left(\eta^\varphi+\mu_{N_K}^\varphi\right)N_K(\nu)\}d\nu,
\end{aligned}
\tag{80}
$$

$$
\begin{aligned}
I_{10}(t)-I_{10^\star} &= \frac{1-\varphi}{\mathbb{N}(\varphi)}\left\{\rho_3^{\varphi} I_M(t)T_0(t)\left(\frac{1}{1+\tau_1^{\varphi} I_{10}}\right)-\mu_{I_{10}^{\varphi}(t)}I_{10}(t)\right\}\\
&\quad+\frac{\varphi}{\mathbb{N}(\varphi)\Gamma(\varphi)}\times\int_0^t(t-\nu)^{\varphi-1}\left\{\rho_3^{\varphi} I_M(\nu)T_0(\nu)\left(\frac{1}{1+\tau_1^{\varphi} I_{10}}\right)\right.\\
&\quad\left.-\mu_{I_{10}}^{\varphi} I_{10}(\nu)\right\}d\nu, \qquad (81)\\
F_1(t)-F_{1^\star} &= \frac{1-\varphi}{\mathbb{N}(\varphi)}\left(\varepsilon^{\varphi} I_M(t)-\left(\theta_1^{\varphi}+\mu_{F_1}^{\varphi}\right)F_1(t)\right)\\
&\quad+\frac{\varphi}{\mathbb{N}(\varphi)\Gamma(\varphi)}\times\int_0^t(t-\nu)^{\varphi-1}\left\{\varepsilon^{\varphi} I_M(\nu)\right.\\
&\quad\left.-\left(\theta_1^{\varphi}+\mu_{F_1}^{\varphi}\right)F_1(\nu)\right\}d\nu,\\
F_2(t)-F_{2^\star} &= \frac{1-\varphi}{\mathbb{N}(\varphi)}\left(\eta^{\varphi} N_K(t)-\left(\theta_2^{\varphi}+\mu_{F_2}^{\varphi}\right)F_2(t)\right)\\
&\quad+\frac{\varphi}{\mathbb{N}(\varphi)\Gamma(\varphi)}\times\int_0^t(t-\nu)^{\varphi-1}\left\{\eta^{\varphi} N_K(\nu)\right.\\
&\quad\left.-\left(\theta_2^{\varphi}+\mu_{F_2}^{\varphi}\right)F_2(\nu)\right\}d\nu.
\end{aligned}
$$

To streamline the analysis and enhance clarity, the kernel was chosen to take the following form.

$$
\begin{aligned}
\Phi_1(t,T_0) &= \Lambda^{\varphi}_{T_0} - \rho^{\varphi}_1 I_M(t)T_0(t)I_{10}(t) - \rho^{\varphi}_2 V(t)T_0(t)I_{10}(t) \\
&\quad -\rho^{\varphi}_3 T_0(t)I_M(t)\left(\frac{1}{1+\tau^{\varphi}_1 I_{10}}\right) - \mu^{\varphi}_{T_0}T_0(t), \\
\Phi_2(t,T_1) &= \rho^{\varphi}_1 I_M(t)T_0(t)I_{10}(t) - \pi^{\varphi}I_M(t)T_1(t) - \mu^{\varphi}_{T_1}T_1(t), \\
\Phi_3(t,T_2) &= \rho^{\varphi}_2 V(t)T_0(t)I_{10}(t) - \delta^{\varphi}_3 T_2(t)V(t) - \mu^{\varphi}_{T_2}T_2(t), \\
\Phi_4(t,M_0) &= \Lambda^{\varphi}_{M_0} - \beta^{\varphi}_1 V(t)M_0(t) - \mu^{\varphi}_{M_0}M_0(t), \\
\Phi_5(t,M_1) &= \Lambda^{\varphi}_{M_1} - \beta^{\varphi}_2 V(t)M_1(t) + \zeta^{\varphi}I_M(t) - \mu^{\varphi}_{M_1}M_1(t), \\
\Phi_6(t,I_M) &= \beta^{\varphi}_1 V(t)M_0(t) + \beta^{\varphi}_2 V(t)M_1(t) + \pi^{\varphi}I_M(t)T_1(t) \\
&\quad -\delta^{\varphi}_1\left(1+\chi^{\varphi}_1 F_1(t)\right)I_M(t)N_K(t) \\
&\quad -\delta^{\varphi}_2\left(1+\chi^{\varphi}_2 F_2(t)\right)I_M(t)E(t) - \sigma^{\varphi}I_M(t)E(t) \\
&\quad -\left(\omega^{\varphi}+\varepsilon^{\varphi}+\zeta^{\varphi}+\mu^{\varphi}_{I_M}\right)I_M(t), \\
\Phi_7(t,V) &= \Lambda^{\varphi}_V + \omega^{\varphi}I_M(t) - \delta^{\varphi}_3 T_2(t)V(t) - \delta^{\varphi}_4 A(t)V(t) \\
&\quad -\left(\psi^{\varphi}+\mu^{\varphi}_V\right)V(t), \\
\Phi_8(t,A) &= \Lambda^{\varphi}_A + \psi^{\varphi}V(t) - \delta^{\varphi}_4 A(t)V(t) - \mu^{\varphi}_A A(t), \\
\Phi_9(t,E) &= \Lambda^{\varphi}_E + \sigma^{\varphi}I_M(t)E(t) - \delta^{\varphi}_2\left(1+\chi^{\varphi}_2 F_2\right)I_M(t)E(t) - \mu^{\varphi}_E E(t), \\
\Phi_{10}(t,N_K) &= \Lambda^{\varphi}_{N_K} + \theta^{\varphi}_1 F_1(t) + \theta^{\varphi}_2 F_2(t) - \delta^{\varphi}_1\left(1+\chi^{\varphi}_1 F_1\right)I_M(t)N_K(t) \\
&\quad -\left(\eta^{\varphi}+\mu^{\varphi}_{N_K}\right)N_K(t), \\
\Phi_{11}(t,I_{10}) &= \rho^{\varphi}_3 I_M(t)T_0(t)\left(\frac{1}{1+\tau^{\varphi}_1 I_{10}}\right) - \mu^{\varphi}_{I_{10}}I_{10}(t), \\
\Phi_{12}(t,F_1) &= \varepsilon^{\varphi}I_M(t) - \left(\theta^{\varphi}_1+\mu^{\varphi}_{F_1}\right)F_1(t), \\
\Phi_{13}(t,F_2) &= \eta^{\varphi}N_K(t) - \left(\theta^{\varphi}_2+\mu^{\varphi}_{F_2}\right)F_2(t).
\end{aligned}
\tag{82}
$$

Following the equations in 82, the constants $\Theta_i, i = 1, 2, \ldots, 13$ are obtained to be

$$
\begin{aligned}
\Theta_1 &= \rho^{\varphi}_1 a_6 a_{11} + \rho^{\varphi}_2 a_7 a_{11} + \rho^{\varphi}_3 a_6\left(\frac{1}{1+\tau^{\varphi}_1 a_{11}}\right) + \mu^{\varphi}_{T_0}, \\
\Theta_2 &= \pi^{\varphi}a_6 + \mu^{\varphi}_{T_1},
\end{aligned}
$$

$$
\begin{aligned}
\Theta_3 &= \delta_3^{\varphi} a_7 + \mu_{T_2}^{\varphi}, \\
\Theta_4 &= \beta_1^{\varphi} a_7 + \mu_{M_0}^{\varphi}, \\
\Theta_5 &= \beta_2^{\varphi} a_7 + \mu_{M_1}^{\varphi}, \\
\Theta_6 &= \pi^{\varphi} a_2 + \delta_1^{\varphi} \left(1 + \chi_1^{\varphi} a_{12}\right) a_{10} + \delta_2^{\varphi} \left(1 + \chi_2^{\varphi} a_{13}\right) + \sigma^{\varphi} a_9 \\
&\quad + \left(\omega^{\varphi} + \varepsilon^{\varphi} + \zeta^{\varphi} + \mu_{I_M}^{\varphi}\right), \\
\Theta_7 &= \delta_3^{\varphi} a_3 + \delta_4^{\varphi} a_8 + \left(\psi^{\varphi} + \mu_V^{\varphi}\right), \\
\Theta_8 &= \delta_4^{\varphi} a_7 + \mu_A^{\varphi}, \\
\Theta_9 &= \delta_2^{\varphi} \left(1 + \chi_2^{\varphi} a_{13}\right) a_9 + \sigma^{\varphi} a_6 + \mu_E^{\varphi}, \\
\Theta_{10} &= \delta_1^{\varphi} \left(1 + \chi_1^{\varphi} a_{12}\right) a_6 + \left(\eta^{\varphi} + \mu_{N_K}^{\varphi}\right), \\
\Theta_{11} &= \mu_{I_{10}}^{\varphi}, \\
\Theta_{12} &= \theta_1^{\varphi} + \mu_{F_1}^{\varphi}, \\
\Theta_{13} &= \theta_2^{\varphi} + \mu_{F_2}^{\varphi}.
\end{aligned}
$$

To establish both the existence and uniqueness of solutions for the model system, the following assumption was considered:

H_1 : For the continuous functions

$$
\begin{aligned}
&\{T_0, T_1, T_2, M_0, M_1, I_M, V, A, E, N_K, I_{10}, F_1, F_2, \\
&T_{0^\star}, T_{1^\star}, T_{2^\star}, M_{0^\star}, I_{M^\star}, V_0, A_0, E_0, N_{K^\star}, I_{10^\star}, F_{1^\star}, F_{2^\star}\} \in \mathbb{L}[0,1],
\end{aligned}
$$

it follows that $||T_0|| \leq a_1, ||T_1|| \leq a_2, ||T_2|| \leq a_3, ||M_0|| \leq a_4, ||M_1|| \leq a_5, ||I_M|| \leq a_6, ||V|| \leq a_7, ||A|| \leq a_8, ||E|| \leq a_9, ||N_K|| \leq a_{10}, ||I_{10}|| \leq a_{11}, ||F_1|| \leq a_{12}, ||F_2|| \leq a_{13}$.

Theorem 8

If assumption (H_1) *is true and* $\Phi_i, i = 1, 2, \cdots, 13$ *mollify the Lipschitz condition, then they are contractions and* $\Theta_i < 1; \forall i = 1, 2, \cdots, 13$.

Proof. First, the satisfaction of the Lipschitz condition by $\Phi_1(t, T_0)$ is demonstrated. Let T_0 and $T_{0^\star}$ be two given functions, then

$$\begin{aligned}
||\Phi_1(t,T_0) - \Phi_1(t,T_{0^\star})|| &= ||\Lambda^{\varphi}_{T_0} - \rho^{\varphi}_1 I_M T_0 I_{10} - \rho^{\varphi}_2 V T_0 I_{10} \\
&\quad -\rho^{\varphi}_3 T_0 I_M \left(\frac{1}{1+\tau^{\varphi}_1 I_{10}}\right) - \mu^{\varphi}_{T_0} T_0 \\
&\quad -\{\Lambda^{\varphi}_{T_0} - \rho^{\varphi}_1 I_M T_{0^\star} I_{10} - \rho^{\varphi}_2 V T_{0^\star} I_{10} \\
&\quad -\rho^{\varphi}_3 T_{0^\star} I_M \left(\frac{1}{1+\tau^{\varphi}_1 I_{10}}\right) - \mu^{\varphi}_{T_0} T_{0^\star}\}||, \\
&\leq \left\{\rho^{\varphi}_1 I_M I_{10} + \rho^{\varphi}_2 V I_{10}\right. \\
&\quad \left. +\rho^{\varphi}_3 I_M \left(\frac{1}{1+\tau^{\varphi}_1 I_{10}}\right) + \mu^{\varphi}_{T_0}\right\} ||T_0 - T_{0^\star}||, \\
&\leq \left\{\rho^{\varphi}_1 a_6 a_{11} + \rho^{\varphi}_2 a_7 a_{11} + \rho^{\varphi}_3 a_6 \left(\frac{1}{1+\tau^{\varphi}_1 a_{11}}\right)\right. \\
&\quad \left. +\mu^{\varphi}_{T_0}\right\} ||T_0 - T_{0^\star}||, \\
&= \Theta_1 ||T_0 - T_{0^\star}||.
\end{aligned}$$

Next, the satisfaction of the Lipschitz condition by $\Phi_2(t, T_1)$ is demonstrated. Let T_1 and $T_{1^\star}$ be two given functions, then it means that

$$\begin{aligned}
||\Phi_2(t,T_1) - \Phi_2(t,T_{1^\star})|| &= ||\rho^{\varphi}_1 I_M T_0 I_{10} - \pi^{\varphi} I_M T_1 - \mu^{\varphi}_{T_1} T_1 - \{\rho^{\varphi}_1 I_M T_0 I_{10} \\
&\quad -\pi^{\varphi} I_M T_{1^\star} - \mu^{\varphi}_{T_1} T_{1^\star}\}||, \\
&\leq \left(\pi^{\varphi} I_M - \mu^{\varphi}_{T_1}\right) ||T_1 - T_{1^\star}||, \\
&\leq \left(\pi^{\varphi} a_6 + \mu^{\varphi}_{T_1}\right) ||T_1 - T_{1^\star}||, \\
&= \Theta_2 ||T_1 - T_{1^\star}||.
\end{aligned}$$

Furthermore, the satisfaction of the Lipschitz condition by $\Phi_3(t, T_2)$ is demonstrated. Let T_2 and $T_{2^\star}$ be two given functions. It follows that

$$\begin{aligned}
||\Phi_3(t,T_2)-\Phi_3(t,T_{2^\star})|| &= ||\rho_2^\varphi V T_0 I_{10}-\delta_2^\varphi V T_2-\mu_{T_2}^\varphi T_2-\{\rho_2^\varphi V T_0 I_{10}\\
&\quad -\delta_3^\varphi V T_{2^\star}-\mu_{T_2}^\varphi T_{2^\star}\}||,\\
&\leq \left(\delta_3^\varphi V+\mu_{T_2}^\varphi\right)||T_2-T_{2^\star}||,\\
&\leq \left(\delta_3^\varphi a_7+\mu_{T_2}^\varphi\right)||T_2-T_{2^\star}||,\\
&= \Theta_3||T_2-T_{2^\star}||.
\end{aligned}$$

Next, the satisfaction of the Lipschitz condition by $\Phi_4(t,M_0)$ is demonstrated. Let M_0 and $M_{0^\star}$ be two given functions. It follows that

$$\begin{aligned}
||\Phi_4(t,M_0)-\Phi_4(t,M_{0^\star})|| &= ||\Lambda_{M_0}^\varphi-\beta_1^\varphi V M_0-\mu_{M_0}M_0\\
&\quad -\{\Lambda_{M_0}^\varphi-\beta_1^\varphi V M_{0^\star}-\mu_{M_0}^\varphi M_{0^\star}\}||,\\
&\leq \left(\beta_1^\varphi V+\mu_{M_0}^\varphi\right)||M_0-M_{0^\star}||,\\
&\leq \left(\beta_1^\varphi a_7+\mu_{M_0}^\varphi\right)||M_0-M_{0^\star}||,\\
&= \Theta_4||M_0-M_{0^\star}||.
\end{aligned}$$

Next, the satisfaction of the Lipschitz condition by $\Phi_5(t,M_1)$ is demonstrated. Let M_1 and $M_{1^\star}$ be two given functions. It follows that

$$\begin{aligned}
||\Phi_5(t,M_1)-\Phi_5(t,M_{1^\star})|| &= ||\Lambda_{M_1}^\varphi-\beta_2^\varphi V+\zeta^\varphi I_M-\mu_{M_1}^\varphi M_1\\
&\quad -\{\Lambda_{M_1}^\varphi-\beta_2^\varphi V M_{1^\star}+\zeta^\varphi I_M-\mu_{M_1}^\varphi M_{1^\star}\}||,\\
&\leq \left(\beta_2^\varphi V+\mu_{M_1}^\varphi\right)||M_1-M_{1^\star}||,\\
&\leq \left(\beta_2^\varphi a_7+\mu_{M_1}^\varphi\right)||M_1-M_{1^\star}||,\\
&= \Theta_5||M_1-M_{1^\star}||.
\end{aligned}$$

Next, the satisfaction of the Lipschitz condition by $\Phi_6(t,I_M)$ is demonstrated. Let I_M and $I_{M^\star}$ be two given functions. It implies that

$$
\begin{aligned}
||\Phi_6(t, I_M) - \Phi_6(t, I_{M^\star})|| &= ||\beta_1^\varphi V M_0 + \beta_2^\varphi V M_1 + \pi^\varphi I_M T_1 \\
&\quad -\delta_1^\varphi (1 + \chi_1^\varphi F_1) I_M N_K - \delta_2^\varphi (1 + \chi_2^\varphi F_2) I_M E \\
&\quad -\sigma^\varphi I_M E - \left(\omega^\varphi + \varepsilon^\varphi + \zeta^\varphi + \mu_{I_M}^\varphi\right) I_M \\
&\quad -\{\beta_1^\varphi V M_0 + \beta_2^\varphi V M_1 + \pi^\varphi I_{M^\star} T_1 - \\
&\quad -\delta_1^\varphi (1 + \chi_1^\varphi F_1) I_{M^\star}(t) N_K \\
&\quad -\delta_2^\varphi (1 + \chi_2^\varphi F_2) I_{M^\star} E - \sigma^\varphi I_{M^\star} E \\
&\quad -\left(\omega^\varphi + \varepsilon^\varphi + \zeta^\varphi + \mu_{I_M}^\varphi\right) I_{M^\star}\}||, \\
&\leq \{\pi^\varphi T_1 + \delta_1^\varphi (1 + \chi_1^\varphi F_1) N_K + \delta_2^\varphi (1 + \chi_2^\varphi F_2) E \\
&\quad +\sigma^\varphi E + \left(\omega^\varphi + \varepsilon^\varphi + \zeta^\varphi + \mu_{I_M}^\varphi\right)\}||I_M - I_{M^\star}||, \\
&\leq \{(\pi^\varphi a_2 + \delta_1^\varphi (1 + \chi_1^\varphi a_{12}) a_{10} + \delta_2^\varphi (1 + \chi_2^\varphi a_{13}) a_9 \\
&\quad +\sigma^\varphi a_9 + \left(\omega^\varphi + \varepsilon^\varphi + \zeta^\varphi + \mu_{I_M}^\varphi\right)\}||I_M - I_{M^\star}||, \\
&= \Theta_6 ||I_M - I_{M^\star}||.
\end{aligned}
$$

Next, the satisfaction of the Lipschitz condition by $\Phi_7(t, V)$ is demonstrated. Let V and V_0 be two given functions. It follows that

$$
\begin{aligned}
||\Phi_7(t, V) - \Phi_7(t, V_0)|| &= ||\Lambda_V^\varphi + \omega^\varphi I_M - \delta_3^\varphi T_2 V - \delta_4^\varphi A V - (\psi^\varphi + \mu_V^\varphi) V \\
&\quad -\{\Lambda_V^\varphi + \omega^\varphi I_M - \delta_3^\varphi T_2 V_0 - \delta_4^\varphi A V_0 \\
&\quad -(\psi^\varphi + \mu_V^\varphi) V_0\}||, \\
&\leq (\delta_3^\varphi T_2 + \delta_4^\varphi A + (\psi^\varphi + \mu_V^\varphi))\, ||V - V_0||, \\
&\leq [\delta_3^\varphi a_3 + \delta_4^\varphi a_8 + (\psi^\varphi + \mu_V^\varphi)]\, ||V - V_0||, \\
&= \Theta_7 ||V - V_0||.
\end{aligned}
$$

Next, the satisfaction of the Lipschitz condition by $\Phi_8(t, A)$ is demonstrated. Let A and A_0 be two given functions. It means that

$$\begin{aligned}
||\Phi_8(t,A)-\Phi_8(t,A_0)|| &= ||\Lambda_A^{\varphi}+\psi^{\varphi}V-\delta_4^{\varphi}AV-\mu_A^{\varphi}A \\
&\quad -\{\Lambda_A^{\varphi}+\psi^{\varphi}V-\delta_4^{\varphi}A_0V-\mu_A^{\varphi}A_0\}||, \\
&\leq (\delta_4^{\varphi}V+\mu_A^{\varphi})\,||A-A_0||, \\
&\leq (\delta_4^{\varphi}a_7+\mu_A^{\varphi})\,||A-A_0||, \\
&= \Theta_8||A-A_0||.
\end{aligned}$$

Next, the satisfaction of the Lipschitz condition by $\Phi_9(t,E)$ is demonstrated. Let E and E_0 be two given functions. It means that

$$\begin{aligned}
||\Phi_9(t,E)-\Phi_9(t,E_0)|| &= ||\Lambda_E^{\varphi}+\sigma^{\varphi}I_ME-\delta_2^{\varphi}(1+\chi_2^{\varphi}F_2)\,I_ME \\
&\quad -\mu_E^{\varphi}E-\{\Lambda_E^{\varphi}+\sigma^{\varphi}I_ME_0 \\
&\quad -\delta_2^{\varphi}(1+\chi_2F_2)\,I_ME_0\mu_E^{\varphi}E_0\}||, \\
&\leq (\sigma^{\varphi}I_M+\delta_2^{\varphi}(1+\chi_2^{\varphi}F_2)\,I_M+\mu_E^{\varphi})\,||E-E_0||, \\
&\leq [\sigma^{\varphi}a_6+\delta_2^{\varphi}(1+\chi_2^{\varphi}a_{13})\,a_6+\mu_E^{\varphi}]\,||E-E_0||, \\
&= \Theta_9||E-E_0||.
\end{aligned}$$

Next, the satisfaction of the Lipschitz condition by $\Phi_{10}(t,N_K)$ is demonstrated. Let N_K and $N_{K^\star}$ be two given functions. It means that

$$\begin{aligned}
||\Phi_{10}(t,N_K)-\Phi_{10}(t,N_{K^\star})|| &= ||\{\Lambda_{N_K}^{\varphi}+\theta_1^{\varphi}F_1+\theta_2^{\varphi}F_2 \\
&\quad -\delta_1^{\varphi}(1+\chi_1^{\varphi}F_1)\,I_MN_K-\left(\eta^{\varphi}+\mu_{N_K}^{\varphi}\right)N_K\} \\
&\quad -\{\Lambda_{N_K}^{\varphi}+\theta_1^{\varphi}F_1+\theta_2^{\varphi}F_2-\delta_1^{\varphi}(1+\chi_1^{\varphi}F_1) \\
&\quad \times I_MN_{K^\star}-\left(\eta^{\varphi}+\mu_{N_K}^{\varphi}\right)N_{K^\star}\}||, \\
&\leq \left(\delta_1^{\varphi}(1+\chi_1^{\varphi}F_1)\,I_M+\left(\eta^{\varphi}+\mu_{N_K}^{\varphi}\right)\right) \\
&\quad \times||N_K-N_{K^\star}||,
\end{aligned}$$

$$\begin{aligned}||\Phi_{10}(t,N_K)-\Phi_{10}(t,N_{K^\star})||&\leq\left[\delta_1^\varphi(1+\chi_1^\varphi a_{12})a_6+\left(\eta^\varphi+\mu_{N_K}^\varphi\right)\right]\\&\quad\times||N_K-N_{K^\star}||,\\&=\Theta_{10}||N_K-N_{K^\star}||.\end{aligned}$$

Next, the satisfaction of the Lipschitz condition by $\Phi_{11}(t,I_{10})$ is demonstrated. Let I_{10} and $I_{10^\star}$ be two given functions. It implies that

$$\begin{aligned}||\Phi_{11}(t,I_{10})-\Phi_{11}(t,I_{10^\star})||&=||\rho_3^\varphi I_M T_0\left(\frac{1}{1+\tau_1^\varphi I_{10}}\right)-\mu_{I_{10}}^\varphi I_{10}\\&\quad-\{\rho_3^\varphi I_M T_0\left(\frac{1}{1+\tau_1^\varphi I_{10}}\right)-\mu_{I_{10}}^\varphi I_{10^\star}\}||,\\&\leq\mu_{I_{10}}^\varphi||I_{10}-I_{10^\star}||,\\&=\Theta_{11}||I_{10}-I_{10^\star}||.\end{aligned}$$

Next, the satisfaction of the Lipschitz condition by $\Phi_{12}(t,F_1)$ is demonstrated. Let F_1 and $F_{1^\star}$ be two given functions. It follows that

$$\begin{aligned}||\Phi_{12}(t,F_1)-\Phi_{12}(t,F_{1^\star})||&=||\varepsilon^\varphi I_M-\left(\theta_1^\varphi+\mu_{F_1}^\varphi\right)F_1\\&\quad-\left[\varepsilon^\varphi I_M-\left(\theta_1^\varphi+\mu_{F_1}^\varphi\right)F_{1^\star}\right]||,\\&\leq\left(\theta_1^\varphi+\mu_{F_1}^\varphi\right)||F_1-F_{1^\star}||,\\&=\Theta_{12}||F_1-F_{1^\star}||.\end{aligned}$$

Finally, the satisfaction of the Lipschitz condition by $\Phi_{13}(t,F_2)$ is demonstrated. Let F_2 and $F_{2^\star}$ be two given functions. It follows that

$$\begin{aligned}||\Phi_{13}(t,F_2)-\Phi_{13}(t,F_{2^\star})||&=||\eta^\varphi N_K-\left(\theta_2^\varphi+\mu_{F_2}^\varphi\right)F_2\\&\quad-\left[\eta^\varphi N_K-\left(\theta_1^\varphi+\mu_{F_2}^\varphi\right)F_{2^\star}\right]||,\\&\leq\left(\theta_2^\varphi+\mu_{F_2}^\varphi\right)||F_2-F_{2^\star}||,\\&=\Theta_{13}||F_2-F_{2^\star}||.\end{aligned}$$

It is evident that each of the kernels $\Phi_i, i = 1, 2, \cdots, 13$, meets the Lipschitz condition, indicating that they are contractions with $\Theta_i < 1, i \in 1, 2, \cdots, 13$ as well.

Moreover, when the initial conditions approach zero, the model systems 79, 80, and 81 transform into 83, 84 and 85 respectively.

$$
\begin{aligned}
T_0(t) &= \frac{1-\varphi}{\mathbb{N}(\varphi)}\left\{\Lambda^{\varphi}_{T_0} - \rho^{\varphi}_1 I_M(t)T_0(t)I_{10}(t) - \rho^{\varphi}_2 V(t)T_0(t)I_{10}(t)\right.\\
&\quad \left.-\rho^{\varphi}_3 T_0(t)I_M(t)\left(\frac{1}{1+\tau^{\varphi}_1 I_{10}}\right) - \mu^{\varphi}_{T_0}T_0(t)\right\}\\
&\quad +\frac{\varphi}{\mathbb{N}(\varphi)\Gamma(\varphi)}\times\int_0^t (t-\nu)^{\varphi-1}\left\{\Lambda^{\varphi}_{T_0} - \rho^{\varphi}_1 I_M(\nu)T_0(\nu)I_{10}(\nu)\right.\\
&\quad \left.-\rho^{\varphi}_2 V(\nu)T_0(\nu)I_{10}(\nu) - \rho^{\varphi}_3 T_0(\nu)I_M(\nu)\left(\frac{1}{1+\tau^{\varphi}_1 I_{10}}\right)\right.\\
&\quad \left.-\mu^{\varphi}_{T_0}T_0(\nu)\right\}d\nu,\\
T_1(t) &= \frac{1-\varphi}{\mathbb{N}(\varphi)}\left\{\rho^{\varphi}_1 I_M(t)T_0(t)I_{10}(t) - \pi^{\varphi} I_M(t)T_1(t) - \mu^{\varphi}_{T_1}T_1(t)\right\}\\
&\quad +\frac{\varphi}{\mathbb{N}(\varphi)\Gamma(\varphi)}\times\int_0^t (t-\nu)^{\varphi-1}\left\{\rho^{\varphi}_1 I_M(\nu)T_0(\nu)I_{10}(\nu)\right.\\
&\quad \left.-\pi^{\varphi} I_M(\nu)T_1(\nu) - \mu^{\varphi}_{T_1}T_1(\nu)\right\}d\nu, \qquad (83)\\
T_2(t) &= \frac{1-\varphi}{\mathbb{N}(\varphi)}\left\{\rho^{\varphi}_2 V(t)T_0(t)I_{10}(t) - \delta^{\varphi}_3 T_2(t)V(t) - \mu^{\varphi}_{T_2}T_2(t)\right\}\\
&\quad +\frac{\varphi}{\mathbb{N}(\varphi)\Gamma(\varphi)}\times\int_0^t (t-\nu)^{\varphi-1}\left\{\rho^{\varphi}_2 V(\nu)T_0(\nu)I_{10}(\nu)\right.\\
&\quad \left.-\delta^{\varphi}_3 T_2(\nu)V(\nu) - \mu^{\varphi}_{T_2}T_2(\nu)\right\}d\nu,\\
M_0(t) &= \frac{1-\varphi}{\mathbb{N}(\varphi)}\left\{\Lambda^{\varphi}_{M_0} - \beta^{\varphi}_1 V(t)M_0(t) - \mu^{\varphi}_{M_0}M_0(t)\right\}\\
&\quad +\frac{\varphi}{\mathbb{N}(\varphi)\Gamma(\varphi)}\times\int_0^t (t-\nu)^{\varphi-1}\left\{\Lambda^{\varphi}_{M_0} - \beta^{\varphi}_1 V(\nu)M_0(\nu)\right.\\
&\quad \left.-\mu^{\varphi}_{M_0}M_0(\nu)\right\}d\nu,
\end{aligned}
$$

$$
\begin{aligned}
M_1(t) &= \frac{1-\varphi}{\mathbb{N}(\varphi)}\left\{\Lambda_{M_1}^{\varphi} - \beta_2^{\varphi}V(t)M_1(t) + \zeta^{\varphi}I_M(t) - \mu_{M_1}^{\varphi}M_1(t)\right\} \\
&\quad + \frac{\varphi}{\mathbb{N}(\varphi)\Gamma(\varphi)} \times \int_0^t (t-\nu)^{\varphi-1}\left\{\Lambda_{M_1}^{\varphi} - \beta_2^{\varphi}V(\nu)M_1(\nu)\right. \\
&\quad \left. + \zeta^{\varphi}I_M(\nu) - \mu_{M_1}^{\varphi}M_1(\nu)\right\}d\nu, \\
I_M(t) &= \frac{1-\varphi}{\mathbb{N}(\varphi)}\left\{\beta_1^{\varphi}V(t)M_0(t) + \beta_2^{\varphi}V(t)M_1(t) + \pi^{\varphi}I_M(t)T_1(t)\right. \\
&\quad -\delta_1^{\varphi}\left(1+\chi_1^{\varphi}F_1(t)\right)I_M(t)N_K(t) \\
&\quad \left. -\sigma^{\varphi}I_M(t)E(t) - \left(\omega^{\varphi}+\varepsilon^{\varphi}+\zeta^{\varphi}+\mu_{I_M}^{\varphi}\right)I_M(t)\right\} \\
&\quad + \frac{\varphi}{\mathbb{N}(\varphi)\Gamma(\varphi)} \times \int_0^t (t-\nu)^{\varphi-1}\left\{\beta_1^{\varphi}V(\nu)M_0(\nu) + \beta_2^{\varphi}V(\nu)M_1(\nu)\right. \\
&\quad +\pi^{\varphi}I_M(\nu)T_1(\nu) - \delta_1^{\varphi}\left(1+\chi_1^{\varphi}F_1(\nu)\right)I_M(\nu)N_K(\nu) \\
&\quad -\delta_2^{\varphi}\left(1+\chi_2^{\varphi}F_2(\nu)\right)I_M(\nu)E(\nu) - \sigma^{\varphi}I_M(\nu)E(\nu) \qquad (84) \\
&\quad \left. -\left(\omega^{\varphi}+\varepsilon^{\varphi}+\zeta^{\varphi}+\mu_{I_M}^{\varphi}\right)I_M(\nu)\right\}d\nu, \\
V(t) &= \frac{1-\varphi}{\mathbb{N}(\varphi)}\left\{\Lambda_V^{\varphi} + \omega^{\varphi}I_M(t) - \delta_3^{\varphi}T_2(t)V(t) - \delta_4^{\varphi}A(t)V(t)\right. \\
&\quad \left. -\left(\psi^{\varphi}+\mu_V^{\varphi}\right)V(t)\right\} \\
&\quad + \frac{\varphi}{\mathbb{N}(\varphi)\Gamma(\varphi)} \times \int_0^t (t-\nu)^{\varphi-1}\left\{\Lambda_V^{\varphi} + \omega^{\varphi}I_M(\nu) - \delta_3^{\varphi}T_2(\nu)V(\nu)\right. \\
&\quad \left. -\delta_4^{\varphi}A(\nu)V(\nu) - \left(\psi^{\varphi}+\mu_V^{\varphi}\right)V(\nu)\right\}d\nu, \\
A(t) &= \frac{1-\varphi}{\mathbb{N}(\varphi)}\left\{\Lambda_A^{\varphi} + \psi^{\varphi}V(t) - \delta_4^{\varphi}A(t)V(t) - \mu_A^{\varphi}A(t)\right\} \\
&\quad + \frac{\varphi}{\mathbb{N}(\varphi)\Gamma(\varphi)} \times \int_0^t (t-\nu)^{\varphi-1}\left\{\Lambda_A^{\varphi} + \psi^{\varphi}V(\nu) - \delta_4^{\varphi}A(\nu)V(\nu)\right. \\
&\quad \left. -\mu_A^{\varphi}A(\nu)\right\}d\nu,
\end{aligned}
$$

$$
\begin{aligned}
E(t) &= \frac{1-\varphi}{\mathbb{N}(\varphi)}\Bigg\{\Lambda_E^{\varphi}+\sigma^{\varphi}I_M(t)E(t)-\delta_2^{\varphi}\left(1+\chi_2^{\varphi}F_2(t)\right)I_M(t)E(t)\\
&\quad -\mu_E^{\varphi}E(t)\Bigg\}\\
&\quad +\frac{\varphi}{\mathbb{N}(\varphi)\Gamma(\varphi)}\times\int_0^t(t-\nu)^{\varphi-1}\Bigg\{\Lambda_E^{\varphi}+\sigma^{\varphi}I_M(\nu)E(\nu)\\
&\quad -\delta_2^{\varphi}\left(1+\chi_2^{\varphi}F_2(\nu)\right)I_M(\nu)E(\nu)-\mu_E^{\varphi}E(\nu)\Bigg\}d\nu,\\
N_K(t) &= \frac{1-\varphi}{\mathbb{N}(\varphi)}\Bigg\{\Lambda_{N_K}^{\varphi}+\theta_{\varphi}^{\varphi}F_1(t)+\theta_2^{\varphi}F_2(t)\\
&\quad -\delta_1^{\varphi}\left(1+\chi_1^{\varphi}F_1(t)\right)I_M(t)N_K(t)-\left(\eta^{\varphi}+\mu_{N_K}^{\varphi}\right)N_K(t)\Bigg\}\\
&\quad +\frac{\varphi}{\mathbb{N}(\varphi)\Gamma(\varphi)}\times\int_0^t(t-\nu)^{\varphi-1}\Bigg\{\Lambda_{N_K}^{\varphi}+\theta_1^{\varphi}F_1(\nu)+\theta_2^{\varphi}F_2(\nu)\\
&\quad -\delta_1^{\varphi}\left(1+\chi_1^{\varphi}F_1(\nu)\right)I_M(\nu)N_K(\nu)-\left(\eta^{\varphi}+\mu_{N_K}^{\varphi}\right)N_K(\nu)\Bigg\}d\nu,\\
I_{10}(t) &= \frac{1-\varphi}{\mathbb{N}(\varphi)}\Bigg\{\rho_3^{\varphi}I_M(t)T_0(t)\left(\frac{1}{1+\tau_1^{\varphi}I_{10}}\right)-\mu_{I_{10}^{\varphi}(t)}I_{10}(t)\Bigg\} \qquad (85)\\
&\quad +\frac{\varphi}{\mathbb{N}(\varphi)\Gamma(\varphi)}\times\int_0^t(t-\nu)^{\varphi-1}\Bigg\{\rho_3^{\varphi}I_M(\nu)T_0(\nu)\left(\frac{1}{1+\tau_1^{\varphi}I_{10}}\right)\\
&\quad -\mu_{I_{10}}^{\varphi}I_{10}(\nu)\Bigg\}d\nu,\\
F_1(t) &= \frac{1-\varphi}{\mathbb{N}(\varphi)}\Bigg\{\varepsilon^{\varphi}I_M(t)-\left(\theta_1^{\varphi}+\mu_{F_1}^{\varphi}\right)F_1(t)\Bigg\}\\
&\quad +\frac{\varphi}{\mathbb{N}(\varphi)\Gamma(\varphi)}\times\int_0^t(t-\nu)^{\varphi-1}\Bigg\{\varepsilon^{\varphi}I_M(\nu)-\left(\theta_1^{\varphi}+\mu_{F_1}^{\varphi}\right)F_1(\nu)\Bigg\}d\nu,\\
F_2(t) &= \frac{1-\varphi}{\mathbb{N}(\varphi)}\Bigg\{\eta^{\varphi}N_K(t)-\left(\theta_2^{\varphi}+\mu_{F_2}^{\varphi}\right)F_2(t)\Bigg\}\\
&\quad +\frac{\varphi}{\mathbb{N}(\varphi)\Gamma(\varphi)}\times\int_0^t(t-\nu)^{\varphi-1}\Bigg\{\eta^{\varphi}N_K(\nu)-\left(\theta_2^{\varphi}+\mu_{F_2}^{\varphi}\right)F_2(\nu)\Bigg\}d\nu.
\end{aligned}
$$

Let $t = t_n$, where $n = 1, 2, \cdots, 13$, define the following recursive formulas for systems 83, 84, and 85 to be in the forms:

$$
\begin{aligned}
T_{0_n}(t) &= \frac{1-\varphi}{\mathbb{N}(\varphi)}\Bigg\{\Lambda^{\varphi}_{T_0} - \rho^{\varphi}_1 I_M(t) T_{0_{n-1}}(t) I_{10}(t) - \rho^{\varphi}_2 V(t) T_{0_{n-1}}(t) I_{10}(t) \\
&\quad -\rho^{\varphi}_3 T_{0_{n-1}}(t) I_M(t)\left(\frac{1}{1+\tau^{\varphi}_1 I_{10}}\right) - \mu^{\varphi}_{T_0} T_{0_{n-1}}(t)\Bigg\} \\
&\quad +\frac{\varphi}{\mathbb{N}(\varphi)\Gamma(\varphi)} \times \int_0^t (t-\nu)^{\varphi-1}\Bigg\{\Lambda^{\varphi}_{T_0} - \rho^{\varphi}_1 I_M(\nu) T_{0_{n-1}}(\nu) I_{10}(\nu) \\
&\quad -\rho^{\varphi}_2 V(\nu) T_{0_{n-1}}(\nu) I_{10}(\nu) - \rho^{\varphi}_3 T_{0_{n-1}}(\nu) I_M(\nu)\left(\frac{1}{1+\tau^{\varphi}_1 I_{10}}\right) \\
&\quad -\mu^{\varphi}_{T_0} T_{0_{n-1}}(\nu)\Bigg\} d\nu, \\
T_{1_n}(t) &= \frac{1-\varphi}{\mathbb{N}(\varphi)}\{\rho^{\varphi}_1 I_M(t) T_0(t) I_{10}(t) - \pi^{\varphi} I_M(t) T_{1_{n-1}}(t) - \mu^{\varphi}_{T_1} T_{1_{n-1}}(t)\} \\
&\quad +\frac{\varphi}{\mathbb{N}(\varphi)\Gamma(\varphi)} \times \int_0^t (t-\nu)^{\varphi-1}\{\rho^{\varphi}_1 I_M(\nu) T_0(\nu) I_{10}(\nu) \\
&\quad -\pi^{\varphi} I_M(\nu) T_{1_{n-1}}(\nu) - \mu^{\varphi}_{T_1} T_{1_{n-1}}(\nu)\} d\nu, \qquad (86) \\
T_{2_n}(t) &= \frac{1-\varphi}{\mathbb{N}(\varphi)}\{\rho^{\varphi}_2 V(t) T_0(t) I_{10}(t) - \delta^{\varphi}_3 T_{2_{n-1}}(t) V(t) - \mu^{\varphi}_{T_2} T_{2_{n-1}}(t)\} \\
&\quad +\frac{\varphi}{\mathbb{N}(\varphi)\Gamma(\varphi)} \times \int_0^t (t-\nu)^{\varphi-1}\{\rho^{\varphi}_2 V(\nu) T_0(\nu) I_{10}(\nu) \\
&\quad -\delta^{\varphi}_3 T_{2_{n-1}}(\nu) V(\nu) - \mu^{\varphi}_{T_2} T_{2_{n-1}}(\nu)\} d\nu, \\
M_{0_n}(t) &= \frac{1-\varphi}{\mathbb{N}(\varphi)}\{\Lambda^{\varphi}_{M_0} - \beta^{\varphi}_1 V(t) M_{0_{n-1}}(t) - \mu^{\varphi}_{M_0} M_{0_{n-1}}(t)\} \\
&\quad +\frac{\varphi}{\mathbb{N}(\varphi)\Gamma(\varphi)} \times \int_0^t (t-\nu)^{\varphi-1}\{\Lambda^{\varphi}_{M_0} - \beta^{\varphi}_1 V(\nu) M_{0_{n-1}}(\nu) \\
&\quad -\mu^{\varphi}_{M_0} M_{0_{n-1}}(\nu)\} d\nu, \\
M_{1_n}(t) &= \frac{1-\varphi}{\mathbb{N}(\varphi)}\{\Lambda^{\varphi}_{M_1} - \beta^{\varphi}_2 V(t) M_{1_{n-1}}(t) + \zeta^{\varphi} I_M(t) - \mu^{\varphi}_{M_1} M_{1_{n-1}}(t)\} \\
&\quad +\frac{\varphi}{\mathbb{N}(\varphi)\Gamma(\varphi)} \times \int_0^t (t-\nu)^{\varphi-1}\{\Lambda^{\varphi}_{M_1} - \beta^{\varphi}_2 V(\nu) M_{1_{n-1}}(\nu) \\
&\quad +\zeta^{\varphi} I_M(\nu) - \mu^{\varphi}_{M_1} M_{1_{n-1}}(\nu)\} d\nu,
\end{aligned}
$$

$$
\begin{aligned}
I_{M_n}(t) &= \frac{1-\varphi}{\mathbb{N}(\varphi)}\{\beta_1^{\varphi}V(t)M_0(t)+\beta_2^{\varphi}V(t)M_1(t)+\pi^{\varphi}I_{M_{n-1}}(t)T_1(t)\\
&\quad -\delta_1^{\varphi}\left(1+\chi_1^{\varphi}F_1(t)\right)I_{M_{n-1}}(t)N_K(t)\\
&\quad -\sigma^{\varphi}I_{M_{n-1}}(t)E(t)-\left(\omega^{\varphi}+\varepsilon^{\varphi}+\zeta^{\varphi}+\mu_{I_M}^{\varphi}\right)I_{M_{n-1}}(t)\}\\
&\quad +\frac{\varphi}{\mathbb{N}(\varphi)\Gamma(\varphi)}\times\int_0^t(t-\nu)^{\varphi-1}\{\beta_1^{\varphi}V(\nu)M_0(\nu)+\beta_2^{\varphi}V(\nu)M_1(\nu)\\
&\quad +\pi^{\varphi}I_{M_{n-1}}(\nu)T_1(\nu)-\delta_1^{\varphi}\left(1+\chi_1^{\varphi}F_1(\nu)\right)I_{M_{n-1}}(\nu)N_K(\nu)\\
&\quad -\delta_2^{\varphi}\left(1+\chi_2^{\varphi}F_2(\nu)\right)I_{M_{n-1}}(\nu)E(\nu)-\sigma^{\varphi}I_{M_{n-1}}(\nu)E(\nu)\\
&\quad -\left(\omega^{\varphi}+\varepsilon^{\varphi}+\zeta^{\varphi}+\mu_{I_M}^{\varphi}\right)I_{M_{n-1}}(\nu)\}d\nu,\\
V_n(t) &= \frac{1-\varphi}{\mathbb{N}(\varphi)}\{\Lambda_V^{\varphi}+\omega^{\varphi}I_M(t)-\delta_3^{\varphi}T_2(t)V_{n-1}(t)-\delta_4^{\varphi}A(t)V_{n-1}(t)\\
&\quad -\left(\psi^{\varphi}+\mu_V^{\varphi}\right)V_{n-1}(t)\} \qquad (87)\\
&\quad +\frac{\varphi}{\mathbb{N}(\varphi)\Gamma(\varphi)}\times\int_0^t(t-\nu)^{\varphi-1}\{\Lambda_V^{\varphi}+\omega^{\varphi}I_M(\nu)-\delta_3^{\varphi}T_2(\nu)V_{n-1}(\nu)\\
&\quad -\delta_4^{\varphi}A(\nu)V_{n-1}(\nu)-\left(\psi^{\varphi}+\mu_V^{\varphi}\right)V_{n-1}(\nu)\}d\nu,\\
A_n(t) &= \frac{1-\varphi}{\mathbb{N}(\varphi)}\{\Lambda_A^{\varphi}+\psi^{\varphi}V(t)-\delta_4^{\varphi}A_{n-1}(t)V(t)-\mu_A^{\varphi}A_{n-1}(t)\}\\
&\quad +\frac{\varphi}{\mathbb{N}(\varphi)\Gamma(\varphi)}\times\int_0^t(t-\nu)^{\varphi-1}\{\Lambda_A^{\varphi}+\psi^{\varphi}V(\nu)-\delta_4^{\varphi}A_{n-1}(\nu)V(\nu)\\
&\quad -\mu_A^{\varphi}A_{n-1}(\nu)\}d\nu,\\
E_n(t) &= \frac{1-\varphi}{\mathbb{N}(\varphi)}\{\Lambda_E^{\varphi}+\sigma^{\varphi}I_M(t)E_{n-1}(t)-\delta_2^{\varphi}\left(1+\chi_2^{\varphi}F_2(t)\right)I_M(t)E_{n-1}(t)\\
&\quad -\mu_E^{\varphi}E_{n-1}(t)\}\\
&\quad +\frac{\varphi}{\mathbb{N}(\varphi)\Gamma(\varphi)}\times\int_0^t(t-\nu)^{\varphi-1}\{\Lambda_E^{\varphi}+\sigma^{\varphi}I_M(\nu)E_{n-1}(\nu)\\
&\quad -\delta_2^{\varphi}\left(1+\chi_2^{\varphi}F_2(\nu)\right)I_M(\nu)E_{n-1}(\nu)-\mu_E^{\varphi}E_{n-1}(\nu)\}d\nu,\\
N_{K_n}(t) &= \frac{1-\varphi}{\mathbb{N}(\varphi)}\{\Lambda_{N_K}^{\varphi}+\theta_{\varphi}^{\varphi}F_1(t)+\theta_2^{\varphi}F_2(t)\\
&\quad -\delta_1^{\varphi}\left(1+\chi_1^{\varphi}F_1(t)\right)I_M(t)N_{K_{n-1}}(t)-\left(\eta^{\varphi}+\mu_{N_K}^{\varphi}\right)N_{K_{n-1}}(t)\}\\
&\quad +\frac{\varphi}{\mathbb{N}(\varphi)\Gamma(\varphi)}\times\int_0^t(t-\nu)^{\varphi-1}\{\Lambda_{N_K}^{\varphi}+\theta_1^{\varphi}F_1(\nu)+\theta_2^{\varphi}F_2(\nu)\\
&\quad -\delta_1^{\varphi}\left(1+\chi_1^{\varphi}F_1(\nu)\right)I_M(\nu)N_{K_{n-1}}(\nu)-\left(\eta^{\varphi}+\mu_{N_K}^{\varphi}\right)N_{K_{n-1}}(\nu)\}d\nu,
\end{aligned}
$$

$$
\begin{aligned}
I_{10_n}(t) &= \frac{1-\varphi}{\mathbb{N}(\varphi)}\left\{\rho_3^{\varphi} I_M(t)T_0(t)\left(\frac{1}{1+\tau_1^{\varphi} I_{10_{n-1}}}\right) - \mu_{I_{10}^{\varphi}(t)} I_{10_{n-1}}(t)\right\} \\
&\quad + \frac{\varphi}{\mathbb{N}(\varphi)\Gamma(\varphi)} \times \int_0^t (t-\nu)^{\varphi-1}\left\{\rho_3^{\varphi} I_M(\nu)T_0(\nu)\left(\frac{1}{1+\tau_1^{\varphi} I_{10_{n-1}}}\right)\right. \\
&\quad \left. - \mu_{I_{10}}^{\varphi} I_{10_{n-1}}(\nu)\right\} d\nu, \qquad (88) \\
F_{1_n}(t) &= \frac{1-\varphi}{\mathbb{N}(\varphi)}\{\varepsilon^{\varphi} I_M(t) - \left(\theta_1^{\varphi} + \mu_{F_1}^{\varphi}\right) F_{1_{n-1}}(t)\} \\
&\quad + \frac{\varphi}{\mathbb{N}(\varphi)\Gamma(\varphi)} \times \int_0^t (t-\nu)^{\varphi-1}\{\varepsilon^{\varphi} I_M(\nu) \\
&\quad - \left(\theta_1^{\varphi} + \mu_{F_1}^{\varphi}\right) F_{1_{n-1}}(\nu)\} d\nu, \\
F_{2_n}(t) &= \frac{1-\varphi}{\mathbb{N}(\varphi)}\{\eta^{\varphi} N_K(t) - \left(\theta_2^{\varphi} + \mu_{F_2}^{\varphi}\right) F_{2_{n-1}}(t)\} \\
&\quad + \frac{\varphi}{\mathbb{N}(\varphi)\Gamma(\varphi)} \times \int_0^t (t-\nu)^{\varphi-1}\{\eta^{\varphi} N_K(\nu) \\
&\quad - \left(\theta_2^{\varphi} + \mu_{F_2}^{\varphi}\right) F_{2_{n-1}}(\nu)\} d\nu.
\end{aligned}
$$

By taking the difference of each equation in systems 86, 87, and 88) and applying norm on both sides, the differences between successive terms in systems 86, 87 and

88 are expressed as follows:

$$
\begin{aligned}
\|T_{0_{n+1}} - T_{0_n}\| &= \frac{1-\varphi}{\mathbb{N}(\varphi)}\|\Bigg\{\Lambda^{\varphi}_{T_0} - \rho^{\varphi}_1 I_M T_{0_n} I_{10} - \rho^{\varphi}_2 V(t) T_{0_n} I_{10} \\
&\quad -\rho^{\varphi}_3 T_{0_n} I_M \left(\frac{1}{1+\tau^{\varphi}_1 I_{10}}\right) - \mu^{\varphi}_{T_0} T_{0_n}\Bigg\} \\
&\quad -\Bigg\{\Lambda^{\varphi}_{T_0} - \rho^{\varphi}_1 I_M T_{0_{n-1}} I_{10} - \rho^{\varphi}_2 V(t) T_{0_{n-1}} I_{10} \\
&\quad -\rho^{\varphi}_3 T_{0_{n-1}} I_M \left(\frac{1}{1+\tau^{\varphi}_1 I_{10}}\right) - \mu^{\varphi}_{T_0} T_{0_{n-1}}\Bigg\}\| \\
&\quad +\frac{\varphi}{\mathbb{N}(\varphi)\Gamma(\varphi)} \times \int_0^t (t-\nu)^{\varphi-1} \|\Bigg\{\Lambda^{\varphi}_{T_0} - \rho^{\varphi}_1 I_M T_{0_n} I_{10} \\
&\quad -\rho^{\varphi}_2 V T_{0_n} I_{10} - \rho^{\varphi}_3 T_{0_n} I_M \left(\frac{1}{1+\tau^{\varphi}_1 I_{10}}\right) - \mu^{\varphi}_{T_0} T_{0_n}\Bigg\} \\
&\quad -\Bigg\{\Lambda^{\varphi}_{T_0} - \rho^{\varphi}_1 I_M T_{0_{n-1}} I_{10} - \rho^{\varphi}_2 V T_{0_{n-1}} I_{10} \\
&\quad -\rho^{\varphi}_3 T_{0_{n-1}} I_M \left(\frac{1}{1+\tau^{\varphi}_1 I_{10}}\right) - \mu^{\varphi}_{T_0} T_{0_{n-1}}\Bigg\}\| d\nu, \\
\|T_{1_{n+1}} - T_{1_n}\| &= \frac{1-\varphi}{\mathbb{N}(\varphi)}\|\{\rho^{\varphi}_1 I_M T_0 I_{10} - \pi^{\varphi} I_M T_{1_n} - \mu^{\varphi}_{T_1} T_{1_n}\} \\
&\quad -\{\rho^{\varphi}_1 I_M T_0 I_{10} - \pi^{\varphi} I_M T_{1_{n-1}} - \mu^{\varphi}_{T_1} T_{1_{n-1}}\}\| \qquad (89) \\
&\quad +\frac{\varphi}{\mathbb{N}(\varphi)\Gamma(\varphi)} \times \int_0^t (t-\nu)^{\varphi-1} \|\{\rho^{\varphi}_1 I_M T_0 I_{10} - \pi^{\varphi} I_M T_{1_n} \\
&\quad -\mu^{\varphi}_{T_1} T_{1_n}\} - \{\rho^{\varphi}_1 I_M T_0 I_{10} - \pi^{\varphi} I_M T_{1_{n-1}} - \mu^{\varphi}_{T_1} T_{1_{n-1}}\}\| d\nu, \\
\|T_{2_{n+1}} - T_{2_n}\| &= \frac{1-\varphi}{\mathbb{N}(\varphi)}\|\{\rho^{\varphi}_2 V T_0 I_{10} - \delta^{\varphi}_3 T_{2_n} V - \mu^{\varphi}_{T_2} T_{2_n}\} \\
&\quad -\{\rho^{\varphi}_2 V T_0 I_{10} - \delta^{\varphi}_3 T_{2_{n-1}} V - \mu^{\varphi}_{T_2} T_{2_{n-1}}\}\| \\
&\quad +\frac{\varphi}{\mathbb{N}(\varphi)\Gamma(\varphi)} \times \int_0^t (t-\nu)^{\varphi-1} \|\{\rho^{\varphi}_2 V T_0 I_{10} - \delta^{\varphi}_3 T_{2_n} V \\
&\quad -\mu^{\varphi}_{T_2} T_{2_n}\} - \{\rho^{\varphi}_2 V T_0 I_{10} - \delta^{\varphi}_3 T_{2_{n-1}} V - \mu^{\varphi}_{T_2} T_{2_{n-1}}\}\| d\nu, \\
\|M_{0_{n+1}} - M_{0_n}\| &= \frac{1-\varphi}{\mathbb{N}(\varphi)}\|\{\Lambda^{\varphi}_{M_0} - \beta^{\varphi}_1 V M_{0_n} - \mu^{\varphi}_{M_0} M_{0_n}\} \\
&\quad -\{\Lambda^{\varphi}_{M_0} - \beta^{\varphi}_1 V M_{0_{n-1}} - \mu^{\varphi}_{M_0} M_{0_{n-1}}\}\| \\
&\quad +\frac{\varphi}{\mathbb{N}(\varphi)\Gamma(\varphi)} \times \int_0^t (t-\nu)^{\varphi-1} \|\{\Lambda^{\varphi}_{M_0} - \beta^{\varphi}_1 V M_{0_n} \\
&\quad -\mu^{\varphi}_{M_0} M_{0_n}\} - \{\Lambda^{\varphi}_{M_0} - \beta^{\varphi}_1 V M_{0_{n-1}} - \mu^{\varphi}_{M_0} M_{0_{n-1}}\}\| d\nu,
\end{aligned}
$$

$$
\begin{aligned}
\|M_{1_{n+1}} - M_{1_n}\| &= \frac{1-\varphi}{\mathbb{N}(\varphi)}\|\{\Lambda^{\varphi}_{M_1} - \beta^{\varphi}_2 V M_{1_n} + \zeta^{\varphi} I_M - \mu^{\varphi}_{M_1} M_{1_n}\} \\
&\quad -\{\Lambda^{\varphi}_{M_1} - \beta^{\varphi}_2 V M_{1_{n-1}} - \mu^{\varphi}_{M_1} M_{1_{n-1}}\}\| \\
&\quad + \frac{\varphi}{\mathbb{N}(\varphi)\Gamma(\varphi)} \times \int_0^t (t-\nu)^{\varphi-1} \|\{\Lambda^{\varphi}_{M_1} - \beta^{\varphi}_2 V M_{1_n} + \zeta^{\varphi} I_M \\
&\quad -\mu^{\varphi}_{M_1} M_{1_n}\} - \{\Lambda^{\varphi}_{M_1} - \beta^{\varphi}_2 V M_{1_{n-1}} + \zeta^{\varphi} I_M \\
&\quad -\mu^{\varphi}_{M_1} M_{1_{n-1}}\}\| d\nu, \\
\|I_{M_{n+1}} - I_{M_n}\| &= \frac{1-\varphi}{\mathbb{N}(\varphi)}\|\{\beta^{\varphi}_1 V M_0 + \beta^{\varphi}_2 V M_1 + \pi^{\varphi} I_{M_n} T_1 \\
&\quad -\delta^{\varphi}_1 \left(1 + \chi^{\varphi}_1 F_1\right) I_{M_n} N_K - \delta^{\varphi}_2 \left(1 + \chi^{\varphi}_2 F_2\right) I_{M_n} E \\
&\quad -\sigma^{\varphi} I_{M_n} E - \left(\omega^{\varphi} + \varepsilon^{\varphi} + \zeta^{\varphi} + \mu^{\varphi}_{I_M}\right) I_{M_n}\} \\
&\quad -\{\beta^{\varphi}_1 V M_0 + \beta^{\varphi}_2 V M_1 + \pi^{\varphi} I_{M_{n-1}} T_1 \\
&\quad -\delta^{\varphi}_1 \left(1 + \chi^{\varphi}_1 F_1\right) I_{M_{n-1}} N_K \delta^{\varphi}_2 \left(1 + \chi^{\varphi}_2 F_2\right) I_{Mn-1} E \\
&\quad -\sigma^{\varphi} I_{M_{n-1}} E - \left(\omega^{\varphi} + \varepsilon^{\varphi} + \zeta^{\varphi} + \mu^{\varphi}_{I_M}\right) I_{M_{n-1}}\}\| \qquad (90) \\
&\quad + \frac{\varphi}{\mathbb{N}(\varphi)\Gamma(\varphi)} \times \int_0^t (t-\nu)^{\varphi-1} \|\{\beta^{\varphi}_1 V M_0 + \beta^{\varphi}_2 V M_1 \\
&\quad +\pi^{\varphi} I_M T_1 - \delta^{\varphi}_1 \left(1 + \chi^{\varphi}_1 F_1\right) I_{M_n} N_K \\
&\quad -\delta^{\varphi}_2 \left(1 + \chi^{\varphi}_2 F_2\right) I_{M_n} E \\
&\quad -\sigma^{\varphi} I_{M_n} E - \left(\omega^{\varphi} + \varepsilon^{\varphi} + \zeta^{\varphi} + \mu^{\varphi}_{I_M}\right) I_{M_n}\} \\
&\quad -\{\beta^{\varphi}_1 V M_0 + \beta^{\varphi}_2 V M_1 + \pi^{\varphi} I_{M_{n-1}} T_1 \\
&\quad -\delta^{\varphi}_1 \left(1 + \chi^{\varphi}_1 F_1\right) I_{M_{n-1}} N_K - \delta^{\varphi}_2 \left(1 + \chi^{\varphi}_2 F_2\right) I_{M_{n-1}} E \\
&\quad -\sigma^{\varphi} I_{M_{n-1}} E - \left(\omega^{\varphi} + \varepsilon^{\varphi} + \zeta^{\varphi} + \mu^{\varphi}_{I_M}\right) I_{M_{n-1}}\} \| d\nu,
\end{aligned}
$$

$$
\begin{aligned}
\|V_{n+1}-V_n\| &= \frac{1-\varphi}{\mathbb{N}(\varphi)}\|\{\Lambda_V^{\varphi}+\omega^{\varphi}I_M-\delta_3^{\varphi}T_2V_n-\delta_4^{\varphi}AV_n \\
&\quad -\left(\psi^{\varphi}+\mu_V^{\varphi}\right)V_n\} \\
&\quad -\{\Lambda_V^{\varphi}+\omega^{\varphi}I_M-\delta_3^{\varphi}T_2V_{n-1}-\delta_4^{\varphi}AV_{n-1} \\
&\quad -\left(\psi^{\varphi}+\mu_V^{\varphi}\right)V_{n-1}\}\| \\
&\quad +\frac{\varphi}{\mathbb{N}(\varphi)\Gamma(\varphi)}\times\int_0^t(t-\nu)^{\varphi-1}\|\{\Lambda_V^{\varphi}+\omega^{\varphi}I_M-\delta_3^{\varphi}T_2V_n \\
&\quad -\delta_4^{\varphi}AV_n-\left(\psi^{\varphi}+\mu_V^{\varphi}\right)V_n\}-\{\Lambda_V^{\varphi}+\omega^{\varphi}I_M \\
&\quad -\delta_3^{\varphi}T_2V_{n-1}-\delta_4^{\varphi}AV_{n-1}-\left(\psi^{\varphi}+\mu_V^{\varphi}\right)V_{n-1}\}\|d\nu, \\
\|A_{n+1}-A_n\| &= \frac{1-\varphi}{\mathbb{N}(\varphi)}\|(\Lambda_A^{\varphi}+\psi^{\varphi}V-\delta_4^{\varphi}A_nV-\mu_A^{\varphi}A_n) \\
&\quad -(\Lambda_A^{\varphi}+\psi^{\varphi}V-\delta_4^{\varphi}A_{n-1}V-\mu_A^{\varphi}A_{n-1})\| \\
&\quad +\frac{\varphi}{\mathbb{N}(\varphi)\Gamma(\varphi)}\times\int_0^t(t-\nu)^{\varphi-1}\|\{\Lambda_A^{\varphi}+\psi^{\varphi}V-\delta_4^{\varphi}A_{n-1}V \\
&\quad -\mu_A^{\varphi}A_{n-1}\}-\{\Lambda_A^{\varphi}+\psi^{\varphi}V-\delta_4^{\varphi}A_{n-1}V-\mu_A^{\varphi}A_{n-1}\}\|d\nu, \\
\|E_{n+1}-E_n\| &= \frac{1-\varphi}{\mathbb{N}(\varphi)}\|(\Lambda_E^{\varphi}+\sigma^{\varphi}I_ME_n-\delta_2^{\varphi}\left(1+\chi_2^{\varphi}F_2\right)I_ME_n-\mu_E^{\varphi}E_n) \\
&\quad -\{\Lambda_E^{\varphi}+\sigma^{\varphi}I_ME_{n-1}-\delta_2^{\varphi}\left(1+\chi_2^{\varphi}F_2\right)I_ME_{n-1} \\
&\quad -\mu_E^{\varphi}E_{n-1}\}\| \\
&\quad +\frac{\varphi}{\mathbb{N}(\varphi)\Gamma(\varphi)}\times\int_0^t(t-\nu)^{\varphi-1}\|\{\Lambda_E^{\varphi}+\sigma^{\varphi}I_ME_n \\
&\quad -\delta_2^{\varphi}\left(1+\chi_2^{\varphi}F_2\right)I_ME_n-\mu_E^{\varphi}E_n\}-\{\Lambda_E^{\varphi}+\sigma^{\varphi}I_ME_{n-1} \\
&\quad -\delta_2^{\varphi}\left(1+\chi_2^{\varphi}F_2\right)I_ME_{n-1}-\mu_E^{\varphi}E_{n-1}\}\|d\nu, \qquad (91) \\
\|N_{K_{n+1}}-N_{K_n}\| &= \frac{1-\varphi}{\mathbb{N}(\varphi)}\|\{\Lambda_{N_K}^{\varphi}+\theta_1^{\varphi}F_1+\theta_2^{\varphi}F_2-\delta_1^{\varphi}\left(1+\chi_1^{\varphi}F_1\right)I_MN_{K_n}\} \\
&\quad -\left(\eta^{\varphi}+\mu_{N_K}^{\varphi}\right)N_{K_n}-\{\Lambda_{N_K}^{\varphi}+\theta_1^{\varphi}F_1+\theta_2^{\varphi}F_2 \\
&\quad -\delta_1^{\varphi}\left(1+\chi_1^{\varphi}F_1\right)I_MN_{K_{n-1}}-\left(\eta^{\varphi}+\mu_{N_K}^{\varphi}\right)N_{K_{n-1}}\}\| \\
&\quad +\frac{\varphi}{\mathbb{N}(\varphi)\Gamma(\varphi)}\times\int_0^t(t-\nu)^{\varphi-1}\|\{\Lambda_{N_K}^{\varphi}+\theta_1^{\varphi}F_1+\theta_2^{\varphi}F_2 \\
&\quad -\delta_1^{\varphi}\left(1+\chi_1^{\varphi}F_1\right)I_MN_{K_n}-\left(\eta^{\varphi}+\mu_{N_K}^{\varphi}\right)N_{K_n}\} \\
&\quad -\{\Lambda_{N_K}^{\varphi}+\theta_1^{\varphi}F_1+\theta_2^{\varphi}F_2-\delta_1^{\varphi}\left(1+\chi_1^{\varphi}F_1\right)I_MN_{K_{n-1}} \\
&\quad -\left(\eta^{\varphi}+\mu_{N_K}^{\varphi}\right)N_{K_{n-1}}\}\|d\nu,
\end{aligned}
$$

$$
\begin{aligned}
\|I_{10_{n+1}} - I_{10_n}\| &= \frac{1-\varphi}{\mathbb{N}(\varphi)}\|\left\{\rho_3^{\varphi} I_M T_0\left(\frac{1}{1+\tau_1^{\varphi} I_{10}}\right) - \mu_{I_{10}}^{\varphi} I_{10_n}\right\} \\
&\quad -\left\{\rho_3^{\varphi} I_M T_0\left(\frac{1}{1+\tau_1^{\varphi} I_{10}}\right)\mu_{I_{10}}^{\varphi} I_{10_{n-1}}\right\}\| \\
&\quad +\frac{\varphi}{\mathbb{N}(\varphi)\Gamma(\varphi)} \times \int_0^t (t-\nu)^{\varphi-1}\|\left\{\rho_3^{\varphi} I_M T_0\left(\frac{1}{1+\tau_1^{\varphi} I_{10}}\right)\right. \\
&\quad \left.-\mu_{I_{10}}^{\varphi} I_{10_{n-1}}\right\} - \left\{\rho_3^{\varphi} I_M T_0\left(\frac{1}{1+\tau_1^{\varphi} I_{10}}\right) - \mu_{I_{10}}^{\varphi} I_{10_n}\right\}\|d\nu, \\
\|F_{1_{n+1}} - F_{1_n}\| &= \frac{1-\varphi}{\mathbb{N}(\varphi)}\|\left(\varepsilon^{\varphi} I_M - \left(\theta_1^{\varphi} + \mu_{F_1}^{\varphi}\right) F_{1_n}\right) \\
&\quad -\left(\varepsilon^{\varphi} I_M - \left(\theta_1^{\varphi} + \mu_{F_1}^{\varphi}\right) F_{1_{n-1}}\right)\| \\
&\quad +\frac{\varphi}{\mathbb{N}(\varphi)\Gamma(\varphi)} \times \int_0^t (t-\nu)^{\varphi-1}\|\left(\varepsilon^{\varphi} I_M - \left(\theta_1^{\varphi} + \mu_{F_1}^{\varphi}\right) F_{1_n}\right) \\
&\quad -\left(\varepsilon^{\varphi} I_M - \left(\theta_1^{\varphi} + \mu_{F_1}^{\varphi}\right) F_{1_{n-1}}\right)\|d\nu, \qquad (92) \\
\|F_{2_{n+1}} - F_{2_n}\| &= \frac{1-\varphi}{\mathbb{N}(\varphi)}\|\left(\eta^{\varphi} N_K(t) - \left(\theta_2^{\varphi} + \mu_{F_2}^{\varphi}\right) F_{2_n}\right) \\
&\quad -\left(\eta^{\varphi} N_K(t) - \left(\theta_2^{\varphi} + \mu_{F_2}^{\varphi}\right) F_{2_{n-1}}\right)\| \\
&\quad +\frac{\varphi}{\mathbb{N}(\varphi)\Gamma(\varphi)} \times \int_0^t (t-\nu)^{\varphi-1}\|\left(\eta^{\varphi} N_K - \left(\theta_2^{\varphi} + \mu_{F_2}^{\varphi}\right) F_{2_n}\right) \\
&\quad -\left(\eta^{\varphi} N_K(t) - \left(\theta_2^{\varphi} + \mu_{F_2}^{\varphi}\right) F_{2_{n-1}}\right)\|d\nu.
\end{aligned}
$$

Theorem 9

If the following inequality holds for t_0, then the considered model 39 has a solution:

$$\mathbb{Z}_i = \max\{\Psi_i\} < 1, \quad i = 1, 2, \cdots, 13.$$

Where

$$\Psi_i = \frac{1-\varphi}{\mathbb{N}(\varphi)}\Theta_i + \frac{t_0^{\varphi}}{\mathbb{N}(\varphi)\Gamma(\varphi)}\Theta_i < 1.$$

Proof. Suppose the following equations: $\Omega_{1n} = T_{0_{n+1}}(t) - T_{0_n}(t)$, $\Omega_{2n} = T_{1_{n+1}}(t) - T_{1_n}(t)$, $\Omega_{3n} = T_{2_{n+1}}(t) - T_{2_n}(t)$, $\Omega_{4n} = M_{0_{n+1}}(t) - M_{0_n}(t)$, $\Omega_{5n} = M_{1_{n+1}}(t) - M_{1_n}(t)$, $\Omega_{6n} = I_{M_{n+1}}(t) - I_{M_n}(t)$, $\Omega_{7n} = V_{n+1}(t) - V_n(t)$, $\Omega_{8n} = A_{n+1}(t) - A_n(t)$, $\Omega_{9n} = E_{n+1}(t) - E_n(t)$, $\Omega_{10n} = N_{K_{n+1}}(t) - N_{K_n}(t)$, $\Omega_{11n} = I_{10_{n+1}}(t) - I_{10_n}(t)$,

$\Omega_{12n} = F_{1_{n+1}}(t) - F_{1_n}(t), \Omega_{13n} = F_{2_{n+1}}(t) - F_{2_n}(t).$

First, the analysis begins with Ω_{1n} for the first compartment

$$\begin{aligned}
\|\Omega_{1n}\| &= \frac{1-\varphi}{\mathbb{N}(\varphi)}\|\Phi_1(t, T_{0_n}) - \Phi_1(t - T_0)\| + \frac{\varphi}{\mathbb{N}(\varphi)\Gamma(\varphi)} \\
&\quad \times \int_0^t (t-\nu)^{\varphi-1} \|\Phi_1(\nu, T_{0_n}(\nu)) - \Phi_1(\nu - T_0(\nu))\| d\nu, \\
&\leq \left(\frac{1-\varphi}{\mathbb{N}(\varphi)} + \frac{\varphi}{\mathbb{N}(\varphi)\Gamma(\varphi)} t^{\varphi}\right) \Psi_1 \|T_{0_n} - T_0\|, \\
&\leq \left(\frac{1-\varphi}{\mathbb{N}(\varphi)} + \frac{\varphi}{\mathbb{N}(\varphi)\Gamma(\varphi)} t^{\varphi}\right)^n \mathbb{Z}_1^n \|T_0 - T_{0_1}\|.
\end{aligned}$$

Next, the analysis proceeds with the second compartment

$$\begin{aligned}
\|\Omega_{2n}\| &= \frac{1-\varphi}{\mathbb{N}(\varphi)}\|\Phi_2(t, T_{1n}) - \Phi_2(t - T_1)\| + \frac{\varphi}{\mathbb{N}(\varphi)\Gamma(\varphi)} \\
&\quad \times \int_0^t (t-\nu)^{\varphi-1} \|\Phi_2(\nu, T_{1_n}(\nu)) - \Phi_2(\nu - T_1(\nu))\| d\nu, \\
&\leq \left(\frac{1-\varphi}{\mathbb{N}(\varphi)} + \frac{\varphi}{\mathbb{N}(\varphi)\Gamma(\varphi)} t^{\varphi}\right) \Psi_2 \|T_{1_n} - T_1\|, \\
&\leq \left(\frac{1-\varphi}{\mathbb{N}(\varphi)} + \frac{\varphi}{\mathbb{N}(\varphi)\Gamma(\varphi)} t^{\varphi}\right)^n \mathbb{Z}_2^n \|T_1 - T_{1_1}\|.
\end{aligned}$$

Next, the analysis proceeds with the third compartment

$$\begin{aligned}
\|\Omega_{3n}\| &= \frac{1-\varphi}{\mathbb{N}(\varphi)}\|\Phi_3(t, T_{2_n}) - \Phi_3(t - T_2)\| + \frac{\varphi}{\mathbb{N}(\varphi)\Gamma(\varphi)} \\
&\quad \times \int_0^t (t-\nu)^{\varphi-1} \|\Phi_3(\nu, T_{2_n}(\nu)) - \Phi_3(\nu - T_2(\nu))\| d\nu, \\
&\leq \left(\frac{1-\varphi}{\mathbb{N}(\varphi)} + \frac{\varphi}{\mathbb{N}(\varphi)\Gamma(\varphi)} t^{\varphi}\right) \Psi_3 \|T_{2_n} - T_2\|, \\
&\leq \left(\frac{1-\varphi}{\mathbb{N}(\varphi)} + \frac{\varphi}{\mathbb{N}(\varphi)\Gamma(\varphi)} t^{\varphi}\right)^n \mathbb{Z}_3^n \|T_2 - T_{2_1}\|.
\end{aligned}$$

Next, the analysis proceeds with the fourth compartment

$$\begin{aligned}
\|\Omega_{4n}\| &= \frac{1-\varphi}{\mathbb{N}(\varphi)}\|\Phi_4(t, M_{0_n}) - \Phi_4(t - M_0)\| + \frac{\varphi}{\mathbb{N}(\varphi)\Gamma(\varphi)} \\
&\quad \times \int_0^t (t-\nu)^{\varphi-1} \|\Phi_4(\nu, M_{0_n}(\nu)) - \Phi_4(\nu - M_0(\nu))\| d\nu, \\
&\leq \left(\frac{1-\varphi}{\mathbb{N}(\varphi)} + \frac{\varphi}{\mathbb{N}(\varphi)\Gamma(\varphi)} t^{\varphi}\right) \Psi_4 \|M_{0_n} - M_0\|, \\
&\leq \left(\frac{1-\varphi}{\mathbb{N}(\varphi)} + \frac{\varphi}{\mathbb{N}(\varphi)\Gamma(\varphi)} t^{\varphi}\right)^n \mathbb{Z}_4^n \|M_0 - M_{0_1}\|.
\end{aligned}$$

Next, the analysis proceeds with the fifth compartment

$$\begin{aligned}
\|\Omega_{5n}\| &= \frac{1-\varphi}{\mathbb{N}(\varphi)}\|\Phi_5(t, M_{1_n}) - \Phi_5(t - M_1)\| + \frac{\varphi}{\mathbb{N}(\varphi)\Gamma(\varphi)} \\
&\quad \times \int_0^t (t-\nu)^{\varphi-1} \|\Phi_5(\nu, M_{1_n}(\nu)) - \Phi_5(\nu - M_1(\nu))\| d\nu, \\
&\leq \left(\frac{1-\varphi}{\mathbb{N}(\varphi)} + \frac{\varphi}{\mathbb{N}(\varphi)\Gamma(\varphi)} t^{\varphi}\right) \Psi_5 \|M_{1_n} - M_1\|, \\
&\leq \left(\frac{1-\varphi}{\mathbb{N}(\varphi)} + \frac{\varphi}{\mathbb{N}(\varphi)\Gamma(\varphi)} t^{\varphi}\right)^n \mathbb{Z}_5^n \|M_1 - M_{1_1}\|.
\end{aligned}$$

Next, the analysis proceeds with the sixth compartment

$$\begin{aligned}
\|\Omega_{6n}\| &= \frac{1-\varphi}{\mathbb{N}(\varphi)}\|\Phi_6(t, I_{M_n}) - \Phi_6(t - I_M)\| + \frac{\varphi}{\mathbb{N}(\varphi)\Gamma(\varphi)} \\
&\quad \times \int_0^t (t-\nu)^{\varphi-1} \|\Phi_6(\nu, I_{M_n}(\nu)) - \Phi_6(\nu - I_M(\nu))\| d\nu, \\
&\leq \left(\frac{1-\varphi}{\mathbb{N}(\varphi)} + \frac{\varphi}{\mathbb{N}(\varphi)\Gamma(\varphi)} t^{\varphi}\right) \Psi_6 \|I_{M_n} - I_M\|, \\
&\leq \left(\frac{1-\varphi}{\mathbb{N}(\varphi)} + \frac{\varphi}{\mathbb{N}(\varphi)\Gamma(\varphi)} t^{\varphi}\right)^n \mathbb{Z}_6^n \|I_M - I_{M_1}\|.
\end{aligned}$$

Next, the analysis proceeds with the seventh compartment

$$\begin{aligned}
\|\Omega_{7n}\| &= \frac{1-\varphi}{\mathbb{N}(\varphi)}\|\Phi_7(t, V_n) - \Phi_7(t - V)\| + \frac{\varphi}{\mathbb{N}(\varphi)\Gamma(\varphi)} \\
&\quad \times \int_0^t (t-\nu)^{\varphi-1} \|\Phi_7(\nu, V_n(\nu)) - \Phi_7(\nu - V(\nu))\| d\nu, \\
&\leq \left(\frac{1-\varphi}{\mathbb{N}(\varphi)} + \frac{\varphi}{\mathbb{N}(\varphi)\Gamma(\varphi)} t^{\varphi}\right) \Psi_7 \|V_n - V\|, \\
&\leq \left(\frac{1-\varphi}{\mathbb{N}(\varphi)} + \frac{\varphi}{\mathbb{N}(\varphi)\Gamma(\varphi)} t^{\varphi}\right)^n \mathbb{Z}_7^n \|V - V_1\|.
\end{aligned}$$

Next, the analysis proceeds with the eighth compartment

$$\begin{aligned}\|\Omega_{8n}\| &= \frac{1-\varphi}{\mathbb{N}(\varphi)}\|\Phi_8(t,A_n)-\Phi_8(t-A)\|+\frac{\varphi}{\mathbb{N}(\varphi)\Gamma(\varphi)}\\ &\quad\times\int_0^t(t-\nu)^{\varphi-1}\|\Phi_8(\nu,A_n(\nu))-\Phi_8(\nu-A(\nu))\|d\nu,\\ &\leq \left(\frac{1-\varphi}{\mathbb{N}(\varphi)}+\frac{\varphi}{\mathbb{N}(\varphi)\Gamma(\varphi)}t^{\varphi}\right)\Psi_8\|A_n-A\|,\\ &\leq \left(\frac{1-\varphi}{\mathbb{N}(\varphi)}+\frac{\varphi}{\mathbb{N}(\varphi)\Gamma(\varphi)}t^{\varphi}\right)^n\mathbb{Z}_8^n\|A-A_1\|.\end{aligned}$$

Next, the analysis proceeds with the ninth compartment

$$\begin{aligned}\|\Omega_{9n}\| &= \frac{1-\varphi}{\mathbb{N}(\varphi)}\|\Phi_9(t,E_n)-\Phi_9(t-E)\|+\frac{\varphi}{\mathbb{N}(\varphi)\Gamma(\varphi)}\\ &\quad\times\int_0^t(t-\nu)^{\varphi-1}\|\Phi_9(\nu,E_n(\nu))-\Phi_9(\nu-E(\nu))\|d\nu,\\ &\leq \left(\frac{1-\varphi}{\mathbb{N}(\varphi)}+\frac{\varphi}{\mathbb{N}(\varphi)\Gamma(\varphi)}t^{\varphi}\right)\Psi_9\|E_n-E\|,\\ &\leq \left(\frac{1-\varphi}{\mathbb{N}(\varphi)}+\frac{\varphi}{\mathbb{N}(\varphi)\Gamma(\varphi)}t^{\varphi}\right)^n\mathbb{Z}_9^n\|E-E_1\|.\end{aligned}$$

Next, the analysis proceeds with the tenth compartment

$$\begin{aligned}\|\Omega_{10n}\| &= \frac{1-\varphi}{\mathbb{N}(\varphi)}\|\Phi_{10}(t,N_{K_n})-\Phi_{10}(t-N_K)\|+\frac{\varphi}{\mathbb{N}(\varphi)\Gamma(\varphi)}\\ &\quad\times\int_0^t(t-\nu)^{\varphi-1}\|\Phi_{10}(\nu,N_{K_n}(\nu))-\Phi_{10}(\nu-N_K(\nu))\|d\nu,\\ &\leq \left(\frac{1-\varphi}{\mathbb{N}(\varphi)}+\frac{\varphi}{\mathbb{N}(\varphi)\Gamma(\varphi)}t^{\varphi}\right)\Psi_{10}\|N_{K_n}-N_K\|,\\ &\leq \left(\frac{1-\varphi}{\mathbb{N}(\varphi)}+\frac{\varphi}{\mathbb{N}(\varphi)\Gamma(\varphi)}t^{\varphi}\right)^n\mathbb{Z}_{10}^n\|N_K-N_{K_1}\|.\end{aligned}$$

Next, the analysis proceeds with the eleventh compartment

$$\begin{aligned}\|\Omega_{11n}\| &= \frac{1-\varphi}{\mathbb{N}(\varphi)}\|\Phi_{11}(t,I_{10_n})-\Phi_{11}(t-I_{10})\|+\frac{\varphi}{\mathbb{N}(\varphi)\Gamma(\varphi)}\\ &\quad\times\int_0^t(t-\nu)^{\varphi-1}\|\Phi_{11}(\nu,I_{10_n}(\nu))-\Phi_{10}(\nu-I_{10}(\nu))\|d\nu,\\ &\leq \left(\frac{1-\varphi}{\mathbb{N}(\varphi)}+\frac{\varphi}{\mathbb{N}(\varphi)\Gamma(\varphi)}t^{\varphi}\right)\Psi_{11}\|I_{10_n}-I_{10}\|,\\ &\leq \left(\frac{1-\varphi}{\mathbb{N}(\varphi)}+\frac{\varphi}{\mathbb{N}(\varphi)\Gamma(\varphi)}t^{\varphi}\right)^n\mathbb{Z}_{11}^n\|I_{10}-I_{10_1}\|.\end{aligned}$$

Next, the analysis proceeds with the twelveth compartment

$$\begin{aligned}
\|\Omega_{12n}\| &= \frac{1-\varphi}{\mathbb{N}(\varphi)}||\Phi_{12}\left(t,F_{1_n}\right)-\Phi_{12}\left(t-F_{1_1}\right)\|+\frac{\varphi}{\mathbb{N}(\varphi)\Gamma(\varphi)}\\
&\quad\times\int_0^t(t-\nu)^{\varphi-1}\left\|\Phi_{12}\left(\nu,F_{1_n}(\nu)\right)-\Phi_{12}\left(\nu-F_1(\nu)\right)\right\|d\nu,\\
&\leq \left(\frac{1-\varphi}{\mathbb{N}(\varphi)}+\frac{\varphi}{\mathbb{N}(\varphi)\Gamma(\varphi)}t^{\varphi}\right)\Psi_{12}\|F_{1_n}-F_1\|,\\
&\leq \left(\frac{1-\varphi}{\mathbb{N}(\varphi)}+\frac{\varphi}{\mathbb{N}(\varphi)\Gamma(\varphi)}t^{\varphi}\right)^n\mathbb{Z}_{12}^n\|F_1-F_{1_1}\|.
\end{aligned}$$

Finally, the analysis proceeds with the thirteenth compartment

$$\begin{aligned}
\|\Omega_{13n}\| &= \frac{1-\varphi}{\mathbb{N}(\varphi)}\|\Phi_{13}\left(t,F_{2_n}\right)-\Phi_{13}\left(t-F_2\right)\|+\frac{\varphi}{\mathbb{N}(\varphi)\Gamma(\varphi)}\\
&\quad\times\int_0^t(t-\nu)^{\varphi-1}\left\|\Phi_{13}\left(\nu,F_{2_n}(\nu)\right)-\Phi_{13}\left(\nu-F_2(\nu)\right)\right\|d\nu,\\
&\leq \left(\frac{1-\varphi}{\mathbb{N}(\varphi)}+\frac{\varphi}{\mathbb{N}(\varphi)\Gamma(\varphi)}t^{\varphi}\right)\Psi_{13}\|F_{2_n}-F_2\|,\\
&\leq \left(\frac{1-\varphi}{\mathbb{N}(\varphi)}+\frac{\varphi}{\mathbb{N}(\varphi)\Gamma(\varphi)}t^{\varphi}\right)^n\mathbb{Z}_{13}^n\|F_2-F_{2_1}\|.
\end{aligned}$$

Following the analysis above, it can be seen that

$$\begin{aligned}
\|\Omega_{1n}\| &= \|T_{0_{n+k}}(t)-T_{0_n}(t)\|\leq\sum_{j=n+1}^{n+k}Z_1^j=\frac{Z_1^{n+1}-Z_1^{n+k+1}}{1-Z_1},\\
\|\Omega_{2n}\| &= \|T_{1_{n+k}}(t)-T_{1_n}(t)\|\leq\sum_{j=n+1}^{n+k}Z_2^j=\frac{Z_2^{n+1}-Z_2^{n+k+1}}{1-Z_2},\\
\|\Omega_{3n}\| &= \|T_{2_{n+k}}(t)-T_{2_n}(t)\|\leq\sum_{j=n+1}^{n+k}Z_3^j=\frac{Z_3^{n+1}-Z_3^{n+k+1}}{1-Z_3},\\
\|\Omega_{4n}\| &= \|M_{0_{n+k}}(t)-M_{0_n}(t)\|\leq\sum_{j=n+1}^{n+k}Z_4^j=\frac{Z_4^{n+1}-Z_4^{n+k+1}}{1-Z_4},\\
\|\Omega_{5n}\| &= \|M_{1_{n+k}}(t)-M_{1_n}(t)\|\leq\sum_{j=n+1}^{n+k}Z_5^j=\frac{Z_5^{n+1}-Z_5^{n+k+1}}{1-Z_5},\\
\|\Omega_{6n}\| &= \|I_{M_{n+k}}(t)-I_{M_n}(t)\|\leq\sum_{j=n+1}^{n+k}Z_6^j=\frac{Z_6^{n+1}-Z_6^{n+k+1}}{1-Z_6},\\
\|\Omega_{7n}\| &= \|V_{n+k}(t)-V_n(t)\|\leq\sum_{j=n+1}^{n+k}Z_7^j=\frac{Z_7^{n+1}-Z_7^{n+k+1}}{1-Z_7},
\end{aligned}$$

$$\begin{aligned}
\|\Omega_{8n}\| &= \|A_{n+k}(t) - A_n(t)\| \leq \sum_{j=n+1}^{n+k} Z_8^j = \frac{Z_8^{n+1} - Z_8^{n+k+1}}{1 - Z_8}, \\
\|\Omega_{9n}\| &= \|E_{n+k}(t) - E_n(t)\| \leq \sum_{j=n+1}^{n+k} Z_9^j = \frac{Z_9^{n+1} - Z_9^{n+k+1}}{1 - Z_9}, \\
\|\Omega_{10n}\| &= \|N_{K_{n+k}}(t) - N_{K_n}(t)\| \leq \sum_{j=n+1}^{n+k} Z_{10}^j = \frac{Z_{10}^{n+1} - Z_{10}^{n+k+1}}{1 - Z_{10}}, \\
\|\Omega_{11n}\| &= \|I_{10_{n+k}}(t) - I_{10_n}(t)\| \leq \sum_{j=n+1}^{n+k} Z_{11}^j = \frac{Z_{11}^{n+1} - Z_{11}^{n+k+1}}{1 - Z_{11}}, \\
\|\Omega_{12n}\| &= \|F_{1_{n+k}}(t) - F_{1_n}(t)\| \leq \sum_{j=n+1}^{n+k} Z_{12}^j = \frac{Z_{12}^{n+1} - Z_{12}^{n+k+1}}{1 - Z_{12}}, \\
\|\Omega_{13n}\| &= \|F_{2_{n+k}}(t) - F_{2_n}(t)\| \leq \sum_{j=n+1}^{n+k} Z_{13}^j = \frac{Z_{13}^{n+1} - Z_{13}^{n+k+1}}{1 - Z_{13}},
\end{aligned}$$

for some k.

Hence, we have found that the sequence $\|\Omega_{in}(t)\| \to 0$ (i.e tends to zero)

$$\forall i = 1, 2, \cdots, 13$$

as $n \to \infty$ (tends to infinity). Therefore,

$$T_0, T_1, T_2, M_0, M_1, I_M, V, A, E, N_K, I_{10}, F_1$$

and F_2 can be viewed as Cauchy sequences within the Banach space $B(S)$. Applying the limit theorem as n tends to infinity confirms that the limit of these sequences is the singular solution of 39. This demonstrates their uniform convergence (Taylor & Lay, 1986; X. Liu et al., 2022), and establishes the existence of a solution for 39 under Theorem 9. Thus, the proof is concluded.

Next, the uniqueness of the solution for the considered model in Eq. (33) was demonstrated.

Theorem 10

The system has a unique solution if the following holds:

$$\left(\frac{1-\varphi}{\mathbb{N}(\varphi)}+\frac{\varphi}{\mathbb{N}(\varphi)\Gamma(\varphi)}t^{\varphi}\right)\Psi_i \quad \leq \quad 1, i=1,2,\cdots,13.$$

Proof. Suppose the considered model 78 has solutions $T_0(t)$, $T_1(t)$, $T_2(t)$, $M_0(t)$, $M_1(t)$, $I_M(t)$, $V(t)$, $A(t)$, $E(t)$, $N_K(t)$, $I_{10}(t)$, $F_1(t)$, $F_2(t)$ as well as $\hat{T}_0(t)$, $\hat{T}_1(t)$, $\hat{T}_2(t)$, $\hat{M}_0(t)$, $\hat{M}_1(t)$, $\hat{I_M}(t)$, $\hat{V}(t)$, $\hat{A}(t)$, $\hat{E}(t)$, $\hat{N_K}(t)$, $\hat{I_{10}}(t)$, $\hat{F}_1(t)$, $\hat{F}_2(t)$, then the model system can be written as

$$\begin{aligned}
\hat{T_0}(t) &= \frac{1-\varphi}{\mathbb{N}(\varphi)}\Bigg\{\Lambda_{T_0}^{\varphi}-\rho_1^{\varphi}I_M(t)\hat{T}_0(t)I_{10}(t)-\rho_2^{\varphi}V(t)\hat{T}_0(t)I_{10}(t)\\
&\quad -\rho_3^{\varphi}\hat{T}_0(t)I_M(t)\left(\frac{1}{1+\tau_1^{\varphi}I_{10}}\right)-\mu_{T_0}^{\varphi}\hat{T}_0(t)\Bigg\}\\
&\quad +\frac{\varphi}{\mathbb{N}(\varphi)\Gamma(\varphi)}\times\int_0^t(t-\nu)^{\varphi-1}\Bigg\{\Lambda_{T_0}^{\varphi}-\rho_1^{\varphi}I_M(\nu)\hat{T}_0(\nu)I_{10}(\nu)\\
&\quad -\rho_2^{\varphi}V(\nu)\hat{T}_0(\nu)I_{10}(\nu)-\rho_3^{\varphi}\hat{T}_0(\nu)I_M(\nu)\left(\frac{1}{1+\tau_1^{\varphi}I_{10}}\right)\\
&\quad -\mu_{T_0}^{\varphi}\hat{T}_0(\nu)\Bigg\}d\nu,\\
\hat{T}_1(t) &= \frac{1-\varphi}{\mathbb{N}(\varphi)}\left(\rho_1^{\varphi}I_M(t)T_0(t)I_{10}(t)-\pi^{\varphi}I_M(t)\hat{T}_1(t)-\mu_{T_1}^{\varphi}\hat{T}_1(t)\right)\\
&\quad +\frac{\varphi}{\mathbb{N}(\varphi)\Gamma(\varphi)}\times\int_0^t(t-\nu)^{\varphi-1}\{\rho_1^{\varphi}I_M(\nu)T_0(\nu)I_{10}(\nu)\\
&\quad -\pi^{\varphi}I_M(\nu)\hat{T}_1(\nu)-\mu_{T_1}^{\varphi}\hat{T}_1(\nu)\}d\nu,\\
\hat{T}_2(t) &= \frac{1-\varphi}{\mathbb{N}(\varphi)}\left(\rho_2^{\varphi}V(t)T_0(t)I_{10}(t)-\delta_3^{\varphi}\hat{T}_2(t)V(t)-\mu_{T_2}^{\varphi}\hat{T}_2(t)\right) \qquad (93)\\
&\quad +\frac{\varphi}{\mathbb{N}(\varphi)\Gamma(\varphi)}\times\int_0^t(t-\nu)^{\varphi-1}\{\rho_2^{\varphi}V(\nu)T_0(\nu)I_{10}(\nu)\\
&\quad -\delta_3^{\varphi}\hat{T}_2(\nu)V(\nu)-\mu_{T_2}^{\varphi}\hat{T}_2(\nu)\}d\nu,\\
\hat{M}_0(t) &= \frac{1-\varphi}{\mathbb{N}(\varphi)}\left(\Lambda_{M_0}^{\varphi}-\beta_1^{\varphi}V(t)\hat{M}_0(t)-\mu_{M_0}^{\varphi}\hat{M}_0(t)\right)\\
&\quad +\frac{\varphi}{\mathbb{N}(\varphi)\Gamma(\varphi)}\times\int_0^t(t-\nu)^{\varphi-1}\{\Lambda_{M_0}^{\varphi}-\beta_1^{\varphi}V(\nu)\hat{M}_0(\nu)\\
&\quad -\mu_{M_0}^{\varphi}\hat{M}_0(\nu)\}d\nu,
\end{aligned}$$

$$
\begin{aligned}
\hat{M_1}(t) &= \frac{1-\varphi}{\mathbb{N}(\varphi)}\left(\Lambda_{M_1}^{\varphi}-\beta_2^{\varphi}V(t)\hat{M_1}(t)+\zeta^{\varphi}I_M(t)-\mu_{M_1}^{\varphi}\hat{M_1}(t)\right)\\
&+\frac{\varphi}{\mathbb{N}(\varphi)\Gamma(\varphi)}\times\int_0^t(t-\nu)^{\varphi-1}\left\{\Lambda_{M_1}^{\varphi}-\beta_2^{\varphi}V(\nu)\hat{M_1}(\nu)\right.\\
&\left.+\zeta^{\varphi}I_M(\nu)-\mu_{M_1}^{\varphi}\hat{M_1}(\nu)\right\}d\nu,\\
\hat{I_M}(t) &= \frac{1-\varphi}{\mathbb{N}(\varphi)}\{\beta_1^{\varphi}V(t)M_0(t)+\beta_2^{\varphi}V(t)M_1(t)+\pi^{\varphi}\hat{I_M}(t)T_1(t)\\
&-\delta_1^{\varphi}\left(1+\chi_1^{\varphi}F_1(t)\right)\hat{I_M}(t)N_K(t)-\delta_2^{\varphi}\left(1+\chi_2^{\varphi}F_2(t)\right)\hat{I_M}(t)E(t)\\
&-\sigma^{\varphi}\hat{I_M}(t)E(t)-\left(\omega^{\varphi}+\varepsilon^{\varphi}+\zeta^{\varphi}+\mu_{I_M}^{\varphi}\right)\hat{I_M}(t)\}\\
&+\frac{\varphi}{\mathbb{N}(\varphi)\Gamma(\varphi)}\times\int_0^t(t-\nu)^{\varphi-1}\{\beta_1^{\varphi}V(\nu)M_0(\nu)+\beta_2^{\varphi}V(\nu)M_1(\nu)\\
&+\pi^{\varphi}\hat{I_M}(\nu)T_1(\nu)-\delta_1^{\varphi}\left(1+\chi_1^{\varphi}F_1(\nu)\right)\hat{I_M}(\nu)N_K(\nu)\\
&-\delta_2^{\varphi}\left(1+\chi_2^{\varphi}F_2(\nu)\right)\hat{I_M}(\nu)E(\nu)-\sigma^{\varphi}\hat{I_M}(\nu)E(\nu)\\
&-\left(\omega^{\varphi}+\varepsilon^{\varphi}+\zeta^{\varphi}+\mu_{I_M}^{\varphi}\right)\hat{I_M}(\nu)\}d\nu,\\
\hat{V}(t) &= \frac{1-\varphi}{\mathbb{N}(\varphi)}\{\Lambda_V^{\varphi}+\omega^{\varphi}I_M(t)-\delta_3^{\varphi}T_2(t)\hat{V}(t)-\delta_4^{\varphi}A(t)\hat{V}(t)\\
&-\left(\psi^{\varphi}+\mu_V^{\varphi}\right)\hat{V}(t)\}\\
&+\frac{\varphi}{\mathbb{N}(\varphi)\Gamma(\varphi)}\times\int_0^t(t-\nu)^{\varphi-1}\{\Lambda_V^{\varphi}+\omega^{\varphi}I_M(\nu)-\delta_3^{\varphi}T_2(\nu)\hat{V}(\nu)\\
&-\delta_4^{\varphi}A(\nu)\hat{V}(\nu)-\left(\psi^{\varphi}+\mu_V^{\varphi}\right)\hat{V}(\nu)\}d\nu, \qquad (94)\\
\hat{A}(t) &= \frac{1-\varphi}{\mathbb{N}(\varphi)}\left(\Lambda_A^{\varphi}+\psi^{\varphi}V(t)-\delta_4^{\varphi}\hat{A}(t)V(t)-\mu_A^{\varphi}\hat{A}(t)\right)\\
&+\frac{\varphi}{\mathbb{N}(\varphi)\Gamma(\varphi)}\times\int_0^t(t-\nu)^{\varphi-1}\{\Lambda_A^{\varphi}+\psi^{\varphi}V(\nu)-\delta_4^{\varphi}\hat{A}(\nu)V(\nu)\\
&-\mu_A^{\varphi}\hat{A}(\nu)\}d\nu,\\
\hat{E}(t) &= \frac{1-\varphi}{\mathbb{N}(\varphi)}\{\Lambda_E^{\varphi}+\sigma^{\varphi}I_M(t)\hat{E}(t)-\delta_2^{\varphi}\left(1+\chi_2^{\varphi}F_2\right)I_M(t)\hat{E}(t)\\
&-\mu_E^{\varphi}\hat{E}(t)\}\\
&+\frac{\varphi}{\mathbb{N}(\varphi)\Gamma(\varphi)}\times\int_0^t(t-\nu)^{\varphi-1}\{\Lambda_E^{\varphi}+\sigma^{\varphi}I_M(\nu)\hat{E}(\nu)\\
&-\delta_2^{\varphi}\left(1+\chi_2^{\varphi}F_2(\nu)\right)I_M(\nu)\hat{E}(\nu)-\mu_E^{\varphi}\hat{E}(\nu)\}d\nu,
\end{aligned}
$$

$$
\begin{aligned}
\hat{N_K}(t) &= \frac{1-\varphi}{\mathbb{N}(\varphi)}\{\Lambda^{\varphi}_{N_K} + \theta^{\varphi}_1 F_1(t) + \theta^{\varphi}_2 F_2(t) - \delta^{\varphi}_1 \left(1+\chi^{\varphi}_1 F_1\right) I_M(t)\hat{N_K}(t) \\
&\quad - \left(\eta^{\varphi} + \mu^{\varphi}_{N_K}\right)\hat{N_K}(t)\} \\
&\quad + \frac{\varphi}{\mathbb{N}(\varphi)\Gamma(\varphi)} \times \int_0^t (t-\nu)^{\varphi-1}\{\Lambda^{\varphi}_{N_K} + \theta^{\varphi}_1 F_1(\nu) + \theta^{\varphi}_2 F_2(\nu) \\
&\quad - \delta^{\varphi}_1 \left(1+\chi^{\varphi}_1 F_1(\nu)\right) I_M(\nu)\hat{N_K}(\nu) - \left(\eta^{\varphi} + \mu^{\varphi}_{N_K}\right)\hat{N_K}(\nu)\}d\nu, \\
\hat{I_{10}}(t) &= \frac{1-\varphi}{\mathbb{N}(\varphi)}\left(\rho^{\varphi}_3 I_M(t)T_0(t)\left(\frac{1}{1+\tau^{\varphi}_1 I_{10}}\right) - \mu^{\varphi}_{I_{10}(t)}\hat{I_{10}}(t)\right) \\
&\quad + \frac{\varphi}{\mathbb{N}(\varphi)\Gamma(\varphi)} \times \int_0^t (t-\nu)^{\varphi-1}\{\rho^{\varphi}_3 I_M(\nu)T_0(\nu)\left(\frac{1}{1+\tau^{\varphi}_1 I_{10}}\right) \\
&\quad - \mu^{\varphi}_{I_{10}}\hat{I_{10}}(\nu)\}d\nu, \\
\hat{F_1}(t) &= \frac{1-\varphi}{\mathbb{N}(\varphi)}\left(\varepsilon^{\varphi} I_M(t) - \left(\theta^{\varphi}_1 + \mu^{\varphi}_{F_1}\right)\hat{F_1}(t)\right) \\
&\quad + \frac{\varphi}{\mathbb{N}(\varphi)\Gamma(\varphi)} \times \int_0^t (t-\nu)^{\varphi-1}\left(\varepsilon^{\varphi} I_M(t) - \left(\theta^{\varphi}_1 + \mu^{\varphi}_{F_1}\right)\hat{F_1}(t)\right)d\nu, \\
\hat{F_2}(t) &= \frac{1-\varphi}{\mathbb{N}(\varphi)}\left(\eta^{\varphi} N_K(t) - \left(\theta^{\varphi}_2 + \mu^{\varphi}_{F_2}\right)\hat{F_2}(t)\right) \qquad (95) \\
&\quad + \frac{\varphi}{\mathbb{N}(\varphi)\Gamma(\varphi)} \times \int_0^t (t-\nu)^{\varphi-1}\left(\eta^{\varphi} N_K(\nu) - \left(\theta^{\varphi}_2 + \mu^{\varphi}_{F_2}\right)\hat{F_2}(\nu)\right)d\nu.
\end{aligned}
$$

Upon applying the norm to both sides of systems 93, 94, and 95, along with systems 79, 80, and 81, the following expression are obtained:

$$
\begin{aligned}
\|T_0 - \hat{T_0}\| &\leq \frac{1-\varphi}{\mathbb{N}(\varphi)}\|\{\Lambda^{\varphi}_{T_0} - \rho^{\varphi}_1 I_M(t)T_0(t)I_{10}(t) - \rho^{\varphi}_2 V(t)T_0(t)I_{10}(t) \\
&\quad - \rho^{\varphi}_3 T_0(t)I_M(t)\left(\frac{1}{1+\tau^{\varphi}_1 I_{10}}\right) - \mu^{\varphi}_{T_0}T_0(t) \\
&\quad - \{\Lambda^{\varphi}_{T_0} - \rho^{\varphi}_1 I_M(t)\hat{T_0}(t)I_{10}(t) - \rho^{\varphi}_2 V(t)T_0(t)I_{10}(t) \\
&\quad - \rho^{\varphi}_3 \hat{T_0}(t)I_M(t)\left(\frac{1}{1+\tau^{\varphi}_1 I_{10}}\right) - \mu^{\varphi}_{T_0}\hat{T_0}(t)\}\| \\
&\quad + \frac{\varphi}{\mathbb{N}(\varphi)\Gamma(\varphi)} \times \int_0^t (t-\nu)^{\varphi-1}\|\{\Lambda^{\varphi}_{T_0} - \rho^{\varphi}_1 I_M(t)T_0(t)I_{10}(t) \\
&\quad - \rho^{\varphi}_2 V(t)T_0(t)I_{10}(t) - \rho^{\varphi}_3 T_0(t)I_M(t)\left(\frac{1}{1+\tau^{\varphi}_1 I_{10}}\right) - \mu^{\varphi}_{T_0}T_0(t)\} \\
&\quad - \{\Lambda^{\varphi}_{T_0} - \rho^{\varphi}_1 I_M(t)\hat{T_0}(t)I_{10}(t) - \rho^{\varphi}_2 V(t)\hat{T_0}(t)I_{10}(t) \\
&\quad - \rho^{\varphi}_3 \hat{T_0}(t)I_M(t)\left(\frac{1}{1+\tau^{\varphi}_1 I_{10}}\right) - \mu^{\varphi}_{T_0}\hat{T_0}(t)\}\|,
\end{aligned}
$$

$$\begin{aligned}\|T_0-\hat{T}_0\| &\leq \frac{1-\varphi}{\mathbb{N}(\varphi)}\Psi_1\|T_0-\hat{T}_0\|+\frac{\varphi\Psi_1}{\mathbb{N}(\varphi)\Gamma(\varphi)}t^{\varphi}\|T_0-\hat{T}_0\|,\\ &\Longrightarrow \left(\frac{1-\varphi}{\mathbb{N}(\varphi)}+\frac{\varphi\Psi_1}{\mathbb{N}(\varphi)\Gamma(\varphi)}t^{\varphi}\right)\|T_0-\hat{T}_0\|\geq 0.\end{aligned}$$

$$\begin{aligned}\|T_1-\hat{T}_1\| &\leq \frac{1-\varphi}{\mathbb{N}(\varphi)}\|\left(\rho_1^{\varphi}I_M(t)T_0(t)I_{10}(t)-\pi^{\varphi}I_M(t)T_1(t)-\mu_{T_1}^{\varphi}T_1(t)\right)\\ &\quad-\left(\rho_1^{\varphi}I_M(t)T_0(t)I_{10}(t)-\pi^{\varphi}I_M(t)\hat{T}_1(t)-\mu_{T_1}^{\varphi}\hat{T}_1(t)\right)\|\\ &\quad+\frac{\varphi}{\mathbb{N}(\varphi)\Gamma(\varphi)}\times\int_0^t(t-\nu)^{\varphi-1}\|\{\rho_1^{\varphi}I_M(t)T_0(t)I_{10}(t)\}\\ &\quad-\pi^{\varphi}I_M(t)T_1(t)-\mu_{T_1}^{\varphi}T_1(t)\\ &\quad-\left(\rho_1^{\varphi}I_M(t)T_0(t)I_{10}(t)-\pi^{\varphi}I_M(t)\hat{T}_1(t)-\mu_{T_1}^{\varphi}\hat{T}_1(t)\right)\|,\\ &\leq \frac{1-\varphi}{\mathbb{N}(\varphi)}\Psi_2\|T_1-\hat{T}_1\|+\frac{\varphi\Psi_2}{\mathbb{N}(\varphi)\Gamma(\varphi)}t^{\varphi}\|T_1-\hat{T}_1\|,\\ &\Longrightarrow \left(\frac{1-\varphi}{\mathbb{N}(\varphi)}+\frac{\varphi\Psi_2}{\mathbb{N}(\varphi)\Gamma(\varphi)}t^{\varphi}\right)\|T_1-\hat{T}_1\|\geq 0.\end{aligned}$$

$$\begin{aligned}\|T_2-\hat{T}_2\| &\leq \frac{1-\varphi}{\mathbb{N}(\varphi)}\|\left(\rho_2^{\varphi}V(t)T_0(t)I_{10}(t)-\delta_3^{\varphi}T_2(t)V(t)-\mu_{T_2}^{\varphi}T_2(t)\right)\\ &\quad-\left(\rho_2^{\varphi}V(t)T_0(t)I_{10}(t)-\delta_3^{\varphi}\hat{T}_2(t)V(t)-\mu_{T_2}^{\varphi}\hat{T}_2(t)\right)\|\\ &\quad+\frac{\varphi}{\mathbb{N}(\varphi)\Gamma(\varphi)}\times\int_0^t(t-\nu)^{\varphi-1}\|\{\rho_2^{\varphi}V(t)T_0(t)I_{10}(t)\\ &\quad-\delta_3^{\varphi}T_2(t)V(t)-\mu_{T_2}^{\varphi}T_2(t)\}\\ &\quad-\{\rho_2^{\varphi}V(t)T_0(t)I_{10}(t)-\delta_3^{\varphi}\hat{T}_2(t)V(t)-\mu_{T_2}^{\varphi}\hat{T}_2(t)\}\|,\\ &\leq \frac{1-\varphi}{\mathbb{N}(\varphi)}\Psi_3\|T_2-\hat{T}_2\|+\frac{\varphi\Psi_3}{\mathbb{N}(\varphi)\Gamma(\varphi)}t^{\varphi}\|T_2-\hat{T}_2\|,\\ &\Longrightarrow \left(\frac{1-\varphi}{\mathbb{N}(\varphi)}+\frac{\varphi\Psi_3}{\mathbb{N}(\varphi)\Gamma(\varphi)}t^{\varphi}\right)\|T_2-\hat{T}_2\|\geq 0.\end{aligned}$$

$$
\begin{aligned}
\|M_0 - \hat{M}_0\| &\leq \frac{1-\varphi}{\mathbb{N}(\varphi)}\|\left(\Lambda^{\varphi}_{M_0} - \beta_1^{\varphi}V(t)M_0(t) - \mu_{M_0}M_0(t)\right) \\
&\quad - \left(\Lambda^{\varphi}_{M_0} - \beta_1^{\varphi}V(t)\hat{M}_0(t) - \mu^{\varphi}_{M_0}\hat{M}_0(t)\right)\| \\
&\quad + \frac{\varphi}{\mathbb{N}(\varphi)\Gamma(\varphi)} \times \int_0^t (t-\nu)^{\varphi-1}\|\{\Lambda^{\varphi}_{M_0} - \beta_1^{\varphi}V(t)M_0(t) \\
&\quad - \mu^{\varphi}_{M_0}M_0(t)\} - \{\Lambda^{\varphi}_{M_0} - \beta_1^{\varphi}V(t)\hat{M}_0(t) - \mu^{\varphi}_{M_0}\hat{M}_0(t)\}\|, \\
&\leq \frac{1-\varphi}{\mathbb{N}(\varphi)}\Psi_4\|M_0 - \hat{M}_0\| + \frac{\varphi\Psi_4}{\mathbb{N}(\varphi)\Gamma(\varphi)}t^{\varphi}\|M_0 - \hat{M}_0\|, \\
&\quad \Longrightarrow \left(\frac{1-\varphi}{\mathbb{N}(\varphi)} + \frac{\varphi\Psi_4}{\mathbb{N}(\varphi)\Gamma(\varphi)}t^{\varphi}\right)\|M_0 - \hat{M}_0\| \geq 0.
\end{aligned}
$$

$$
\begin{aligned}
\|M_1 - \hat{M}_1\| &\leq \frac{1-\varphi}{\mathbb{N}(\varphi)}\|\left(\Lambda^{\varphi}_{M_1} - \beta_2^{\varphi}V(t)M_1(t) + \zeta^{\varphi}I_M(t) - \mu^{\varphi}_{M_1}M_1(t)\right) \\
&\quad - \left(\Lambda^{\varphi}_{M_1} - \beta_2^{\varphi}V(t)\hat{M}_1(t) + \zeta^{\varphi}I_M(t) - \mu^{\varphi}_{M_1}\hat{M}_1(t)\right)\| \\
&\quad + \frac{\varphi}{\mathbb{N}(\varphi)\Gamma(\varphi)} \times \int_0^t (t-\nu)^{\varphi-1}\|\{\Lambda^{\varphi}_{M_1} - \beta_2^{\varphi}V(t)M_1(t) \\
&\quad + \zeta^{\varphi}I_M(t) - \mu^{\varphi}_{M_1}M_1(t)\} - \{\Lambda^{\varphi}_{M_1} - \beta_2^{\varphi}V(t)\hat{M}_1(t) \\
&\quad + \zeta^{\varphi}I_M(t) - \mu^{\varphi}_{M_1}\hat{M}_1(t)\}\|, \\
&\leq \frac{1-\varphi}{\mathbb{N}(\varphi)}\Psi_5\|M_1 - \hat{M}_1\| + \frac{\varphi\Psi_5}{\mathbb{N}(\varphi)\Gamma(\varphi)}t^{\varphi}\|M_1 - \hat{M}_1\|, \\
&\quad \Longrightarrow \left(\frac{1-\varphi}{\mathbb{N}(\varphi)} + \frac{\varphi\Psi_5}{\mathbb{N}(\varphi)\Gamma(\varphi)}t^{\varphi}\right)\|M_1 - \hat{M}_1\| \geq 0.
\end{aligned}
$$

$$
\begin{aligned}
\|I_M - \hat{I_M}\| \leq\ & \frac{1-\varphi}{\mathbb{N}(\varphi)}\|\{\beta_1^{\varphi}V(t)M_0(t) + \beta_2^{\varphi}V(t)M_1(t) + \pi^{\varphi}I_M(t)T_1(t) \\
& -\delta_1^{\varphi}\left(1+\chi_1^{\varphi}F_1(t)\right)I_M(t)N_K(t) - \delta_2^{\varphi}\left(1+\chi_2^{\varphi}F_2(t)\right)I_M(t)E(t) \\
& -\sigma^{\varphi}I_M(t)E(t) - \left(\omega^{\varphi}+\varepsilon^{\varphi}+\zeta^{\varphi}+\mu_{I_M}^{\varphi}\right)I_M(t)\} \\
& -\{\beta_1^{\varphi}V(t)M_0(t) + \beta_2^{\varphi}V(t)M_1(t) + \pi^{\varphi}\hat{I_M}(t)T_1(t) \\
& -\delta_1^{\varphi}\left(1+\chi_1^{\varphi}F_1(t)\right)\hat{I_M}(t)N_K(t) - \delta_2^{\varphi}\left(1+\chi_2^{\varphi}F_2(t)\right)\hat{I_M}(t)E(t) \\
& -\sigma^{\varphi}\hat{I_M}(t)E(t) - \left(\omega^{\varphi}+\varepsilon^{\varphi}+\zeta^{\varphi}+\mu_{I_M}^{\varphi}\right)\hat{I_M}(t)\}\| \\
& +\frac{\varphi}{\mathbb{N}(\varphi)\Gamma(\varphi)}\times\int_0^t(t-\nu)^{\varphi-1}\|\{\beta_1^{\varphi}V(t)M_0(t) + \beta_2^{\varphi}V(t)M_1(t) \\
& +\pi^{\varphi}I_M(t)T_1(t) - \delta_1^{\varphi}\left(1+\chi_1^{\varphi}F_1(t)\right)I_M(t)N_K(t) \\
& -\delta_2^{\varphi}\left(1+\chi_2^{\varphi}F_2(t)\right)I_M(t)E(t) - \sigma^{\varphi}I_M(t)E(t) \\
& -\left(\omega^{\varphi}+\varepsilon^{\varphi}+\zeta^{\varphi}+\mu_{I_M}^{\varphi}\right)I_M(t)\} - \{\beta_1^{\varphi}V(t)M_0(t) \\
& +\beta_2^{\varphi}V(t)M_1(t) + \pi^{\varphi}\hat{I_M}(t)T_1(t) \\
& -\delta_1^{\varphi}\left(1+\chi_1^{\varphi}F_1(t)\right)\hat{I_M}(t)N_K(t) - \delta_2^{\varphi}\left(1+\chi_2^{\varphi}F_2(t)\right)\hat{I_M}(t)E(t) \\
& -\sigma^{\varphi}\hat{I_M}(t)E(t) - \left(\omega^{\varphi}+\varepsilon^{\varphi}+\zeta^{\varphi}+\mu_{I_M}^{\varphi}\right)\hat{I_M}(t)\}\|, \\
\leq\ & \frac{1-\varphi}{\mathbb{N}(\varphi)}\Psi_6\|I_M - \hat{I_M}\| + \frac{\varphi\Psi_6}{\mathbb{N}(\varphi)\Gamma(\varphi)}t^{\varphi}\|I_M - \hat{I_M}\|, \\
& \Longrightarrow \left(\frac{1-\varphi}{\mathbb{N}(\varphi)} + \frac{\varphi\Psi_6}{\mathbb{N}(\varphi)\Gamma(\varphi)}t^{\varphi}\right)\|I_M - \hat{I_M}\| \geq 0.
\end{aligned}
$$

$$
\begin{aligned}
\|V - \hat{V}\| \leq\ & \frac{1-\varphi}{\mathbb{N}(\varphi)}\|\{\Lambda_V^{\varphi} + \omega^{\varphi}I_M(t) - \delta_3^{\varphi}T_2(t)V(t) - \delta_4^{\varphi}A(t)V(t) \\
& -\left(\psi^{\varphi}+\mu_V^{\varphi}\right)V(t)\} - \{\Lambda_V^{\varphi} + \omega^{\varphi}I_M(t) \\
& -\delta_3^{\varphi}T_2(t)\hat{V}(t) - \delta_4^{\varphi}A(t)\hat{V}(t) - \left(\psi^{\varphi}+\mu_V^{\varphi}\right)\hat{V}(t)\}\| \\
& +\frac{\varphi}{\mathbb{N}(\varphi)\Gamma(\varphi)}\times\int_0^t(t-\nu)^{\varphi-1}\|\{\Lambda_V^{\varphi} + \omega^{\varphi}I_M(t) - \delta_3^{\varphi}T_2(t)V(t) \\
& -\delta_4^{\varphi}A(t)V(t) - \left(\psi^{\varphi}+\mu_V^{\varphi}\right)V(t)\} - \{\Lambda_V^{\varphi} + \omega^{\varphi}I_M(t) \\
& -\delta_3^{\varphi}T_2(t)\hat{V}(t) - \delta_4^{\varphi}A(t)\hat{V}(t) - \left(\psi^{\varphi}+\mu_V^{\varphi}\right)\hat{V}(t)\}\|,
\end{aligned}
$$

$$\begin{aligned}\|V-\hat{V}\| &\leq \frac{1-\varphi}{\mathbb{N}(\varphi)}\Psi_7\|V-\hat{V}\|+\frac{\varphi\Psi_7}{\mathbb{N}(\varphi)\Gamma(\varphi)}t^{\varphi}\|V-\hat{V}\|,\\ &\Longrightarrow \left(\frac{1-\varphi}{\mathbb{N}(\varphi)}+\frac{\varphi\Psi_7}{\mathbb{N}(\varphi)\Gamma(\varphi)}t^{\varphi}\right)\|V-\hat{V}\|\geq 0.\end{aligned}$$

$$\begin{aligned}\|A-\hat{A}\| &\leq \frac{1-\varphi}{\mathbb{N}(\varphi)}\|(\Lambda_A^{\varphi}+\psi V(t)-\delta_4^{\varphi}A(t)V(t)-\mu_A^{\varphi}A(t))\\ &\quad-\left(\Lambda_A^{\varphi}+\psi^{\varphi}V(t)-\delta_4^{\varphi}\hat{A}(t)V(t)-\mu_A^{\varphi}\hat{A}(t)\right)\|\\ &\quad+\frac{\varphi}{\mathbb{N}(\varphi)\Gamma(\varphi)}\times\int_0^t(t-\nu)^{\varphi-1}\|\{\Lambda_A^{\varphi}+\psi^{\varphi}V(t)-\delta_4A(t)V(t)\\ &\quad-\mu_A^{\varphi}A(t)\}-\{\Lambda_A^{\varphi}+\psi^{\varphi}V(t)-\delta_4^{\varphi}\hat{A}(t)V(t)-\mu_A^{\varphi}\hat{A}(t)\}\|,\\ &\leq \frac{1-\varphi}{\mathbb{N}(\varphi)}\Psi_8\|A-\hat{A}\|+\frac{\varphi\Psi_8}{\mathbb{N}(\varphi)\Gamma(\varphi)}t^{\varphi}\|A-\hat{A}\|,\\ &\Longrightarrow \left(\frac{1-\varphi}{\mathbb{N}(\varphi)}+\frac{\varphi\Psi_8}{\mathbb{N}(\varphi)\Gamma(\varphi)}t^{\varphi}\right)\|A-\hat{A}\|\geq 0.\end{aligned}$$

$$\begin{aligned}\|E-\hat{E}\| &\leq \frac{1-\varphi}{\mathbb{N}(\varphi)}\|\{\Lambda_E^{\varphi}+\sigma^{\varphi}I_M(t)E(t)-\delta_2^{\varphi}\left(1+\chi_2^{\varphi}F_2\right)I_M(t)E(t)\\ &\quad-\mu_E^{\varphi}E(t)\}-\{\Lambda_E^{\varphi}+\sigma^{\varphi}I_M(t)\hat{E}(t)-\delta_2^{\varphi}\left(1+\chi_2^{\varphi}F_2\right)I_M(t)\hat{E}(t)\\ &\quad-\mu_E^{\varphi}\hat{E}(t)\}\|+\frac{\varphi}{\mathbb{N}(\varphi)\Gamma(\varphi)}\times\int_0^t(t-\nu)^{\varphi-1}\|\{\Lambda_E^{\varphi}+\sigma^{\varphi}I_M(t)E(t)\\ &\quad-\delta_2^{\varphi}\left(1+\chi_2^{\varphi}F_2\right)I_M(t)E(t)-\mu_E^{\varphi}E(t)\}-\{\Lambda_E^{\varphi}+\sigma^{\varphi}I_M(t)\hat{E}(t)\\ &\quad-\delta_2^{\varphi}\left(1+\chi_2^{\varphi}F_2\right)I_M(t)\hat{E}(t)-\mu_E^{\varphi}\hat{E}(t)\}\|,\\ &\leq \frac{1-\varphi}{\mathbb{N}(\varphi)}\Psi_9\|E-\hat{E}\|+\frac{\varphi\Psi_9}{\mathbb{N}(\varphi)\Gamma(\varphi)}t^{\varphi}\|E-\hat{E}\|,\\ &\Longrightarrow \left(\frac{1-\varphi}{\mathbb{N}(\varphi)}+\frac{\varphi\Psi_9}{\mathbb{N}(\varphi)\Gamma(\varphi)}t^{\varphi}\right)\|E-\hat{E}\|\geq 0.\end{aligned}$$

$$
\begin{aligned}
\|N_K - \hat{N}_K\| \leq\ & \frac{1-\varphi}{\mathbb{N}(\varphi)}\|\{\Lambda^{\varphi}_{N_K} + \theta^{\varphi}_1 F_1(t) + \theta^{\varphi}_2 F_2(t) \\
& -\delta^{\varphi}_1 (1+\chi^{\varphi}_1 F_1) I_M(t) N_K(t) - \left(\eta^{\varphi} + \mu^{\varphi}_{N_K}\right) N_K(t)\} \\
& -\{\Lambda^{\varphi}_{N_K} + \theta^{\varphi}_1 F_1(t) + \theta^{\varphi}_2 F_2(t) \\
& -\delta^{\varphi}_1 (1+\chi^{\varphi}_1 F_1) I_M(t) \hat{N}_K(t) - \left(\eta^{\varphi} + \mu^{\varphi}_{N_K}\right) \hat{N}_K(t)\}\| \\
& +\frac{\varphi}{\mathbb{N}(\varphi)\Gamma(\varphi)} \times \int_0^t (t-\nu)^{\varphi-1} \|\{\Lambda^{\varphi}_{N_K} + \theta^{\varphi}_1 F_1(t) + \theta^{\varphi}_2 F_2(t) \\
& -\delta^{\varphi}_1 (1+\chi^{\varphi}_1 F_1) I_M(t) N_K(t) - \left(\eta^{\varphi} + \mu^{\varphi}_{N_K}\right) N_K(t)\} \\
& -\{\Lambda^{\varphi}_{N_K} + \theta^{\varphi}_1 F_1(t) + \theta^{\varphi}_2 F_2(t) - \delta^{\varphi}_1 (1+\chi^{\varphi}_1 F_1) I_M(t) \hat{N}_K(t) \\
& -\left(\eta^{\varphi} + \mu^{\varphi}_{N_K}\right) \hat{N}_K(t)\}\|, \\
\leq\ & \frac{1-\varphi}{\mathbb{N}(\varphi)}\Psi_{10}\|N_K - \hat{N}_K\| + \frac{\varphi\Psi_{10}}{\mathbb{N}(\varphi)\Gamma(\varphi)} t^{\varphi}\|N_K - \hat{N}_K\|, \\
& \Longrightarrow \left(\frac{1-\varphi}{\mathbb{N}(\varphi)} + \frac{\varphi\Psi_{10}}{\mathbb{N}(\varphi)\Gamma(\varphi)} t^{\varphi}\right)\|N_K - \hat{N}_K\| \geq 0.
\end{aligned}
$$

$$
\begin{aligned}
\|I_{10} - \hat{I_{10}}\| \leq\ & \frac{1-\varphi}{\mathbb{N}(\varphi)}\|\left(\rho^{\varphi}_3 I_M(t) T_0(t)\left(\frac{1}{1+\tau^{\varphi}_1 I_{10}}\right) - \mu^{\varphi}_{I_{10}} I_{10}(t)\right) \\
& -\left(\rho^{\varphi}_3 I_M(t) T_0(t)\left(\frac{1}{1+\tau^{\varphi}_1 I_{10}}\right) - \mu^{\varphi}_{I_{10}(t)} \hat{I_{10}}(t)\right)\| \\
& +\frac{\varphi}{\mathbb{N}(\varphi)\Gamma(\varphi)} \times \int_0^t (t-\nu)^{\varphi-1} \|\left\{\rho^{\varphi}_3 I_M(t) T_0(t)\left(\frac{1}{1+\tau^{\varphi}_1 I_{10}}\right)\right. \\
& \left.-\mu^{\varphi}_{I_{10}} I_{10}(t)\right\} - \left\{\rho^{\varphi}_3 I_M(t) T_0(t)\left(\frac{1}{1+\tau^{\varphi}_1 I_{10}}\right) - \mu_{I_{10}} \hat{I_{10}}(t)\right\}\|, \\
\leq\ & \frac{1-\varphi}{\mathbb{N}(\varphi)}\Psi_{11}\|I_{10} - \hat{I_{10}}\| + \frac{\varphi\Psi_{11}}{\mathbb{N}(\varphi)\Gamma(\varphi)} t^{\varphi}\|I_{10} - \hat{I_{10}}\|, \\
& \Longrightarrow \left(\frac{1-\varphi}{\mathbb{N}(\varphi)} + \frac{\varphi\Psi_{11}}{\mathbb{N}(\varphi)\Gamma(\varphi)} t^{\varphi}\right)\|I_{10} - \hat{I_{10}}\| \geq 0.
\end{aligned}
$$

$$\begin{aligned}
\|F_1 - \hat{F}_1\| &\leq \frac{1-\varphi}{\mathbb{N}(\varphi)}\|\left[\varepsilon^{\varphi} I_M(t) - \left(\theta_1^{\varphi} + \mu_{F_1}^{\varphi}\right) F_1(t)\right] \\
&\quad - \left[\varepsilon^{\varphi} I_M(t) - \left(\theta_1^{\varphi} + \mu_{F_1}^{\varphi}\right) \hat{F}_1(t)\right]\| \\
&\quad + \frac{\varphi}{\mathbb{N}(\varphi)\Gamma(\varphi)} \times \int_0^t (t-\nu)^{\varphi-1} \|\left[\varepsilon^{\varphi} I_M(t) - \left(\theta_1^{\varphi} + \mu_{F_1}^{\varphi}\right) F_1(t)\right] \\
&\quad - \left[\varepsilon I_M(t) - \left(\theta_1^{\varphi} + \mu_{F_1}^{\varphi}\right) \hat{F}_1(t)\right]\|, \\
&\leq \frac{1-\varphi}{\mathbb{N}(\varphi)}\Psi_{12}\|F_1 - \hat{F}_1\| + \frac{\varphi\Psi_{12}}{\mathbb{N}(\varphi)\Gamma(\varphi)} t^{\varphi}\|F_1 - \hat{F}_1\|, \\
&\quad \Longrightarrow \left(\frac{1-\varphi}{\mathbb{N}(\varphi)} + \frac{\varphi\Psi_{12}}{\mathbb{N}(\varphi)\Gamma(\varphi)} t^{\varphi}\right) \|F_1 - \hat{F}_1\| \geq 0.
\end{aligned}$$

$$\begin{aligned}
\|F_2 - \hat{F}_2\| &\leq \frac{1-\varphi}{\mathbb{N}(\varphi)}\|\left[\eta^{\varphi} N_K(t) - \left(\theta_2^{\varphi} + \mu_{F_2}^{\varphi}\right) F_2(t)\right] \\
&\quad - \left[\eta^{\varphi} N_K(t) - \left(\theta_2^{\varphi} + \mu_{F_2}^{\varphi}\right) \hat{F}_2(t)\right]\| \\
&\quad + \frac{\varphi}{\mathbb{N}(\varphi)\Gamma(\varphi)} \times \int_0^t (t-\nu)^{\varphi-1} \|\left[\eta^{\varphi} N_K(t) - \left(\theta_2^{\varphi} + \mu_{F_2}^{\varphi}\right) F_2(t)\right] \\
&\quad - \left[\eta^{\varphi} N_K(t) - \left(\theta_2^{\varphi} + \mu_{F_2}^{\varphi}\right) \hat{F}_2(t)\right]\| \\
&\leq \frac{1-\varphi}{\mathbb{N}(\varphi)}\Psi_{13}\|F_2 - \hat{F}_2\| + \frac{\varphi\Psi_{13}}{\mathbb{N}(\varphi)\Gamma(\varphi)} t^{\varphi}\|F_2 - \hat{F}_2\|, \\
&\quad \Longrightarrow \left(\frac{1-\varphi}{\mathbb{N}(\varphi)} + \frac{\varphi\Psi_{13}}{\mathbb{N}(\varphi)\Gamma(\varphi)} t^{\varphi}\right) \|F_2 - \hat{F}_2\| \geq 0.
\end{aligned}$$

Therefore, $\|T_0 - \hat{T}_0\| = 0$ which implies that $T_0 = \hat{T}_0$. In a similarly way, we have $T_1 = \hat{T}_1$, $T_2 = \hat{T}_2$, $M_0 = \hat{M}_0$, $M_1 = \hat{M}_1$, $I_M = \hat{I_M}$, $V = \hat{V}$, $A = \hat{A}$, $E = \hat{E}$, $N_K = \hat{N_K}$, $I_{10} = \hat{I_{10}}$, $F_1 = \hat{F}_1$ and $F_2 = \hat{F}_2$. Thus, the proposed model has a unique solution.

Virus-persistence Equilibrium Analysis (VPE)

In this section, the equilibrium points for viral persistence are delineated by concurrently resolving system 5 for the state variables $T_0^{\star}$, $T_1^{\star}$, $T_2^{\star}$, $M_0^{\star}$, $I_M^{\star}$, $V^{\star}$, $A^{\star}$, $E^{\star}$, $N_K^{\star}$, $I_{10}^{\star}$, $F_1^{\star}$, and $F_2^{\star}$. These equilibrium points represent steady-state configurations where the hepatitis B virus remains active, persistently infiltrating the entire hepatic cell population. In this scenario, the viral compartment does not diminish to

zero, indicating sustained infection within the hepatic cells of the host. Therefore, the system is contingent upon all state variables.

At the equilibrium state of viral persistence, uninfected macrophages transition into an infected state, which subsequently activates the infected cells through cytokine-mediated signaling. It is important to note that the state of viral persistence encapsulates two potential prognoses: an acute condition or progression into a chronic ailment. The manifestation of an acute infection is contingent upon a specific constellation of parameters, whereas the transition to chronic pathology ensues upon the modulation of these variables. Consequently, an analytical exploration is undertaken to scrutinize the gradual cytolytic interactions among the constituents of the immune system within the fractional-order model. Accordingly, the subsequent equations are maintained at the equilibrium point of viral persistence:

$$
\begin{cases}
0 &= \Lambda^{\varphi}_{T_0} - \rho^{\varphi}_1 I_M T_0 I_{10} - \rho^{\varphi}_2 V T_0 I_{10} - \rho^{\varphi}_3 T_0 I_M \left(\frac{1}{1+\tau^{\varphi}_1 I_{10}}\right) - \mu^{\varphi}_{T_0} T_0, \\
0 &= \rho^{\varphi}_1 I_M T_0 I_{10} - \pi^{\varphi} I_M T_1 - \mu^{\varphi}_{T_1} T_1, \\
0 &= \rho^{\varphi}_2 V T_0 I_{10} - \delta^{\varphi}_3 T_2 V - \mu^{\varphi}_{T_2} T_2, \\
0 &= \Lambda^{\varphi}_{M_0} - \beta^{\varphi}_1 V M_0 - \mu^{\varphi}_{M_0} M_0, \\
0 &= \Lambda^{\varphi}_{M_1} - \beta^{\varphi}_2 V M_1 + \zeta^{\varphi} I_M - \mu^{\varphi}_{M_1} M_1, \\
0 &= \beta^{\varphi}_1 V M_0 + \beta^{\varphi}_2 V M_1 + \pi^{\varphi} I_M T_1 - \delta^{\varphi}_1 \left(1 + \chi^{\varphi}_1 F_1\right) I_M N_K \\
&\quad -\delta^{\varphi}_2 \left(1 + \chi^{\varphi}_2 F_2\right) I_M E - \sigma^{\varphi} I_M E - \left(\omega^{\varphi} + \varepsilon^{\varphi} + \zeta^{\varphi} + \mu^{\varphi}_{I_M}\right) I_M, \\
0 &= \Lambda^{\varphi}_V + \omega^{\varphi} I_M - \delta^{\varphi}_3 T_2 V - \delta^{\varphi}_4 A V - \left(\psi^{\varphi} + \mu^{\varphi}_V\right) V, \\
0 &= \Lambda^{\varphi}_A + \psi^{\varphi} V - \delta^{\varphi}_4 A V - \mu^{\varphi}_A A, \\
0 &= \Lambda^{\varphi}_E - \delta^{\varphi}_2 \left(1 + \chi^{\varphi}_2 F_2\right) I_M E + \sigma^{\varphi} I_M E - \mu^{\varphi}_E E, \\
0 &= \Lambda^{\varphi}_{N_K} - \delta^{\varphi}_1 \left(1 + \chi^{\varphi}_1 F_1\right) I_M N_K + \theta^{\varphi}_1 F_1 + \theta^{\varphi}_2 F_2 - \left(\eta^{\varphi} + \mu^{\varphi}_{N_K}\right) N_K, \\
0 &= \rho^{\varphi}_3 I_M T_0 \left(\frac{1}{1+\tau^{\varphi}_1 I_{10}}\right) - \mu^{\varphi}_{I_{10}} I_{10}, \\
0 &= \varepsilon^{\varphi} I_M - \left(\theta^{\varphi}_1 + \mu^{\varphi}_{F_1}\right) F_1, \\
0 &= \eta^{\varphi} N_K - \left(\theta^{\varphi}_2 + \mu^{\varphi}_{F_2}\right) F_2.
\end{cases}
$$

The endemic infection equilibrium state is represented by

$$\varepsilon_0^\star = (T_0^\star, T_1^\star, T_2^\star, M_0^\star, M_1^\star, I_M^\star, V^\star, A^\star, E^\star, N_K^\star, I_{10}^\star, F_1^\star, F_2^\star).$$

The equilibrium value for naive T cells ($T_0^\star$) at the viral persistence state in system 5 is determined by

$$T_0^\star = \frac{\Lambda_{T_0}^\varphi}{\rho_1^\varphi I_M^\star I_{10}^\star + \rho_2^\varphi V^\star I_{10}^\star + \frac{\rho_3^\varphi I_M^\star}{1+\tau_1^\varphi I_{10}^\star} + \mu_{T_0}^\varphi}. \tag{96}$$

The equation in Eq. (96) elucidates that during the endemic phase, there is a continuous influx of naive T cells from the bone marrow into the host system. Conversely, the denominator denotes that elevated concentrations of both intracellular and extracellular viruses deleteriously affect the proliferation of naive T cells. This is attributed to the virus and infected macrophages stimulating the differentiation of naive T cells. Nonetheless, this differentiation is contingent upon the clonal expansion rates (ρ_i, where $i = 1, 2, 3$) and the decay rate μ_{T_0}. As the viral burden recedes, the naive T cells revert to their baseline production rate of $\frac{\Lambda_{T_0}}{\mu_{T_0}}$.

For the T helper 1 cells at the viral persistence state, the population is given by

$$T_1^\star = \frac{\rho_1^\varphi I_M^\star T_0^\star I_{10}^\star}{\pi^\varphi I_M^\star + \mu_{T_1}^\varphi}. \tag{97}$$

The equation in Eq. (97) denotes that the numerator encapsulates the interaction between infected macrophages, the proliferation rate of T_0 cells secreting I_{10}, and the naive T cells (T_0), which collectively enhance the augmentation of T helper 1 (T_1) cells. Conversely, the concentration of cytokines generated through the activation of T_0 cells by infected macrophages (I_M), in conjunction with the decay rate of T_1 cells, mitigates the proliferation of the T_1 cell population.

The expression for T helper 2 cells, also known as cytotoxic T lymphocytes, produced from naive T cells at the viral persistence state is given by

$$T_2^\star = \frac{\rho_2^\varphi V^\star T_0^\star I_{10}^\star}{\delta_3^\varphi V^\star + \mu_{T_2}^\varphi}. \tag{98}$$

In equation Eq. (98), the interplay between the virus and naive T cells, alongside the presence of interleukin-10, augments and sustains the genesis of T2 cells. However, the magnitude of the virus's lytic activity, characterized by the rate (δ_3) and modulated by the decay rate (μ_{T_2}), obstructs the expansion of the T2 cell population.

Expression Eq. (99) delineates the equilibrium concentration of non-cancerous, uninfected macrophages in the presence of the virus as follows:

$$M_0^\star = \frac{\Lambda_{M_0}^\varphi}{\beta_1^\varphi V^\star + \mu_{M_0}^\varphi}. \tag{99}$$

In this equation, the numerator quantifies the influx of non-malignant, uninfected macrophages originating from the bloodstream. Conversely, the impact of the viral burden on these macrophages, coupled with an elevation in their inherent degradation rate, leads to a diminished macrophage population. As the viral load abates, the uninfected macrophages stabilize to their baseline concentration, articulated as $\frac{\Lambda_{M_0}^\varphi}{\mu_{M_0}^\varphi}$. Furthermore, the denominator illustrates that augmented interactions between non-malignant macrophages and the virus further exacerbate the attrition of macrophage numbers.

Similarly, expression Eq. (100) represents the equilibrium concentration of uninfected macrophages associated with cancer under the viral presence:

$$M_1^\star = \frac{\Lambda_{M_1^\varphi} + \zeta^\varphi I_M^\star}{\beta_2^\varphi V^\star + \mu_{M_1}^\varphi}. \tag{100}$$

The numerator in equation Eq. (100) signifies the influx of cancer-compromised, uninfected macrophages from the bloodstream. However, the presence of the viral population adversely affects these macrophages, exacerbated by an elevated intrinsic decay rate. As the viral burden recedes, the concentration of cancer-compromised, uninfected macrophages returns to its equilibrium baseline, represented by $\frac{\Lambda_{M_1}^\varphi}{\mu_{M_1}^\varphi}$. Additionally, the denominator reveals that intensified interactions between these cells and the virus further exacerbate the diminution of their population.

The equation for infected macrophages under the viral presence is given by:

$$I_M^\star = \frac{\beta_1^\varphi V^\star M_0^\star + \beta_2^\varphi V^\star M_1^\star}{\left[\delta_1^\varphi \left(1+\chi_1^\varphi F_1^\star\right) N_K^\star + \delta_2^\varphi \left(1+\chi_2^\varphi F_2^\star\right) E^\star + H\right]}, \tag{101}$$

where $H = \sigma^\varphi E^\star + \left(\omega^\varphi + \varepsilon^\varphi + \zeta^\varphi + \mu_{I_M}^\varphi\right) - \pi^\varphi T_1^\star$.

Expression Eq. (101) elucidates that the interaction between the virus and both non-malignant and cancer-afflicted macrophages leads to an augmentation in the population of infected macrophages. However, factors such as the heightened cytotoxicity of type 1 and type 2 interferons, denoted by the rates χ_1 and χ_2 respectively, the production of effector B cells during the infection, as well as the synthesis of novel virions and type-1 interferon by activated infected macrophages, contribute to a diminution in the infected macrophage population. Furthermore, the degradation rate (μ_{I_M}) of infected macrophages also significantly influences their reduction.

The equilibrium concentration of the viral population in the endemic state is expressed as:

$$V^\star = \frac{\Lambda_V^\varphi + \omega^\varphi I_M^\star}{\delta_3^\varphi T_2^\star + \delta_4^\varphi A^\star + \left(\psi^\varphi + \mu_V^\varphi\right)}. \tag{102}$$

Equation Eq. (102) elucidates that the viral load escalates both extracellularly and intracellularly. Extracellularly, the virus proliferates due to its influx rate, represented by Λ_V, especially when interleukin-2 (I_2) fails to trigger apoptosis, a mechanism responsible for the programmed demise of infected macrophages. Intracellularly, the replication of the hepatitis B virus within infected cells, originating from an initially negligible viral load that does not provoke an immune response, leads to a gradual augmentation of the viral population at a rate denoted by ω. Nonetheless, the proliferation of the viral population is mitigated by decay rates and the cytotoxic effects of both adaptive and humoral immune responses.

The equilibrium concentration of antibodies in the endemic state is given by:

$$A^\star = \frac{\Lambda_A^\varphi + \psi^\varphi V^\star}{\delta_4^\varphi V^\star + \mu_A^\varphi}. \tag{103}$$

During the endemic phase, antibodies (A) are synthesized as a consequence of the viral cytolytic activity and the antibody production rate. Consequently, an upsurge in viral proliferation is positively correlated with the antibody population. However, the rate at which antibodies neutralize the virus attenuates this proliferation. Additionally, the antibody population is diminished by its decay rate (μ_A), as articulated in equation Eq. (103). It is observed that as the viral burden recedes, antibody concentrations stabilize to $\frac{\Lambda_A^{\varphi}}{\mu_A^{\varphi}}$.

The equilibrium value for the population of effector B cells in the endemic state is expressed as:

$$E^{\star} = \frac{\Lambda_E^{\varphi}}{\delta_2^{\varphi}\left(1+\chi_2^{\varphi}F_2^{\star}\right)I_M^{\star}+\mu_E^{\varphi}-\sigma^{\varphi}I_M^{\star}}. \tag{104}$$

In equation Eq. (104), the numerator denotes the influx of effector B cells. However, the presence of infected macrophages deleteriously impacts the effector B cell population, compounded by an elevation in their intrinsic degradation rate. As the infected macrophage population nears zero, effector B cells revert to their equilibrium level of $\frac{\Lambda_E^{\varphi}}{\mu_E^{\varphi}}$. Additionally, the denominator elucidates that augmented interactions between type-2 interferon and infected macrophages further attenuate the effector B cell population.

The equilibrium concentration of natural killer (N_K) cells in the endemic state is given by:

$$N_K^{\star} = \frac{\Lambda_{N_K}^{\varphi}+\theta_1^{\varphi}F_1^{\star}+\theta_2^{\varphi}F_2^{\star}}{\delta_1^{\varphi}\left(1+\chi_1^{\varphi}F_1^{\star}\right)I_M^{\star}+\left(\eta^{\varphi}+\mu_{N_K}^{\varphi}\right)}. \tag{105}$$

Equation Eq. (105) elucidates the influx of natural killer (NK) cells. Moreover, it indicates that the activity of both interferons facilitates an augmentation in the NK cell population. However, the presence of infected macrophages and an escalation in their intrinsic decay rate detrimentally influence the NK cell population. As the infected macrophage population diminishes to near zero, NK cells stabilize at their equilibrium level denoted by $\frac{\Lambda_{N_K}^{\varphi}}{\mu_{N_K}^{\varphi}}$. Additionally, the denominator signifies that heightened interactions between type-1 interferon and infected macrophages further

contribute to a diminution in the NK cell population.

The endemic equilibrium concentration of interleukin-10 cytokines is expressed as:

$$I_{10}^{\star} = \frac{\rho_3^{\varphi} I_M^{\star} T_0^{\star}}{\mu_{I_{10}}^{\varphi}\left(1+\tau_1^{\varphi} I_{10}^{\star}\right)}. \tag{106}$$

In equation Eq. (106), the numerator delineates that regulatory T cells are the principal origin of interleukin-10 (I_{10}), synthesized through interactions among naive T cells (T_0), infected macrophages (I_M), and the virus. Furthermore, the equation reveals that I_{10} production is modulated by a temporal factor $(1+\tau_1 I_{10}^{\star})$, particularly when intracellular viral burdens in infected macrophages (I_M) are insufficient to elicit a robust immune response. The denominator additionally encompasses the attenuation of I_{10} levels due to its intrinsic degradation rate $\mu_{I_{10}}$.

The endemic equilibrium level of type-1 interferon cytokines is given by:

$$F_1^{\star} = \frac{\varepsilon^{\varphi} I_M^{\star}}{\theta_1^{\varphi} + \mu_{F_1}^{\varphi}}. \tag{107}$$

Equation Eq. (107) illustrates that the synthesis of type-1 interferon (alpha-beta) cytokines is catalyzed by the proliferation of infected macrophages (I_M) at a rate denoted by ε. Consequently, an augmentation in the F_1 population correlates with increased proliferation of infected macrophages. Nonetheless, this population encounters suppression from natural killer cells (N_K), which continuously counteract its production, and is also diminished by its intrinsic decay rate μ_{F_1}.

The endemic equilibrium concentration of type-2 interferon cytokines is given by:

$$F_2^{\star} = \frac{\eta^{\varphi} N_K^{\star}}{\theta_2^{\varphi} + \mu_{F_2}^{\varphi}}. \tag{108}$$

In equation Eq. (108), the biosynthesis of type-2 interferon (gamma) cytokines is propelled by the proliferation of natural killer cells (N_K) at a rate signified by η.

Consequently, the concentration of F_2 escalates with heightened natural killer cell activity. However, this cytokine level is regulated by the natural killer cells themselves, which perpetually endeavor to suppress its production, and is also attenuated by the intrinsic decay rate μ_{F_2}.

Local Stability Analysis of Virus-free Equilibrium

This section presents a localized stability assessment utilizing fractional-order operators. It is crucial to emphasize that although the equilibrium point of the fractional-order system mirrors that of the corresponding classical-order system, the underlying conditions diverge markedly. Specifically, when the eigenvalue is non-negative, the equilibrium point for the integer-order system is generally unstable, whereas it tends to exhibit stability in fractional-order systems.

Theorem 11

Local stability analysis of virus-free equilibrium.

The points of equilibrium for system 39, where $\varphi \in [0,1]$ are said to be asymptotically (local) stable, if for the Jacobian matrix $\dfrac{\partial}{\partial y} f(t,y)$, all the eigenvalues λ_i computed at the points of equilibrium satisfy

$$|arg(\lambda_i)| > \frac{\varphi\pi}{2}, i = 1, 2, \cdots, 13.$$

Proof. From the corresponding fractional-order system below,

$$ {}_0^{ABC}\mathbb{D}_t^{\varphi} y_i(t) = f(t, y_i(t)), \quad y_i(t_0) = y_0, \tag{109}$$

where ${}_0^{ABC}\mathbb{D}_t^{\varphi}$ represent classical fractional derivative (CFD) of order $\varphi \in [0,1]$.

Next, the points of equilibrium would be evaluated using ${}_0^{ABC}\mathbb{D}_t^{\varphi} y_i(t) = 0$ which means that $f_i(f_1, f_2, f_3, f_4, f_5, f_6, f_7, f_8, f_9, f_{10}, f_{11}, f_{12}, f_{13}) = 0$ for which we can get the equilibrium points

$$f_1, f_2, f_3, f_4, f_5, f_6, f_7, f_8, f_9, f_{10}, f_{11}, f_{12}, f_{13}.$$

To compute for asymptotic stability, the system ${}_0^{ABC}\mathbb{D}_t^{\varphi} f(x) = f(x,y)$ would be

considered in Atangana-Baleanu in Caputo sense; let $y_i(t) = y_i\mathbb{E}_i(t)$. The following equilibrium points $(f_1, f_2, f_3, f_4, f_5, f_6, f_7, f_8, f_9, f_{10}, f_{11}, f_{12}, f_{13})$ are said to be locally asymptotically stable provided all the Jacobian eigenvalues from the matrix

$$\begin{pmatrix}
\frac{\partial f_1}{\partial y_1} & \frac{\partial f_1}{\partial y_2} & \frac{\partial f_1}{\partial y_3} & \frac{\partial f_1}{\partial y_4} & \frac{\partial f_1}{\partial y_5} & \frac{\partial f_1}{\partial y_6} & \frac{\partial f_1}{\partial y_7} & \frac{\partial f_1}{\partial y_8} & \frac{\partial f_1}{\partial y_9} & \frac{\partial f_1}{\partial y_{10}} & \frac{\partial f_1}{\partial y_{11}} & \frac{\partial f_1}{\partial y_{12}} & \frac{\partial f_1}{\partial y_{13}} \\
\frac{\partial f_2}{\partial y_1} & \frac{\partial f_2}{\partial y_2} & \frac{\partial f_2}{\partial y_3} & \frac{\partial f_2}{\partial y_4} & \frac{\partial f_2}{\partial y_5} & \frac{\partial f_2}{\partial y_6} & \frac{\partial f_2}{\partial y_7} & \frac{\partial f_2}{\partial y_8} & \frac{\partial f_2}{\partial y_9} & \frac{\partial f_2}{\partial y_{10}} & \frac{\partial f_2}{\partial y_{11}} & \frac{\partial f_2}{\partial y_{12}} & \frac{\partial f_2}{\partial y_{13}} \\
\frac{\partial f_3}{\partial y_1} & \frac{\partial f_3}{\partial y_2} & \frac{\partial f_3}{\partial y_3} & \frac{\partial f_3}{\partial y_4} & \frac{\partial f_3}{\partial y_5} & \frac{\partial f_3}{\partial y_6} & \frac{\partial f_3}{\partial y_7} & \frac{\partial f_3}{\partial y_8} & \frac{\partial f_3}{\partial y_9} & \frac{\partial f_3}{\partial y_{10}} & \frac{\partial f_3}{\partial y_{11}} & \frac{\partial f_3}{\partial y_{12}} & \frac{\partial f_3}{\partial y_{13}} \\
\frac{\partial f_4}{\partial y_1} & \frac{\partial f_4}{\partial y_2} & \frac{\partial f_4}{\partial y_3} & \frac{\partial f_4}{\partial y_4} & \frac{\partial f_4}{\partial y_5} & \frac{\partial f_4}{\partial y_6} & \frac{\partial f_4}{\partial y_7} & \frac{\partial f_4}{\partial y_8} & \frac{\partial f_4}{\partial y_9} & \frac{\partial f_4}{\partial y_{10}} & \frac{\partial f_4}{\partial y_{11}} & \frac{\partial f_4}{\partial y_{12}} & \frac{\partial f_4}{\partial y_{13}} \\
\frac{\partial f_5}{\partial y_1} & \frac{\partial f_5}{\partial y_2} & \frac{\partial f_5}{\partial y_3} & \frac{\partial f_5}{\partial y_4} & \frac{\partial f_5}{\partial y_5} & \frac{\partial f_5}{\partial y_6} & \frac{\partial f_5}{\partial y_7} & \frac{\partial f_5}{\partial y_8} & \frac{\partial f_5}{\partial y_9} & \frac{\partial f_5}{\partial y_{10}} & \frac{\partial f_5}{\partial y_{11}} & \frac{\partial f_5}{\partial y_{12}} & \frac{\partial f_5}{\partial y_{13}} \\
\frac{\partial f_6}{\partial y_1} & \frac{\partial f_6}{\partial y_2} & \frac{\partial f_6}{\partial y_3} & \frac{\partial f_6}{\partial y_4} & \frac{\partial f_6}{\partial y_5} & \frac{\partial f_6}{\partial y_6} & \frac{\partial f_6}{\partial y_7} & \frac{\partial f_6}{\partial y_8} & \frac{\partial f_6}{\partial y_9} & \frac{\partial f_6}{\partial y_{10}} & \frac{\partial f_6}{\partial y_{11}} & \frac{\partial f_6}{\partial y_{12}} & \frac{\partial f_6}{\partial y_{13}} \\
\frac{\partial f_7}{\partial y_1} & \frac{\partial f_7}{\partial y_2} & \frac{\partial f_7}{\partial y_3} & \frac{\partial f_7}{\partial y_4} & \frac{\partial f_7}{\partial y_5} & \frac{\partial f_7}{\partial y_6} & \frac{\partial f_7}{\partial y_7} & \frac{\partial f_7}{\partial y_8} & \frac{\partial f_7}{\partial y_9} & \frac{\partial f_7}{\partial y_{10}} & \frac{\partial f_7}{\partial y_{11}} & \frac{\partial f_7}{\partial y_{12}} & \frac{\partial f_7}{\partial y_{13}} \\
\frac{\partial f_8}{\partial y_1} & \frac{\partial f_8}{\partial y_2} & \frac{\partial f_8}{\partial y_3} & \frac{\partial f_8}{\partial y_4} & \frac{\partial f_8}{\partial y_5} & \frac{\partial f_8}{\partial y_6} & \frac{\partial f_8}{\partial y_7} & \frac{\partial f_8}{\partial y_8} & \frac{\partial f_8}{\partial y_9} & \frac{\partial f_8}{\partial y_{10}} & \frac{\partial f_8}{\partial y_{11}} & \frac{\partial f_8}{\partial y_{12}} & \frac{\partial f_8}{\partial y_{13}} \\
\frac{\partial f_9}{\partial y_1} & \frac{\partial f_9}{\partial y_2} & \frac{\partial f_9}{\partial y_3} & \frac{\partial f_9}{\partial y_4} & \frac{\partial f_9}{\partial y_5} & \frac{\partial f_9}{\partial y_6} & \frac{\partial f_9}{\partial y_7} & \frac{\partial f_9}{\partial y_8} & \frac{\partial f_9}{\partial y_9} & \frac{\partial f_9}{\partial y_{10}} & \frac{\partial f_9}{\partial y_{11}} & \frac{\partial f_9}{\partial y_{12}} & \frac{\partial f_9}{\partial y_{13}} \\
\frac{\partial f_{10}}{\partial y_1} & \frac{\partial f_{10}}{\partial y_2} & \frac{\partial f_{10}}{\partial y_3} & \frac{\partial f_{10}}{\partial y_4} & \frac{\partial f_{10}}{\partial y_5} & \frac{\partial f_{10}}{\partial y_6} & \frac{\partial f_{10}}{\partial y_7} & \frac{\partial f_{10}}{\partial y_8} & \frac{\partial f_{10}}{\partial y_9} & \frac{\partial f_{10}}{\partial y_{10}} & \frac{\partial f_{10}}{\partial y_{11}} & \frac{\partial f_{10}}{\partial y_{12}} & \frac{\partial f_{10}}{\partial y_{13}} \\
\frac{\partial f_{11}}{\partial y_1} & \frac{\partial f_{11}}{\partial y_2} & \frac{\partial f_{11}}{\partial y_3} & \frac{\partial f_{11}}{\partial y_4} & \frac{\partial f_{11}}{\partial y_5} & \frac{\partial f_{11}}{\partial y_6} & \frac{\partial f_{11}}{\partial y_7} & \frac{\partial f_{11}}{\partial y_8} & \frac{\partial f_{11}}{\partial y_9} & \frac{\partial f_{11}}{\partial y_{10}} & \frac{\partial f_{11}}{\partial y_{11}} & \frac{\partial f_{11}}{\partial y_{12}} & \frac{\partial f_2}{\partial y_{13}} \\
\frac{\partial f_{12}}{\partial y_1} & \frac{\partial f_{12}}{\partial y_2} & \frac{\partial f_{12}}{\partial y_3} & \frac{\partial f_{12}}{\partial y_4} & \frac{\partial f_{12}}{\partial y_5} & \frac{\partial f_{12}}{\partial y_6} & \frac{\partial f_{12}}{\partial y_7} & \frac{\partial f_{12}}{\partial y_8} & \frac{\partial f_{12}}{\partial y_9} & \frac{\partial f_{12}}{\partial y_{10}} & \frac{\partial f_{12}}{\partial y_{11}} & \frac{\partial f_{12}}{\partial y_{12}} & \frac{\partial f_{12}}{\partial y_{13}} \\
\frac{\partial f_{13}}{\partial y_1} & \frac{\partial f_{13}}{\partial y_2} & \frac{\partial f_{13}}{\partial y_3} & \frac{\partial f_{13}}{\partial y_4} & \frac{\partial f_{13}}{\partial y_5} & \frac{\partial f_{13}}{\partial y_6} & \frac{\partial f_{13}}{\partial y_7} & \frac{\partial f_{13}}{\partial y_8} & \frac{\partial f_{13}}{\partial y_9} & \frac{\partial f_{13}}{\partial y_{10}} & \frac{\partial f_{13}}{\partial y_{11}} & \frac{\partial f_{13}}{\partial y_{12}} & \frac{\partial f_{13}}{\partial y_{13}}
\end{pmatrix},$$

computed at the points of equilibrium satisfy the condition

$$|arg\,(\lambda_1, \lambda_2, \lambda_3, \cdots, \lambda_{13})| > \frac{\varphi\pi}{2}.$$

It follows that, the linearized Jacobian Matrix at the virus-free equilibrium is obtained to be where

$$J_0(\varepsilon_0)^\star = \begin{pmatrix}
-\mu_{T_0}^{\varphi} & 0 & 0 & 0 & 0 & -\mathfrak{S}_1^{\varphi} & 0 & 0 & 0 & 0 & 0 & 0 & 0 \\
0 & -\mu_{T_1}^{\varphi} & 0 & 0 & 0 & 0 & 0 & 0 & 0 & 0 & 0 & 0 & 0 \\
0 & 0 & -\kappa_1^{\varphi} & 0 & 0 & 0 & 0 & 0 & 0 & 0 & 0 & 0 & 0 \\
0 & 0 & 0 & -\kappa_2^{\varphi} & 0 & 0 & -\mathfrak{S}_2^{\varphi} & 0 & 0 & 0 & 0 & 0 & 0 \\
0 & 0 & 0 & 0 & -\kappa_3^{\varphi} & \zeta^{\varphi} & -\mathfrak{S}_3^{\varphi} & 0 & 0 & 0 & 0 & 0 & 0 \\
0 & 0 & 0 & 0 & 0 & -\kappa_4^{\varphi} & \kappa_{11}^{\varphi} & 0 & 0 & 0 & 0 & 0 & 0 \\
0 & 0 & 0 & 0 & 0 & \omega^{\varphi} & -\kappa_5^{\varphi} & 0 & 0 & 0 & 0 & 0 & 0 \\
0 & 0 & 0 & 0 & 0 & 0 & \kappa_6^{\varphi} & -\kappa_7^{\varphi} & 0 & 0 & 0 & 0 & 0 \\
0 & 0 & 0 & 0 & 0 & 0 & 0 & 0 & -\mu_E^{\varphi} & 0 & 0 & 0 & 0 \\
0 & 0 & 0 & 0 & 0 & 0 & 0 & 0 & 0 & -\kappa_8^{\varphi} & 0 & \theta_1^{\varphi} & \theta_2^{\varphi} \\
0 & 0 & 0 & 0 & 0 & \mathfrak{S}_4^{\varphi} & 0 & 0 & 0 & 0 & -\mu_{I_{10}}^{\varphi} & 0 & 0 \\
0 & 0 & 0 & 0 & 0 & \varepsilon^{\varphi} & 0 & 0 & 0 & 0 & 0 & -\kappa_9^{\varphi} & 0 \\
0 & 0 & 0 & 0 & 0 & 0 & 0 & 0 & 0 & \eta & 0 & 0 & -\kappa_{10}^{\varphi}
\end{pmatrix},$$

$$\kappa_1 = \mu_{T_2}^{\varphi}, \qquad \kappa_2 = \mu_{M_0}^{\varphi}, \qquad \kappa_3 = \mu_{M_1}^{\varphi},$$

$$\kappa_4 = \left(\omega^{\varphi} + \varepsilon^{\varphi} + \zeta^{\varphi} + \mu_{I_M}^{\varphi}\right), \qquad \kappa_5 = \left(\psi^{\varphi} + \mu_V^{\varphi}\right), \qquad \kappa_6 = \psi^{\star},$$

$$\kappa_7 = \mu_A^{\varphi}, \qquad \kappa_8 = \left(\eta^{\varphi} + \mu_{N_K}^{\varphi}\right), \qquad \kappa_9 = \left(\theta_1^{\varphi} + \mu_{F_1}^{\varphi}\right),$$

$$\kappa_{10} = \left(\theta_2^{\varphi} + \mu_{F_2}^{\varphi}\right), \qquad \kappa_{11} = \beta_1^{\varphi} M_0^{\star} + \beta_2^{\varphi} M_1^{\star}, \qquad \mathfrak{S}_1 = \rho_3^{\varphi} T_0^{\star},$$
$$\mathfrak{S}_2 = \beta_1^{\varphi} M_0^{\star}, \qquad \mathfrak{S}_3 = \beta_2^{\varphi} M_1^{\star}, \qquad \mathfrak{S}_4 = \mathfrak{S}_1.$$

By examining columns 1, 2, 3, 4, 5, 8, 9, and 11, it is observed that

$$\lambda_1 = -\mu_{T_0}^{\varphi}, \qquad \lambda_2 = -\mu_{T_1}^{\varphi}, \qquad \lambda_3 = -\mu_{T_2}^{\varphi},$$
$$\lambda_4 = -\mu_{M_0}^{\varphi}, \qquad \lambda_5 = -\mu_{M_1}^{\varphi}, \qquad \lambda_6 = -\mu_{A}^{\varphi},$$
$$\lambda_7 = -\mu_{E}^{\varphi}, \qquad \lambda_8 = -\mu_{I_{10}}^{\varphi}.$$

The remaining five eigenvalues are the eigenvalues of the 5×5 matrix given by

$$J_1\left(\varepsilon_0^{\star}\right) = \begin{pmatrix} -\kappa_4^{\varphi} & \kappa_{11}^{\varphi} & 0 & 0 & 0 \\ \omega^{\varphi} & -\kappa_5^{\varphi} & 0 & 0 & 0 \\ 0 & 0 & -\kappa_8^{\varphi} & \theta_1^{\varphi} & \theta_2^{\varphi} \\ \varepsilon^{\varphi} & 0 & 0 & -\kappa_9^{\varphi} & 0 \\ 0 & 0 & \eta^{\varphi} & 0 & -\kappa_{10}^{\varphi} \end{pmatrix}.$$

The row echelon method was used to determine the remaining eigenvalues. Consider $\frac{\eta^{\varphi}}{\kappa_8^{\varphi}} R_3 + R_5 \to R_5$. It follows that the Jacobian matrix $J_1(\varepsilon_0^{\star})$ becomes

$$J_1\left(\varepsilon_0^{\star}\right) = \begin{pmatrix} -\kappa_4^{\varphi} & \kappa_{11}^{\varphi} & 0 & 0 & 0 \\ \omega^{\varphi} & -\kappa_5^{\varphi} & 0 & 0 & 0 \\ 0 & 0 & -\kappa_8^{\varphi} & \theta_1^{\varphi} & \theta_2^{\varphi} \\ \varepsilon^{\varphi} & 0 & 0 & -\kappa_9^{\varphi} & 0 \\ 0 & 0 & 0 & 0 & -\kappa_{10}^{\varphi} \end{pmatrix}.$$

TBy considering column 3, λ_9 is obtained as $\lambda_9 = -\kappa_8^{\varphi} = -\left(\eta^{\varphi} + \mu_{N_K}^{\varphi}\right)$. The

remaining four eigenvalues are the eigenvalues of the 4×4 matrix given by

$$J_2\left(\varepsilon_0^\star\right) = \begin{pmatrix} -\kappa_4^\varphi & \kappa_{11}^\varphi & 0 & 0 \\ \omega^\varphi & -\kappa_5^\varphi & 0 & 0 \\ \varepsilon^\varphi & 0 & -\kappa_9^\varphi & 0 \\ 0 & 0 & 0 & -\kappa_{10}^\varphi \end{pmatrix}.$$

By considering columns 3 and 4, λ_{10} and λ_{11} are obtained as

$$\lambda_{10} = -\kappa_9^\varphi = -\left(\theta_1^\varphi + \mu_{F_1}^\varphi\right)$$

and $\lambda_{11} = -\kappa_{10}^\varphi = -\left(\theta_2^\varphi + \mu_{F_2}^\varphi\right)$, respectively. The remaining two eigenvalues are the eigenvalues of the 2×2 matrix given by

$$J_3\left(\varepsilon_0^\star\right) = \begin{pmatrix} -\kappa_4^\varphi & \kappa_{11}^\varphi \\ \omega^\varphi & -\kappa_5^\varphi \end{pmatrix}.$$

The characteristics polynomial of the Jacobian matrix $J_3\left(\varepsilon_0^\star\right)$ is given by

$$\lambda^2 + \lambda\left[\left(\omega^\varphi + \varepsilon^\varphi + \zeta^\varphi + \mu_{I_M}^\varphi\right) + \left(\psi^\varphi + \mu_V^\varphi\right)\right] + 1 - \mathbb{R}_0 \;=\; 0. \qquad (110)$$

Given that all coefficients of the characteristic polynomial in Eq. (110) are positive when $\mathbb{R}_0 < 1$, the Routh-Hurwitz criterion indicates that the roots of the characteristic polynomial possess negative real parts. Consequently, all eigenvalues of the Jacobian matrix $J_0(\varepsilon_0^\star)$ have negative real components when $\mathbb{R}_0 < 1$. Thus, it can be inferred, based on the Routh-Hurwitz criterion, that the virus-free equilibrium $\varepsilon_0^\star$ of system 39 is locally asymptotically stable.

Global Stability Analysis of Virus-free Equilibrium

To analyze the global stability of the considered fractional model 39, we use the Ulam-Hyers sense approach.

Ulam-Hyers (UH) Stability Scheme

Ulam-Hyers stability is a concept that provides an approximate solution for the exact solution in a simple form for fractional differential equations. This section establishes the stability of the proposed model 39. To achieve this effectively, the following definition was utilized.

Definition 12

The systems in Eq. (86), Eq. (87) and Eq. (88) is UH stable if there exists a constant $\mathbb{P}_i > 0, i = 1, 2, 3, \cdots, 13$ satisfying $\mho_i > 0, i = 1, 2, 3, \cdots, 13$, if

$$\begin{aligned}
\left|T_0(t) - \tfrac{1-\varphi}{\mathbb{N}(\varphi)}\Phi_1(t, T_0(t)) \tfrac{\varphi}{\mathbb{N}(\varphi)\Gamma(\varphi)} \int_0^t (1-\nu)^{\varphi-1} \Phi_1(\nu, T_0(\nu))\, d\nu\right| &< \mho_1,\\
\left|T_1(t) - \tfrac{1-\varphi}{\mathbb{N}(\varphi)}\Phi_2(t, T_1(t)) \tfrac{\varphi}{\mathbb{N}(\varphi)\Gamma(\varphi)} \int_0^t (1-\nu)^{\varphi-1} \Phi_2(\nu, T_1(\nu))\, d\nu\right| &< \mho_2,\\
\left|T_2(t) - \tfrac{1-\varphi}{\mathbb{N}(\varphi)}\Phi_3(t, T_2(t)) \tfrac{\varphi}{\mathbb{N}(\varphi)\Gamma(\varphi)} \int_0^t (1-\nu)^{\varphi-1} \Phi_3(\nu, T_2(\nu))\, d\nu\right| &< \mho_3,\\
\left|M_0(t) - \tfrac{1-\varphi}{\mathbb{N}(\varphi)}\Phi_4(t, M_0(t)) \tfrac{\varphi}{\mathbb{N}(\varphi)\Gamma(\varphi)} \int_0^t (1-\nu)^{\varphi-1} \Phi_4(\nu, M_0(\nu))\, d\nu\right| &< \mho_4,\\
\left|M_1(t) - \tfrac{1-\varphi}{\mathbb{N}(\varphi)}\Phi_5(t, M_1(t)) \tfrac{\varphi}{\mathbb{N}(\varphi)\Gamma(\varphi)} \int_0^t (1-\nu)^{\varphi-1} \Phi_5(\nu, M_1(\nu))\, d\nu\right| &< \mho_5,\\
\left|I_M(t) - \tfrac{1-\varphi}{\mathbb{N}(\varphi)}\Phi_6(t, I_M(t)) \tfrac{\varphi}{\mathbb{N}(\varphi)\Gamma(\varphi)} \int_0^t (1-\nu)^{\varphi-1} \Phi_6(\nu, I_M(\nu))\, d\nu\right| &< \mho_6,\\
\left|V(t) - \tfrac{1-\varphi}{\mathbb{N}(\varphi)}\Phi_7(t, V(t)) \tfrac{\varphi}{\mathbb{N}(\varphi)\Gamma(\varphi)} \int_0^t (1-\nu)^{\varphi-1} \Phi_7(\nu, V(\nu))\, d\nu\right| &< \mho_7,\\
\left|A(t) - \tfrac{1-\varphi}{\mathbb{N}(\varphi)}\Phi_8(t, A(t)) \tfrac{\varphi}{\mathbb{N}(\varphi)\Gamma(\varphi)} \int_0^t (1-\nu)^{\varphi-1} \Phi_8(\nu, A(\nu))\, d\nu\right| &< \mho_8,
\end{aligned} \tag{111}$$

and

$$\begin{aligned}
\left|E(t) - \tfrac{1-\varphi}{\mathbb{N}(\varphi)}\Phi_9(t, E(t)) \tfrac{\varphi}{\mathbb{N}(\varphi)\Gamma(\varphi)} \int_0^t (1-\nu)^{\varphi-1} \Phi_9(\nu, E(\nu))\, d\nu\right| &< \mho_9,\\
\left|N_K(t) - \tfrac{1-\varphi}{\mathbb{N}(\varphi)}\Phi_{10}(t, N_K(t)) \tfrac{\varphi}{\mathbb{N}(\varphi)\Gamma(\varphi)} \int_0^t (1-\nu)^{\varphi-1} \Phi_{10}(\nu, N_K(\nu))\, d\nu\right| &< \mho_{10},\\
\left|I_{10}(t) - \tfrac{1-\varphi}{\mathbb{N}(\varphi)}\Phi_{11}(t, I_{10}(t)) \tfrac{\varphi}{\mathbb{N}(\varphi)\Gamma(\varphi)} \int_0^t (1-\nu)^{\varphi-1} \Phi_{11}(\nu, I_{10}(\nu))\, d\nu\right| &< \mho_{11},\\
\left|F_1(t) - \tfrac{1-\varphi}{\mathbb{N}(\varphi)}\Phi_{12}(t, F_1(t)) \tfrac{\varphi}{\mathbb{N}(\varphi)\Gamma(\varphi)} \int_0^t (1-\nu)^{\varphi-1} \Phi_{12}(\nu, F_1(\nu))\, d\nu\right| &< \mho_{12},\\
\left|F_2(t) - \tfrac{1-\varphi}{\mathbb{N}(\varphi)}\Phi_{13}(t, F_2(t)) \tfrac{\varphi}{\mathbb{N}(\varphi)\Gamma(\varphi)} \int_0^t (1-\nu)^{\varphi-1} \Phi_{13}(\nu, F_2(\nu))\, d\nu\right| &< \mho_{13},
\end{aligned} \tag{112}$$

and also satisfying for $\hat{T}_0, \hat{T}_1, \hat{T}_2, \hat{M}_0, \hat{M}_1, \hat{I_M}, \hat{V}, \hat{A}, \hat{E}, \hat{N_K}, \hat{I_{10}}, \hat{F_1}, \hat{F_2}$ such that

$$
\begin{aligned}
\hat{T_0}(t) &= \frac{1-\varphi}{\mathbb{N}(\varphi)}\Phi_1(t,\hat{T_0}(t))\frac{\varphi}{\mathbb{N}(\varphi)\Gamma(\varphi)}\int_0^t (1-\nu)^{\varphi-1}\,\Phi_1\left(\nu,\hat{T_0}(\nu)\right)d\nu,\\
\hat{T_1}(t) &= \frac{1-\varphi}{\mathbb{N}(\varphi)}\Phi_2(t,\hat{T_1}(t))\frac{\varphi}{\mathbb{N}(\varphi)\Gamma(\varphi)}\int_0^t (1-\nu)^{\varphi-1}\,\Phi_2\left(\nu,\hat{T_1}(\nu)\right)d\nu,\\
\hat{T_2}(t) &= \frac{1-\varphi}{\mathbb{N}(\varphi)}\Phi_3(t,\hat{T_2}(t))\frac{\varphi}{\mathbb{N}(\varphi)\Gamma(\varphi)}\int_0^t (1-\nu)^{\varphi-1}\,\Phi_3\left(\nu,\hat{T_2}(\nu)\right)d\nu,\\
\hat{M_0}(t) &= \frac{1-\varphi}{\mathbb{N}(\varphi)}\Phi_4(t,\hat{M_0}(t))\frac{\varphi}{\mathbb{N}(\varphi)\Gamma(\varphi)}\int_0^t (1-\nu)^{\varphi-1}\,\Phi_4\left(\nu,\hat{M_0}(\nu)\right)d\nu,\\
\hat{M_1}(t) &= \frac{1-\varphi}{\mathbb{N}(\varphi)}\Phi_5(t,\hat{M_1}(t))\frac{\varphi}{\mathbb{N}(\varphi)\Gamma(\varphi)}\int_0^t (1-\nu)^{\varphi-1}\,\Phi_5\left(\nu,\hat{M_1}(\nu)\right)d\nu,\\
\hat{I_M}(t) &= \frac{1-\varphi}{\mathbb{N}(\varphi)}\Phi_6(t,\hat{I_M}(t))\frac{\varphi}{\mathbb{N}(\varphi)\Gamma(\varphi)}\int_0^t (1-\nu)^{\varphi-1}\,\Phi_6\left(\nu,\hat{I_M}(\nu)\right)d\nu,\\
\hat{V}(t) &= \frac{1-\varphi}{\mathbb{N}(\varphi)}\Phi_7(t,\hat{V}(t))\frac{\varphi}{\mathbb{N}(\varphi)\Gamma(\varphi)}\int_0^t (1-\nu)^{\varphi-1}\,\Phi_7\left(\nu,\hat{V}(\nu)\right)d\nu,\\
\hat{A}(t) &= \frac{1-\varphi}{\mathbb{N}(\varphi)}\Phi_8(t,\hat{A}(t))\frac{\varphi}{\mathbb{N}(\varphi)\Gamma(\varphi)}\int_0^t (1-\nu)^{\varphi-1}\,\Phi_8\left(\nu,\hat{A}(\nu)\right)d\nu,\\
\hat{E}(t) &= \frac{1-\varphi}{\mathbb{N}(\varphi)}\Phi_9(t,\hat{E}(t))\frac{\varphi}{\mathbb{N}(\varphi)\Gamma(\varphi)}\int_0^t (1-\nu)^{\varphi-1}\,\Phi_9\left(\nu,\hat{E}(\nu)\right)d\nu,\\
\hat{N_K}(t) &= \frac{1-\varphi}{\mathbb{N}(\varphi)}\Phi_{10}(t,\hat{N_K}(t))\frac{\varphi}{\mathbb{N}(\varphi)\Gamma(\varphi)}\int_0^t (1-\nu)^{\varphi-1}\,\Phi_{10}\left(\nu,\hat{N_K}(\nu)\right)d\nu,\\
\hat{I_{10}}(t) &= \frac{1-\varphi}{\mathbb{N}(\varphi)}\Phi_{11}(t,\hat{I_{10}}(t))\frac{\varphi}{\mathbb{N}(\varphi)\Gamma(\varphi)}\int_0^t (1-\nu)^{\varphi-1}\,\Phi_{11}\left(\nu,\hat{I_{10}}(\nu)\right)d\nu,\\
\hat{F_1}(t) &= \frac{1-\varphi}{\mathbb{N}(\varphi)}\Phi_{12}(t,\hat{F_1}(t))\frac{\varphi}{\mathbb{N}(\varphi)\Gamma(\varphi)}\int_0^t (1-\nu)^{\varphi-1}\,\Phi_{12}\left(\nu,\hat{F_1}(\nu)\right)d\nu,\\
\hat{F_2}(t) &= \frac{1-\varphi}{\mathbb{N}(\varphi)}\Phi_{13}(t,\hat{F_2}(t))\frac{\varphi}{\mathbb{N}(\varphi)\Gamma(\varphi)}\int_0^t (1-\nu)^{\varphi-1}\,\Phi_{13}\left(\nu,\hat{F_2}(\nu)\right)d\nu.
\end{aligned}
\tag{113}
$$

Theorem 12

With assumption (H_1) the fractional model 39 is UH stable.

Proof. Theorem 10 demonstrates that each compartment

$$T_0(t), T_1(t), T_2(t), M_0(t), M_1(t), I_M(t), V(t), A(t), E(t),$$

$$N_K(t), I_{10}(t), F_1(t), F_2(t)$$

has a unique solution. Let

$$\hat{T_0}(t), \hat{T_1}(t), \hat{T_2}(t), \hat{M_0}(t), \hat{M_1}(t), \hat{I_M}(t), \hat{V}(t), \hat{A}(t), \hat{E}(t),$$
$$\hat{N_K}(t), \hat{I_{10}}(t), \hat{F_1}(t), \hat{F_2}(t)$$

be the estimated solution of model system 39 and satisfying systems 83, 84 and 85 respectively. It can be stated that

$$\begin{aligned}
\|T_0 - \hat{T_0}\| &\leq \frac{1-\varphi}{\mathbb{N}(\varphi)}\|\Phi_1(t, T_0) - \Phi_1\left(t, \hat{T_0}\right)\| \\
&\quad + \frac{\varphi}{\mathbb{N}(\varphi)\Gamma(\varphi)}\int_0^t \|\Phi_1(\nu, T_0) - \Phi_1\left(\nu, \hat{T_0}\right)\|, \\
&\leq \left(\frac{1-\varphi}{\mathbb{N}(\varphi)} + \frac{\varphi}{\mathbb{N}(\varphi)\Gamma(\varphi)}t\right)\Psi_1\|T_0 - \hat{T_0}\|,
\end{aligned}$$

$$\begin{aligned}
\|T_1 - \hat{T_1}\| &\leq \frac{1-\varphi}{\mathbb{N}(\varphi)}\|\Phi_2(t, T_1) - \Phi_2\left(t, \hat{T_1}\right)\| \\
&\quad + \frac{\varphi}{\mathbb{N}(\varphi)\Gamma(\varphi)}\int_0^t \|\Phi_2(\nu, T_1) - \Phi_2\left(\nu, \hat{T_1}\right)\|, \\
&\leq \left(\frac{1-\varphi}{\mathbb{N}(\varphi)} + \frac{\varphi}{\mathbb{N}(\varphi)\Gamma(\varphi)}t\right)\Psi_2\|T_1 - \hat{T_1}\|,
\end{aligned}$$

$$\begin{aligned}
\|T_2 - \hat{T_2}\| &\leq \frac{1-\varphi}{\mathbb{N}(\varphi)}\|\Phi_3(t, T_2) - \Phi_3\left(t, \hat{T_2}\right)\| \\
&\quad + \frac{\varphi}{\mathbb{N}(\varphi)\Gamma(\varphi)}\int_0^t \|\Phi_3(\nu, T_2) - \Phi_3\left(\nu, \hat{T_2}\right)\|, \\
&\leq \left(\frac{1-\varphi}{\mathbb{N}(\varphi)} + \frac{\varphi}{\mathbb{N}(\varphi)\Gamma(\varphi)}t\right)\Psi_3\|T_2 - \hat{T_2}\|,
\end{aligned}$$

$$\begin{aligned}
\|M_0 - \hat{M_0}\| &\leq \frac{1-\varphi}{\mathbb{N}(\varphi)}\|\Phi_4(t, M_0) - \Phi_4\left(t, \hat{M_0}\right)\| \\
&\quad + \frac{\varphi}{\mathbb{N}(\varphi)\Gamma(\varphi)}\int_0^t \|\Phi_4(\nu, M_0) - \Phi_4\left(\nu, \hat{M_0}\right)\|,
\end{aligned}$$

$$\|M_0 - \hat{M}_0\| \leq \left(\frac{1-\varphi}{\mathbb{N}(\varphi)} + \frac{\varphi}{\mathbb{N}(\varphi)\Gamma(\varphi)}t\right)\Psi_4\|M_0 - \hat{M}_0\|,$$

$$\begin{aligned}\|M_1 - \hat{M}_1\| &\leq \frac{1-\varphi}{\mathbb{N}(\varphi)}\|\Phi_5(t, M_1) - \Phi_5\left(t, \hat{M}_1\right)\| \\ &\quad + \frac{\varphi}{\mathbb{N}(\varphi)\Gamma(\varphi)}\int_0^t \|\Phi_5(\nu, M_1) - \Phi_5\left(\nu, \hat{M}_1\right)\|, \\ &\leq \left(\frac{1-\varphi}{\mathbb{N}(\varphi)} + \frac{\varphi}{\mathbb{N}(\varphi)\Gamma(\varphi)}t\right)\Psi_5\|M_1 - \hat{M}_1\|,\end{aligned}$$

$$\begin{aligned}\|I_M - \hat{I_M}\| &\leq \frac{1-\varphi}{\mathbb{N}(\varphi)}\|\Phi_6(t, I_M) - \Phi_6\left(t, \hat{I_M}\right)\| \\ &\quad + \frac{\varphi}{\mathbb{N}(\varphi)\Gamma(\varphi)}\int_0^t \|\Phi_6(\nu, I_M) - \Phi_6\left(\nu, \hat{I_M}\right)\|, \\ &\leq \left(\frac{1-\varphi}{\mathbb{N}(\varphi)} + \frac{\varphi}{\mathbb{N}(\varphi)\Gamma(\varphi)}t\right)\Psi_6\|I_M - \hat{I_M}\|,\end{aligned}$$

$$\begin{aligned}\|V - \hat{V}\| &\leq \frac{1-\varphi}{\mathbb{N}(\varphi)}\|\Phi_7(t, V) - \Phi_7\left(t, \hat{V}\right)\| \\ &\quad + \frac{\varphi}{\mathbb{N}(\varphi)\Gamma(\varphi)}\int_0^t \|\Phi_7(\nu, V) - \Phi_7\left(\nu, \hat{V}\right)\|, \\ &\leq \left(\frac{1-\varphi}{\mathbb{N}(\varphi)} + \frac{\varphi}{\mathbb{N}(\varphi)\Gamma(\varphi)}t\right)\Psi_7\|V - \hat{V}\|,\end{aligned}$$

$$\begin{aligned}\|A - \hat{A}\| &\leq \frac{1-\varphi}{\mathbb{N}(\varphi)}\|\Phi_8(t, A) - \Phi_8\left(t, \hat{A}\right)\| \\ &\quad + \frac{\varphi}{\mathbb{N}(\varphi)\Gamma(\varphi)}\int_0^t \|\Phi_8(\nu, A) - \Phi_8\left(\nu, \hat{A}\right)\|, \\ &\leq \left(\frac{1-\varphi}{\mathbb{N}(\varphi)} + \frac{\varphi}{\mathbb{N}(\varphi)\Gamma(\varphi)}t\right)\Psi_8\|A - \hat{A}\|,\end{aligned}$$

$$\begin{aligned}\|E-\hat{E}\| &\leq \frac{1-\varphi}{\mathbb{N}(\varphi)}\|\Phi_9(t,E)-\Phi_9\left(t,\hat{E}\right)\| \\ &\quad +\frac{\varphi}{\mathbb{N}(\varphi)\Gamma(\varphi)}\int_0^t\|\Phi_9(\nu,E)-\Phi_9\left(\nu,\hat{E}\right)\|, \\ &\leq \left(\frac{1-\varphi}{\mathbb{N}(\varphi)}+\frac{\varphi}{\mathbb{N}(\varphi)\Gamma(\varphi)}t\right)\Psi_9\|E-\hat{E}\|,\end{aligned}$$

$$\begin{aligned}\|N_K-\hat{N_K}\| &\leq \frac{1-\varphi}{\mathbb{N}(\varphi)}\|\Phi_{10}(t,N_K)-\Phi_{10}\left(t,\hat{N_K}\right)\| \\ &\quad +\frac{\varphi}{\mathbb{N}(\varphi)\Gamma(\varphi)}\int_0^t\|\Phi_{10}(\nu,N_K)-\Phi_{10}\left(\nu,\hat{N_K}\right)\|, \\ &\leq \left(\frac{1-\varphi}{\mathbb{N}(\varphi)}+\frac{\varphi}{\mathbb{N}(\varphi)\Gamma(\varphi)}\right)\Psi_{10}\|N_K-\hat{N_K}\|,\end{aligned}$$

$$\begin{aligned}\|I_{10}-\hat{I_{10}}\| &\leq \frac{1-\varphi}{\mathbb{N}(\varphi)}\|\Phi_{11}(t,I_{10})-\Phi_{11}\left(t,\hat{I_{10}}\right)\| \\ &\quad +\frac{\varphi}{\mathbb{N}(\varphi)\Gamma(\varphi)}\int_0^t\|\Phi_{11}(\nu,I_{10})-\Phi_{11}\left(\nu,\hat{I_{10}}\right)\|, \\ &\leq \left(\frac{1-\varphi}{\mathbb{N}(\varphi)}+\frac{\varphi}{\mathbb{N}(\varphi)\Gamma(\varphi)}t\right)\Psi_{11}\|I_{10}-\hat{I_{10}}\|,\end{aligned}$$

$$\begin{aligned}\|F_1-\hat{F_1}\| &\leq \frac{1-\varphi}{\mathbb{N}(\varphi)}\|\Phi_{12}(t,F_1)-\Phi_{12}\left(t,\hat{F_1}\right)\| \\ &\quad +\frac{\varphi}{\mathbb{N}(\varphi)\Gamma(\varphi)}\int_0^t\|\Phi_{12}(\nu,F_1)-\Phi_{12}\left(\nu,\hat{F_1}\right)\|, \\ &\leq \left(\frac{1-\varphi}{\mathbb{N}(\varphi)}+\frac{\varphi}{\mathbb{N}(\varphi)\Gamma(\varphi)}t\right)\Psi_{12}\|F_1-\hat{F_1}\|,\end{aligned}$$

$$\begin{aligned}\|F_2 - \hat{F}_2\| &\leq \frac{1-\varphi}{\mathbb{N}(\varphi)}\|\Phi_{13}(t, F_2) - \Phi_{13}\left(t, \hat{F}_2\right)\| \\ &\quad + \frac{\varphi}{\mathbb{N}(\varphi)\Gamma(\varphi)}\int_0^t \|\Phi_{13}(\nu, F_2) - \Phi_{13}\left(\nu, \hat{F}_2\right)\|, \\ &\leq \left(\frac{1-\varphi}{\mathbb{N}(\varphi)} + \frac{\varphi}{\mathbb{N}(\varphi)\Gamma(\varphi)}t\right)\Psi_{13}\|F_2 - \hat{F}_2\|.\end{aligned}$$

Taking into account

$$\mho_1, \mho_2, \cdots \mho_{13} = \Psi_1, \Psi_2, \cdots, \Psi_{13}$$

and

$$\mathbb{P}_1, \mathbb{P}_2, \cdots, \mathbb{P}_{13} = \left(\frac{1-\varphi}{\mathbb{N}(\varphi)} + \frac{\varphi}{\mathbb{N}(\varphi)\Gamma(\varphi)}t\right),$$

the following are obtained.

$$\begin{aligned}&\|T_0 - \hat{T}_0\| \leq \mho_1\mathbb{P}_1, && \|T_1 - \hat{T}_1\| \leq \mho_2\mathbb{P}_2, && \|T_2 - \hat{T}_2\| \leq \mho_3\mathbb{P}_3, \\ &\|M_0 - \hat{M}_0\| \leq \mho_4\mathbb{P}_4, && \|M_1 - \hat{M}_1\| \leq \mho_5\mathbb{P}_5, && \|I_M - \hat{I_M}\| \leq \mho_6\mathbb{P}_6, \\ &\|V - \hat{V}\| \leq \mho_7\mathbb{P}_7, && \|A - \hat{A}\| \leq \mho_8\mathbb{P}_8, && \|E - \hat{E}\| \leq \mho_9\mathbb{P}_9, \\ &\|N_K - \hat{N_K}\| \leq \mho_{10}\mathbb{P}_{10}, && \|I_{10} - \hat{I_{10}}\| \leq \mho_{11}\mathbb{P}_{11}, && \|F_1 - \hat{F}_1\| \leq \mho_{12}\mathbb{P}_{12}, \\ &\|F_2 - \hat{F}_2\| \leq \mho_{13}\mathbb{P}_{13}. && && && (114)\end{aligned}$$

From the inequalities in Eq. (114) above, it follows that system 39 is UH stable and this complete the proof.

Fractional-order Model With Treatment

The focus now shifts to the pivotal role of antiviral interventions in managing HBV and liver cancer. While there are no specific treatments available for acute hepatitis B, two principal classes of pharmacological agents are utilized for the management of chronic HBV infection Chenar et al. (2018); Fatehi et al. (2022). These include nucleotide (nucleoside) analogues (NAs) such as lamivudine, adefovir, ente-

cavir, tenofovir, telbivudine, famciclovir, and clevudine, as well as interferon-based modalities, encompassing either standard interferon-α (roferon, intron) or pegylated interferon (peg-IFN-$\alpha 2a/2b$) (Takkenberg et al., 2010; Kim et al., 2012; Dahari et al., 2009; Sypsa et al., 2005; Packer et al., 2014; Chenar et al., 2018). These therapeutic approaches, whether administered as monotherapy (Nowak et al., 1996; Min et al., 2008) or in combination regimens (Lewin et al., 2001; Colombatto et al., 2006; Chenar et al., 2018), are designed to either attenuate the synthesis of new viral particles or prevent the initiation of novel infections. In this context, "de novo" refers to the emergence of hepatitis B surface antigen in a patient with previously negative hepatitis B serology following an orthotopic liver transplantation (OTLX).

The primary objective of these interventions is to suppress HBV replication, thereby impeding the progression of liver disease and averting the advancement to cirrhosis and hepatocellular carcinoma. This is mathematically represented by modifying the viral production rate to $(1-\varrho^{\varphi})\,\omega^{\varphi}$, and adjusting the transmission rates to $(1-\vartheta^{\varphi})\,\beta_1^{\varphi}$ and $(1-\vartheta^{\varphi})\,\beta_2^{\varphi}$ (Chenar et al., 2018). Here, $0 \leq \varrho^{\varphi} \leq 1$ and $0 \leq \vartheta^{\varphi} \leq 1$ denote the efficacy of the drugs in diminishing viral production and preventing new infections, respectively (Chenar et al., 2018; Fatehi et al., 2022). Consequently, the revised equations for the populations of uninfected macrophages, both with and without malignancy, infected macrophages, and viral loads, are formulated as follows:

$$
\begin{cases}
{}_0^{ABC}\mathbb{D}_t^{\varphi} M_0 &= \Lambda_{M_0}^{\varphi} - \beta_1^{\varphi}\,(1-\vartheta^{\varphi})\,V M_0 - \mu_{M_0}^{\varphi} M_0, \\
{}_0^{ABC}\mathbb{D}_t^{\varphi} M_1 &= \Lambda_{M_1}^{\varphi} - \beta_2^{\varphi}\,(1-\vartheta^{\varphi})\,V M_1 + \zeta^{\varphi} I_M - \mu_{M_1}^{\varphi} M_1, \\
{}_0^{ABC}\mathbb{D}_t^{\varphi} I_M &= \beta_1^{\varphi}\,(1-\vartheta^{\varphi})\,V M_0 + \beta_2^{\varphi}\,(1-\vartheta^{\varphi})\,V M_1 + \pi^{\varphi} I_M T_1 \\
&\quad -\delta_1^{\varphi}\,(1+\chi_1^{\varphi} F_1)\,I_M N_K - \delta_2^{\varphi}\,(\,1+\chi_2^{\varphi} F_2)\,I_M E \\
&\quad -\sigma^{\varphi} I_M E - \left[\omega^{\varphi}\,(1-\varrho^{\varphi}) + \varepsilon^{\varphi} + \zeta^{\varphi} + \mu_{I_M}^{\varphi}\right] I_M, \\
{}_0^{ABC}\mathbb{D}_t^{\varphi} V &= \Lambda_V^{\varphi} + \omega^{\varphi}\,(1-\varrho^{\varphi})\,I_M - \delta_3^{\varphi} T_2 V - \delta_4^{\varphi} A V - (\psi^{\varphi} + \mu_V^{\varphi})\,V.
\end{cases}
\tag{115}
$$

Control Reproduction Number, $\mathcal{R}_c$

Next, the control reproduction number, $\mathcal{R}_c$, of the model system is determined using the Next Generation Matrix method, as outlined by (Diekmann & Heesterbeek, 2000) and applied in (Chataa et al., 2021). This procedure begins with an analysis of the equations within the model framework that characterize the proliferation of new infected macrophages and the transitions in the state of these infected macrophages. The relevant equations are expressed as follows:

$$\begin{cases} {}_0^{ABC}\mathbb{D}_t^{\varphi} I_M(t) & = \beta_1^{\varphi}\left(1-\vartheta^{\varphi}\right) V M_0 + \beta_2^{\varphi}\left(1-\vartheta^{\varphi}\right) V M_1 + \pi^{\varphi} I_M T_1 \\ & \quad -\delta_1\left(1+\chi_1^{\varphi} F_1\right) I_M N_K - \delta_2^{\varphi}\left(1+\chi_2^{\varphi} F_2\right) I_M E \\ & \quad -\sigma^{\varphi} I_M E - \mathfrak{E} I_M, \\ {}_0^{ABC}\mathbb{D}_t^{\varphi} V(t) & = \Lambda_V^{\varphi} + \omega^{\varphi}\left(1-\varrho^{\varphi}\right) I_M - \delta_3^{\varphi} T_2 V - \delta_4^{\varphi} A V - \left(\psi^{\varphi}+\mu_V^{\varphi}\right) V, \end{cases} \tag{116}$$

where

$$\mathfrak{E} \;=\; \left(\omega^{\varphi}\left(1-\varrho^{\varphi}\right)+\varepsilon^{\varphi}+\zeta^{\varphi}+\mu_{I_M}^{\varphi}\right).$$

We designate this set of equations in system 116 as the infected subsystem. Adhering to the established principle of the next-generation matrix approach, the initial step involves linearizing the infected subsystem around the virus-free steady state. If we set

$$\mathbb{X} = \left(T_0, T_1, T_2, M_0, M_1, I_M, V, A, E, N_K, I_{10}, F_1, F_2\right)^T;$$

where T denote the transpose, then the infected subsection can be written in the form:

$${}_0^{ABC}\mathbb{D}_t^{\varphi}\mathbb{X}(t) \;=\; \mathbb{F}(\mathbb{X}) - \mathbb{V}(\mathbb{X}),$$

where

$$\mathbb{F}(\mathbb{X}) = \begin{pmatrix} \beta_1^{\varphi}\left(1-\vartheta^{\varphi}\right)VM_0 + \beta_2^{\varphi}\left(1-\vartheta^{\varphi}\right)VM_1 + \pi^{\varphi}I_M T_1 \\ 0 \end{pmatrix} \quad \text{and}$$

$$\mathbb{V}(\mathbb{X}) = \begin{pmatrix} \delta_1^{\varphi}\left(1+\chi_1^{\varphi}F_1\right)I_M N_K + \delta_2^{\varphi}\left(1+\chi_2^{\varphi}F_2\right)I_M E + \sigma^{\varphi}I_M E + \mathfrak{E}I_M \\ -\Lambda_V^{\varphi} - \omega^{\varphi}\left(1-\varrho^{\varphi}\right)I_M + \delta_3^{\varphi}T_2 V + \delta_4^{\varphi}AV + \left(\psi^{\varphi}+\mu_V^{\varphi}\right)V \end{pmatrix}.$$

Taking the Jacobian of $\mathbb{F}(\mathbb{X})$ at the disease-free equilibrium state gives

$$F = \begin{pmatrix} 0 & \frac{\beta_1^{\varphi}(1-\vartheta^{\varphi})\Lambda_{M_0}^{\varphi}}{\mu_{M_0}^{\varphi}} + \frac{\beta_2^{\varphi}(1-\vartheta^{\varphi})\Lambda_{M_1}^{\varphi}}{\mu_{M_1}^{\varphi}} \\ 0 & 0 \end{pmatrix}.$$

Also, taking the Jacobian of $\mathbb{V}(\mathbb{X})$ at the disease-free equilibrium and substituting gives

$$V = \begin{pmatrix} \left(\omega^{\varphi}\left(1-\varrho^{\varphi}\right)+\varepsilon^{\varphi}+\zeta^{\varphi}+\mu_{I_M}^{\varphi}\right) & 0 \\ -\omega^{\varphi}\left(1-\varrho^{\varphi}\right) & \left(\psi^{\varphi}+\mu_V^{\varphi}\right). \end{pmatrix}$$

It follows that

$$V = \begin{pmatrix} \mathcal{A} & 0 \\ -\omega^{\varphi}\left(1-\varrho^{\varphi}\right) & \mathcal{B} \end{pmatrix},$$

where

$$\begin{aligned} \mathcal{A} &= \left(\omega^{\varphi}\left(1-\varrho^{\varphi}\right)+\varepsilon^{\varphi}+\zeta^{\varphi}+\mu_{I_M}^{\varphi}\right), \\ \mathcal{B} &= \left(\psi^{\varphi}+\mu_V^{\varphi}\right). \end{aligned}$$

Hence,

$$V^{-1} = \begin{pmatrix} \frac{1}{\mathcal{A}} & 0 \\ \frac{\omega^{\varphi}(1-\varrho^{\varphi})}{\mathcal{A}\mathcal{B}} & \frac{1}{\mathcal{B}} \end{pmatrix}.$$

Hence, the next generation matrix which represents the total infectiousness of liver cells during the entire infected period is given as

$$\begin{aligned} FV^{-1} &= \begin{pmatrix} 0 & \beta_1^{\varphi}\left(1-\vartheta^{\varphi}\right)M_0^{\star}+\beta_2^{\varphi}\left(1-\vartheta^{\varphi}\right)M_1^{\star} \\ 0 & 0 \end{pmatrix} \begin{pmatrix} \frac{1}{\mathcal{A}} & 0 \\ \frac{\omega^{\varphi}(1-\varrho^{\varphi})}{\mathcal{A}\mathcal{B}} & \frac{1}{\mathcal{B}} \end{pmatrix} \\ &= \begin{pmatrix} \frac{\omega^{\varphi}(1-\varrho^{\varphi})}{\mathcal{A}\mathcal{B}}\left[\frac{\beta_1^{\varphi}(1-\vartheta^{\varphi})\Lambda_{M_0}^{\varphi}}{\mu_{M_0}^{\varphi}}+\frac{\beta_2^{\varphi}(1-\vartheta^{\varphi})\Lambda_{M_1}^{\varphi}}{\mu_{M_1}^{\varphi}}\right] & \spadesuit \\ 0 & 0 \end{pmatrix}, \end{aligned}$$

where $\spadesuit = \frac{1}{\mathcal{B}}\left[\frac{\beta_1^{\varphi}(1-\vartheta^{\varphi})\Lambda_{M_0}^{\varphi}}{\mu_{M_0}^{\varphi}}+\frac{\beta_2^{\varphi}(1-\vartheta^{\varphi})\Lambda_{M_1}^{\varphi}}{\mu_{M_1}^{\varphi}}\right]$. Hence, we obtain the $\mathcal{R}_c$ to be

$$\mathcal{R}_c = \mathcal{R}_{M_0}+\mathcal{R}_{M_1},$$

where

$$\mathcal{R}_{M_0} = \frac{\beta_1^{\varphi}\left(1-\vartheta^{\varphi}\right)\omega^{\varphi}\left(1-\varrho^{\varphi}\right)\Lambda_{M_0}^{\varphi}}{\mu_{M_0}^{\varphi}\left(\omega^{\varphi}\left(1-\varrho^{\varphi}\right)+\varepsilon^{\varphi}+\zeta^{\varphi}+\mu_{I_M}^{\varphi}\right)\left(\psi^{\varphi}+\mu_V^{\varphi}\right)},$$

$$\mathcal{R}_{M_1} = \frac{\beta_2^{\varphi}\left(1-\vartheta^{\varphi}\right)\omega^{\varphi}\left(1-\varrho^{\varphi}\right)\Lambda_{M_1}^{\varphi}}{\mu_{M_1}^{\varphi}\left(\omega^{\varphi}\left(1-\varrho^{\varphi}\right)+\varepsilon^{\varphi}+\zeta^{\varphi}+\mu_{I_M}^{\varphi}\right)\left(\psi^{\varphi}+\mu_V^{\varphi}\right)}.$$

Chapter Summary

In this chapter, a model capturing the dynamics of coexisting hepatitis B virus and liver cancer transmission, with the immune response incorporated as a regulatory mechanism, was rigorously analyzed. A detailed explanation of the model's foundational assumptions was provided, along with a comprehensive flowchart illustrating its structure, as well as descriptions of the various state variables and parameters. The model encompasses populations of liver cells, viruses, and immune cells, demonstrating that all state variables and their solutions remain non-negative for all time points t and are bounded by upper limits that populations cannot exceed. The system described in 5 has two non-negative equilibrium states, including the virus-free equilibrium (VFE), denoted as $\varepsilon_0^{\star}$, and the virus-persistence equilibrium. The

conditions necessary for the existence of the virus-persistence equilibrium were also examined. These steady states significantly influence virus transmission dynamics within liver cell populations.

Despite the potential for infinite variations in the initial distribution of hepatitis B virus and liver cancer among the cell populations, these equilibrium states represent the ultimate reachable configurations. The stability of these points was further assessed using the reproduction number, $\mathbb{R}_0$. Stability analysis confirms that the virus-free equilibrium is locally asymptotically stable, as verified by the Routh-Hurwitz criterion, and globally asymptotically stable based on the Castillo-Chavez, Feng, and Huang methodology. In contrast, the virus-persistence equilibrium may exhibit stability, instability, or act as a saddle point. Analytical results for the reproduction number suggest that when the rate of new virion replication, ω, exceeds a critical threshold, the model system converges to the virus-persistence equilibrium. The chapter continues by demonstrating the existence and uniqueness of solutions for the model system at the virus-persistence state.

Similarly, the model framework for hepatitis B virus and liver cancer transmission dynamics was revised to incorporate the immune response and treatment of infected cells as regulatory measures in Eq. (39), using fractional-order calculus. Key characteristics of the revised model, including the existence and uniqueness of solutions, as well as its stability, were analyzed using fractional differential equations. The model system 39 also features two non-negative equilibrium states: the virus-free equilibrium (VFE) and the virus-persistent equilibrium (VPE). The control reproduction number was calculated, and its analytical properties were explored. Furthermore, it was observed that increasing the clearance rates of NK cells, effector B cells, and antibodies from infected macrophages helps eliminate the infection. However, the presence of naive T cells, supported by other immune cells, facilitates the faster achievement of the virus-free equilibrium.

CHAPTER FOUR

RESULTS AND DISCUSSIONS

Introduction

Validating an epidemiological model critically involves fitting its parameters, which enhances the model's precision in understanding epidemic transmission and predicting disease trends. In this section, we will explain how to determine parameters using nonlinear least squares curve fitting, perform sensitivity analysis on the estimated parameter values, and conduct numerical simulations with published patient data from acute infections for classical-order systems and literature-sourced parameter values for fractional-order models. Sensitivity analysis is utilized to pinpoint the parameters that exert the greatest influence on the spread of an infectious disease, with a focus on assessing the effect of each parameter on the reproduction number $\mathbb{R}_0$. Computational simulations are carried out to elucidate the role of the immune system in eradicating the hepatitis B virus from hepatic cells and to identify the most effective combination of therapeutic and preventative measures for managing hepatitis B virus and liver cancer infections.

Model Fitting Procedure

The model is typically compared with data after its formulation to validate it. Model validation involves assessing how well a mathematical model represents real-world data. Analyzing data from infectious diseases is a complex problem, and various approaches have been used to address it. These techniques encompass the moments method, the maximum likelihood approach, the minimum χ^2 method, the least squares approach, among others. Inference issues with burst data are often complex due to the data's interdependence and common incompleteness, as the true infection status or process is not always directly observable. Nonetheless, creating a straightforward model that encapsulates the essential aspects of disease spread can serve as a valuable initial basis for inference. This research utilized the nonlinear least squares technique to align the DNA viral load data with the model.

Non-linear Least Square Method

The non-linear least squares technique, also known as the Nelder-Mead algorithm, named after Nelder and Roger Mead in 1975 (Nelder & Mead, 1965), was utilized to optimize the estimation of system parameters. To effectively apply this method, system 5 is reformulated into the following structure:

$$\begin{cases} \frac{d}{dt}u(t,0) = v(t,w,\varpi), \\ u(0,\varpi) = u_0, \end{cases}$$

where the function v is dependent on time t, the state variable w, and the parameter vector ϖ that needs to be estimated. The vector of variables is defined as:

$$\begin{aligned} u(t,\varpi) &= \{T_0(t), T_1(t), T_2(t), M_0(t), M_1(t), I_M(t), V(t), A(t), E(t), \\ &\quad N_K(t), I_{10}(t), F_1(t), F_2(t)\} \in \mathbb{R}^{13}. \end{aligned}$$

The process for performing the least squares estimation involves minimizing the sum of squared differences between the observed data values $u(t_i)$ and the model's predicted values $\hat{u}(t,\varpi)$, which are associated with the parameters ϖ. Thus, given k data points (t_i, u_i), where $i = 1, \cdots, k$, the goal is to minimize the following objective function:

$$H(\varpi) = \sum_{i=1}^{n} \left[\hat{u}(t_i,\varpi) - u(t_i)\right]^2.$$

Therefore, finding the parameter vector ϖ that best fits the model requires solving the optimization problem $\min H(\varpi)$ under the constraints $\varpi_{\min} \leq \varpi_i \leq \varpi_{\max}$ for $i = 1, \cdots, g$, where g denotes the number of parameters to be estimated. The model is implemented using the 'ode15s' solver in MATLAB, which is designed for solving initial value ordinary differential equations. Subsequently, the model is fitted to real data using the 'fminsearch' function in MATLAB.

Model Fitting Results

The behavior of model 5 is examined using a set of plausible parameter values approximated from available experimental data. Interaction rates and kinetics are estimated from this published data. The results are depicted in Figures 2 and 3.

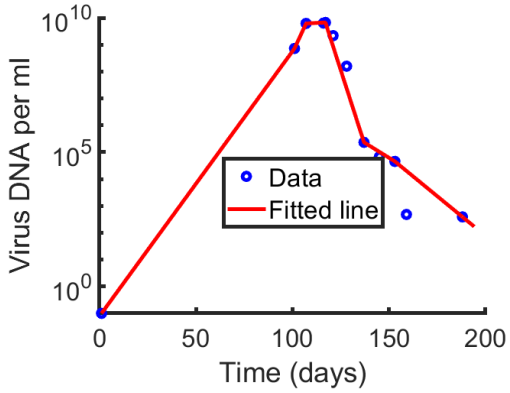

(a) Best fit of V against patient 1 data

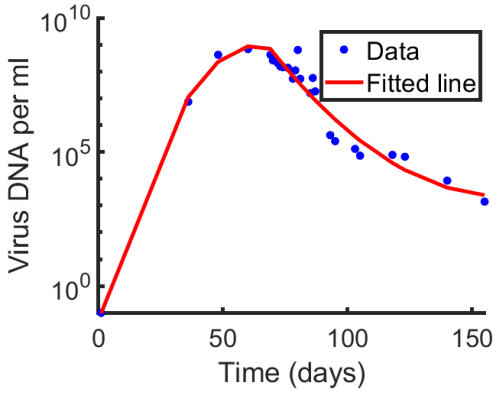

(b) Best fit of V versus patient 2 data

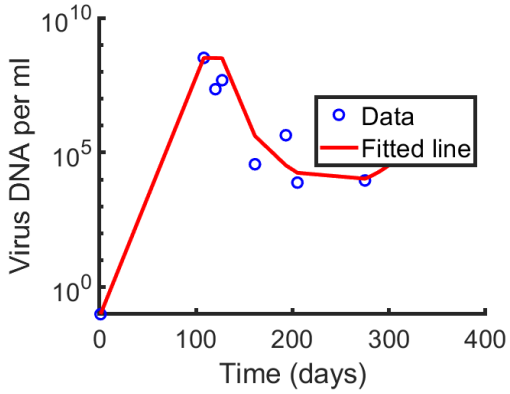

(c) Best fit of V versus patient 3 data

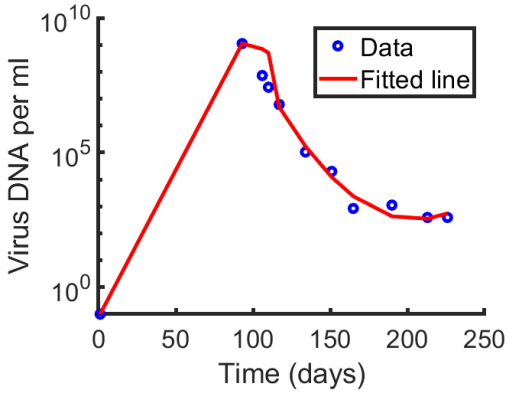

(d) Best fit of V versus patient 4 data

Figure 2: The Optimal Representation of V Provided by Model 1 (Solid Red Lines) is Compared to Patient Data $(\circ)$, Where (a) Represents the Best Fit for Patient 1 Data, (b) Represents the Best Fit for Patient 2 Data, (c) Represents the Best Fit for Patient 3 Data, and (d) Represents the Best Fit for Patient 4 Data (Source: Author's construct, 2023)

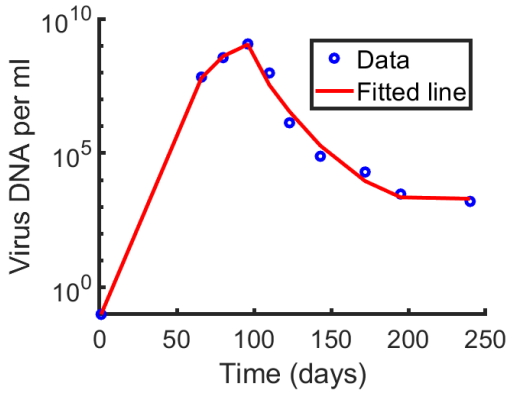

(a) Best fit of V versus patient 5 data

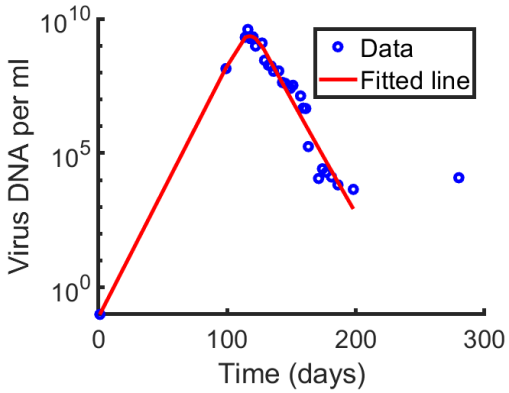

(b) Best fit of V versus patient 6 data

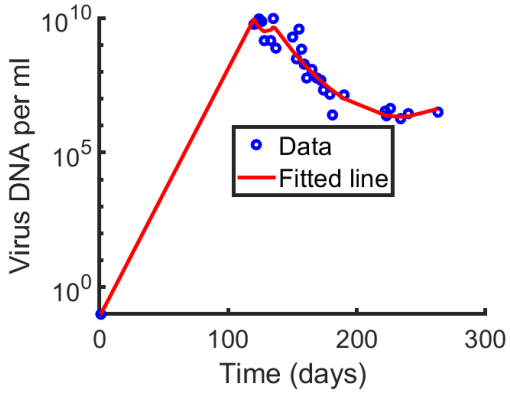

(c) Best fit of V versus patient 7 data

Figure 3: The Optimal Representation of V Provided by Model 1 (Solid Red Lines) is Compared to Patient Data $(\circ)$, Where (a) Represents the Best Fit for Patient 5 Data, (b) Represents the Best Fit for Patient 6 Data, and (c) Represents the Best Fit for Patient 7 Data (Source: Author's construct, 2023)

In 1998, seven individuals were identified in the prodromal stage of infection amidst a singular-source hepatitis B virus (HBV) outbreak Webster, Hallett, et al. (2000); Webster, Reignat, et al. (2000). All were infected with an identical HBV variant and were seronegative for antibodies against hepatitis C virus and hepatitis delta virus Webster, Hallett, et al. (2000); Webster, Reignat, et al. (2000). For patients 1 and 6, who were identified during the latency period, the interval between exposure and the zenith of viral replication was extrapolated to be 117 and 120 days, respectively, based on computations of the viral doubling kinetics prior to the peak Whalley et al. (2001). In the case of patient 2, this temporal window was ascertained to be 80 days Whalley et al. (2001). For the remaining individuals, the precise chronology of infection was indeterminate, prompting the assumption of

an average incubation period of 100 days between viral acquisition and the apogee of viral proliferation. The dataset under scrutiny comprises longitudinal quantifications of HBV DNA concentration per milliliter of plasma for these seven individuals over the initial $8-10$ months post-infection. Each individual underwent between 7 and 29 measurements, with a mean sampling interval of 12 days. Initially, the viral burden escalated exponentially, culminating at a peak of up to 10^{10} HBV DNA copies per milliliter, subsequently declining in a biphasic trajectory and appearing to asymptote approximately six months following infection. However, epidemiological evidence elucidates that patients $1-6$ ultimately achieved viral clearance, whereas patient 7 progressed to chronic HBV infection Webster, Hallett, et al. (2000); Webster, Reignat, et al. (2000) and succumbed shortly thereafter to fibrotic pulmonary pathology.

The model V was fitted as outlined by the HBV and liver cancer co-existence model Eq. (5) using data from seven patients who were identified in the acute stage of infection during a single-source HBV outbreak (for further details, see Webster, Hallett, et al. (2000); Ciupe et al. (2014); Fatehi et al. (2022)). The findings are illustrated in Figures 2 and 3, and the optimal parameter estimates for each patient are provided in Table 4. The model accurately reflects the significant viral surge observed during the acute infection phase for each individual and the subsequent two-phase reduction in viral levels. Furthermore, the most best estimates indicate that viral elimination (defined as having less than one virion present in the body) occurs after infection in the first six individuals, but not in patient 7, who has developed a chronic infection (Ciupe et al., 2014; Fatehi et al., 2022). No relationship was found between $\mathcal{R}_0$ and the time to viral clearance; however, the rapid clearance seen in patient 5 corresponds to a marked second-phase reduction in viral levels, attributed to a high rate of infected cell loss, $\mu_{I_M}(2.1918)$. Conversely, patients 2 and 7, who have the lowest $\mu_{I_M}(0.4908)$ and $\mu_{I_M}(0.00000885)$, respectively, experience the longest duration to viral clearance and no clearance at all. The parameters $\{\psi, \omega, \sigma, \beta_1, \beta_2, \zeta, \delta_1, \delta_2, \delta_3, \delta_4, \rho_1, \rho_2, \rho_3, \mu_{I_M}\}$ were determined by fitting V as specified by the HBV and liver cancer co-existence model Eq. (5) using data from

acute HBV infections (Ciupe, Ribeiro, Nelson, Dusheiko, & Perelson, 2007; Webster, Hallett, et al., 2000; Fatehi et al., 2022). The infection dates for each individual were either known or previously approximated (Ciupe, Ribeiro, Nelson, Dusheiko, & Perelson, 2007; Whalley et al., 2001; Ciupe et al., 2014; Fatehi et al., 2022). The parameter values are detailed in Table 4, and we then adjusted ω, δ_1, δ_2, δ_3, δ_4, and ρ_3 to explore the outcomes. The basic reproduction number ($\mathcal{R}_0$) corresponding to the fitting result was calculated to be $\mathcal{R}_0 = 5,061,469.22$, with $\mathcal{R}_1 = 5,061,469.01$ and $\mathcal{R}_2 = 0.21$, indicating that the primary driver of infection dynamics is the contribution from $\mathcal{R}_1$, which is associated with the uninfected macrophage without cancer population. In the absence of antibodies, natural killer cells, effector B cells, and T-cell responses, the reproduction number exceeds one (i.e., $\mathcal{R}_0 > 1$), indicating a persistent, chronic HBV infection in model 5. The changes in these dynamics are examined in the presence of antibodies, natural killer cells, effector B cells, naive T cells, and cytokines.

Table 4: Estimated Parameter Values for Seven Patients

Patient	ψ	ω	σ	β_1	β_2	ζ	δ_1	δ_2	δ_3	δ_4	ρ_1	ρ_2	ρ_3	μ_{I_M}	RSS
1	5.9511	20.2859	5.6135	5.5746	4.6961	1.7544	6.6342	5.4818	4.0929	5.7133	22.8207	20.2655	6.4256	0.6489	1148.66
2	4.9455	20.0315	0.9836	1.2375	0.9157	0.5516	0.5308	0.4640	1.0708	1.4752	2.8477	2.4894	0.9932	0.4908	18.8765
3	5.0003	19.9999	0.5000	0.8903	0.8915	1.0014	0.7000	0.6976	0.7000	0.6996	0.8913	0.2702	0.0077	0.5636	2.4474
4	5.0000	20.0000	0.5000	0.0001	0.0001	1.0000	0.7000	0.7016	0.7000	0.7000	0.0001	0.0200	0.0006	0.5600	0.0037
5	5.2105	20.0342	0.3698	0.7059	1.0635	1.1476	0.6373	0.9308	1.7567	1.0803	3.7523	3.0210	0.3781	2.1918	9.0212
6	5.0137	20.0659	0.8746	0.5868	0.7980	0.6829	1.2619	1.3411	1.3114	0.5854	4.2445	3.7187	0.6697	0.7786	34.6358
7	4.7512	20.1240	0.2192	1.3863	0.9973	1.2611	0.8358	1.1504	1.4190	0.6839	4.4136	4.0736	0.9025	0.0000885	40.9971
median	5.0003	20.0342	0.5000	0.8903	0.9157	1.0014	0.7000	0.9308	1.3114	0.7000	3.7523	3.0210	0.6697	0.5636	-
mean	5.1246	20.0773	1.2944	1.4831	1.3375	1.0570	1.6143	1.5382	1.5787	1.5625	5.5672	4.8369	1.3396	0.7477	-
stdev	0.3884	0.1014	1.9236	1.8605	1.5236	0.3954	2.2260	1.7640	1.1728	1.8567	7.7922	6.9850	2.2774	0.6819	-

Source: Author's construct (2023)

Parameter Estimation for the Classical-order Model

It is estimated that an adult liver contains about 2×10^{11} cells, with 60% of these being hepatocytes (Ciupe, Ribeiro, Nelson, Dusheiko, & Perelson, 2007; Goyal et al., 2017; Michalopoulos, 2007; Kmiec, 2001; Fatehi et al., 2022). For an adult patient, the assumption is that 3 liters of serum contain complete particles (Murray & Goyal, 2015). Therefore, $\frac{\Lambda_{M_0}}{\mu_{M_0}} = \frac{0.6\times 2\times 10^{11}}{3000} = 4 \times 10^7$ cells/ml. The death rate for uninfected macrophages is estimated at 0.01 per day (Guedj et al., 2013; Kitagawa et al., 2018; Fatehi et al., 2022), making $\mu_{M_0} = 0.01$. Consequently, $\Lambda_{M_0} = 4 \times 10^5$. SIn unvaccinated individuals with a positive HBV-DNA test, the antibody concentration remains below 10 mIU/ml, equivalent to 8.5×10^4 mg/ml or 3.4×10^{12} molecules/ml (Ciupe et al., 2014; Guang et al., 2019; Fatehi et al., 2022). Thus, $\Lambda_A = 3.4 \times 10^{12}$ molecules/ml was assumed. The remaining baseline parameter values are provided in Tables 5 and 6.

Table 5: Parameters and their Values for the Classical-order Model

Parameter	Values	Source
Λ_{T_0}	0.99 cell/ml/day	Assumed
Λ_{M_0}	4×10^5 cell/ml/day	(Fatehi et al., 2022)
Λ_{M_1}	0.015 cell/ml/day	(Bhadauria, 2011)
Λ_V	0.3 cell/ml/day	(Wiah et al., 2011)
Λ_A	3.4×10^{12} cell/ml/day	(Guang et al., 2019)
Λ_E	10 cell/ml/day	(Fatehi et al., 2022)
Λ_{N_K}	0.057 cell/ml/day	(Y. Zhang et al., 2007)
μ_{T_0}	6.7×10^{-7} cell/ml/day	Assumed
μ_{T_1}	0.3333 cell/ml/day	Assumed
μ_{T_2}	0.3333 cell/ml/day	Assumed
μ_{M_0}	0.011 cell/ml/day	(Fatehi et al., 2022)
μ_{M_1}	0.01 cell/ml/day	(Kitagawa et al., 2018)
μ_{I_M}	0.5636 cell/ml/day	Estimated

Source: Author's construct (2023)

Table 6: Parameters and their Values for the Classical-order Model

Parameter	Description	Source
μ_V	0.67 cell/ml/day	(Chenar et al., 2018)
μ_A	0.332 cell/ml/day	(Ciupe et al., 2014)
μ_E	0.5 cell/ml/day	(Ciupe et al., 2014)
μ_{N_K}	0.42 cell/ml/day	Assumed
$\mu_{I_{10}}$	3.70×10^{-2} cell/ml/day	Assumed
μ_{F_1}	4.9 cell/ml/day	(Chenar et al., 2018)
μ_{F_2}	5.16 cell/ml/day	(Chenar et al., 2018)
ρ_1	3.7523 cell/ml/day	Estimated
ρ_2	3.0210 cell/ml/day	Estimated
ρ_3	0.6697 cell/ml/day	Estimated
δ_1	0.7 cell/ml/day	Estimated
δ_2	0.9308 cell/ml/day	Estimated
δ_3	1.3114 cell/ml/day	Estimated
δ_4	0.7 cell/ml/day	Estimated
θ_1	0.8 cell/ml/day	(Chenar et al., 2018)
θ_2	0.6 cell/ml/day	(Chenar et al., 2018)
χ_1	1.5 cell/ml/day	(Chenar et al., 2018)
χ_2	2.0 cell/ml/day	(Chenar et al., 2018)
β_1	0.8903 cell/ml/day	Estimated
β_2	0.9157 cell/ml/day	Estimated
τ_1	0.1642 cell/ml/day	Assumed
ψ	5 cell/ml/day	(Chenar et al., 2018)
σ	0.5 cell/ml/day	Estimated
ω	20.0342 cell/ml/day	Estimated
ε	1 cell/ml/day	(Chenar et al., 2018)
η	0.9 cell/ml/day	(Chenar et al., 2018)
π	0.3359 cell/ml/day	Assumed
ζ	1.0014 cell/ml/day	Estimated

Source: Author's construct (2023)

Numerical Results of Classical-order Model

Assessing the practical utility and performance of system 5 through numerical methods involves applying a set of estimated parameter values derived from published research on HBV patients and other relevant studies. The initial conditions employed are: $T_0(0) = 5 \times 10^5$, $T_1(0) = 0$, $T_2(0) = 0$, $M_0(0) = 4 \times 10^5$, $M_1(0) = 4 \times 10^5$, $I_M(0) = 0$, $V(0) = 300$, $A(0) = 0$, $E(0) = 0$, $N_K(0) = 0$, $I_{10}(0) = 0$, $F_1(0) = 0$, and $F_2(0) = 0$. The parameters used in the simulations are detailed in Tables 5 and 6.

Quantitative Findings at the Virus-free Equilibrium

To elucidate the spectrum of dynamic behaviors that model 5 can exhibit under various parameter configurations, the system is computationally resolved utilizing the baseline parameter values enumerated in Tables 5 and 6. The results are showcased in Figures 4, 5, and 6. Figures 4, 5, and 6 elucidate the immune response dynamics in the absence of hepatitis B virus within the hepatic cell population. In this scenario, the initial viral replication precipitates an augmentation in the levels of antibodies (A), effector B cells (E), natural killer cells (N_K), cytotoxic T lymphocytes (T_2), and both classes of interferons. This culminates in the effective eradication of the HBV infection. Subsequently, type-1 interferons are also eradicated, and the system attains a stable, virus-free equilibrium. The absence of infected macrophages indicates that HBV is not proliferating, implying that naive T lymphocytes do not partake in lytic activity. Consequently, the populations of T helper-1 cells, cytotoxic T lymphocytes, antibodies, effector B cells, natural killer cells, interleukin-10, and interferon-gamma diminish to zero, as depicted in Figures 4, 5, and 6.

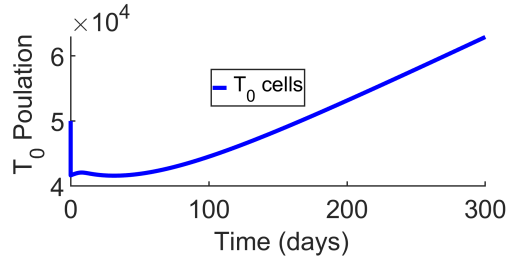

(a) Unactivated T cells (T_0)

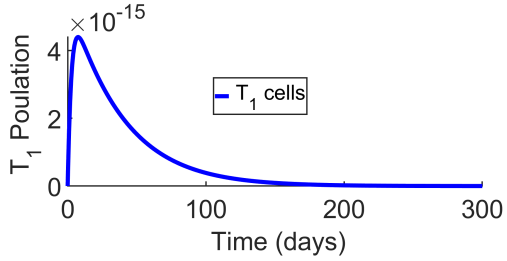

(b) Th1 cells (T_1) cells

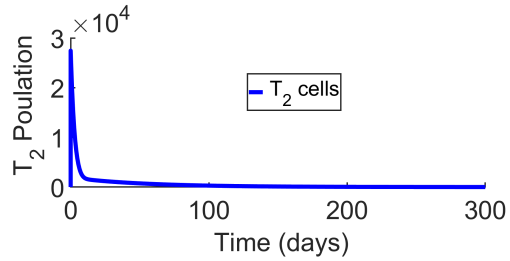

(c) Killer T cells (T_2)

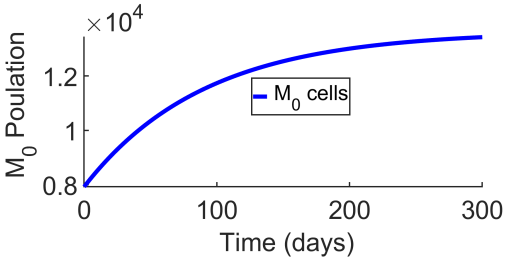

(d) Macrophages not infected and free of cancer cells (M_0)

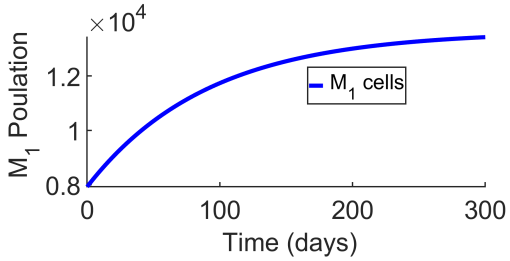

(e) Macrophages not infected but contain cancer cells (M_1)

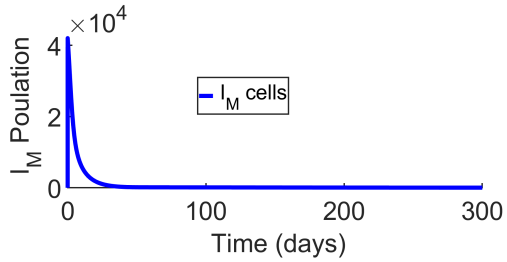

(f) Macrophages with an infection (I_M)

Figure 4: Simulation Results Illustrating the Dynamics of State Variables at the Virus-Free Equilibrium Point, Where (a) Represents the Unactivated T Cell Class, (b) Represents the T Helper 1 Cell Class, (c) Represents the Killer T Cell Class, (d) Represents the Uninfected Macrophage Free of Cancer Cells Class, (e) Represents the Uninfected Macrophage Containing Cancer Cells Class, and (f) Represents the Infected Macrophage Containing Cancer Cells Class (Source: Author's construct, 2023)

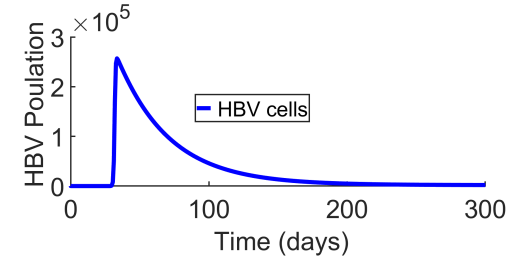

(a) Hepatitis B virus particles (HBV)

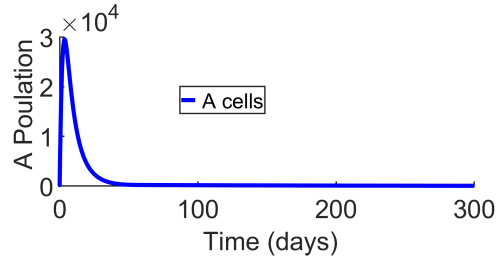

(b) Immune antibodies (A) cells

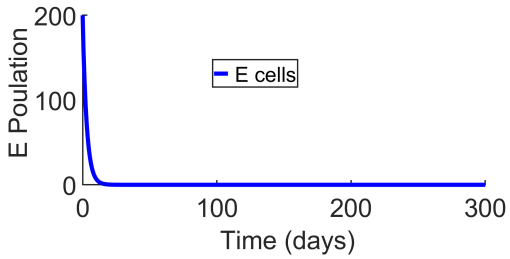

(c) Plasma (effector B cells) (E)

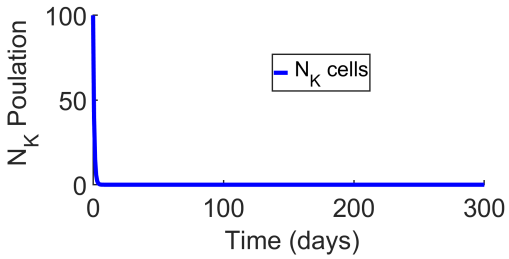

(d) (N_K) cells

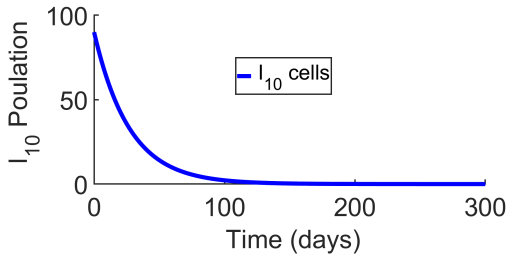

(e) Cells producing Interleukin-10

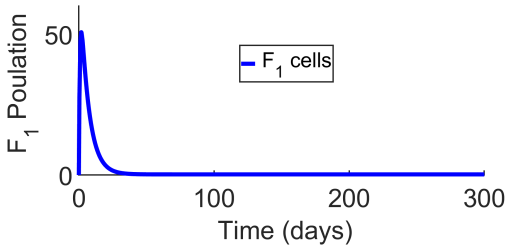

(f) Alpha and beta interferons (F_1)

Figure 5: Simulation Results Illustrating the Dynamics of State Variables at the Virus-Free Equilibrium Point, Where (a) Represents the Hepatitis B Virus Particles Class, (b) Represents the Antibodies Class, (c) Represents the Effector B Cell Class, (d) Represents the Natural Killer Cell Class, (e) Represents the Interleukin-10 Cytokine Class, and (f) Represents the Interferon Alpha and Beta Class (Source: Author's construct, 2023)

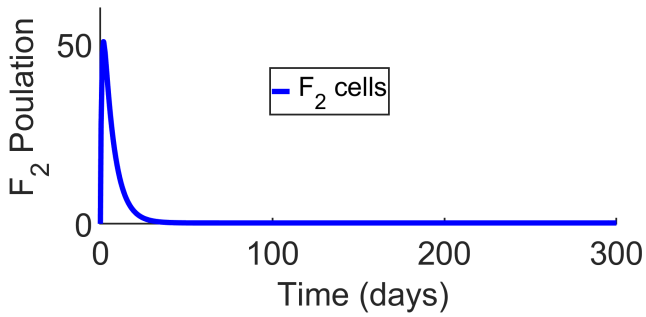

Figure 6: Simulation Outcomes Demonstrating the Dynamics of the F_2 Cytokine Class at the Virus-Free Equilibrium (Source: Author's construct, 2023)

Quantitative Findings at the Virus-persistence Equilibrium

Figures 7, 8, and 9 delineate the dynamics of the state variables model 5 subsequent to infection with a minimal initial burden of hepatitis B viruses, observed at the equilibrium of viral persistence. Figure 7(a) elucidates the dynamics of naive T lymphocytes, which, upon complete maturation, attain their peak density. However, the presence of HBV within hepatic cells induces a modification in these dynamics. As depicted in Figure 8(a), HBV precipitates a diminution in the density of naive T lymphocytes due to their differentiation into T-helper 1 (T_1) cells, cytotoxic T lymphocytes (T_2), and interleukin-10 (I_{10}) cells. A reciprocal relationship was also discerned between HBV levels and naive T lymphocytes, indicating that an augmentation in naive T lymphocyte density correlates with a diminution in HBV levels. As the HBV burden escalates, the rate of decline in naive T lymphocytes accelerates, concomitant with an enhanced production of both pro-inflammatory and anti-inflammatory cells, as illustrated in Figures 8(e), 8(f), and 9. Figures 7(b) and 7(c) further examine the behavior of T-helper 1 and cytotoxic T lymphocytes, respectively, demonstrating an initial increase in both cell types as a consequence of the differentiation process of naive T lymphocytes. Nevertheless, cytotoxic T lymphocytes were observed to diminish almost immediately post-generation, within the shortest conceivable time frame, due to persistent inhibition by HBV. Conversely, T-helper 1 cells decline as a result of the lytic effects induced by HBV replication within macrophages, which impacts the overall rate of disease progression. Figures 7(d) and 7(e) illustrate that uninfected macrophages, whether or not associated with neoplastic cells, commence with their initial densities, which subsequently decrease over time, correlating with the escalating HBV load.

As the HBV replication rate intensifies, an increased recruitment of cells to the infection site occurs to engulf the virus, as depicted in Figure 7(f). This results in a diminution in the density of uninfected macrophages. Consequently, the number of infected macrophages escalates as uninfected macrophages become infected through viral ingestion. This increase in infected macrophages stabilizes once they achieve activation, as shown in Figure 7(f). Furthermore, the density of in-

fected macrophages, positively correlated with interferon-gamma, interferon-alpha and beta cytokines, antibodies, effector B cells, and natural killer cells, is illustrated in Figures 8(b), 8(c), and 8(d). As interferon-gamma concentration escalates, as depicted in Figure 8(f), it triggers the activation of additional infected macrophages, resulting in a rise in the population of uninfected macrophages. Thus, Figures 7, 8, and 9 delineate the dynamics when the endemic steady state is both attainable and stable, demonstrating that the initial viral expansion is regulated by the coordinated actions of various components of the immune system.

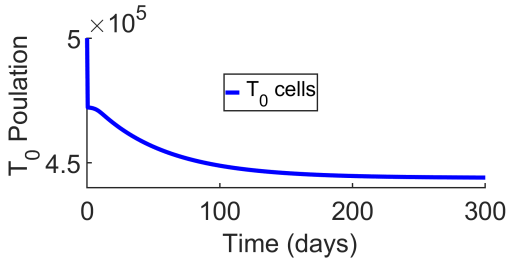

(a) Unactivated T cells (T_0)

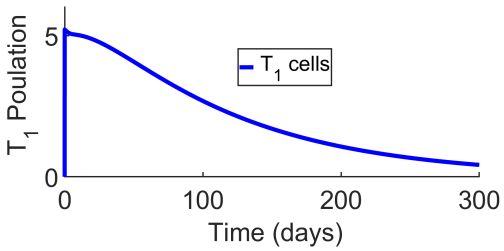

(b) Th1 cells (T_1)

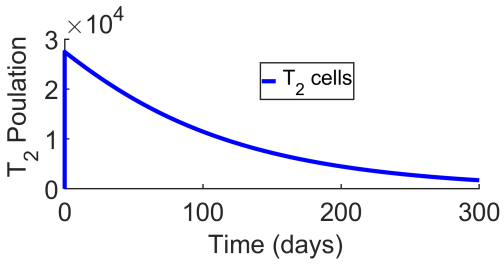

(c) Killer T cells (T_2)

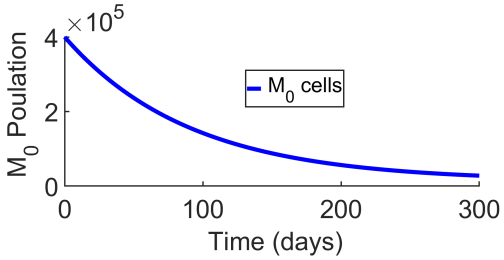

(d) Macrophages not infected and free of cancer cells (M_0)

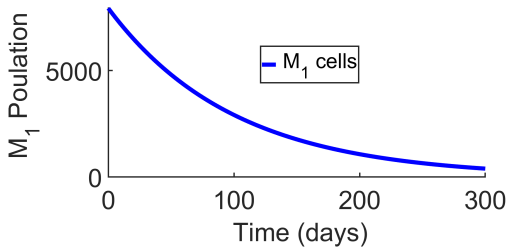

(e) Macrophages not infected but contain cancer cells (M_1)

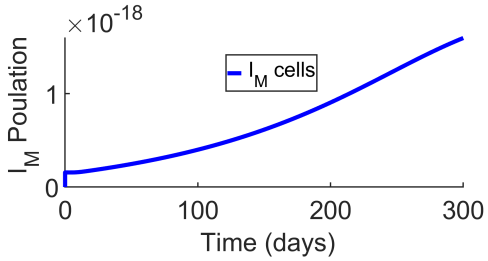

(f) Macrophages with an infection (I_M)

Figure 7: Simulation Results Illustrating the Dynamics of State Variables at the Endemic Equilibrium Point, Where (b) Represents the Unactivated T Cell Class, (b) Represents the T Helper 1 Cell Class, (c) Represents the Killer T Cell Class, (d) Represents the Uninfected Macrophage Free of Cancer Cells Class, (e) Represents the Uninfected Macrophage Containing Cancer Cells Class, and (f) Represents the Infected Macrophage Containing Cancer Cells Class (Source: Author's construct, 2023)

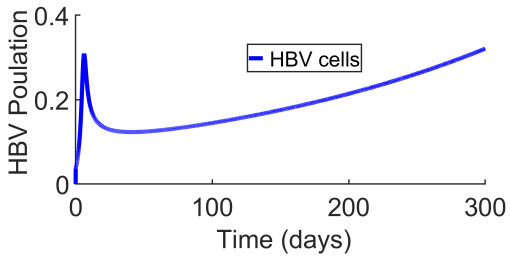

(a) Hepatitis B virus particles (HBV)

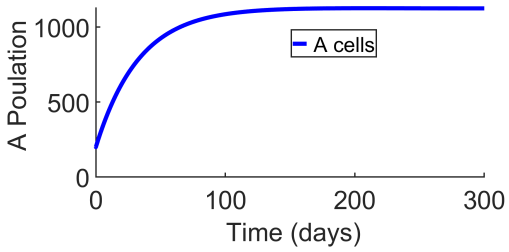

(b) Immune antibodies (A) cells

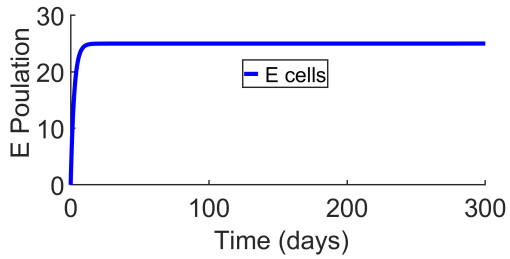

(c) Plasma (Effector B) cells (E)

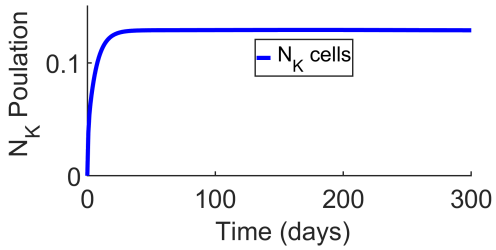

(d) (N_K) cells

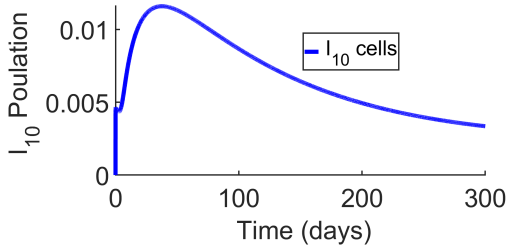

(e) Interleukin-10 cells (I_{10})

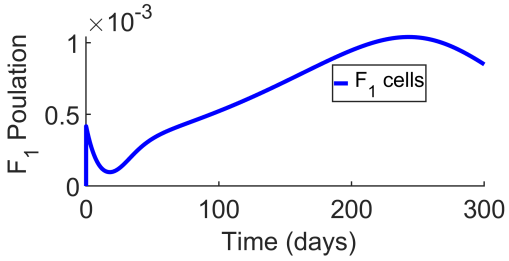

(f) Alpha and beta interferons (F_1)

Figure 8: Simulation Results Illustrating the Dynamics of State Variables at the Endemic Equilibrium Point, Where (a) Represents the Hepatitis B Virus Particles Class, (b) Represents the Antibodies Class, (c) Represents the Effector B Cell Class, (d) Represents the Natural Killer Cell Class, (e) Represents the Interleukin-10 Cytokine Class, and (f) Represents the Interferon Alpha and Beta Class (Source: Author's construct, 2023)

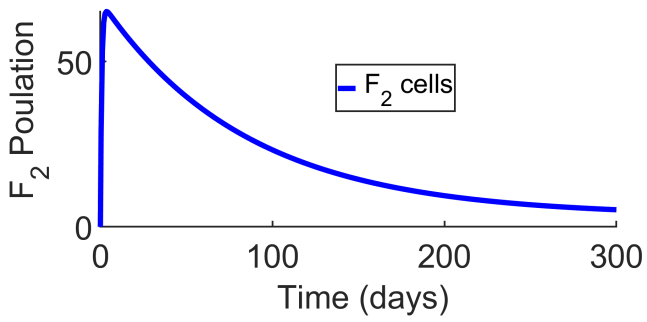

Figure 9: Simulation Outcomes Demonstrating the Dynamics of the F_2 Cytokine Class at the Endemic Equilibrium (Source: Author's construct, 2023)

Impact of Natural Killer Cells on Infected Macrophages Cells

Natural Killer (NK) cells are essential in the immune defense against Hepatitis B virus (HBV) and in preventing the development of liver cancer, referred to as hepatocellular carcinoma (HCC). They address HBV by targeting and killing infected liver cells, as well as secreting cytokines that curtail viral replication and enhance other immune responses. In liver cancer, NK cells recognize and eliminate tumor cells through cytotoxic mechanisms. However, in chronic HBV infection and advanced liver cancer, NK cell function can be impaired, allowing the virus to persist and cancer cells to evade immune detection, contributing to disease progression.

In Figure 10, it is evident that an increase in the rate at which natural killer cells cure and kill infected macrophage cells by 25% from the baseline value ($\delta_1 = 0.7$ to $\delta_1 = 0.875$) corresponds to a 0.23% decrease in infected macrophages. This suggests the effective elimination of infected macrophages causing HBV and liver cancer infections, leading to a reduction in the overall infected liver cell population. Conversely, a 25% reduction in this rate from the baseline ($\delta_1 = 0.7$ to $\delta_1 = 0.525$) results in a 0.05% increase in infected macrophage cells. This implies that increasing the rate at which natural killer cells cure and clear infected macrophage cells from the baseline lowers the basic reproduction number ($\mathbb{R}_0$), subsequently reducing the spread of HBV and liver cancer infections.

Further adjustments in the virus clearance rate by natural killer cells, such as a 50% increase to $\delta_1 = 1.05$ or a 50% decrease to $\delta_1 = 0.35$, lead to corresponding 4.58% decreases or 2.46% increases in the infected macrophage populations. Similar trends are observed when the clearance rate is increased by 75% to $\delta_1 = 1.225$ (i.e., a 6.76% decrease in the infected macrophage population) or decreased by the same percentage to $\delta_1 = 0.175$ (i.e., a 4.94% increase in the infected macrophage population). We also computed the area under the curve (AUC) for different virus clearance rates by natural killer cells to assess the extent of the infected macrophage population over time and summarized the results in Table 7.

The simulation results in Figure 10 underscore the crucial role that natural killer cells, through the immune system response, play in controlling the dynamics

of HBV and liver cancer spread within human liver cells and their elimination.

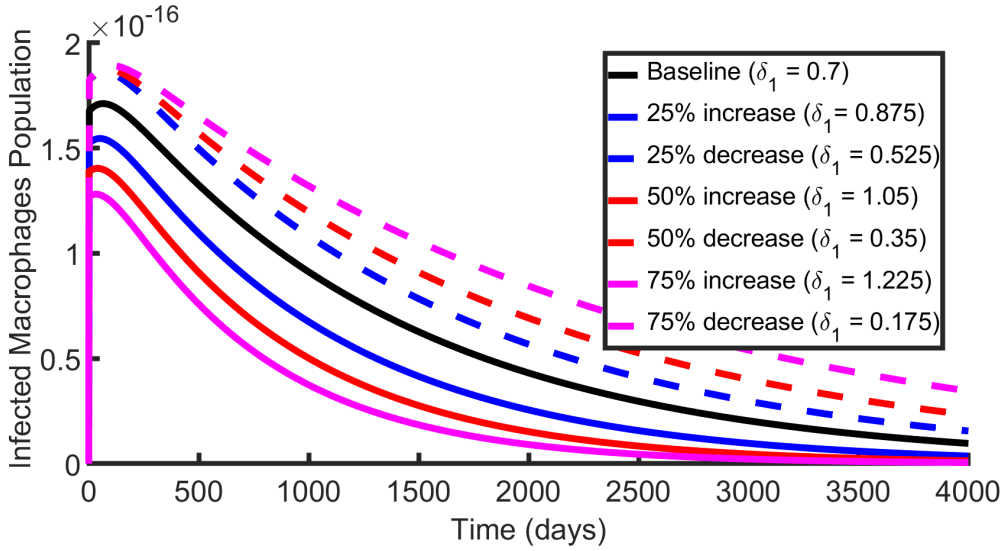

Figure 10: Effects of NK Cell Clearance Rates on Infected Cells (Source: Author's construct, 2023)

Table 7: Effects of NK Cell Clearance Rates on Infected Cells

Parameter Value	AUC	PC %
Baseline ($\delta_1 = 0.7$)	211799712.99	-
25% increase ($\delta_1 = 0.875$)	206870976.17	-0.23%
25% decrease ($\delta_1 = 0.525$)	211898491.99	0.05%
50% increase ($\delta_1 = 1.05$)	202099200.36	-4.58%
50% decrease ($\delta_1 = 0.35$)	2170000903.39	2.46%
75% increase ($\delta_1 = 1.225$)	197478331.85	-6.76%
75% decrease ($\delta_1 = 0.175$)	222264190.28	4.94%

Source: Author's construct (2023)

Impact of Effector B Cells on Infected Macrophages Cells

Effector B cells (plasma cells) are crucial in the immune defense against Hepatitis B virus (HBV) and liver cancer. They represent the mature stage of B cells and are responsible for generating antibodies that target HBV specifically. These antibodies neutralize the virus, stopping it from infecting liver cells and tagging it for elimination by other immune cells. Regarding liver cancer (hepatocellular carcinoma), which can result from chronic HBV infection, Plasma B cells contribute to the immune defense by producing antibodies that target tumor-associated antigens, aiding in the recognition and elimination of cancerous cells. Nonetheless, in persistent HBV infection and advanced hepatic carcinoma, the activity of Plasma B cells

might be compromised, reducing their ability to manage the illness. In Figure 11, it is clear that a 25% increase in the rate at which plasma cells treat and eliminate infected macrophages from the baseline value ($\delta_2 = 0.9308$ to $\delta_2 = 1.1635$) results in a 2.66% decline in infected macrophages. This indicates the successful removal of infected macrophages driving HBV and liver cancer cell replication, thereby decreasing the overall population of infected liver cells. On the other hand, reducing this rate by 25% from the baseline ($\delta_2 = 0.9308$ to $\delta_2 = 0.6981$) causes a 0.99% rise in infected macrophage cells. This shows that boosting the rate at which effector B cells clear infected macrophages from the baseline reduces the basic reproduction number ($\mathbb{R}_0$), which in turn limits the transmission of HBV and liver cancer infections.

Additional changes in the virus elimination rate by effector B cells, such as a 50% increase to $\delta_2 = 1.3962$ or a 50% decrease to $\delta_2 = 0.4654$, result in 4.99% reductions or 1.98% increases in infected macrophage populations, respectively. Similar patterns are observed when the clearance rate is raised by 75% to $\delta_2 = 1.6289$ (leading to a 7.24% decrease in infected macrophages) or lowered by 75% to $\delta_2 = 0.2327$ (leading to a 3.40% increase in infected macrophages). Additionally, we calculated the area under the curve (AUC) for various virus elimination rates by effector B cells to evaluate the progression of infected macrophage populations over time, with the results summarized in Table 8.

The simulation results in Figure 11 highlight the significant role that effector B cells, through their immune response, play in managing the spread of HBV and liver cancer within liver cells and facilitating their clearance.

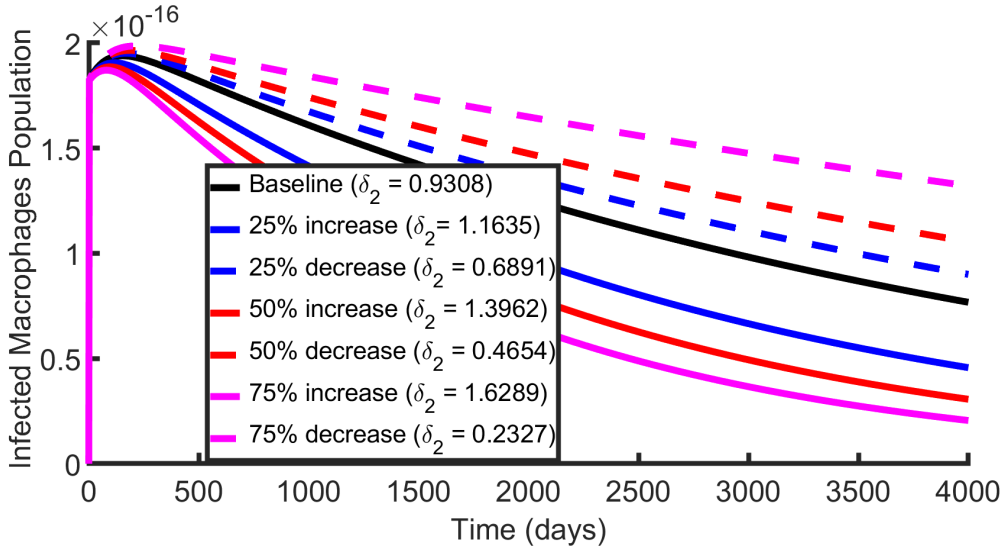

Figure 11: Effects of Plasma Cell Clearance Rates on Infected Cells (Source: Author's construct, 2023)

Table 8: Effects of Plasma Cell Clearance Rates on Infected Cells

Parameter Value	AUC	PC %
Baseline ($\delta_2 = 0.9308$)	233309811.20	-
25% increase ($\delta_2 = 1.1635$)	227103342.58	-2.66%
25% decrease ($\delta_2 = 0.6981$)	235608561.86	0.99%
50% increase ($\delta_2 = 1.3962$)	221677614.71	-4.99%
50% decrease ($\delta_2 = 0.4654$)	237938941.06	1.98%
75% increase ($\delta_2 = 1.6289$)	216426617.26	-7.24%
75% decrease ($\delta_2 = 0.2327$)	241242954.76	3.40%

Source: Author's construct (2023)

Impact of Cytotoxic T Cells on Hepatitis B Virus (HBV) Cells

Cytotoxic T lymphocytes, often referred to as $CD8^+$ T cells, play a crucial role in combating HBV and liver cancer infections. They identify and attach to liver cells that present viral antigens, including those from HBV, on their surface. Upon attachment, these T lymphocytes secrete cytotoxic substances, such as perforin and granzymes, which trigger apoptosis (programmed cell death) in the infected cells, thereby effectively removing the virus. In the context of liver cancer, Cytotoxic T lymphocytes can also detect and destroy cancerous cells that present abnormal antigens, aiding in the management and reduction of cancer progression. Even so, in long-term infections, their functionality could be diminished, lowering their efficiency. In Figure 12, it is clear that a 25% increase in the rate at which cyto-

toxic T lymphocytes target and eliminate hepatitis B virus from the baseline value ($\delta_3 = 1.3114$ to $\delta_3 = 1.6393$) leads to a 7.26% reduction in the HBV population. This shows that effectively removing HBV cells that drive the infection reduces the total count of infected liver cells. Conversely, a 25% decrease in this rate from the baseline ($\delta_3 = 1.3114$ to $\delta_3 = 0.9836$) results in a 5.44% increase in the HBV population. This indicates that raising the rate at which cytotoxic T cells eliminate virus cells from the baseline lowers the basic reproduction number ($\mathbb{R}_0$), thus reducing the spread of HBV and liver cancer infections.

Further changes in the virus elimination rate by cytotoxic T cells, such as a 50% increase to $\delta_3 = 1.9671$ or a 50% decrease to $\delta_3 = 0.6557$, lead to 11.86% decreases or 9.48% increases in HBV populations, respectively. Similar effects are observed when the clearance rate is increased by 75% to $\delta_3 = 2.2950$ (resulting in a 16.02% reduction in HBV population) or decreased by 75% to $\delta_3 = 0.3278$ (causing a 13.94% increase in the virus population). Additionally, we calculated the area under the curve (AUC) for different virus elimination rates by cytotoxic T cells to assess the evolution of virus populations over time, with the results summarized in Table 9.

The simulation results shown in Figure 12 emphasize the important role of cytotoxic T cells in managing the spread of HBV and liver cancer within liver cells and in aiding their clearance through their immune response.

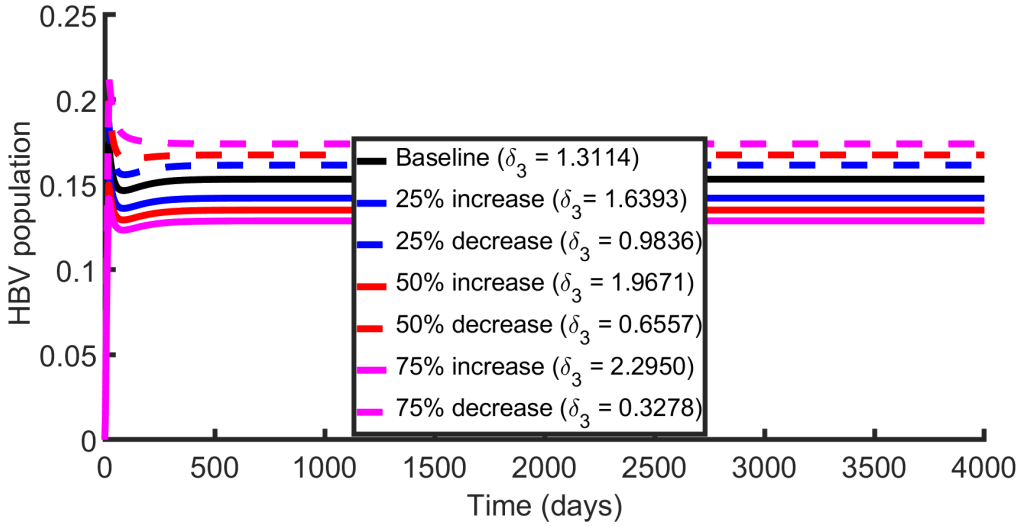

Figure 12: Effects of Cytotoxic T Cells on HBV Cells (Source: Author's construct, 2023)

Table 9: Effects of Cytotoxic Cells Viral Removal Rate on HBV Cells

Parameter Value	AUC	PC %
Baseline ($\delta_3 = 1.3114$)	611.22	-
25% increase ($\delta_3 = 1.6393$)	566.83	-7.26%
25% decrease ($\delta_3 = 0.9836$)	644.44	5.44%
50% increase ($\delta_3 = 1.9671$)	538.73	-11.86%
50% decrease ($\delta_3 = 0.6557$)	669.17	9.48%
75% increase ($\delta_3 = 2.2950$)	513.31	-16.02%
75% decrease ($\delta_3 = 0.3278$)	696.45	13.94%

Source: Author's construct (2023)

Impact of Antibodies Cells on Hepatitis B Virus (HBV) Cells

Antibodies are essential in clearing HBV (hepatitis B virus) and liver cancer infections by targeting and neutralizing pathogens or infected cells. For HBV, antibodies bind to viral particles, preventing them from infecting new cells and marking them for destruction by other immune cells, thus inhibiting replication and spread. In liver cancer, antibodies target and bind to cancer cells, facilitating their destruction by the immune system and potentially interfering with tumor growth. Thus, antibodies enhance the immune system's ability to recognize and eliminate HBV and cancer cells, aiding in the control and resolution of these conditions. In Figure 13, it is apparent that a 25% increase in the rate at which antibodies target and eradicate the hepatitis B virus from the initial value ($\delta_7 = 0.7$ to $\delta_4 = 0.875$) results in

a 22.49% reduction in the HBV population. This indicates that efficiently removing HBV cells responsible for the infection decreases the total number of infected liver cells. Conversely, a 25% decrease in this rate from the initial value ($\delta_4 = 0.7$ to $\delta_3 = 0.525$) leads to a 7.52% increase in the HBV population. This shows that raising the rate at which antibodies eliminate virus cells from the baseline reduces the basic reproduction number ($\mathbb{R}_0$), thereby limiting the transmission of HBV and liver cancer infections.

Further variations in the virus elimination rate by antibodies, such as a 50% increase to $\delta_4 = 1.05$ or a 50% decrease to $\delta_4 = 0.35$, result in 34.36% decreases or 11.73% increases in HBV populations, respectively. Similar patterns are observed when the clearance rate is raised by 75% to $\delta_4 = 1.225$ (leading to a 43.08% decrease in HBV population) or reduced by 75% to $\delta_3 = 0.175$ (causing a 14.01% increase in the virus population). Additionally, we computed the area under the curve (AUC) for various rates of virus elimination by antibodies to evaluate the changes in virus populations over time, with the results detailed in Table 10.

The simulation results shown in Figure 13 underscore the significant role of antibodies in managing the spread of HBV and liver cancer within liver cells and in facilitating their clearance through the immune response.

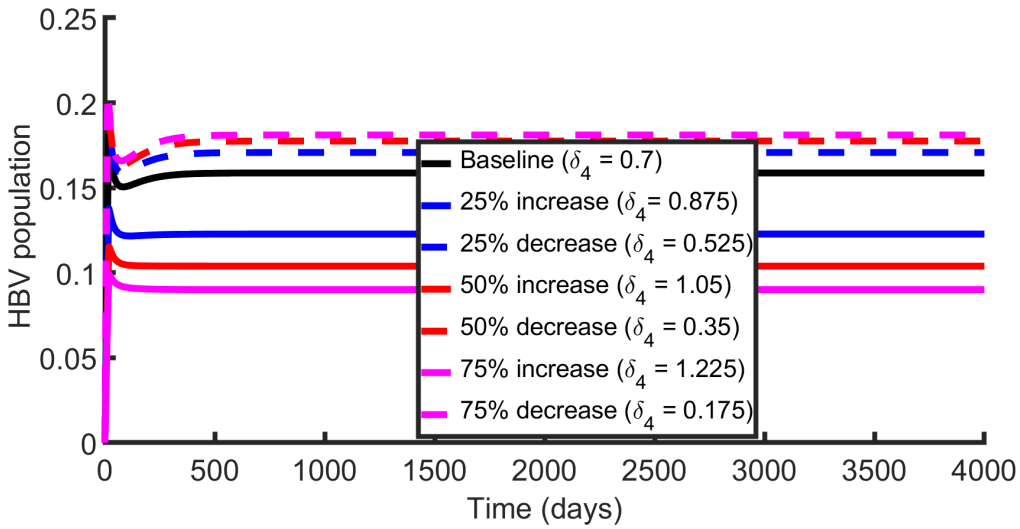

Figure 13: Effects of Antibodies on Hepatitis B Virus Cells (Source: Author's construct, 2023)

Table 10: Effects Antibodies Viral Clearance Rate on HBV Cells

Parameter Value	AUC	PC %
Baseline ($\delta_4 = 0.7$)	632.54	-
25% increase ($\delta_4 = 0.875$)	490.26	-22.49%
25% decrease ($\delta_4 = 0.525$)	680.09	7.52%
50% increase ($\delta_4 = 1.05$)	415.22	-34.36%
50% decrease ($\delta_4 = 0.35$)	706.76	11.73%
75% increase ($\delta_4 = 1.225$)	360.04	-43.08%
75% decrease ($\delta_4 = 0.175$)	721.16	14.01%

Source: Author's construct (2023)

Time to Chronicity

The outcomes of hepatitis B virus (HBV) infection exhibit substantial variability among individuals, highlighting the significance of host genetic determinants in influencing susceptibility to HBV persistence and the progression from hepatic damage to cirrhosis and hepatocellular carcinoma (HCC). An efficacious antiviral response, primarily orchestrated by $CD4^+$ and $CD8^+$ T lymphocytes, natural killer cells, and monocytes, can facilitate immune-mediated containment of HBV replication, potentially culminating in a functional cure. Conversely, in individuals with compromised immune systems, encompassing both pediatric and adult populations, persistent viral replication may persist unabated.

IL-10 predominantly functions as an immunomodulatory cytokine by impeding T cell proliferation and the activity of antigen-presenting cells (APCs), while also modulating the secretion of various cytokines and chemokines (Saraiva & O'garra, 2010). Recently, a specialized subset of IL-10-secreting B cells, termed regulatory B cells (Bregs), has been identified as a modulator of HBV-specific $CD8^+$ T cell responses (Das et al., 2012; Y. Liu et al., 2016). The attenuation of IL-10 has been shown to restore the functionality of exhausted HBV-specific $CD8^+$ T cells (Das et al., 2012). Nevertheless, IL-10 can significantly influence the antiviral immune response by suppressing the production of pro-inflammatory cytokines such as IFN-γ, TNF-α, IL-1β, and IL-6. In chronic HBV infection, there is an elevation in both the quantity of regulatory T cells and the levels of inhibitory cytokines IL-10 and transforming growth factor beta (TGF-β), leading to the exhaustion of HBV-specific

$CD8^+$ T cells and impeding the elimination of the virus from the liver (Peeridogaheh et al., 2018). Consequently, elevated IL-10 expression during chronic viral infections reflects a viral strategy to attenuate the host immune response and facilitate viral persistence (Hyodo et al., 2004; Ohga et al., 2004; Brooks et al., 2006; Kaplan et al., 2008; Brockman et al., 2009).

During the preceding decade, a multitude of researchers have endeavored to utilize mathematical frameworks to predict the advancement of acute hepatitis B infection toward a persistent state and ultimately to hepatic malignancy, a process frequently designated as "chronicity." By employing system 5, our objective is to anticipate the temporal point at which T helper-1 cells (T_1) will surpass cytotoxic T lymphocytes (T_2) in quantity. The aim is to elucidate the determinants that facilitate the transition from the acute phase to a chronic pathological state as the infection progresses. The interval during which T helper-1 (T_1) cells exceed cytotoxic T lymphocytes (T_2) is considered pivotal for the progression from acute infection to chronic disease. In the initial phase of infection within macrophages, the virus generally remains latent while persisting in replication. Within infected macrophages, an ongoing contest ensues between the immune response and the hepatitis B virus. For the infection to evolve into a chronic condition, there must be a commensurate increase in the viral burden. Given the virus's complexity, an elevated viral load constitutes a significant threat to the host, potentially culminating in chronic pathology. Thus, the concept of time to chronicity is employed to ascertain the minimum duration and conditions necessary for T helper-1 (T_1) cells to effectively surpass cytotoxic T lymphocytes (T_2), thereby facilitating the transition of infected macrophages to acute macrophages and ensuring a vigorous immune response. Typically, a diminished transition period correlates with a reduced hepatitis B viral load. In our model, it was apparent that parameters ρ_1, ρ_2, and ρ_3 exert a profound influence on the modulation of transition time and viral load. These parameters are integral to the functions of interferon-alpha and beta, interferon-gamma, and the synthesis of pro-inflammatory cytokines such as IFN-γ, TNF-α, IL-1β, and IL-6. These factors are crucial in the progression from the acute phase of the disease to chronic stages

and potentially to hepatic malignancy. By maintaining all other parameters constant while varying ρ_3, the resultant times to chronicity were observed as follows:

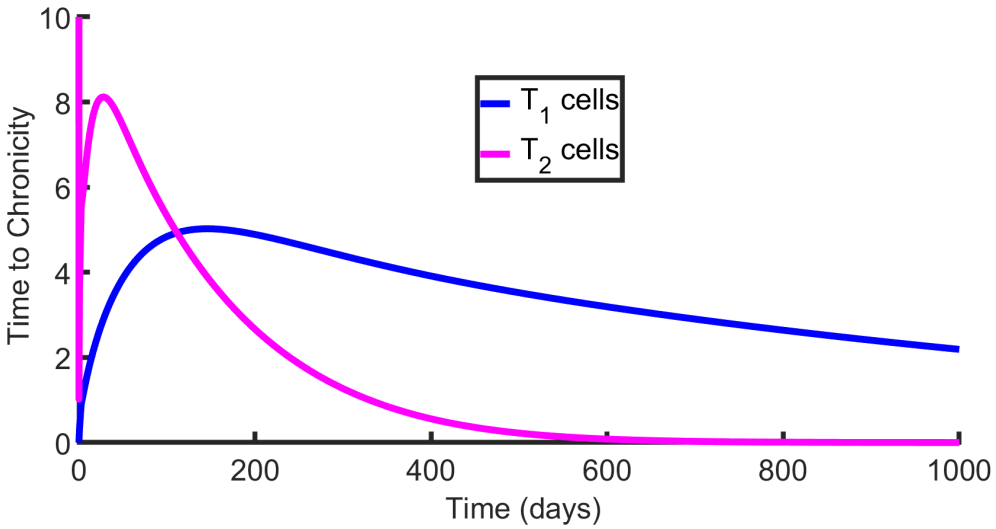

Figure 14: The Graph Represents the Duration to Chronicity at $\rho_3 = 0.6697$ (Source: Author's construct, 2023)

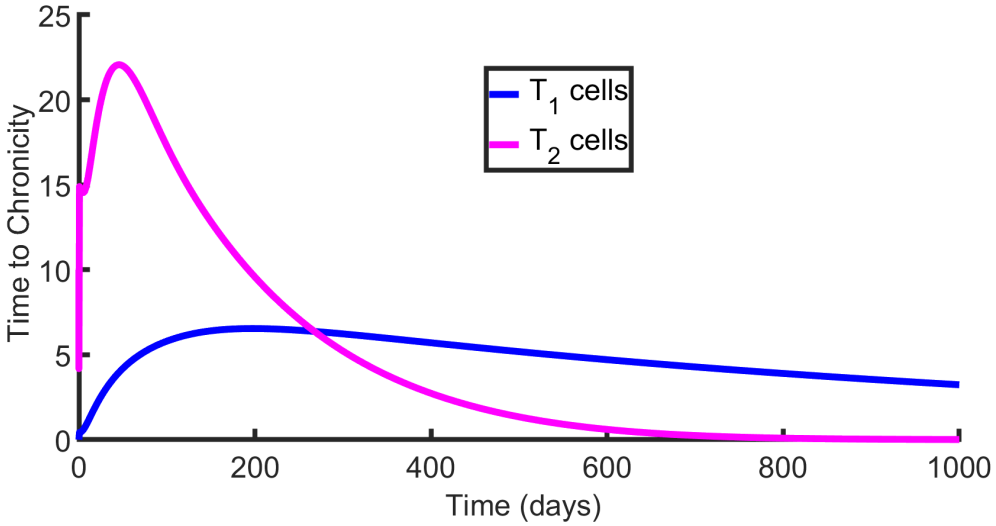

Figure 15: The Graph Represents the Duration to Chronicity at $\rho_3 = 1.0046$ (Source: Author's construct, 2023)

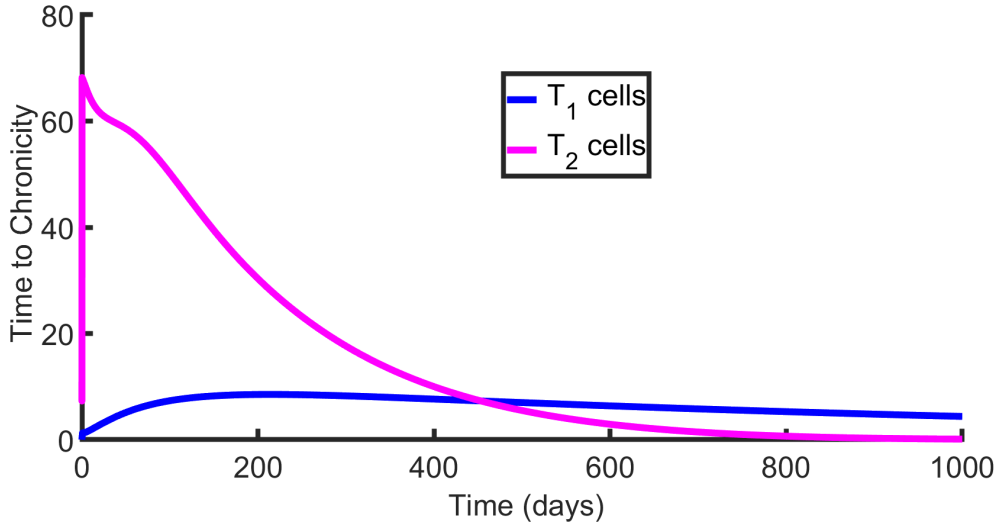

Figure 16: The Graph Represents the Duration to Chronicity at $\rho_3 = 1.1720$ (Source: Author's construct, 2023)

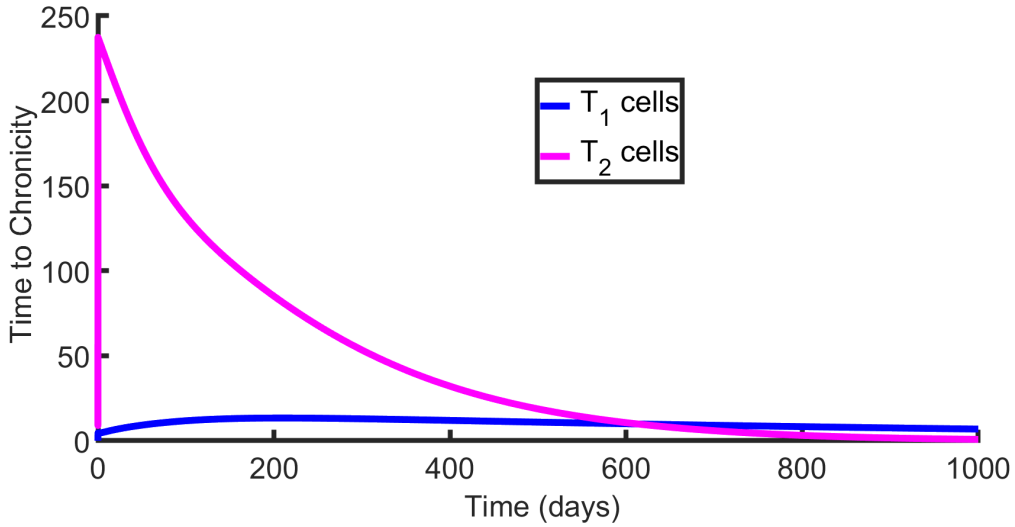

Figure 17: The Graph Represents the Duration to Chronicity at $\rho_3 = 1.3394$ (Source: Author's construct, 2023)

Figures 14, 15, 16, and 17 delineate the diverse time frames to chronicity within the model. Initially, the quantities of cytotoxic T lymphocytes rise during the initial days, but subsequently begin to diminish, eventually being surpassed by the escalating levels of T helper-1 cells. With a parameter value of $\rho_3 = 0.6697$, it was observed that it requires over 100 days (approximately 112 days) for T helper-1 cells to outnumber cytotoxic T lymphocytes. However, when the parameter ρ_3 was modified to $\rho_3 = 1.0046$, $\rho_3 = 1.1720$, and $\rho_3 = 1.3394$, the duration necessary to attain chronicity extended to 266, 457, and 600 days, respectively. This

result is counter-intuitive, as one might anticipate that augmenting the production of interleukin-10 cytokines would generally facilitate infection resolution for a given viral load. Nonetheless, these findings substantiate the hypothesis that sustained antigen exposure from infected cells and elevated antigen concentrations in HBV infections correlate with $CD8^+$ T cell exhaustion (Revill et al., 2019; Fatehi et al., 2022). Biologically, persistent production of interleukin-10 cytokines impedes cytotoxic T lymphocytes (T_2), thereby prolonging the duration to chronicity. A chronicity period of approximately 112 days reflects the early phase following exposure to the core hepatitis B virus (i.e., the acute phase of HBV infection), which is the optimal time frame for the immune system to mount an effective response to the virus.

To enhance our comprehension of how hepatitis B virus (HBV) load dynamics shift as the latency to chronicity extends, we adjust the parameter ω in relation to its association with the temporal span to chronicity and scrutinize the HBV compartment to observe resultant variations. As depicted in Figure 18, we noted that an extension in the duration to chronicity correlates with an elevated viral load. With an ω value of 20.7039, the HBV density is illustrated by the black trajectory on the graph. Augmenting ω to 20.8713, 21.0388, and 21.2062 transitions the virus density representation to the blue, red, and magma curves, respectively. Generally, a reduced time to chronicity is associated with a diminished HBV load. The graph demonstrates that decreasing the ω value from 20.7039 to 20.5365, 20.3691, and 20.2016, indicating a shorter latency to chronicity, results in a lower HBV load as signified by the blue, red, and magma dashed lines. This outcome is expected, given that the model does not incorporate temporal delays in naïve T cell dynamics. The absence of a temporal lag in naïve T cell production implies continuous exposure to elevated antigen concentrations, leading to functional impairment. Consequently, the model suggests that delaying the maturation of naïve T cells into T helper 1 cells influences the determination of the duration to chronicity.

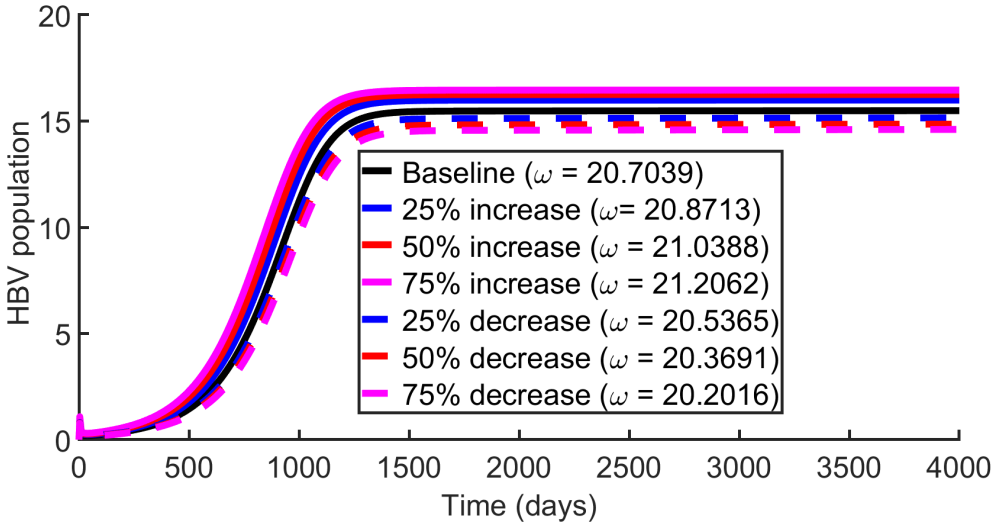

Figure 18: Graph Showing HBV Load Fluctuations Over Time to Chronicity (Source: Author's construct, 2023)

Sensitivity Analysis

The reproduction number $\mathbb{R}_0$ is often affected by uncertainties in data collection and the estimation of parameter values. Sensitivity analysis is conducted to assess the relative importance of each epidemic parameter for the transmission and control of both hepatitis B virus and liver cancer, as well as alterations in the model's structure. The reproduction number $\mathbb{R}_0$ is influenced by parameters such as β_1, β_2, Λ_{M_0}, Λ_{M_1}, ζ, ω, μ_{M_0}, μ_{M_1}, μ_V, μ_{I_M}, ψ, and ε. Effective management of a viral outbreak requires controlling parameter values to achieve $\mathbb{R}_0 < 1$, as these parameters significantly impact the dynamics of virus transmission. Thus, the goal is to determine how $\mathbb{R}_0$ varies with changes in parameter values. The rate of change of $\mathbb{R}_0$ in response to a change in a parameter, referred to as Π, can be estimated using a normalized sensitivity index defined as follows:

Definition 13

The normalized sensitivity index of the reproduction number $\mathbb{R}_0$, depending upon the differentiability with respect to a parameter is given by

$$S_\Pi = \frac{\Pi}{\mathbb{R}_0}\frac{\partial \mathbb{R}_0}{\partial \Pi} \tag{117}$$

The sensitivity of $\mathbb{R}_0$ can be analyzed through sensitivity index calculation.

For this analysis, Eq. (117) was utilized as outlined by (Chitnis et al., 2008; Tilahun et al., 2018; Chataa et al., 2021), yielding the following results.

$$\frac{\partial \mathbb{R}_0}{\partial \beta_1} = \frac{\omega \Lambda_{M_0}}{\mu_{M_0}\left(\omega+\varepsilon+\zeta+\mu_{I_M}\right)\left(\psi+\mu_V\right)} > 0,$$

$$\frac{\partial \mathbb{R}_0}{\partial \beta_2} = \frac{\omega \Lambda_{M_1}}{\mu_{M_1}\left(\omega+\varepsilon+\zeta+\mu_{I_M}\right)\left(\psi+\mu_V\right)} > 0,$$

$$\frac{\partial \mathbb{R}_0}{\partial \Lambda_{M_0}} = \frac{\beta_1 \omega}{\mu_{M_0}\left(\omega+\varepsilon+\zeta+\mu_{I_M}\right)\left(\psi+\mu_V\right)} > 0,$$

$$\frac{\partial \mathbb{R}_0}{\partial \Lambda_{M_1}} = \frac{\beta_2 \omega}{\mu_{M_1}\left(\omega+\varepsilon+\zeta+\mu_{I_M}\right)\left(\psi+\mu_V\right)} > 0,$$

$$\frac{\partial \mathbb{R}_0}{\partial \mu_{M_0}} = -\frac{\beta_1 \omega \Lambda_{M_0}}{\mu_{M_0}^2\left(\omega+\varepsilon+\zeta+\mu_{I_M}\right)\left(\psi+\mu_V\right)} < 0,$$

$$\frac{\partial \mathbb{R}_0}{\partial \mu_{M_1}} = -\frac{\beta_2 \omega \Lambda_{M_1}}{\mu_{M_1}^2\left(\omega+\varepsilon+\zeta+\mu_{I_M}\right)\left(\psi+\mu_V\right)} < 0,$$

$$\frac{\partial \mathbb{R}_0}{\partial \psi} = -\frac{\beta_1 \omega \Lambda_{M_0}\mu_{M_0}\left(\omega+\varepsilon+\zeta+\mu_{I_M}\right)}{\left[\mu_{M_0}\left(\omega+\varepsilon+\zeta+\mu_{I_M}\right)\left(\psi+\mu_V\right)\right]^2} - \frac{\beta_2 \omega \Lambda_{M_1}\mu_{M_1}\left(\omega+\varepsilon+\zeta+\mu_{I_M}\right)}{\left[\mu_{M_1}\left(\omega+\varepsilon+\zeta+\mu_{I_M}\right)\left(\psi+\mu_V\right)\right]^2} < 0,$$

$$\frac{\partial \mathbb{R}_0}{\partial \mu_V} = -\frac{\beta_1 \omega \Lambda_{M_0}\mu_{M_0}\left(\omega+\varepsilon+\zeta+\mu_{I_M}\right)}{\left[\mu_{M_0}\left(\omega+\varepsilon+\zeta+\mu_{I_M}\right)\left(\psi+\mu_V\right)\right]^2} - \frac{\beta_2 \omega \Lambda_{M_1}\mu_{M_1}\left(\omega+\varepsilon+\zeta+\mu_{I_M}\right)}{\left[\mu_{M_1}\left(\omega+\varepsilon+\zeta+\mu_{I_M}\right)\left(\psi+\mu_V\right)\right]^2} < 0,$$

$$\frac{\partial \mathbb{R}_0}{\partial \varepsilon} = -\frac{\beta_1 \omega \Lambda_{M_0}\left(\psi+\mu_V\right)}{\left[\mu_{M_0}\left(\omega+\varepsilon+\zeta+\mu_{I_M}\right)\left(\psi+\mu_V\right)\right]^2} - \frac{\beta_2 \omega \Lambda_{M_1}\left(\psi+\mu_V\right)}{\left[\mu_{M_1}\left(\omega+\varepsilon+\zeta+\mu_{I_M}\right)\left(\psi+\mu_V\right)\right]^2} < 0,$$

$$\frac{\partial \mathbb{R}_0}{\partial \zeta} = -\frac{\beta_1 \omega \Lambda_{M_0} (\psi + \mu_V)}{\left[\mu_{M_0} (\omega + \varepsilon + \zeta + \mu_{I_M}) (\psi + \mu_V)\right]^2} - \frac{\beta_2 \omega \Lambda_{M_1} (\psi + \mu_V)}{\left[\mu_{M_1} (\omega + \varepsilon + \zeta + \mu_{I_M}) (\psi + \mu_V)\right]^2} < 0,$$

$$\frac{\partial \mathbb{R}_0}{\partial \mu_{I_M}} = -\frac{\beta_1 \omega \Lambda_{M_0} (\psi + \mu_V)}{\left[\mu_{M_0} (\omega + \varepsilon + \zeta + \mu_{I_M}) (\psi + \mu_V)\right]^2} - \frac{\beta_2 \omega \Lambda_{M_1} (\psi + \mu_V)}{\left[\mu_{M_1} (\omega + \varepsilon + \zeta + \mu_{I_M}) (\psi + \mu_V)\right]^2} < 0,$$

$$\frac{\partial \mathbb{R}_0}{\partial \omega} = \frac{\left(\frac{\beta_1 \Lambda_{M_0}}{\mu_{M_0}} + \frac{\beta_2 \Lambda_{M_1}}{\mu_{M_1}}\right) (\varepsilon + \zeta + \mu_{I_M})}{(\omega + \varepsilon + \zeta + \mu_{I_M})^2 (\psi + \mu_V)} > 0.$$

Furthermore, Latin Hypercube Sampling (LHS) and Partial Rank Correlation Coefficients (PRCC) are employed numerically to pinpoint which parameters of the model have the most significant impact, using the reproduction number $(\mathbb{R}_0)$ as the response variable. The purpose of this analysis is to assess how parameters influence the results of the model. Parameters that demonstrate high sensitivity need to be estimated with greater accuracy, as even minor changes in these parameters can lead to considerable differences in the outcomes (Cariboni et al., 2007; Blower & Dowlatabadi, 1994; Iboi & Gumel, 2018). Conversely, parameters with lower sensitivity require less precise estimation, as small variations in these parameters have minimal impact on the response (Blower & Dowlatabadi, 1994).

Parameters with PRCC values above $+0.50$ are regarded as having a strong positive correlation with the response variable, while those with values below -0.50 are seen as having a strong negative correlation with the response variable (Cariboni et al., 2007; Blower & Dowlatabadi, 1994; Iboi & Gumel, 2018). The PRCC analysis encompasses various factors: the interaction rates between V and M_0 (β_1) and between V and M_1 (β_2), the supply rates of uninfected macrophages without cancer (Λ_{M_0}) and with cancer (Λ_{M_1}), the rate at which infected macrophages transition to liver cancer (ζ), the replication rate of new infectious virions (ω), the decay rates of uninfected macrophages without cancer (μ_{M_0}) and with cancer (μ_{M_1}), the virus decay rate (μ_V), the decay rate of infected macrophages (μ_{I_M}), the virus lytic effect

rate for antibody release (ψ), and the lytic effect rate of infected macrophages for releasing interferon alpha and beta cytokines (ε).

Although the PRCC analysis was conducted across five different periods, the parameters showed consistent effects on the dependent variable throughout all periods. Therefore, we chose to present a single plot from the final time point of the analysis, as depicted in Figure 19, and summarized the results in Table 11. The results indicate that the twelve parameters most significantly impacting the response variable $(\mathbb{R}_0)$ are β_1, β_2, Λ_{M_0}, Λ_{M_1}, ζ, ω, μ_{M_0}, μ_{M_1}, μ_V, μ_{I_M}, ψ, and ε. According to the PRCC values, parameters β_1, β_2, Λ_{M_0}, Λ_{M_1}, and ω positively affect $(\mathbb{R}_0)$, meaning that an increase (or decrease) in these parameters will result in a rise (or fall) in $(\mathbb{R}_0)$. Conversely, parameters ζ, μ_{M_0}, μ_{M_1}, μ_V, μ_{I_M}, ψ, and ε have a negative impact on $(\mathbb{R}_0)$, with increases in these parameters leading to a decrease in $(\mathbb{R}_0)$.

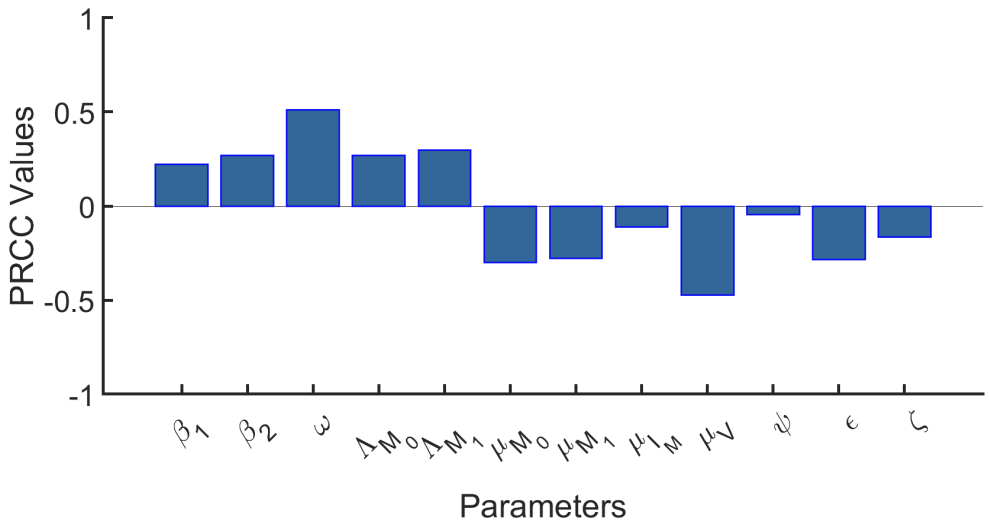

Figure 19: Partial Rank Correlation Coefficients Demonstrating the Effect of Twelve Model Parameters on the Basic Reproduction Number $(\mathbb{R}_0)$ of the Model Framework (Source: Author's construct, 2023)

Table 11: Parameters and their Relationship With $\mathbb{R}_0$

Parameter	Sensitivity Index (SI)	Parameter	Sensitivity Index (SI)
Λ_{M_0}	+ 0.1854	μ_V	- 0.5145
Λ_{M_1}	+ 0.2282	β_1	+ 0.2253
μ_{I_M}	- 0.0487	β_2	+ 0.2850
μ_{M_0}	- 0.2608	ε	- 0.2886
μ_{M_1}	-0.2850	ζ	- 0.1390
ψ	-0.0060	ω	+ 0.5038

Source: Author's construct (2023)

The sensitivity analysis highlights that the most influential parameters on the reproduction number $\mathbb{R}_0$ are the new virion replication rate ω and the HBV decay rate μ_V, both of which play critical roles in the dynamics of HBV transmission. The high sensitivity of these parameters indicates that even small changes in their values can have significant effects on the spread of HBV. As such, future research should prioritize efforts to better understand and target these parameters, particularly in the context of antiviral treatments, to reduce viral replication and enhance the control of HBV transmission. Investigating strategies that could lower these rates such as developing more effective antiviral drugs or therapeutic interventions could provide key insights for improving treatment outcomes and preventing the further spread of the virus.

Numerical Simulation of Fractional-order Model

Fractional-order models extend traditional integer-order differential equations by incorporating derivatives of non-integer order. These models can capture complex dynamic behaviors and memory effects in various systems, making them particularly useful in fields like epidemiology, control systems, and physics. The primary goal of numerical simulation for fractional-order models is to approximate the solutions of differential equations that involve fractional derivatives. This allows researchers to analyze system dynamics, predict behavior, and validate theoretical models. Thus, this study employed the parameter values in Tables 12 and 13 for numerical simulations.

Numerical Scheme

In this section, the iterative method was use to find the approximate solution to the proposed hepatitis B virus and liver cancer co-existence model system 39 in ABC sense since it is implausible to determine the exact solution of the model and then perform numerical simulations for various values of arbitrary order $\varphi \in (0, 1]$.

Iterative Method

To effectively find the approximate solution of system 39 using the iterative method, the numerical scheme developed in recent literature (see (Diethelm & Ford, 2002) and (Gnitchogna Batogna & Atangana, 2017)) is applied. To proceed further, system 39 is expressed in a compact form as follows:

$$\begin{cases} {}_0^{ABC}\mathbb{D}_t^{\varphi} y(t) & = g\left(t, y(t)\right), \\ y(0) & = y_0, \quad 0 < t < T < \infty, \end{cases} \tag{118}$$

where, $y = (T_0, T_1, T_2, M_0, M_1, I_M, V, A, E, N_K, I_{10}, F_1, F_2) \in \Re^{13}$ denotes continuous real valued vector function satisfying Lipschitz condition and y_0 denotes the corresponding initial state vector. Taking the ABC integral on both sides of Eq. (118), we arrived at the following results:

$$\begin{aligned} y(t) - y(0) &= \frac{1-\varphi}{G(\varphi)} g\left(t, y(t)\right) \\ &\quad + \frac{\varphi}{G(\varphi)\Gamma(\varphi)} \int_0^t (t-\theta)^{\varphi-1} g\left(\theta, y(\theta)\right) d\theta. \end{aligned} \tag{119}$$

Now, an approximate solution is proposed by considering approximation at the points $t = t_n$ and $t = t_{n+1}$. Consequently, at $t = t_{n+1}$, $n = 0, 1, 2, \cdots$, we have

$$\begin{aligned} y(t_{n+1}) - y(0) &= \frac{1-\varphi}{G(\varphi)} g\left(t_n, y_n\right) \\ &\quad + \frac{\varphi}{G(\varphi)\Gamma(\varphi)} \int_0^{t_{n+1}} (t_{n+1}-t)^{\varphi-1} g\left(t, y(t)\right) dt. \end{aligned} \tag{120}$$

Similarly, at $t = t_n$, where $n = 0, 1, 2, \cdots$, the following expression was obtained

$$\begin{aligned} y(t_n) - y(0) &= \frac{1-\varphi}{G(\varphi)} g\left(t_{n-1}, y_{n-1}\right) \\ &+ \frac{\varphi}{G(\varphi)\Gamma(\varphi)} \int_0^{t_n} (t_n - t)^{\varphi-1} g\left(t, y(t)\right) dt. \end{aligned} \tag{121}$$

Subtracting Eq. (121) from Eq. (120), lead to the following:

$$\begin{aligned} y(t_{n+1}) - y(t_n) &= \frac{1-\varphi}{G(\varphi)} \left[g\left(t_n, y_n\right) - g\left(t_{n-1}, y_{n-1}\right)\right] \\ &+ \frac{\varphi}{G(\varphi)\Gamma(\varphi)} \int_0^{t_{n+1}} (t_{n+1} - t)^{\varphi-1} g\left(t, y(t)\right) dt \\ &- \frac{\varphi}{G(\varphi)\Gamma(\varphi)} \int_0^{t_n} (t_n - t)^{\varphi-1} g\left(t, y(t)\right) dt. \end{aligned} \tag{122}$$

Hence,

$$\begin{aligned} y(t_{n+1}) - y(t_n) &= \frac{1-\varphi}{G(\varphi)} \left[g\left(t_n, y_n\right) - g\left(t_{n-1}, y_{n-1}\right)\right] \\ &+ \mathbb{B}_{\varphi,1} - \mathbb{B}_{\varphi,2}, \end{aligned} \tag{123}$$

where

$$\begin{aligned} \mathbb{B}_{\varphi,1} &= \frac{\varphi}{G(\varphi)\Gamma(\varphi)} \int_0^{t_{n+1}} (t_{n+1} - t)^{\varphi-1} g\left(t, y(t)\right) dt \\ \mathbb{B}_{\varphi,2} &= \frac{\varphi}{G(\varphi)\Gamma(\varphi)} \int_0^{t_n} (t_n - t)^{\varphi-1} g\left(t, y(t)\right) dt. \end{aligned}$$

Let us consider

$$\mathbb{B}_{\varphi,1} = \frac{\varphi}{G(\varphi)\Gamma(\varphi)} \int_0^{t_{n+1}} (t_{n+1} - t)^{\varphi-1} g\left(t, y(t)\right) dt. \tag{124}$$

The proposed method is of order 2; therefore, taking the Lagrange interpolation with two interpolating functions of y_n, y_{n-1} are required to evaluate the approximate solutions as follows:

$$p(t) \cong g(t, y(t)) = \frac{t - t_{n-1}}{t_n - t_{n-1}} g(t_n, y_n) + \frac{t - t_{n-1}}{t_{n-1} - t_n} g(t_{n-1}, y_{n-1}). \tag{125}$$

Substituting Eq. (125) into Eq. (124) leads to

$$\begin{aligned}\mathbb{B}_{\varphi,1} &= \frac{\varphi}{G(\varphi)\Gamma(\varphi)}\int_0^{t_{n+1}}(t_{n+1}-t)^{\varphi-1}\left\{\frac{t-t_{n-1}}{\hbar}g\left(t_n,y_n\right)\right.\\ &\left.-\frac{t-t_n}{\hbar}g\left(t_{n-1},y_{n-1}\right)\right\}dt. \end{aligned} \tag{126}$$

Further simplification of Eq. (126) leads to

$$\begin{aligned}\mathbb{B}_{\varphi,1} &= \frac{\varphi g\left(t_n,y_n\right)}{G(\varphi)\Gamma(\varphi)\hbar}\left[\int_0^{t_{n+1}}(t_{n+1}-t)^{\varphi-1}\left(t-t_{n-1}\right)\right]dt\\ &-\frac{\varphi g\left(t_{n-1},y_{n-1}\right)}{G(\varphi)\Gamma(\varphi)\hbar}\left[\int_0^{t_{n+1}}(t_{n+1}-t)^{\varphi-1}\left(t-t_{n-1}\right)\right]dt. \end{aligned} \tag{127}$$

Following Eq. (127) and without loss of generality;

$$\begin{aligned}\mathbb{B}_{\varphi,1} &= \frac{\varphi g\left(t_n,y_n\right)}{G(\varphi)\Gamma(\varphi)\hbar}\left(\frac{2\hbar t_{n+1}^{\varphi}}{\varphi}-\frac{t_{n+1}^{\varphi+1}}{\varphi+1}\right)\\ &-\frac{\varphi g\left(t_{n-1},y_{n-1}\right)}{G(\varphi)\Gamma(\varphi)\hbar}\left(\frac{\hbar t^{\varphi}}{\varphi}-\frac{t_{n+1}^{\varphi+1}}{\varphi+1}\right), \end{aligned} \tag{128}$$

where $\hbar = t_{n+1}-t_n$. Similarly, the expression can be written as follows

$$\mathbb{B}_{\varphi,2} = \frac{\varphi g\left(t_n,y_n\right)}{G(\varphi)\Gamma(\varphi)\hbar}\left(\frac{2\hbar t_{n+1}^{\varphi}}{\varphi}-\frac{t_{n+1}^{\varphi+1}}{\varphi+1}\right)-\frac{\varphi g\left(t_{n-1},y_{n-1}\right)}{G(\varphi)\Gamma(\varphi)\hbar}. \tag{129}$$

Finally,

$$\begin{aligned}y_{n+1} &= y_n+g\left(t_n,y_n\right)\left\{\frac{1-\varphi}{G(\varphi)}+\frac{\varphi}{G(\varphi)\hbar}\left(\frac{2\hbar t_{n+1}^{\varphi}}{\varphi}-\frac{t_{n+1}^{\varphi+1}}{\varphi+1}\right)\right.\\ &\left.-\frac{\varphi}{G(\varphi)\Gamma(\varphi)\hbar}\left(\frac{\hbar t_{n+1}^{\varphi}}{\varphi}-\frac{t_{n+1}^{\varphi+1}}{\varphi+1}\right)\right\}\\ &+g\left(t_{n-1},y_{n-1}\right)\left\{\frac{1-\varphi}{G(\varphi)}-\frac{\varphi}{G(\varphi)\Gamma(\varphi)\hbar}\right.\\ &\left.\times\left(\frac{\hbar t_{n+1}^{\varphi}}{\varphi}-\frac{t_{n+1}^{\varphi+1}}{\varphi+1}+\frac{t^{\varphi+1}}{G(\varphi)\Gamma(\varphi)\hbar}\right)\right\}+R_{\varphi}, \end{aligned} \tag{130}$$

where $||R_{\varphi}||_{\infty} < M$. Eq. (130) is known as the two-step Adams-Bashforth technique for fractional derivative in the sense of Caputo.

Theorem 13

Suppose $y(t)$ *is the solution for* ${}_0^{ABC}\mathbb{D}_t^{\varphi} y(t) = g\left(t, y(t)\right)$*, where* g *is bounded and continuous. The numerical solution of* $y(t)$ *is given as*

$$\begin{aligned} y_{n+1} &= y_n + g\left(t_n, y_n\right)\left\{\frac{1-\varphi}{G(\varphi)} + \frac{\varphi}{G(\varphi)\hbar}\left(\frac{2\hbar t_{n+1}^{\varphi}}{\varphi} - \frac{t_{n+1}^{\varphi+1}}{\varphi+1}\right)\right. \\ &\quad \left. - \frac{\varphi}{G(\varphi)\Gamma(\varphi)\hbar}\left(\frac{\hbar t_{n+1}^{\varphi}}{\varphi} - \frac{t_{n+1}^{\varphi+1}}{\varphi+1}\right)\right\} \\ &\quad + g\left(t_{n-1}, y_{n-1}\right)\left\{\frac{1-\varphi}{G(\varphi)} - \frac{\varphi}{G(\varphi)\Gamma(\varphi)\hbar}\right. \\ &\quad \left. \times \left(\frac{\hbar t_{n+1}^{\varphi}}{\varphi} - \frac{t_{n+1}^{\varphi+1}}{\varphi+1} + \frac{t^{\varphi+1}}{G(\varphi)\Gamma(\varphi)\hbar}\right)\right\} + R_{\varphi}, \end{aligned} \tag{131}$$

where $||R_{\varphi}||_{\infty} < M$.

Numerical Scheme of the Fractional Model System

The fractional hepatitis B virus and liver cancer co-existence system under the ABC fractional derivative was presented in Eq. (39), and the values for Φ_i, where

$i = 1, 2, \ldots, 13$, was obtained. Thus,

$$
\begin{aligned}
T_0(t) - T_0(0) &= \frac{1-\varphi}{G(\varphi)}\Phi_1\left(t, T_0(t)\right) \\
&\quad + \frac{\varphi}{G(\varphi)\Gamma(\varphi)}\int_0^t (t-\Theta)^{\varphi-1}\Phi_1\left(\Theta, T_0(\Theta)\right)d\Theta, \\
T_1(t) - T_1(0) &= \frac{1-\varphi}{G(\varphi)}\Phi_2\left(t, T_1(t)\right) \\
&\quad + \frac{\varphi}{G(\varphi)\Gamma(\varphi)}\int_0^t (t-\Theta)^{\varphi-1}\Phi_2\left(\Theta, T_1(\Theta)\right)d\Theta, \\
T_2(t) - T_2(0) &= \frac{1-\varphi}{G(\varphi)}\Phi_3\left(t, T_2(t)\right) \\
&\quad + \frac{\varphi}{G(\varphi)\Gamma(\varphi)}\int_0^t (t-\Theta)^{\varphi-1}\Phi_3\left(\Theta, T_2(\Theta)\right)d\Theta, \\
M_0(t) - M_0(0) &= \frac{1-\varphi}{G(\varphi)}\Phi_4\left(t, M_0(t)\right) \\
&\quad + \frac{\varphi}{G(\varphi)\Gamma(\varphi)}\int_0^t (t-\Theta)^{\varphi-1}\Phi_4\left(\Theta, M_0(\Theta)\right)d\Theta, \\
M_1(t) - M_1(0) &= \frac{1-\varphi}{G(\varphi)}\Phi_5\left(t, M_1(t)\right) \\
&\quad + \frac{\varphi}{G(\varphi)\Gamma(\varphi)}\int_0^t (t-\Theta)^{\varphi-1}\Phi_5\left(\Theta, M_1(\Theta)\right)d\Theta, \\
I_M(t) - I_M(0) &= \frac{1-\varphi}{G(\varphi)}\Phi_6\left(t, I_M(t)\right) \\
&\quad + \frac{\varphi}{G(\varphi)\Gamma(\varphi)}\int_0^t (t-\Theta)^{\varphi-1}\Phi_6\left(\Theta, I_M(\Theta)\right)d\Theta, \\
V(t) - V(0) &= \frac{1-\varphi}{G(\varphi)}\Phi_7\left(t, V(t)\right) \\
&\quad + \frac{\varphi}{G(\varphi)\Gamma(\varphi)}\int_0^t (t-\Theta)^{\varphi-1}\Phi_7\left(\Theta, V(\Theta)\right)d\Theta, \\
A(t) - A(0) &= \frac{1-\varphi}{G(\varphi)}\Phi_8\left(t, A(t)\right) \\
&\quad + \frac{\varphi}{G(\varphi)\Gamma(\varphi)}\int_0^t (t-\Theta)^{\varphi-1}\Phi_8\left(\Theta, A(\Theta)\right)d\Theta,
\end{aligned}
\tag{132}
$$

$$
\begin{aligned}
E(t)-E(0) &= \frac{1-\varphi}{G(\varphi)}\Phi_9\left(t,E(t)\right) \\
&\quad +\frac{\varphi}{G(\varphi)\Gamma(\varphi)}\int_0^t (t-\Theta)^{\varphi-1}\Phi_9\left(\Theta,E(\Theta)\right)d\Theta, \\
N_K(t)-N_K(0) &= \frac{1-\varphi}{G(\varphi)}\Phi_{10}\left(t,N_K(t)\right) \\
&\quad +\frac{\varphi}{G(\varphi)\Gamma(\varphi)}\int_0^t (t-\Theta)^{\varphi-1}\Phi_{10}\left(\Theta,N_K(\Theta)\right)d\Theta, \\
I_{10}(t)-I_{10}(0) &= \frac{1-\varphi}{G(\varphi)}\Phi_{11}\left(t,I_{10}(t)\right) \\
&\quad +\frac{\varphi}{G(\varphi)\Gamma(\varphi)}\int_0^t (t-\Theta)^{\varphi-1}\Phi_{11}\left(\Theta,I_{10}(\Theta)\right)d\Theta, \\
F_1(t)-F_1(0) &= \frac{1-\varphi}{G(\varphi)}\Phi_{12}\left(t,F_1(t)\right) \\
&\quad +\frac{\varphi}{G(\varphi)\Gamma(\varphi)}\int_0^t (t-\Theta)^{\varphi-1}\Phi_{12}\left(\Theta,F_1(\Theta)\right)d\Theta, \\
F_2(t)-F_2(0) &= \frac{1-\varphi}{G(\varphi)}\Phi_{13}\left(t,F_2(t)\right) \\
&\quad +\frac{\varphi}{G(\varphi)\Gamma(\varphi)}\int_0^t (t-\Theta)^{\varphi-1}\Phi_{13}\left(\Theta,F_2(\Theta)\right)d\Theta.
\end{aligned}
\tag{133}
$$

Thus t_{n+1} lead to

$$
\begin{aligned}
T_{0_{n+1}}(t)-T_0(0) &= \frac{1-\varphi}{G(\varphi)}\Phi_1\left(t_n,T_{0_n}(t)\right) \\
&\quad +\frac{\varphi}{G(\varphi)\Gamma(\varphi)}\int_0^{t_{n+1}} (t_{n+1}-t)^{\varphi-1}\Phi_1\left(t,T_0(t)\right)dt, \\
T_{1_{n+1}}(t)-T_1(0) &= \frac{1-\varphi}{G(\varphi)}\Phi_2\left(t_n,T_{1_n}(t)\right) \\
&\quad +\frac{\varphi}{G(\varphi)\Gamma(\varphi)}\int_0^{t_{n+1}} (t_{n+1}-t)^{\varphi-1}\Phi_2\left(t,T_1(t)\right)dt, \\
T_{2_{n+1}}(t)-T_2(0) &= \frac{1-\varphi}{G(\varphi)}\Phi_3\left(t_n,T_{2_n}(t)\right) \\
&\quad +\frac{\varphi}{G(\varphi)\Gamma(\varphi)}\int_0^{t_{n+1}} (t_{n+1}-t)^{\varphi-1}\Phi_3\left(t,T_2(t)\right)dt, \\
M_{0_{n+1}}(t)-M_0(0) &= \frac{1-\varphi}{G(\varphi)}\Phi_4\left(t_n,M_{0_n}(t)\right) \\
&\quad +\frac{\varphi}{G(\varphi)\Gamma(\varphi)}\int_0^{t_{n+1}} (t_{n+1}-t)^{\varphi-1}\Phi_4\left(t,M_0(t)\right)dt,
\end{aligned}
\tag{134}
$$

$$
\begin{aligned}
M_{1_{n+1}}(t) - M_1(0) &= \frac{1-\varphi}{G(\varphi)}\Phi_5\left(t_n, M_{1_n}(t)\right) \\
&\quad + \frac{\varphi}{G(\varphi)\Gamma(\varphi)}\int_0^{t_{n+1}} (t_{n+1}-t)^{\varphi-1}\,\Phi_5\left(t, M_1(t)\right)dt, \\
I_{M_{n+1}}(t) - I_M(0) &= \frac{1-\varphi}{G(\varphi)}\Phi_6\left(t_n, I_{M_n}(t)\right) \\
&\quad + \frac{\varphi}{G(\varphi)\Gamma(\varphi)}\int_0^{t_{n+1}} (t_{n+1}-t)^{\varphi-1}\,\Phi_6\left(t, I_M(t)\right)dt, \\
V_{n+1}(t) - V(0) &= \frac{1-\varphi}{G(\varphi)}\Phi_7\left(t_n, V_n(t)\right) \\
&\quad + \frac{\varphi}{G(\varphi)\Gamma(\varphi)}\int_0^{t_{n+1}} (t_{n+1}-t)^{\varphi-1}\,\Phi_7\left(t, V(t)\right)dt, \\
A_{n+1}(t) - A(0) &= \frac{1-\varphi}{G(\varphi)}\Phi_8\left(t_n, A_n(t)\right) \\
&\quad + \frac{\varphi}{G(\varphi)\Gamma(\varphi)}\int_0^{t_{n+1}} (t_{n+1}-t)^{\varphi-1}\,\Phi_8\left(t, A(t)\right)dt, \\
E_{n+1}(t) - E(0) &= \frac{1-\varphi}{G(\varphi)}\Phi_9\left(t_n, E_n(t)\right) \\
&\quad + \frac{\varphi}{G(\varphi)\Gamma(\varphi)}\int_0^{t_{n+1}} (t_{n+1}-t)^{\varphi-1}\,\Phi_9\left(t, E(t)\right)dt, \\
N_{K_{n+1}}(t) - N_K(0) &= \frac{1-\varphi}{G(\varphi)}\Phi_{10}\left(t_n, N_{K_n}(t)\right) \\
&\quad + \frac{\varphi}{G(\varphi)\Gamma(\varphi)}\int_0^{t_{n+1}} (t_{n+1}-t)^{\varphi-1}\,\Phi_{10}\left(t, N_K(t)\right)dt, \\
I_{10_{n+1}}(t) - I_{10}(0) &= \frac{1-\varphi}{G(\varphi)}\Phi_{11}\left(t_n, I_{10_n}(t)\right) \qquad (135) \\
&\quad + \frac{\varphi}{G(\varphi)\Gamma(\varphi)}\int_0^{t_{n+1}} (t_{n+1}-t)^{\varphi-1}\,\Phi_{11}\left(t, I_{10}(t)\right)dt, \\
F_{1_{n+1}}(t) - F_1(0) &= \frac{1-\varphi}{G(\varphi)}\Phi_{12}\left(t_n, F_{1_n}(t)\right) \\
&\quad + \frac{\varphi}{G(\varphi)\Gamma(\varphi)}\int_0^{t_{n+1}} (t_{n+1}-t)^{\varphi-1}\,\Phi_{12}\left(t, F_1(t)\right)dt, \\
F_{2_{n+1}}(t) - F_2(0) &= \frac{1-\varphi}{G(\varphi)}\Phi_{13}\left(t_n, F_{2_n}(t)\right) \\
&\quad + \frac{\varphi}{G(\varphi)\Gamma(\varphi)}\int_0^{t_{n+1}} (t_{n+1}-t)^{\varphi-1}\,\Phi_{13}\left(t, F_1(t)\right)dt.
\end{aligned}
$$

For t_n, the following expression holds

$$
\begin{aligned}
T_{0_n}(t) - T_0(0) &= \frac{1-\varphi}{G(\varphi)}\Phi_1\left(t_{n-1}, T_{0_{n-1}}(t)\right) \\
&\quad + \frac{\varphi}{G(\varphi)\Gamma(\varphi)}\int_0^{t_n}(t_n - t)^{\varphi-1}\,\Phi_1\left(t, T_0(t)\right)dt, \\
T_{1_n}(t) - T_1(0) &= \frac{1-\varphi}{G(\varphi)}\Phi_2\left(t_{n-1}, T_{1_{n-1}}(t)\right) \\
&\quad + \frac{\varphi}{G(\varphi)\Gamma(\varphi)}\int_0^{t_n}(t_n - t)^{\varphi-1}\,\Phi_2\left(t, T_1(t)\right)dt, \\
T_{2_n}(t) - T_2(0) &= \frac{1-\varphi}{G(\varphi)}\Phi_3\left(t_{n-1}, T_{2_{n-1}}(t)\right) \\
&\quad + \frac{\varphi}{G(\varphi)\Gamma(\varphi)}\int_0^{t_n}(t_n - t)^{\varphi-1}\,\Phi_3\left(t, T_2(t)\right)dt, \\
M_{0_n}(t) - M_0(0) &= \frac{1-\varphi}{G(\varphi)}\Phi_4\left(t_{n-1}, M_{0_{n-1}}(t)\right) \\
&\quad + \frac{\varphi}{G(\varphi)\Gamma(\varphi)}\int_0^{t_n}(t_n - t)^{\varphi-1}\,\Phi_4\left(t, M_0(t)\right)dt, \\
M_{1_n}(t) - M_1(0) &= \frac{1-\varphi}{G(\varphi)}\Phi_5\left(t_{n-1}, M_{1_{n-1}}(t)\right) \\
&\quad + \frac{\varphi}{G(\varphi)\Gamma(\varphi)}\int_0^{t_n}(t_n - t)^{\varphi-1}\,\Phi_5\left(t, M_1(t)\right)dt, \\
I_{M_n}(t) - I_M(0) &= \frac{1-\varphi}{G(\varphi)}\Phi_6\left(t_{n-1}, I_{M_{n-1}}(t)\right) \\
&\quad + \frac{\varphi}{G(\varphi)\Gamma(\varphi)}\int_0^{t_n}(t_n - t)^{\varphi-1}\,\Phi_6\left(t, I_M(t)\right)dt, \\
V_n(t) - V(0) &= \frac{1-\varphi}{G(\varphi)}\Phi_7\left(t_{n-1}, V_{n-1}(t)\right) \\
&\quad + \frac{\varphi}{G(\varphi)\Gamma(\varphi)}\int_0^{t_n}(t_n - t)^{\varphi-1}\,\Phi_7\left(t, V(t)\right)dt, \\
A_n(t) - A(0) &= \frac{1-\varphi}{G(\varphi)}\Phi_8\left(t_{n-1}, A_{n-1}(t)\right) \\
&\quad + \frac{\varphi}{G(\varphi)\Gamma(\varphi)}\int_0^{t_n}(t_n - t)^{\varphi-1}\,\Phi_8\left(t, A(t)\right)dt, \\
E_n(t) - E(0) &= \frac{1-\varphi}{G(\varphi)}\Phi_9\left(t_{n-1}, E_{n-1}(t)\right) \\
&\quad + \frac{\varphi}{G(\varphi)\Gamma(\varphi)}\int_0^{t_n}(t_n - t)^{\varphi-1}\,\Phi_9\left(t, E(t)\right)dt, \\
N_{K_n}(t) - N_K(0) &= \frac{1-\varphi}{G(\varphi)}\Phi_{10}\left(t_{n-1}, N_{K_{n-1}}(t)\right) \\
&\quad + \frac{\varphi}{G(\varphi)\Gamma(\varphi)}\int_0^{t_n}(t_n - t)^{\varphi-1}\,\Phi_{10}\left(t, N_K(t)\right)dt,
\end{aligned}
\tag{136}
$$

$$
\begin{aligned}
I_{10_n}(t) - I_{10}(0) &= \frac{1-\varphi}{G(\varphi)}\Phi_{11}\left(t_{n-1}, I_{10_{n-1}}(t)\right) \\
&\quad + \frac{\varphi}{G(\varphi)\Gamma(\varphi)}\int_0^{t_n}(t_n - t)^{\varphi-1}\,\Phi_{11}\left(t, I_{10}(t)\right)dt, \\
F_{1_n}(t) - F_1(0) &= \frac{1-\varphi}{G(\varphi)}\Phi_{12}\left(t_{n-1}, F_{1_{n-1}}(t)\right) \\
&\quad + \frac{\varphi}{G(\varphi)\Gamma(\varphi)}\int_0^{t_n}(t_n - t)^{\varphi-1}\,\Phi_{12}\left(t, F_1(t)\right)dt, \\
F_{2_n}(t) - F_2(0) &= \frac{1-\varphi}{G(\varphi)}\Phi_{13}\left(t_{n-1}, F_{2_{n-1}}(t)\right) \\
&\quad + \frac{\varphi}{G(\varphi)\Gamma(\varphi)}\int_0^{t_n}(t_n - t)^{\varphi-1}\,\Phi_{13}\left(t, F_1(t)\right)dt.
\end{aligned} \tag{137}
$$

Upon subtracting Eq. (136) from Eq. (134) and Eq. (137) from Eq. (135), it leads to Eq. (138), Eq. (139) and Eq. (140) below.

$$
\begin{aligned}
T_{0_{n+1}}(t) - T_{0_n}(t) &= \frac{1-\varphi}{G(\varphi)}\left[\Phi_1\left(t_n, T_{0_n(t)}\right) - \Phi_1\left(t_{n-1}, T_{0_{n-1}(t)}\right)\right] \\
&\quad + \frac{\varphi}{G(\varphi)\Gamma(\varphi)}\int_0^{t_{n+1}}(t_{n+1} - t)^{\varphi-1}\,\Phi_1\left(t, T_0(t)\right)dt \\
&\quad - \frac{\varphi}{G(\varphi)\Gamma(\varphi)}\int_0^{t_{n+1}}(t_{n+1} - 1)^{\varphi-1}\,\Phi_1\left(t, T_0(t)\right)dt, \\
T_{1_{n+1}}(t) - T_{1_n}(t) &= \frac{1-\varphi}{G(\varphi)}\left[\Phi_2\left(t_n, T_{1_n(t)}\right) - \Phi_2\left(t_{n-1}, T_{1_{n-1}(t)}\right)\right] \\
&\quad + \frac{\varphi}{G(\varphi)\Gamma(\varphi)}\int_0^{t_{n+1}}(t_{n+1} - t)^{\varphi-1}\,\Phi_2\left(t, T_1(t)\right)dt \\
&\quad - \frac{\varphi}{G(\varphi)\Gamma(\varphi)}\int_0^{t_{n+1}}(t_{n+1} - 1)^{\varphi-1}\,\Phi_2\left(t, T_1(t)\right)dt, \\
T_{2_{n+1}}(t) - T_{2_n}(t) &= \frac{1-\varphi}{G(\varphi)}\left[\Phi_3\left(t_n, T_{2_n(t)}\right) - \Phi_3\left(t_{n-1}, T_{2_{n-1}(t)}\right)\right] \\
&\quad + \frac{\varphi}{G(\varphi)\Gamma(\varphi)}\int_0^{t_{n+1}}(t_{n+1} - t)^{\varphi-1}\,\Phi_3\left(t, T_2(t)\right)dt \\
&\quad - \frac{\varphi}{G(\varphi)\Gamma(\varphi)}\int_0^{t_{n+1}}(t_{n+1} - 1)^{\varphi-1}\,\Phi_3\left(t, T_2(t)\right)dt, \\
M_{0_{n+1}}(t) - M_{0_n}(t) &= \frac{1-\varphi}{G(\varphi)}\left[\Phi_4\left(t_n, M_{0_n(t)}\right) - \Phi_4\left(t_{n-1}, M_{0_{n-1}(t)}\right)\right] \\
&\quad + \frac{\varphi}{G(\varphi)\Gamma(\varphi)}\int_0^{t_{n+1}}(t_{n+1} - t)^{\varphi-1}\,\Phi_4\left(t, M_0(t)\right)dt \\
&\quad - \frac{\varphi}{G(\varphi)\Gamma(\varphi)}\int_0^{t_{n+1}}(t_{n+1} - 1)^{\varphi-1}\,\Phi_4\left(t, M_0(t)\right)dt,
\end{aligned} \tag{138}
$$

$$
\begin{aligned}
M_{1_{n+1}}(t) - M_{1_n}(t) &= \frac{1-\varphi}{G(\varphi)}\left[\Phi_5\left(t_n, M_{1_{n(t)}}\right) - \Phi_5\left(t_{n-1}, M_{1_{n-1(t)}}\right)\right] \\
&+\frac{\varphi}{G(\varphi)\Gamma(\varphi)}\int_0^{t_{n+1}}(t_{n+1}-t)^{\varphi-1}\Phi_5\left(t, M_1(t)\right)dt \\
&-\frac{\varphi}{G(\varphi)\Gamma(\varphi)}\int_0^{t_{n+1}}(t_{n+1}-1)^{\varphi-1}\Phi_5\left(t, M_1(t)\right)dt, \\
I_{M_{n+1}}(t) - I_{M_n}(t) &= \frac{1-\varphi}{G(\varphi)}\left[\Phi_6\left(t_n, I_{M_n(t)}\right) - \Phi_6\left(t_{n-1}, I_{M_{n-1(t)}}\right)\right] \\
&+\frac{\varphi}{G(\varphi)\Gamma(\varphi)}\int_0^{t_{n+1}}(t_{n+1}-t)^{\varphi-1}\Phi_6\left(t, I_M(t)\right)dt \\
&-\frac{\varphi}{G(\varphi)\Gamma(\varphi)}\int_0^{t_{n+1}}(t_{n+1}-1)^{\varphi-1}\Phi_6\left(t, I_M(t)\right)dt, \\
V_{n+1}(t) - V_n(t) &= \frac{1-\varphi}{G(\varphi)}\left[\Phi_7\left(t_n, V_n(t)\right) - \Phi_7\left(t_{n-1}, V_{n-1}(t)\right)\right] \\
&+\frac{\varphi}{G(\varphi)\Gamma(\varphi)}\int_0^{t_{n+1}}(t_{n+1}-t)^{\varphi-1}\Phi_7\left(t, V(t)\right)dt \\
&-\frac{\varphi}{G(\varphi)\Gamma(\varphi)}\int_0^{t_{n+1}}(t_{n+1}-1)^{\varphi-1}\Phi_7\left(t, V(t)\right)dt, \\
A_{n+1}(t) - A_n(t) &= \frac{1-\varphi}{G(\varphi)}\left[\Phi_8\left(t_n, A_n(t)\right) - \Phi_8\left(t_{n-1}, A_{n-1}(t)\right)\right] \qquad (139) \\
&+\frac{\varphi}{G(\varphi)\Gamma(\varphi)}\int_0^{t_{n+1}}(t_{n+1}-t)^{\varphi-1}\Phi_8\left(t, A(t)\right)dt \\
&-\frac{\varphi}{G(\varphi)\Gamma(\varphi)}\int_0^{t_{n+1}}(t_{n+1}-1)^{\varphi-1}\Phi_8\left(t, A(t)\right)dt, \\
E_{n+1}(t) - E_n(t) &= \frac{1-\varphi}{G(\varphi)}\left[\Phi_9\left(t_n, E_n(t)\right) - \Phi_9\left(t_{n-1}, E_{n-1}(t)\right)\right] \\
&+\frac{\varphi}{G(\varphi)\Gamma(\varphi)}\int_0^{t_{n+1}}(t_{n+1}-t)^{\varphi-1}\Phi_9\left(t, E(t)\right)dt \\
&-\frac{\varphi}{G(\varphi)\Gamma(\varphi)}\int_0^{t_{n+1}}(t_{n+1}-1)^{\varphi-1}\Phi_9\left(t, E(t)\right)dt, \\
N_{K_{n+1}}(t) - N_{K_n}(t) &= \frac{1-\varphi}{G(\varphi)}\left[\Phi_{10}\left(t_n, N_{K_n(t)}\right) - \Phi_{10}\left(t_{n-1}, N_{K_{n-1(t)}}\right)\right] \\
&+\frac{\varphi}{G(\varphi)\Gamma(\varphi)}\int_0^{t_{n+1}}(t_{n+1}-t)^{\varphi-1}\Phi_{10}\left(t, N_K(t)\right)dt \\
&-\frac{\varphi}{G(\varphi)\Gamma(\varphi)}\int_0^{t_{n+1}}(t_{n+1}-1)^{\varphi-1}\Phi_{10}\left(t, N_K(t)\right)dt,
\end{aligned}
$$

$$
\begin{aligned}
I_{10_{n+1}}(t) - I_{10_n}(t) &= \frac{1-\varphi}{G(\varphi)}\left[\Phi_{11}\left(t_n, I_{10_{n(t)}}\right) - \Phi_{11}\left(t_{n-1}, I_{11_{n-1(t)}}\right)\right] \\
&+\frac{\varphi}{G(\varphi)\Gamma(\varphi)}\int_0^{t_{n+1}}(t_{n+1}-t)^{\varphi-1}\,\Phi_{11}\left(t, I_{10}(t)\right)dt \\
&-\frac{\varphi}{G(\varphi)\Gamma(\varphi)}\int_0^{t_{n+1}}(t_{n+1}-1)^{\varphi-1}\,\Phi_{11}\left(t, I_{11}(t)\right)dt, \\
F_{1_{n+1}}(t) - F_{1_n}(t) &= \frac{1-\varphi}{G(\varphi)}\left[\Phi_{12}\left(t_n, F_{1_{n(t)}}\right) - \Phi_{12}\left(t_{n-1}, F_{1_{n-1(t)}}\right)\right] \\
&+\frac{\varphi}{G(\varphi)\Gamma(\varphi)}\int_0^{t_{n+1}}(t_{n+1}-t)^{\varphi-1}\,\Phi_{12}\left(t, F_1(t)\right)dt \\
&-\frac{\varphi}{G(\varphi)\Gamma(\varphi)}\int_0^{t_{n+1}}(t_{n+1}-1)^{\varphi-1}\,\Phi_{12}\left(t, F_1(t)\right)dt, \\
F_{2_{n+1}}(t) - F_{2_n}(t) &= \frac{1-\varphi}{G(\varphi)}\left[\Phi_{13}\left(t_n, F_{2_{n(t)}}\right) - \Phi_{13}\left(t_{n-1}, F_{2_{n-1(t)}}\right)\right] \qquad (140) \\
&+\frac{\varphi}{G(\varphi)\Gamma(\varphi)}\int_0^{t_{n+1}}(t_{n+1}-t)^{\varphi-1}\,\Phi_{13}\left(t, F_2(t)\right)dt \\
&-\frac{\varphi}{G(\varphi)\Gamma(\varphi)}\int_0^{t_{n+1}}(t_{n+1}-1)^{\varphi-1}\,\Phi_{13}\left(t, F_2(t)\right)dt.
\end{aligned}
$$

Applying Theorem 13 to Eq. (138), Eq. (139), and Eq. (140) yields the following

$$
\begin{aligned}
T_{0_{n+1}} &= T_{0_n} + \Phi_1\left(t_n, T_{0_n}\right)\left\{\frac{1-\varphi}{G(\varphi)} + \frac{\varphi}{G(\varphi)}\hbar\left(\frac{2\hbar t_{n+1}^{\varphi}}{\varphi} - \frac{t_{n+1}^{\varphi+1}}{\varphi+1}\right)\right. \\
&\left.-\frac{\varphi}{G(\varphi)\Gamma(\varphi)\hbar}\left(\frac{\hbar t_{n+1}^{\varphi}}{\varphi} - \frac{t_{n+1}^{\varphi+1}}{\varphi+1}\right)\right\} \\
&+\Phi_1\left(t_{n-1}, T_{0_{n-1}}\right)\left\{\frac{\varphi-1}{G(\varphi)} - \frac{\varphi}{G(\varphi)\Gamma(\varphi)\hbar}\right. \\
&\left.\times\left(\frac{\hbar t_{n+1}^{\varphi}}{\varphi} - \frac{t_{n+1}^{\varphi+1}}{\varphi+1} + \frac{t^{\varphi+1}}{G(\varphi)\Gamma(\varphi)}\hbar\right)\right\} + \quad {}^1R_{\varphi},
\end{aligned}
$$

where $||^1R_{\varphi}||_{\infty} < M$.

Next

$$\begin{aligned} T_{1_{n+1}} &= T_{1_n} + \Phi_2\left(t_n, T_{1_n}\right)\left\{\frac{1-\varphi}{G(\varphi)} + \frac{\varphi}{G(\varphi)}\hbar\left(\frac{2\hbar t_{n+1}^{\varphi}}{\varphi} - \frac{t_{n+1}^{\varphi+1}}{\varphi+1}\right)\right. \\ &\left. -\frac{\varphi}{G(\varphi)\Gamma(\varphi)\hbar}\left(\frac{\hbar t_{n+1}^{\varphi}}{\varphi} - \frac{t_{n+1}^{\varphi+1}}{\varphi+1}\right)\right\} \\ &+\Phi_2\left(t_{n-1}, T_{1_{n-1}}\right)\left\{\frac{\varphi-1}{G(\varphi)} - \frac{\varphi}{G(\varphi)\Gamma(\varphi)\hbar}\right. \\ &\left.\times\left(\frac{\hbar t_{n+1}^{\varphi}}{\varphi} - \frac{t_{n+1}^{\varphi+1}}{\varphi+1} + \frac{t^{\varphi+1}}{G(\varphi)\Gamma(\varphi)}\hbar\right)\right\} + \quad {}^{2}R_{\varphi}, \end{aligned}$$

where $||^2R_{\varphi}||_{\infty} < M$.

Next

$$\begin{aligned} T_{2_{n+1}} &= T_{2_n} + \Phi_3\left(t_n, T_{2_n}\right)\left\{\frac{1-\varphi}{G(\varphi)} + \frac{\varphi}{G(\varphi)}\hbar\left(\frac{2\hbar t_{n+1}^{\varphi}}{\varphi} - \frac{t_{n+1}^{\varphi+1}}{\varphi+1}\right)\right. \\ &\left. -\frac{\varphi}{G(\varphi)\Gamma(\varphi)\hbar}\left(\frac{\hbar t_{n+1}^{\varphi}}{\varphi} - \frac{t_{n+1}^{\varphi+1}}{\varphi+1}\right)\right\} \\ &+\Phi_3\left(t_{n-1}, T_{2_{n-1}}\right)\left\{\frac{\varphi-1}{G(\varphi)} - \frac{\varphi}{G(\varphi)\Gamma(\varphi)\hbar}\right. \\ &\left.\times\left(\frac{\hbar t_{n+1}^{\varphi}}{\varphi} - \frac{t_{n+1}^{\varphi+1}}{\varphi+1} + \frac{t^{\varphi+1}}{G(\varphi)\Gamma(\varphi)}\hbar\right)\right\} + \quad {}^{3}R_{\varphi}, \end{aligned}$$

where $||^3R_{\varphi}||_{\infty} < M$.

Next

$$\begin{aligned} M_{0_{n+1}} &= M_{0_n} + \Phi_4\left(t_n, M_{0_n}\right)\left\{\frac{1-\varphi}{G(\varphi)} + \frac{\varphi}{G(\varphi)}\hbar\left(\frac{2\hbar t_{n+1}^{\varphi}}{\varphi} - \frac{t_{n+1}^{\varphi+1}}{\varphi+1}\right)\right. \\ &\left. -\frac{\varphi}{G(\varphi)\Gamma(\varphi)\hbar}\left(\frac{\hbar t_{n+1}^{\varphi}}{\varphi} - \frac{t_{n+1}^{\varphi+1}}{\varphi+1}\right)\right\} \\ &+\Phi_4\left(t_{n-1}, M_{0_{n-1}}\right)\left\{\frac{\varphi-1}{G(\varphi)} - \frac{\varphi}{G(\varphi)\Gamma(\varphi)\hbar}\right. \\ &\left.\times\left(\frac{\hbar t_{n+1}^{\varphi}}{\varphi} - \frac{t_{n+1}^{\varphi+1}}{\varphi+1} + \frac{t^{\varphi+1}}{G(\varphi)\Gamma(\varphi)}\hbar\right)\right\} + \quad {}^{4}R_{\varphi}, \end{aligned}$$

where $||^4R_{\varphi}||_{\infty} < M$.

Next

$$\begin{aligned} M_{1_{n+1}} &= M_{1_n} + \Phi_5\left(t_n, M_{1_n}\right)\left\{\frac{1-\varphi}{G(\varphi)} + \frac{\varphi}{G(\varphi)}\hbar\left(\frac{2\hbar t_{n+1}^{\varphi}}{\varphi} - \frac{t_{n+1}^{\varphi+1}}{\varphi+1}\right)\right. \\ &\left. -\frac{\varphi}{G(\varphi)\Gamma(\varphi)\hbar}\left(\frac{\hbar t_{n+1}^{\varphi}}{\varphi} - \frac{t_{n+1}^{\varphi+1}}{\varphi+1}\right)\right\} \\ &+\Phi_5\left(t_{n-1}, M_{1_{n-1}}\right)\left\{\frac{\varphi-1}{G(\varphi)} - \frac{\varphi}{G(\varphi)\Gamma(\varphi)\hbar}\right. \\ &\left.\times\left(\frac{\hbar t_{n+1}^{\varphi}}{\varphi} - \frac{t_{n+1}^{\varphi+1}}{\varphi+1} + \frac{t^{\varphi+1}}{G(\varphi)\Gamma(\varphi)}\hbar\right)\right\} + \quad {}^5R_{\varphi}, \end{aligned}$$

where $||^5R_{\varphi}||_{\infty} < M$.

Next

$$\begin{aligned} I_{M_{n+1}} &= I_{M_n} + \Phi_6\left(t_n, I_{M_n}\right)\left\{\frac{1-\varphi}{G(\varphi)} + \frac{\varphi}{G(\varphi)}\hbar\left(\frac{2\hbar t_{n+1}^{\varphi}}{\varphi} - \frac{t_{n+1}^{\varphi+1}}{\varphi+1}\right)\right. \\ &\left. -\frac{\varphi}{G(\varphi)\Gamma(\varphi)\hbar}\left(\frac{\hbar t_{n+1}^{\varphi}}{\varphi} - \frac{t_{n+1}^{\varphi+1}}{\varphi+1}\right)\right\} \\ &+\Phi_6\left(t_{n-1}, I_{M_{n-1}}\right)\left\{\frac{\varphi-1}{G(\varphi)} - \frac{\varphi}{G(\varphi)\Gamma(\varphi)\hbar}\right. \\ &\left.\times\left(\frac{\hbar t_{n+1}^{\varphi}}{\varphi} - \frac{t_{n+1}^{\varphi+1}}{\varphi+1} + \frac{t^{\varphi+1}}{G(\varphi)\Gamma(\varphi)}\hbar\right)\right\} + \quad {}^6R_{\varphi}, \end{aligned}$$

where $||^6R_{\varphi}||_{\infty} < M$.

Next

$$\begin{aligned} V_{n+1} &= V_n + \Phi_7\left(t_n, V_n\right)\left\{\frac{1-\varphi}{G(\varphi)} + \frac{\varphi}{G(\varphi)}\hbar\left(\frac{2\hbar t_{n+1}^{\varphi}}{\varphi} - \frac{t_{n+1}^{\varphi+1}}{\varphi+1}\right)\right. \\ &\left. -\frac{\varphi}{G(\varphi)\Gamma(\varphi)\hbar}\left(\frac{\hbar t_{n+1}^{\varphi}}{\varphi} - \frac{t_{n+1}^{\varphi+1}}{\varphi+1}\right)\right\} \\ &+\Phi_7\left(t_{n-1}, V_{n-1}\right)\left\{\frac{\varphi-1}{G(\varphi)} - \frac{\varphi}{G(\varphi)\Gamma(\varphi)\hbar}\right. \\ &\left.\times\left(\frac{\hbar t_{n+1}^{\varphi}}{\varphi} - \frac{t_{n+1}^{\varphi+1}}{\varphi+1} + \frac{t^{\varphi+1}}{G(\varphi)\Gamma(\varphi)}\hbar\right)\right\} + \quad {}^7R_{\varphi}. \end{aligned}$$

where $||^7R_{\varphi}||_{\infty} < M$.

Next

$$\begin{aligned} A_{n+1} &= A_n + \Phi_8\left(t_n, A_n\right)\left\{\frac{1-\varphi}{G(\varphi)} + \frac{\varphi}{G(\varphi)}\hbar\left(\frac{2\hbar t_{n+1}^{\varphi}}{\varphi} - \frac{t_{n+1}^{\varphi+1}}{\varphi+1}\right)\right. \\ &\left. -\frac{\varphi}{G(\varphi)\Gamma(\varphi)\hbar}\left(\frac{\hbar t_{n+1}^{\varphi}}{\varphi} - \frac{t_{n+1}^{\varphi+1}}{\varphi+1}\right)\right\} \\ &+\Phi_8\left(t_{n-1}, A_{n-1}\right)\left\{\frac{\varphi-1}{G(\varphi)} - \frac{\varphi}{G(\varphi)\Gamma(\varphi)\hbar}\right. \\ &\left.\times\left(\frac{\hbar t_{n+1}^{\varphi}}{\varphi} - \frac{t_{n+1}^{\varphi+1}}{\varphi+1} + \frac{t^{\varphi+1}}{G(\varphi)\Gamma(\varphi)}\hbar\right)\right\} + \quad {}^{8}R_{\varphi}, \end{aligned}$$

where $||^{8}R_{\varphi}||_{\infty} < M$.

Next

$$\begin{aligned} E_{n+1} &= E_n + \Phi_9\left(t_n, E_n\right)\left\{\frac{1-\varphi}{G(\varphi)} + \frac{\varphi}{G(\varphi)}\hbar\left(\frac{2\hbar t_{n+1}^{\varphi}}{\varphi} - \frac{t_{n+1}^{\varphi+1}}{\varphi+1}\right)\right. \\ &\left. -\frac{\varphi}{G(\varphi)\Gamma(\varphi)\hbar}\left(\frac{\hbar t_{n+1}^{\varphi}}{\varphi} - \frac{t_{n+1}^{\varphi+1}}{\varphi+1}\right)\right\} \\ &+\Phi_9\left(t_{n-1}, E_{n-1}\right)\left\{\frac{\varphi-1}{G(\varphi)} - \frac{\varphi}{G(\varphi)\Gamma(\varphi)\hbar}\right. \\ &\left.\times\left(\frac{\hbar t_{n+1}^{\varphi}}{\varphi} - \frac{t_{n+1}^{\varphi+1}}{\varphi+1} + \frac{t^{\varphi+1}}{G(\varphi)\Gamma(\varphi)}\hbar\right)\right\} + \quad {}^{9}R_{\varphi}, \end{aligned}$$

where $||^{9}R_{\varphi}||_{\infty} < M$.

Next

$$\begin{aligned} N_{K_{n+1}} &= N_{K_n} + \Phi_{10}\left(t_n, N_{K_n}\right)\left\{\frac{1-\varphi}{G(\varphi)} + \frac{\varphi}{G(\varphi)}\hbar\left(\frac{2\hbar t_{n+1}^{\varphi}}{\varphi} - \frac{t_{n+1}^{\varphi+1}}{\varphi+1}\right)\right. \\ &\left. -\frac{\varphi}{G(\varphi)\Gamma(\varphi)\hbar}\left(\frac{\hbar t_{n+1}^{\varphi}}{\varphi} - \frac{t_{n+1}^{\varphi+1}}{\varphi+1}\right)\right\} \\ &+\Phi_{10}\left(t_{n-1}, N_{K_{n-1}}\right)\left\{\frac{\varphi-1}{G(\varphi)} - \frac{\varphi}{G(\varphi)\Gamma(\varphi)\hbar}\right. \\ &\left.\times\left(\frac{\hbar t_{n+1}^{\varphi}}{\varphi} - \frac{t_{n+1}^{\varphi+1}}{\varphi+1} + \frac{t^{\varphi+1}}{G(\varphi)\Gamma(\varphi)}\hbar\right)\right\} + \quad {}^{10}R_{\varphi}, \end{aligned}$$

where $||^{10}R_{\varphi}||_{\infty} < M$.

Next

$$\begin{aligned} I_{10_{n+1}} &= I_{10_n} + \Phi_{11}\left(t_n, I_{10_n}\right)\left\{\frac{1-\varphi}{G(\varphi)} + \frac{\varphi}{G(\varphi)}\hbar\left(\frac{2\hbar t_{n+1}^{\varphi}}{\varphi} - \frac{t_{n+1}^{\varphi+1}}{\varphi+1}\right)\right. \\ &\left. -\frac{\varphi}{G(\varphi)\Gamma(\varphi)\hbar}\left(\frac{\hbar t_{n+1}^{\varphi}}{\varphi} - \frac{t_{n+1}^{\varphi+1}}{\varphi+1}\right)\right\} \\ &+\Phi_{11}\left(t_{n-1}, I_{10_{n-1}}\right)\left\{\frac{\varphi-1}{G(\varphi)} - \frac{\varphi}{G(\varphi)\Gamma(\varphi)\hbar}\right. \\ &\left.\times\left(\frac{\hbar t_{n+1}^{\varphi}}{\varphi} - \frac{t_{n+1}^{\varphi+1}}{\varphi+1} + \frac{t^{\varphi+1}}{G(\varphi)\Gamma(\varphi)}\hbar\right)\right\} + \quad {}^{11}R_{\varphi}, \end{aligned}$$

where $||^{11}R_{\varphi}||_{\infty} < M$.

Next

$$\begin{aligned} F_{1_{n+1}} &= F_{1_n} + \Phi_{12}\left(t_n, F_{1_n}\right)\left\{\frac{1-\varphi}{G(\varphi)} + \frac{\varphi}{G(\varphi)}\hbar\left(\frac{2\hbar t_{n+1}^{\varphi}}{\varphi} - \frac{t_{n+1}^{\varphi+1}}{\varphi+1}\right)\right. \\ &\left. -\frac{\varphi}{G(\varphi)\Gamma(\varphi)\hbar}\left(\frac{\hbar t_{n+1}^{\varphi}}{\varphi} - \frac{t_{n+1}^{\varphi+1}}{\varphi+1}\right)\right\} \\ &+\Phi_{12}\left(t_{n-1}, F_{1_{n-1}}\right)\left\{\frac{\varphi-1}{G(\varphi)} - \frac{\varphi}{G(\varphi)\Gamma(\varphi)\hbar}\right. \\ &\left.\times\left(\frac{\hbar t_{n+1}^{\varphi}}{\varphi} - \frac{t_{n+1}^{\varphi+1}}{\varphi+1} + \frac{t^{\varphi+1}}{G(\varphi)\Gamma(\varphi)}\hbar\right)\right\} + \quad {}^{12}R_{\varphi}, \end{aligned}$$

where $||^{12}R_{\varphi}||_{\infty} < M$.

Finally,

$$\begin{aligned} F_{2_{n+1}} &= F_{2_n} + \Phi_{13}\left(t_n, F_{2_n}\right)\left\{\frac{1-\varphi}{G(\varphi)} + \frac{\varphi}{G(\varphi)}\hbar\left(\frac{2\hbar t_{n+1}^{\varphi}}{\varphi} - \frac{t_{n+1}^{\varphi+1}}{\varphi+1}\right)\right. \\ &\left. -\frac{\varphi}{G(\varphi)\Gamma(\varphi)\hbar}\left(\frac{\hbar t_{n+1}^{\varphi}}{\varphi} - \frac{t_{n+1}^{\varphi+1}}{\varphi+1}\right)\right\} \\ &+\Phi_{13}\left(t_{n-1}, F_{2_{n-1}}\right)\left\{\frac{\varphi-1}{G(\varphi)} - \frac{\varphi}{G(\varphi)\Gamma(\varphi)\hbar}\right. \\ &\left.\times\left(\frac{\hbar t_{n+1}^{\varphi}}{\varphi} - \frac{t_{n+1}^{\varphi+1}}{\varphi+1} + \frac{t^{\varphi+1}}{G(\varphi)\Gamma(\varphi)}\hbar\right)\right\} + \quad {}^{13}R_{\varphi}, \end{aligned}$$

where $||^{13}R_{\varphi}||_{\infty} < M$.

Quantitative Findings for the Fractional-order Model

This section examines the results of the numerical simulations obtained from the iterative numerical scheme applied to the hepatitis B virus and liver cancer model 39. The numerical method used for equation 39 is based on the Adams-Bashforth technique. The simulations are performed with parameter values in Tables 12, 13 with initial conditions $T_0(0) = 5 \times 10^5$, $T_1(0) = 0$, $T_2(0) = 0$, $M_0(0) = 4 \times 10^5$, $M_1(0) = 4 \times 10^5$, $I_M(0) = 0$, $V(0) = 300$, $A(0) = 0$, $E(0) = 0$, $N_k(0) = 0$, $I_{10}(0) = 0$, $F_1(0) = 0$, and $F_2(0) = 0$.

Table 12: Parameters and their Values for the Fractional-order Model

Parameter	Values	Source
Λ_{T_0}	0.99 cell/ml/day	Assumed
Λ_{M_0}	4×10^5 cell/ml/day	(Murray & Goyal, 2015)
Λ_{M_1}	0.015 cell/ml/day	(Bhadauria, 2011)
Λ_V	100 cell/ml/day	(Wiah et al., 2011)
Λ_A	0.43×10^{12} cell/ml/day	(Wiah et al., 2011)
Λ_E	11.5 cell/ml/day	(Wiah et al., 2011)
Λ_{N_K}	0.057 cell/ml/day	(Y. Zhang et al., 2007)
μ_{T_0}	6.7×10^{-7} cell/ml/day	Assumed
μ_{T_1}	0.3333 cell/ml/day	Assumed
μ_{T_2}	0.3333 cell/ml/day	Assumed
μ_{M_0}	0.011 cell/ml/day	(Guedj et al., 2013)
μ_{M_1}	0.01 cell/ml/day	(Kitagawa et al., 2018)
μ_{I_M}	0.3264 cell/ml/day	(Chenar et al., 2018)
μ_V	0.67 cell/ml/day	(Chenar et al., 2018)
μ_A	0.43 cell/ml/day	(Wiah et al., 2011)
μ_E	0.4 cell/ml/day	(Wiah et al., 2011)
μ_{N_K}	0.42 cell/ml/day	Assumed

Source: Author's construct (2023)

Table 13: Parameters and their Values for the Fractional-order Model

Parameter	Description	Source
$\mu_{I_{10}}$	3.70×10^{-2} cell/ml/day	Assumed
μ_{F_1}	8 cell/ml/day	(Wiah et al., 2011)
μ_{F_2}	5.16 cell/ml/day	(Chenar et al., 2018)
ρ_1	2.9×10^{-4}cell/ml/day	Assumed
ρ_2	0.02 cell/ml/day	Assumed
ρ_3	2.03×10^{-7} cell/ml/day	Assumed
δ_1	1.7 cell/ml/day	(Wiah et al., 2011)
δ_2	0.066 cell/ml/day	(Wiah et al., 2011)
δ_3	0.67 cell/ml/day	(Ciupe et al., 2014)
δ_4	0.67 cell/day	(Ciupe et al., 2014)
θ_1	0.8 cell/ml/day	(Chenar et al., 2018)
θ_2	0.6 cell/ml/day	(Chenar et al., 2018)
χ_1	1.5 cell/ml/day	(Chenar et al., 2018)
χ_2	2.0 cell/ml/day	(Chenar et al., 2018)
β_1	1.02 cell/ml/day	(Wiah et al., 2011)
β_2	1.02 cell/ml/day	(Wiah et al., 2011)
τ_1	0.1642 cell/ml/day	Assumed
ψ	5 cell/ml/day	(Chenar et al., 2018)
σ	8.3 cell/ml/day	(Wiah et al., 2011)
ω	20 cell/ml/day	(Chenar et al., 2018)
ε	200 cell/ml/day	(Wiah et al., 2011)
η	2500 cell/ml/day	(Wiah et al., 2011)
π	0.3359 cell/ml/day	Assumed
ζ	0.01 cell/ml/day	(Bhadauria, 2011)
ϑ	$0 \leq \vartheta \leq 1$	(Chenar et al., 2018)
ϱ	$0 \leq \varrho \leq 1$	(Chenar et al., 2018)

Source: Author's construct (2023)

Numerical Simulations of State Trajectories at Varying Fractional Orders

The simulation results in Figures 20, 21, and 22 provide a comprehensive view of how different values of the fractional-order parameter (φ) influence the immune system's response to the co-existence dynamics of the Hepatitis B virus (HBV) and liver cancer. The simulation includes fractional values ranging from 0.4 to 0.9, as well as the integer-order case ($\varphi = 1$), allowing for a detailed comparison between fractional-order and traditional integer-order models. When $\varphi = 0.4$, the trajectory of the fractional-order model converges to the virus-free equilibrium point, similar to the integer-order case, as illustrated in Figure 20 (b), (c), (f), and Figure 21 (a), (b), and (d). However, the trajectories of the fractional-order model with $\varphi = 0.4$ take different paths from the integer-order model, as seen in Figure 20 (a), (d), (e), Figure 21 (c), (e), (f), and Figure 22. The plots reveal pronounced fluctuations in immune cell populations, HBV, and liver cancer levels at fractional-order $\varphi = 0.4$, indicating an unstable immune response characteristic of lower fractional values. The fractional-order model with $\varphi = 0.4$ captures more complex, real-world behaviors such as memory effects and irregular dynamics, which are challenging to model with integer-order equations. This lower value reflects a system that is sensitive to changes and exhibits erratic behavior, highlighting the model's ability to represent intricate and non-linear interactions within the immune system.

As φ increases to 0.5 and 0.6, the simulation graphs show a transition toward greater stability, with a smoother and more controlled immune response, reduced fluctuations in liver cell populations, and viral load. This shift illustrates how intermediate fractional values provide a more refined and stable depiction of the system's dynamics, capturing intermediate behaviors between erratic and stable responses, thus representing the system's complexity more effectively. At $\varphi = 0.7$ and $\varphi = 0.8$, the simulation plots demonstrate further stabilization of the immune system's dynamics, with improved control over HBV and liver cancer infections and a more balanced interaction between immune cells and virus levels. This stability indicates that higher fractional values enhance the model's accuracy, offering a clearer understanding of how the immune system responds to HBV and liver cancer

infections over time, with dynamics becoming more predictable and aligning with observed real-world behaviors, showcasing the model's improved resolution.

When $\varphi = 0.9$, the plots reveal near-optimal stability and control, with the immune response and viral dynamics approaching a state of equilibrium, reflecting the model's ability to closely match observed data as φ nears 1. This high fractional value signifies that the system's behavior is becoming more predictable and less erratic, closely resembling integer-order models. Finally, when $\varphi = 1$, the simulation represents the integer-order model, where the plots show stable and predictable dynamics. The immune response and viral load behaviors closely resemble those observed with other fractional values, indicating that the fractional-order model effectively transitions to the integer-order model when φ is set to 1. This convergence highlights the integer-order model's ability to provide clear and straightforward insights, consistent with traditional modeling approaches, while underscoring the fractional model's flexibility and enhanced resolution in capturing complex dynamics.

This means that, in the context of HBV, an integer-order model might predict that, due to the immune system's response and effective antiviral treatments, the disease could be eradicated in the population (i.e., convergence to the virus-free equilibrium). This is akin to the virus-free equilibrium (VFE) prediction, where no new infections occur, and the infection eventually dies out. However, because a significant number of individuals can develop chronic HBV infection, a fractional-order model that incorporates memory effects might suggest that the virus remains endemic in the population. Hence, our model predicts that, even with a high cell clearance rate by immune cells and treatment of infected macrophages, chronic carriers continue to transmit the virus at a low level, leading to an endemic equilibrium where HBV persists. The fractional-order model accounts for the history of the disease and long-term effects, such as chronic infection, delayed responses to treatment, and the slow clearance of the virus. These dynamics are not captured by a standard integer-order model. Thus, while the integer-order model predicts elimination, the fractional-order model could predict a stable endemic state where a portion of the population remains infected over the long term. The fractional-order model

offers a detailed and nuanced view of the immune system's response to the coexistence of HBV and liver cancer infections, with the ability to smoothly transition to the integer-order model. By varying φ the model captures a spectrum of behaviors, ranging from highly erratic to stable, providing a more comprehensive understanding of the system's dynamics compared to traditional integer-order models.

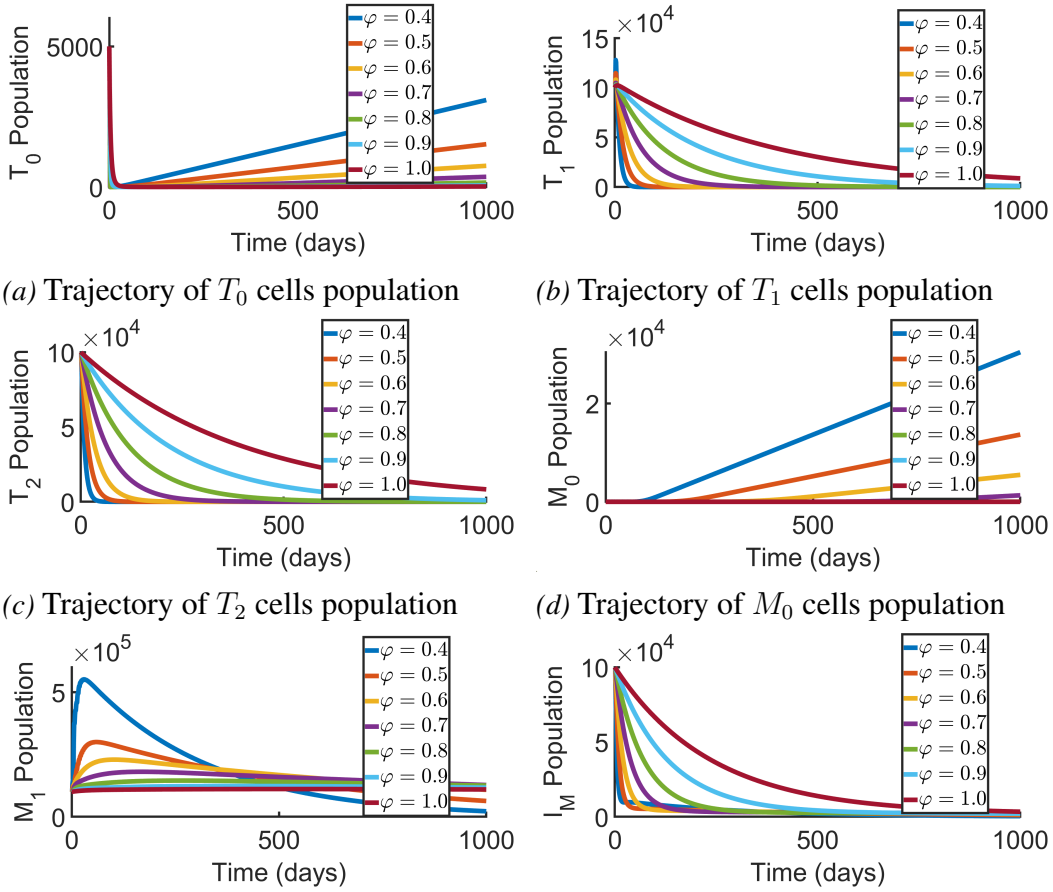

(a) Trajectory of T_0 cells population

(b) Trajectory of T_1 cells population

(c) Trajectory of T_2 cells population

(d) Trajectory of M_0 cells population

(e) Trajectory of M_1 cells population

(f) Trajectory of I_M population

Figure 20: Simulation Results Showing the Trajectories of the State Variables at Different Fractional Orders, Where (a) Represents the Trajectory of T_0 Cell Class, (b) Represents the Trajectory of T_1 Cell Class, (c) Represents the Trajectory of T_2 Cell Class, (d) Represents the Trajectory of M_0 Cell Class, (e) Represents the Trajectory of M_1 Cell Class, and (f) Represents the Trajectory of I_M Cell Class (Source: Author's construct, 2023)

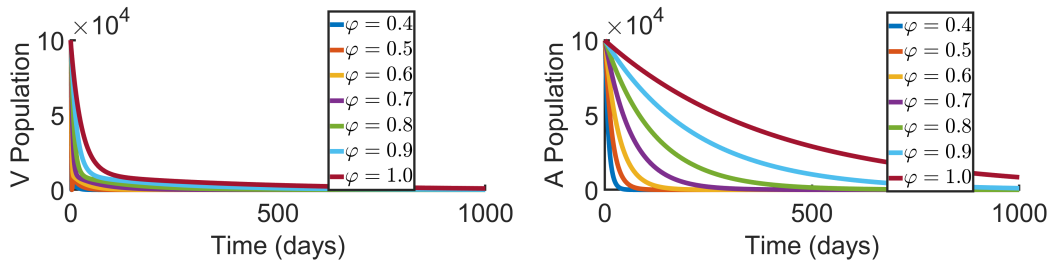

(a) Trajectory of HBV population

(b) Trajectory of A cells population

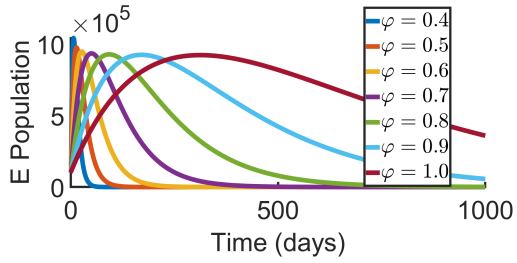

(c) Trajectory of E cells population

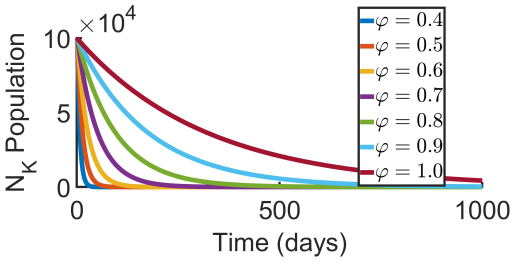

(d) Trajectory of N_K cells population

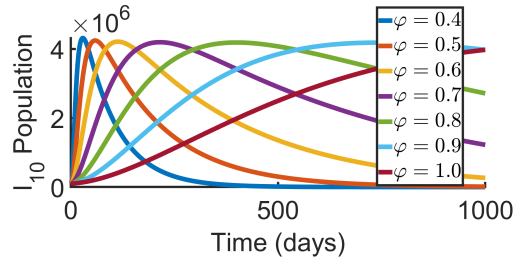

(e) Trajectory of I_{10} cells population

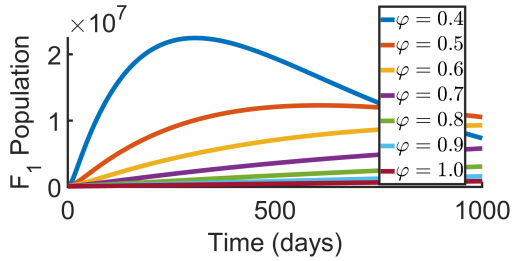

(f) Trajectory of F_1 cells population

Figure 21: Simulation Results Showing the Trajectories of the State Variables at Different Fractional Orders, Where (a) Represents the Trajectory of V Cell Class, (b) Represents the Trajectory of A Cell Class, (c) Represents the Trajectory of E Cell Class, (d) Represents the Trajectory of N_K Cell Class, (e) Represents the Trajectory of I_{10} Cell Class, and (f) Represents the Trajectory of F_1 Cell Class (Source: Author's construct, 2023)

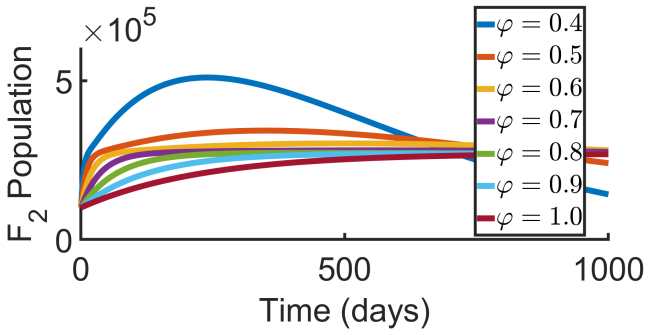

Figure 22: Simulation Results Showing the Trajectories of (F_2) Cells at Different Fractional Orders (Source: Author's construct, 2023)

Impact of Antiviral Treatment on HBV and Liver Cancer

The contour plots in Figures 23 and 24 visually represent how different combinations of two key drug efficacies, ϑ and ϱ, impact the control reproduction number, $\mathcal{R}_c$, in the context of co-existence with HBV and liver cancer. Here, ϑ represents the efficacy of nucleotide (nucleoside) analogues (NAs), including lamivudine, adefovir, entecavir, tenofovir, telbivudine, and clevudine, that obstruct viral production by blocking HBV replication (Chenar et al., 2018; Fatehi et al., 2022). ϱ represents the efficacy of IFN-based therapies, such as interferon-alpha (IFN-α) or pegylated IFN (peg-IFN-$\alpha 2a/2b$), which boost the immune response and prevent new infections of liver cells (Chenar et al., 2018; Fatehi et al., 2022). The objective of HBV treatment is to lower $\mathcal{R}_c$ below unity, as this indicates successful control of the infection, where each infected cell causes less than one new infection on average, leading to the eventual clearance of the virus.

The contour lines in Figures 23 and 24 show regions of constant $\mathcal{R}_c$, with lower values indicating more effective control of the infection. In particular, Figure 23 indicates that a higher drug efficacy of approximately 96% for both NAs and IFN-based therapies is sufficient to shift $\mathcal{R}_c$ below unity. The optimal treatment strategy is found in regions where $\mathcal{R}_c$ is less than one, as illustrated in Figure 24, highlighting the importance of combination therapy that targets both viral production and the prevention of new infections. For instance, achieving a minimum nucleotide drug efficacy rate of approximately 74%, coupled with an IFN-based therapy efficacy rate of 71%, proves adequate in shifting $\mathcal{R}_c$ to 0.0875, indicative of reduced disease transmission. The plots underscore the need for a balanced and personalized treatment approach, where both types of drugs are effectively combined to achieve optimal outcomes in managing HBV and liver cancer co-existence infection.

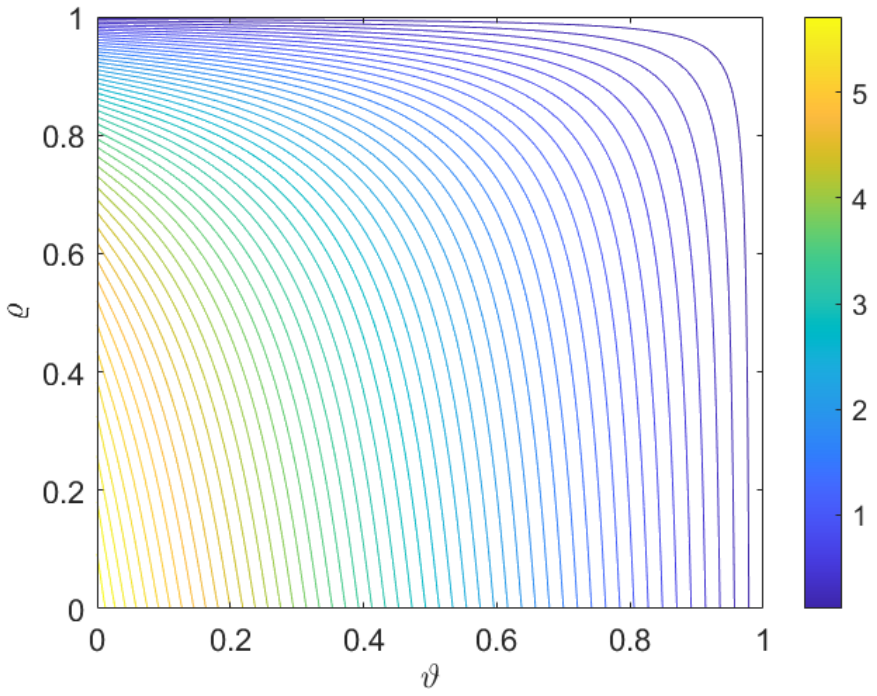

Figure 23: Effect of Antiviral Treatments on HBV and Liver Cancer (Source: Author's construct, 2023)

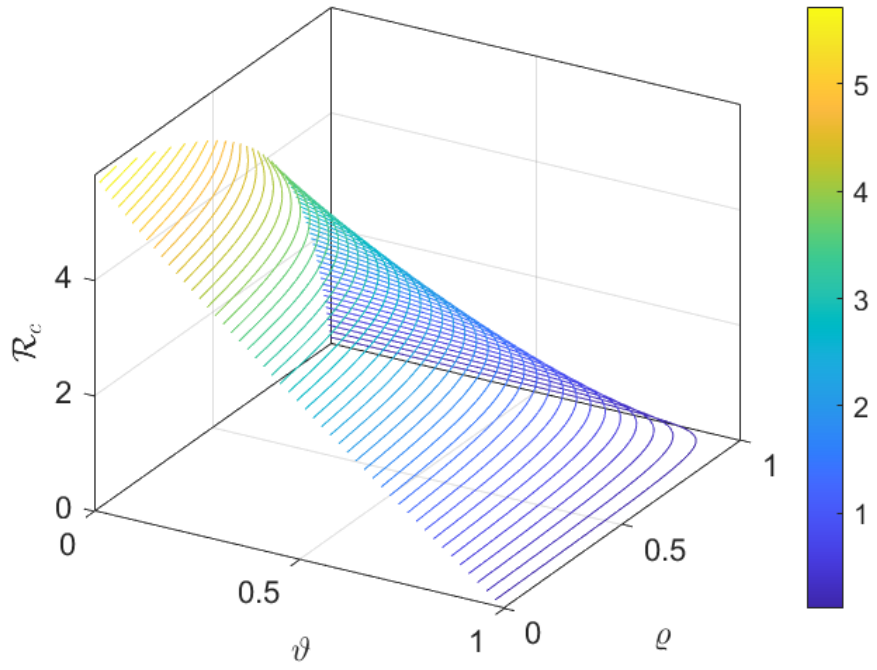

Figure 24: Optimal Control Strategy (Source: Author's construct, 2023)

Discussions

This research proposed and examined a new model for hepatitis B virus (HBV) infection and its concurrent presence with liver cancer, with a specific emphasis on the interactions between various components of the immune system. This model integrates the innate immune response, represented by natural killer (NK) cells, and the adaptive immune response, which encompasses effector B cells and naïve T cells that develop into T helper-1 cells, cytotoxic T cells, interleukin-10, antibodies, and other cytokines. During infection, cytokines play a vital role in recruiting both innate and adaptive immune elements, boosting their efficacy, and aiding in the non-cytolytic elimination of infected cells.

The stability assessment of equilibrium states demonstrated the influence of various parameters on immune response dynamics. Some results, such as the destabilization of the virus persistence equilibrium due to the presence of T cells, were fairly predictable. However, other findings, such as the inadequate infection clearance despite higher levels of antibodies, NK cells, and plasma cells, were unexpectedly surprising. Generally, increasing the quantities of NK cells, the efficiency of antibodies in clearing free virus, the rate at which effector B (plasma) cells eliminate infected cells, the effectiveness of cytotoxic T lymphocytes in clearing infected cells, and the rate at which IFN-γ inhibits viral replication all enhance infection clearance, thereby stabilizing the disease-free steady-state solutions. However, we discovered that extremely high rates of free virus clearance by antibodies, NK cells, and effector B cells have little effect on the stability of the endemic steady state. On the other hand, higher production of naïve T cells leads to destabilization of the virus-persistence equilibrium. This is unexpected, as one might assume that higher production rates of antibodies, NK cells, and effector B cells would promote infection clearance rather than stabilize a chronic infection. This indicates that it is not just the production rates of antibodies, NK cells, and effector B cells that drive viral clearance, but rather the balance among these rates that determines whether the system sustains a chronic infection or achieves viral clearance.

The dynamics of model 5 are examined using a set of reasonably approximated

parameter values derived from published experimental data. The results are depicted in Figures 2 and 3, with the optimal parameter estimates for each patient listed in Table 4. The model effectively captures the high viral peak seen during each person's acute infection phase and the subsequent biphasic decline in viral levels. Furthermore, the best estimates indicate that virus elimination defined as having fewer than one virion remaining in the body occurs after infection in the first six individuals but not in individual 7, who is known to have developed a chronic infection. No correlation was observed between $\mathbb{R}_0$ and the time to clearance; however, the rapid clearance time noted in patient 5 aligns with a sharp second-phase viral decline due to a high loss rate of infected cells, $\mu_{I_M}(2.1918)$. In contrast, patients 2 and 7, with the lowest $\mu_{I_M}(0.4908)$ and $\mu_{I_M}(0.00000885)$ respectively, experience the longest time to viral clearance and no clearance, respectively.

Natural Killer (NK) cells are crucial for the immune response to Hepatitis B virus (HBV) and for preventing liver cancer (hepatocellular carcinoma, HCC). They work by killing infected liver cells and producing cytokines that inhibit viral replication and activate other immune responses. In chronic HBV infection and advanced liver cancer, NK cell functionality can be compromised, which allows the virus to persist and cancer cells to evade immune detection, leading to disease progression. The data in Figure 10 shows that increasing the rate at which NK cells clear infected macrophages by 25% reduces the infected macrophage population by 0.23%, indicating more effective elimination of infected cells. Conversely, a 25% reduction in this clearance rate increases the infected macrophage population by 0.05%. Larger adjustments to the clearance rate, either increases or decreases, lead to more significant changes in the infected macrophage populations, demonstrating the importance of NK cell activity in controlling HBV and liver cancer spread. Similarly, effector B cells (plasma cells) are vital for managing HBV and liver cancer. They produce antibodies that neutralize HBV and target tumor-associated antigens in liver cancer. Figure 11 shows that a 25% increase in the rate at which plasma cells clear infected macrophages results in a 2.66% decrease in infected macrophages, reflecting their effective role in reducing HBV and liver cancer replication. Decreasing this rate by

25% leads to a 0.99% increase in infected macrophages. Overall, changes in the plasma cells' clearance rate also significantly affect the infected macrophage population, highlighting their crucial role in managing these infections.

Moreover, cytotoxic T cells and antibodies are crucial in managing HBV and liver cancer. Cytotoxic T cells eliminate infected and tumor cells by inducing apoptosis, with increased activity leading to significant reductions in HBV populations up to 16.02% while decreased activity causes increases in the virus. Similarly, antibodies neutralize HBV and target cancer cells, with a 25% increase in their elimination rate resulting in a 22.49% reduction in HBV levels, whereas a decrease leads to a 7.52% rise. Both immune components' effectiveness in controlling infections is evident from the simulation results, highlighting their essential roles in managing and reducing the spread of HBV and liver cancer.

Antiviral treatments are crucial in developing strategies to control HBV and liver cancer infections. Figures 23 and 24 show how varying combinations of two key drug efficacies, ϑ and ϱ, influence the control reproduction number, $\mathcal{R}_c$, for managing these two infection co-existence. Here, ϑ represents the effectiveness of nucleotide analogues (NAs) like lamivudine and tenofovir, which inhibit viral replication, while ϱ denotes the efficacy of IFN-based therapies, such as interferon-alpha, which boost immune responses and prevent new infections. The goal is to reduce $\mathcal{R}_c$ below one, indicating effective infection control. The contour lines show regions of constant $\mathcal{R}_c$, with lower values indicating better control. Optimal strategies are those where $\mathcal{R}_c$ falls below one, emphasizing the benefit of combining therapies that both suppress viral production and prevent new infections. For instance, achieving a nucleotide drug efficacy of around 74% combined with an IFN therapy efficacy of 71% can reduce $\mathcal{R}_c$ to 0.0875, demonstrating effective disease management. These plots highlight the need for a balanced, personalized approach that integrates both types of drugs for the best control of HBV and liver cancer.

Interleukin-10 (IL-10) is a pleiotropic anti-inflammatory cytokine with a critical role in modulating the host's immunological defenses against hepatitis B virus (HBV) infection. IL-10 is primarily recognized for its immunosuppressive prop-

erties, particularly its ability to dampen pro-inflammatory immune responses. It is well-established that IL-10 suppresses the synthesis of pro-inflammatory mediators such as interleukin-1 (IL-1), interleukin-6 (IL-6), tumor necrosis factor-alpha TNF_{α}, and interferon-gamma IFN_{γ}. Through the regulation of these cytokines, IL-10 contributes to the attenuation of hepatic inflammation during HBV infection. IL-10 sustains a finely tuned balance between promoting an adequate immune defense to combat the virus and curbing excessive inflammation that could precipitate hepatocellular injury. This equilibrium is paramount, as an overzealous immune response can trigger acute liver pathologies like fulminant hepatitis, whereas an insufficient immune reaction might lead to viral persistence and chronic infection. During HBV pathogenesis, IL-10 suppresses the activity of multiple immune effectors, including T lymphocytes, macrophages, and dendritic cells. This immunosuppression mitigates hepatic inflammation and limits tissue injury, thereby potentially preventing severe liver damage. However, despite its crucial role in immune regulation, IL-10 may paradoxically promote viral persistence by attenuating the host's antiviral immunity. By suppressing the immune response, IL-10 may facilitate the virus's evasion of immune surveillance, allowing it to establish chronicity. The reduced activity of cytotoxic T lymphocytes (CTLs), which are essential for the clearance of infected hepatocytes, may permit the virus to persist and evade immune eradication, as illustrated in Figure 18. Augmented IL-10 concentrations have been associated with deleterious outcomes in patients undergoing antiviral therapy for HBV, as excessive IL-10 can compromise the immunological response requisite for effective viral eradication during intervention.

Heterogeneous temporal intervals culminating in chronicity within the model were discerned. Initially, the concentration of cytotoxic T lymphocytes ascends during the initial phases but subsequently diminishes, ultimately being eclipsed by the persistently augmenting levels of T helper-1 cells. However, when we amplified the synthesis rate of IL-10, the latency to chronicity was protracted. This phenomenon is paradoxical, as one might conjecture that elevated IL-10 concentrations, given a stable viral load, would expedite infection resolution. Thus, these findings substantiate

the postulation that in HBV infection, sustained antigenic presentation by infected hepatocytes and prolonged antigen exposure are concomitant with the attrition of $CD8^+$ T lymphocytes. Biologically, the incessant secretion of IL-10 cytokines attenuates cytotoxic T lymphocyte (T_2) functionality, thereby extending the duration to chronicity. An interval of approximately 112 days corresponds to the initial phase post-exposure to the core hepatitis B virus (i.e., the acute phase of HBV infection), which represents the optimal temporal window for the immune system's activation. Nevertheless, continued IL-10 production beyond this critical juncture precipitates immune dysregulation. The model further elucidates that under specific parameters (refer to Figures 14, 15, 16, 17, and 18), the duration to chronicity can be modulated. As depicted in Figure 18, a reduction in the parameter ω, indicative of a shortened duration to chronicity, correlates with a diminished hepatitis B viral load, as represented by the blue, red, and magma dashed lines. This outcome is anticipated since our model did not account for a temporal lag in the dynamics of naïve T lymphocytes. Consequently, the model posits that delays in the maturation of naïve T lymphocytes into T helper 1 cells significantly influence the determination of the duration to chronicity. The model's projections align with our expectations; logically, an extended duration to chronicity correlates with an elevated viral load and vice versa.

To ameliorate the deleterious effects of IL-10 in hepatitis B virus (HBV) infection, it is essential to meticulously modulate the immunological response to achieve effective viral clearance while preventing excessive immune suppression that could incite chronic infection or hepatocellular injury. Consequently, we advocate for the development of pharmacotherapeutic agents that specifically target IL-10 signaling within discrete cellular subsets or microenvironments to attenuate systemic adverse effects. Furthermore, employing monoclonal antibodies or small molecular antagonists to inhibit IL-10 receptors on distinct immune cell populations may mitigate the attenuation of antiviral responses while preserving the advantageous anti-inflammatory effects within hepatic tissues. Integrating IL-10 modulation with robust antiviral therapeutics can reduce the viral burden, thereby lessening the ne-

cessity for immune suppression. Additionally, co-administering IL-10 antagonists alongside other immunomodulatory agents that enhance T cell functionality or bolster antiviral immune responses can facilitate an optimal balance between immune activation and inhibition.

In the absence of immunoglobulins (antibodies), natural killer (NK) cells, effector B lymphocytes, and T cell-mediated responses, the basic reproduction number surpasses unity (i.e., $\mathbb{R}_0 > 1$), indicating a persistent, chronic HBV infection within the model framework 5. We analyze how these dynamics are modulated by the presence of antibodies, NK lymphocytes, effector B cells, naïve T lymphocytes, and a spectrum of cytokines. The simulation results presented in Figures 20, 21, and 22 reveal how varying the fractional-order parameter (φ) impacts the immune response to hepatitis B virus (HBV) and liver cancer dynamics. For $\varphi = 0.4$, the model's trajectory converges to the virus-free equilibrium, akin to the classical-order model, but with distinct paths and significant fluctuations in immune cell populations, indicating an unstable response characteristic of lower fractional values. As φ increases to 0.5 and 0.6, the immune response becomes smoother and more stable, reflecting a more refined depiction of the system's dynamics. Further increases to $\varphi = 0.7$ and 0.8 enhance stabilization, showing improved control over HBV and liver cancer infections, and aligning more closely with real-world behaviors. At $\varphi = 0.9$, the model exhibits near-optimal stability, with dynamics approaching equilibrium and resembling classical-order models. Finally, at $\varphi = 1$, the fractional-order model aligns with the classical-order case, demonstrating stable and predictable dynamics. Thus, the fractional-order model provides a detailed and flexible perspective on the immune system's response, smoothly transitioning to classical-order behavior and offering a comprehensive understanding of the system's dynamics compared to classical models.

Although both arbitrary and estimated parameters were utilized for the model simulations, incorporating temporal aspects of the immune response to the virus would enhance the model's accuracy. Temporal delays in the immune response to HBV infection profoundly affect immune dynamics. Consequently, future re-

search might expand upon this work by integrating time-delay variables into the immune response model. Additionally, refining the model to encompass diverse immunotherapeutic strategies, such as antibody-based therapies under clinical evaluation, chimeric antigen receptor T-cell (CAR-T) therapy, molecular interventions, and exhaustion therapy, would be advantageous. These therapeutic approaches are comprehensively reviewed in (Fatehi et al., 2022; Chenar et al., 2018; Abernathy et al., 2020; Cho & Levy, 2020; Bukkuri, 2020) to elucidate optimal treatment modalities for managing HBV and hepatic malignancies.

Chapter Summary

In this chapter, simulations were conducted for both the classical-order and fractional-order frameworks. The simulations for the classical-order model utilized parameters from both literature and estimates, while the fractional-order model relied solely on parameter values obtained from existing literature to examine the behavior of hepatitis B virus and liver cancer co-existence. The results are thoroughly discussed. These simulations were performed using MATLAB. The classical-order model was adjusted using HBV viral load data to estimate various parameters, which were then applied in different simulation scenarios. The findings revealed that the interleukin-10 cytokine plays a key role in influencing the time to chronic infection in patients. Sensitivity analysis was conducted on the reproduction number to identify the parameters that most significantly affect the spread of hepatitis B virus and the co-existence of liver tumors. The results show that the rate of new virus production by infected macrophages and the decay rate of the hepatitis B virus are the most critical factors. Therefore, efforts to control the transmission dynamics of hepatitis B virus and liver cancer should focus on minimizing these two parameters to effectively manage the infections.

CHAPTER FIVE

SUMMARY, CONCLUSIONS AND RECOMMENDATIONS

Overview

A classical-order and fractional-order mathematical models for the transmission dynamics of hepatitis B virus and liver cancer diseases has been presented in this dissertation. The body immune system was incorporate to examine its role on hepatitis B virus and liver cancer transmission dynamics and their totally clearance. The analytical and numerical results of these models were discussed. The results obtained from the models presented in CHAPTERS THREE and FOUR are summarized below.

Summary

This dissertation introduces and examines novel models for HBV infection and its coexistence with liver cancer, concentrating on the interactions among different elements of the immune system, such as natural killer (NK) cells, effector B lymphocytes, naïve T lymphocytes, T helper-1 cells, cytotoxic T lymphocytes, and signaling molecules like interleukin-10 (IL-10). The research demonstrates that boosting NK cells, antibody-driven virus elimination rates, and the activity of effector B cells and cytotoxic T lymphocytes generally improves infection clearance and maintains a disease-free condition. However, extremely high or low rates of virus elimination by antibodies, NK cells, or effector B cells have little influence on the stability of the endemic state. Conversely, increased production rates of naïve T lymphocytes, combined with any of the other immune components, can disrupt the equilibrium of persistent virus infection. IL-10 plays a dual role: it regulates inflammation but can also suppress essential immune responses, potentially contributing to viral persistence and poor outcomes with antiviral therapy. The model shows that increasing IL-10 production unexpectedly prolongs immune responses, suggesting that managing IL-10 levels is crucial for effective treatment. Antiviral treatments are crucial for developing strategies to control HBV and liver cancer infections. Therefore, the treatment of HBV was incorporated with two drug types: nucleotide analogues

(NAs) and IFN-based therapies. The goal is to reduce $\mathcal{R}_c$ below one, indicating effective infection control. Simulation results reveal that a nucleotide drug efficacy of around 74%, combined with an IFN therapy efficacy of 71%, can reduce $\mathcal{R}_c$ and shift the infection dynamics to a safer zone, demonstrating effective disease management. The study recommends developing targeted IL-10 inhibitors, combining them with antiviral drugs, and incorporating time delays and advanced immunotherapy techniques in future research to improve HBV and liver cancer management.

Conclusions

A mathematical framework, including both classical-order and fractional-order models, was created to capture the transmission dynamics of hepatitis B virus and liver tumors, integrating the vital role of the immune system's reaction to the infection. The model was structured with the aid of a diagram depicted in Figure 1, and the model parameters are outlined in Tables 1, 2, and 3. The proposed models were both mathematically consistent and biologically significant, as all solutions were shown to be positive and bounded. Furthermore, the virus-free and virus-persistent equilibrium states of the models were identified. The fractional model was also employed to evaluate the effects of treating infected individuals with nucleotide analogs (NAs) and interferon-based (IFN) treatment, as well as the immune system's reaction to the hepatitis B virus, on the transmission patterns of hepatitis B virus and liver cancer.

The fractional model was also solved numerically using $ode15s$ in MATLAB with the iterated-Adams-Bashforth numerical approach, and the outcomes from these simulations were carefully analyzed. Additionally, a sensitivity analysis was performed on the reproduction number with respect to all the model parameters that influence it. This analysis revealed that the most sensitive parameters are ε, μ_{M_0}, μ_{M_1}, μ_V, μ_{I_M}, ψ, and ζ. These parameters need close consideration when developing methods to manage hepatitis B virus and liver tumor infections. Integrating the immune response into the treatment of infected individuals is essential for identifying the most efficient control methods and the best timing for therapy. This strategy aids in minimizing the spread of hepatitis B virus and liver cancer.

Recommendations

From the results of this work, the study suggests developing targeted drugs to selectively inhibit IL-10 activity or block IL-10 receptors on specific immune cells to minimize its negative effects. Combining IL-10 modulation with potent antiviral drugs could help reduce viral load and minimize immune suppression.

Additionally, HBV treatments should be initiated when the viral load is decreasing rather than increasing.

Future research should incorporate time delays in immune responses and explore advanced immunotherapy methods, such as antibody therapies, chimeric antigen receptor T-cell treatment, and molecular treatment, to enhance the management of hepatitis B virus and liver tumors.

Furthermore, future studies should aim to incorporate datasets that include patients with liver cancer to evaluate the generalizability of the results and explore disease-specific dynamics.

REFERENCES

Abbas, A. K., Lichtman, A. H., & Pillai, S. (2014). *Cellular and molecular immunology E-Book*. Philadelphia, USA: Elsevier Health Sciences.

Abernathy, Z., Abernathy, K., & Stevens, J. (2020). A mathematical model for tumor growth and treatment using virotherapy. *AIMS Mathematics*, *5*(5), 4136–4150.

Ahmad, S., Ullah, A., Arfan, M., & Shah, K. (2020). On analysis of the fractional mathematical model of rotavirus epidemic with the effects of breastfeeding and vaccination under atangana-baleanu (AB) derivative. *Chaos, Solitons & Fractals*, *140*, 110233.

Ahmed, E., Hashish, A., & Rihan, F. (2012). On fractional order cancer model. *Journal of Fractional Calculus & Applied Analysis*, *3*(2), 1–6.

Akman Yıldız, T., Arshad, S., & Baleanu, D. (2018). Optimal chemotherapy and immunotherapy schedules for a cancer-obesity model with caputo time fractional derivative. *Mathematical Methods in the Applied Sciences*, *41*(18), 9390–9407.

Albertsen, P. C. (2003). The use of models in the estimation of disease epidemiology. *The Journal of Urology*, *170*(2 Pt 1), 697.

Alzahrani, E., El-Dessoky, M., & Baleanu, D. (2021). Mathematical modeling and analysis of the novel coronavirus using atangana–baleanu derivative. *Results in Physics*, *25*, 104240.

Amin, M., Farman, M., Akgül, A., & Alqahtani, R. T. (2022). Effect of vaccination to control COVID-19 with fractal fractional operator. *Alexandria Engineering Journal*, *61*(5), 3551–3557.

Anderson, L., Jang, S., & Yu, J.-L. (2015). Qualitative behavior of systems of tumor–$CD4^+$–cytokine interactions with treatments. *Mathematical Methods in the Applied Sciences*, *38*(17), 4330–4344.

Anderson, R. M., & May, R. M. (1991). *Infectious diseases of humans: dynamics and control*. New York, USA: Oxford University Press.

Arabameri, A., Asemani, D., & Hajati, J. (2018). Mathematical modeling of in-vivo tumor-immune interactions for the cancer immunotherapy using matured dendritic cells. *Journal of Biological Systems*, *26*(01), 167–188.

Atangana, A. (2018). Blind in a commutative world: simple illustrations with functions and chaotic attractors. *Chaos, Solitons & Fractals*, *114*, 347–363.

Atangana, A., & Baleanu, D. (2016). New fractional derivatives with nonlocal and non-singular kernel: theory and application to heat transfer model. *arXiv preprint*, arXiv:1602.03408.

Babiker, Z. O. E., Hogan, C., Ustianowski, A., & Wilkins, E. (2012). Does interferon-sparing tenofovir disoproxil fumarate-based therapy have a role in the management of severe acute hepatitis delta superinfection? *Journal of Medical Microbiology*, *61*(12), 1780–1783.

Baleanu, D., Diethelm, K., Scalas, E., & Trujillo, J. J. (2012). *Fractional calculus: models and numerical methods* (Vol. 3). 5Toh Tuck Link, Singapore 596224: World Scientific.

Bellomo, N., Li, N., & Maini, P. K. (2008). On the foundations of cancer modelling: selected topics, speculations, and perspectives. *Mathematical Models & Methods in Applied Sciences*, *18*(04), 593–646.

Beňová, K., Hancková, M., Koči, K., Kúdelová, M., & Betáková, T. (2020). T cells and their function in the immune response to viruses. *Acta Virologica*, *64*(2), 131–143.

Bhadauria, A. (2011). Correlation between hepatitis and cancer: A mathematical model. *International Journal of Mathematical Sciences & Computing*, *1*(2), 79–86.

Blower, S. M., & Dowlatabadi, H. (1994). Sensitivity and uncertainty analysis of complex models of disease transmission: an HIV model, as an example. *International Statistical Review/Revue Internationale de Statistique*, *62*(2), 229–243.

Bodnar, M., & Foryś, U. (2000a). Behaviour of solutions to marchuk's model depending on a time delay. *International Journal of Applied Mathematics & Computer Science*, *10*(1), 97–112.

Bodnar, M., & Foryś, U. (2000b). Periodic dynamics in a model of immune system. *Applicationes Mathematicae*, *27*(1), 113–126.

Brockman, M. A., Kwon, D. S., Tighe, D. P., Pavlik, D. F., Rosato, P. C., Sela, J., ... Moss, K. (2009). IL-10 is up-regulated in multiple cell types during viremic HIV infection and reversibly inhibits virus-specific T cells. *Blood, The Journal of the American Society of Hematology*, *114*(2), 346–356.

Brooks, D. G., Trifilo, M. J., Edelmann, K. H., Teyton, L., McGavern, D. B., & Oldstone, M. B. (2006). Interleukin-10 determines viral clearance or persistence in vivo. *Nature Medicine*, *12*(11), 1301–1309.

Bukkuri, A. (2020). Optimal control analysis of combined chemotherapy-immunotherapy treatment regimens in a PKPD cancer evolution model. *Biomath*, *9*(1), ID–2002137.

Bunimovich-Mendrazitsky, S., Shochat, E., & Stone, L. (2007). Mathematical model of BCG immunotherapy in superficial bladder cancer. *Bulletin of Mathematical Biology*, *69*, 1847–1870.

Busca, A., & Kumar, A. (2014). Innate immune responses in hepatitis B virus (HBV) infection. *Virology Journal*, *11*, 1–8.

Caputo, M., & Fabrizio, M. (2015). A new definition of fractional derivative without singular kernel. *Progress in Fractional Differentiation & Applications*, *1*(2), 73–85.

Cariboni, J., Gatelli, D., Liska, R., & Saltelli, A. (2007). The role of sensitivity analysis in ecological modelling. *Ecological Modelling*, *203*(1-2), 167–182.

Castillo-Chavez, C., & Song, B. (2004). Dynamical models of tuberculosis and their applications. *Mathematical Biosciences & Engineering*, *1*(2), 361–404.

Chataa, P., Nyabadza, F., & Naandam, S. M. (2021). Mathematical modelling of the transmission dynamics of hepatitis B virus in the presence of imperfect vaccination. *Journal of Mathematical & Computational Sciences*, *11*(6), 6949–6979.

Chenar, F. F., Kyrychko, Y., & Blyuss, K. (2018). Mathematical model of immune response to hepatitis B. *Journal of Theoretical Biology*, *447*, 98–110.

Chitnis, N., Hyman, J. M., & Cushing, J. M. (2008). Determining important parameters in the spread of malaria through the sensitivity analysis of a mathematical model. *Bulletin of Mathematical Biology*, *70*, 1272–1296.

Cho, H., & Levy, D. (2020). The impact of competition between cancer cells and healthy cells on optimal drug delivery. *Mathematical Modelling of Natural Phenomena*, *15*, 42.

Ciupe, S. M., Ribeiro, R. M., Nelson, P. W., Dusheiko, G., & Perelson, A. S. (2007). The role of cells refractory to productive infection in acute hepatitis B viral dynamics. *Proceedings of the National Academy of Sciences*, *104*(12), 5050–5055.

Ciupe, S. M., Ribeiro, R. M., Nelson, P. W., & Perelson, A. S. (2007). Modeling the mechanisms of acute hepatitis B virus infection. *Journal of Theoretical Biology*, *247*(1), 23–35.

Ciupe, S. M., Ribeiro, R. M., & Perelson, A. S. (2014). Antibody responses during hepatitis B viral infection. *PLoS Computational Biology*, *10*(7), e1003730.

Colombatto, P., Civitano, L., Bizzarri, R., Oliveri, F., Choudhury, S., Gieschke, R., ... Peginterferon Alfa-2a HBeAg-Negative Chronic Hepatitis B Study Group. (2006). A multiphase model of the dynamics of HBV infection in HBeAg-negative patients during pegylated interferon-α2a, lamivudine and combination therapy. *Antiviral Therapy*, *11*(2), 197–212.

Coskun, H., Summerfield, T. L., Kniss, D. A., & Friedman, A. (2010). Mathematical modeling of preadipocyte fate determination. *Journal of Theoretical Biology*, *265*(1), 87–94.

Dahari, H., Shudo, E., Ribeiro, R. M., & Perelson, A. S. (2009). Modeling complex decay profiles of hepatitis B virus during antiviral therapy. *Hepatology*, *49*(1), 32–38.

Das, A., Ellis, G., Pallant, C., Lopes, A. R., Khanna, P., Peppa, D., ... Gill, U. (2012). IL-10–producing regulatory B cells in the pathogenesis of chronic hepatitis b virus infection. *The Journal of Immunology*, *189*(8), 3925–3935.

Dehingia, K., Sarmah, H. K., & Jeelani, M. B. (2021). A brief review on cancer research and its treatment through mathematical modelling. *Annals of Cancer Research & Therapy*, *29*(1), 34–40.

de Pillis, L. G., Fister, K. R., Gu, W., Head, T., Maples, K., Neal, T., ... Kozai, K. (2008). Optimal control of mixed immunotherapy and chemotherapy of tumors. *Journal of Biological Systems*, *16*(01), 51–80.

de Pillis, L. G., Gu, W., & Radunskaya, A. E. (2006). Mixed immunotherapy and chemotherapy of tumors: modeling, applications and biological interpretations. *Journal of Theoretical Biology*, *238*(4), 841–862.

DeVico, A. L., & Gallo, R. C. (2004). Control of HIV-1 infection by soluble factors of the immune response. *Nature Reviews Microbiology*, *2*(5), 401–413.

Diekmann, O., & Heesterbeek, J. A. P. (2000). *Mathematical epidemiology of infectious diseases: model building, analysis and interpretation* (Vol. 5). West Sussex, PO19 1UD, England: John Wiley & Sons.

Diethelm, K., & Ford, N. J. (2002). Analysis of fractional differential equations. *Journal of Mathematical Analysis & Applications*, *265*(2), 229–248.

Dimitriadis, K., Katelani, S., Pappa, M., Fragkoulis, G. E., & Androutsakos, T. (2023). The role of interleukins in HBV infection: A narrative review. *Journal of Personalized Medicine*, *13*(12), 1675.

Eftimie, R., Bramson, J. L., & Earn, D. J. (2010). Modeling anti-tumor Th1 and Th2 immunity in the rejection of melanoma. *Journal of Theoretical Biology*, *265*(3), 467–480.

Elkaranshawy, H. A., Ezzat, H. M., Abouelseoud, Y., & Ibrahim, N. N. (2019). Innovative approximate analytical solution for standard model of viral dynamics: hepatitis C with direct-acting agents as an implemented case. *Mathematical Problems in Engineering*, *2019*(1), 1454739.

Engelhart, M., Lebiedz, D., & Sager, S. (2011). Optimal control for selected cancer chemotherapy ODE models: a view on the potential of optimal schedules and choice of objective function. *Mathematical Biosciences*, *229*(1), 123–134.

Farman, M., Aslam, M., Akgül, A., & Ahmad, A. (2021). Modeling of fractional-order COVID-19 epidemic model with quarantine and social distancing. *Mathematical Methods in the Applied Sciences*, *44*(11), 9334–9350.

Fatehi, F., Bingham, R. J., Dykeman, E. C., Patel, N., Stockley, P. G., & Twarock, R. (2020). An intracellular model of hepatitis B viral infection: an in silico platform for comparing therapeutic strategies. *Viruses*, *13*(1), 11.

Fatehi, F., Bingham, R. J., Stockley, P. G., & Twarock, R. (2022). An age-structured model of hepatitis B viral infection highlights the potential of different therapeutic strategies. *Scientific Reports*, *12*(1), 1252.

Freedman, H., & Pinho, S. T. R. d. (2009). Stability criteria for the cure state in a cancer model with radiation treatment. *Nonlinear Analysis: Real World Applications*, *10*(5), 2709–2715.

Gao, F., Li, X., Li, W., & Zhou, X. (2021). Stability analysis of a fractional-order novel hepatitis B virus model with immune delay based on caputo-fabrizio derivative. *Chaos, Solitons & Fractals*, *142*, 110436.

Ghanbari, B., & Gómez-Aguilar, J. (2018). Modeling the dynamics of nutrient–phytoplankton–zooplankton system with variable-order fractional derivatives. *Chaos, Solitons & Fractals*, *116*, 114–120.

Ghosh, S., & Banerjee, S. (2018). Mathematical modeling of cancer–immune system, considering the role of antibodies. *Theory in Biosciences*, *137*, 67–78.

Ghosh, S., & Samanta, G. (2019). Model justification and stratification for confounding of chlamydia trachomatis disease. *Letters in Biomathematics*, *6*(2), 1–13.

Gnitchogna Batogna, R., & Atangana, A. (2017). New two step laplace adam-bashforth method for integer an non integer order partial differential equations. *arXiv e-prints*, arXiv–1708.

Gómez-Aguilar, J. (2018). Analytical and numerical solutions of a nonlinear alcoholism model via variable-order fractional differential equations. *Physica A: Statistical Mechanics & its Applications*, *494*, 52–75.

Gómez-Aguilar, J., Ali Abro, K., Kolebaje, O., & Yildirim, A. (2019). Chaos in a calcium oscillation model via atangana-baleanu operator with strong memory. *The European Physical Journal Plus*, *134*, 1–9.

Gómez-Aguilar, J. F., López-López, M. G., Alvarado-Martínez, V. M., Baleanu, D., & Khan, H. (2017). Chaos in a cancer model via fractional derivatives with exponential decay and mittag-leffler law. *Entropy*, *19*(12), 681.

Gourley, S. A., Kuang, Y., & Nagy, J. D. (2008). Dynamics of a delay differential equation model of hepatitis B virus infection. *Journal of Biological Dynamics*, *2*(2), 140–153.

Goyal, A., Ribeiro, R. M., & Perelson, A. S. (2017). The role of infected cell proliferation in the clearance of acute HBV infection in humans. *Viruses*, *9*(11), 350.

Guang, Y., Yuzhong, L., & Hui, L. (2019). Establishment of an analysis model based on measurement of hepatitis B viral infection serum markers. *BMC Infectious Diseases*, *19*, 1–5.

Guedj, J., Dahari, H., Rong, L., Sansone, N. D., Nettles, R. E., Cotler, S. J., ... Perelson, A. S. (2013). Modeling shows that the NS5A inhibitor daclatasvir has two modes of action and yields a shorter estimate of the hepatitis C virus half-life. *Proceedings of the National Academy of Sciences*, *110*(10), 3991–3996.

Guidotti, L. G., & Chisari, F. V. (2001). Noncytolytic control of viral infections by the innate and adaptive immuneresponse. *Annual Review of Immunology*, *19*(1), 65–91.

Guidotti, L. G., Guilhot, S., & Chisari, F. V. (1994). Interleukin-2 and alpha/-beta interferon down-regulate hepatitis B virus gene expression in vivo by tumor necrosis factor-dependent and-independent pathways. *Journal of Virology*, *68*(3), 1265–1270.

Hao, W., Gong, S., Wu, S., Xu, J., Go, M. R., Friedman, A., & Zhu, D. (2017). A mathematical model of aortic aneurysm formation. *PloS one*, *12*(2), e0170807.

Hassuneh, M. R., Nagarkatti, M., & Nagarkatti, P. S. (2013). Role of interleukin-10 in the regulation of tumorigenicity of a T cell lymphoma. *Leukemia & Lymphoma*, *54*(4), 827–834.

Herbein, G., & O'brien, W. A. (2000). Tumor necrosis factor (TNF)–α and TNF Receptors in Viral Pathogenesis. *Proceedings of the Society for Experimental Biology & Medicine: Minireviews*, *223*(3), 241–257.

Hews, S., Eikenberry, S., Nagy, J. D., & Kuang, Y. (2010). Rich dynamics of a hepatitis B viral infection model with logistic hepatocyte growth. *Journal of Mathematical Biology*, *60*, 573–590.

Hollinger, F., & Liang, T. (2001). Hepatitis B virus. *Fields Virology*, *37*(1), 2971–3036.

Howard, F. H., Kwan, A., Winder, N., Mughal, A., Collado-Rojas, C., & Muthana, M. (2022). Understanding immune responses to viruses—do underlying Th1/Th2 cell biases predict outcome? *Viruses*, *14*(7), 1493.

Hu, J., & Liu, K. (2017). Complete and incomplete hepatitis B virus particles: formation, function, and application. *Viruses*, *9*(3), 56.

Hu, X., & Jang, S. R.-J. (2018). Dynamics of tumor–$CD4^+$–cytokine–host cells interactions with treatments. *Applied Mathematics & Computation*, *321*, 700–720.

Huang, H., Chen, C., Chang, W., Tao, M., & Huang, C. (2012). Entry of hepatitis B virus into immortalized human primary hepatocytes by clathrin-dependent endocytosis. *Journal of Virology*, *86*(17), 9443–9453.

Hyodo, N., Nakamura, I., & Imawari, M. (2004). Hepatitis B core antigen stimulates interleukin-10 secretion by both T cells and monocytes from peripheral blood of patients with chronic hepatitis B virus infection. *Clinical & Experimental Immunology*, *135*(3), 462–466.

Iboi, E. A., & Gumel, A. B. (2018). Mathematical assessment of the role of dengvaxia vaccine on the transmission dynamics of dengue serotypes. *Mathematical Biosciences*, *304*, 25–47.

Ivanov, A., Beers, S. A., Walshe, C. A., Honeychurch, J., Alduaij, W., Cox, K. L., ... Klymenko, T. (2009). Monoclonal antibodies directed to CD20 and HLA-DR can elicit homotypic adhesion followed by lysosome-mediated cell death in human lymphoma and leukemia cells. *The Journal of Clinical Investigation*, *119*(8), 2143–2159.

Jones, D. S., Plank, M., & Sleeman, B. D. (2009). *Differential equations and mathematical biology*. New York, USA: CRC press.

Kai, D. (2010). *The analysis of fractional differential equations: An application-oriented exposition using differential operators of caputo type* (Vol. 2004). Verlag Berlin Heidelberg 2010: Springer.

Kaplan, D. E., Ikeda, F., Li, Y., Nakamoto, N., Ganesan, S., Valiga, M. E., ... Chang, K.-M. (2008). Peripheral virus-specific T-cell interleukin-10 responses develop early in acute hepatitis C infection and become dominant in chronic hepatitis. *Journal of Hepatology*, *48*(6), 903–913.

Kermack, W. O., & McKendrick, A. G. (1927). A contribution to the mathematical theory of epidemics. *Proceedings of the Royal Society of London. Series A, Containing papers of a Mathematical and Physical Character*, *115*(772), 700–721.

Khan, M., Shah, S. W., Ullah, S., & Gómez-Aguilar, J. (2019). A dynamical model of asymptomatic carrier zika virus with optimal control strategies. *Nonlinear Analysis: Real World Applications*, *50*, 144–170.

Kim, H. Y., Kwon, H.-D., Jang, T. S., Lim, J., & Lee, H.-S. (2012). Mathematical modeling of triphasic viral dynamics in patients with HBeAg-positive chronic hepatitis B showing response to 24-week clevudine therapy. *PLoS One*, *7*(11), e50377.

Kirschner, D., & Panetta, J. C. (1998). Modeling immunotherapy of the tumor–immune interaction. *Journal of Mathematical Biology*, *37*, 235–252.

Kitagawa, K., Nakaoka, S., Asai, Y., Watashi, K., & Iwami, S. (2018). A PDE multiscale model of hepatitis C virus infection can be transformed to a system of ODEs. *Journal of Theoretical Biology*, *448*, 80–85.

Kmiec, Z. (2001). *Cooperation of liver cells in health and disease: with 18 tables*. Verlag Berlin Heidelberg New York: Springer Science & Business Media.

Kuznetsov, V. A., Makalkin, I. A., Taylor, M. A., & Perelson, A. S. (1994). Nonlinear dynamics of immunogenic tumors: parameter estimation and global bifurcation analysis. *Bulletin of Mathematical Biology*, *56*(2), 295–321.

Laing, K. (2022). *Immune responses to viruses* (Tech. Rep.). British Society for Immunology. Retrieved from `https://www.immunology.org/public-information/bitesized-immunology/pathogens-disease/immune-responses-viruses`

Lewin, S. R., Ribeiro, R. M., Walters, T., Lau, G. K., Bowden, S., Locarnini, S., & Perelson, A. S. (2001). Analysis of hepatitis B viral load decline under potent therapy: complex decay profiles observed. *Hepatology*, *34*(5), 1012–1020.

Liu, X., Ur Rahman, M., Arfan, M., Tchier, F., Ahmad, S., Inc, M., & Akinyemi, L. (2022). Fractional mathematical modeling to the spread of polio with the role of vaccination under non-singular kernel. *Fractals*, *30*(05), 2240144.

Liu, Y., Cheng, L.-s., Wu, S.-d., Wang, S.-q., Li, L., She, W.-m., ... Jiang, W. (2016). IL-10-producing regulatory B-cells suppressed effector T-cells but enhanced regulatory T-cells in chronic HBV infection. *Clinical Science*, *130*(11), 907–919.

Long, C., & Qi, H. (2009). Modeling viral and immune system dynamics of HBV infection. In *2009 International Conference on Information Engineering*

and Computer Science (pp. 1–4). Wuhan, China. doi: https://doi.org/10.1109/ICIECS.2009.5363718

Magin, R. (2004). Fractional calculus in bioengineering, part 1. *Critical Reviews™ in Biomedical Engineering*, *32*(1), 104.

Mahoney, F. J., & Kane, M. (1999). Hepatitis B vaccine. *Vaccines*, *3*, 58–82.

Makhlouf, A. M., El-Shennawy, L., & Elkaranshawy, H. A. (2020). Mathematical modelling for the role of $CD4^+$ T cells in tumor-immune interactions. *Computational & Mathematical Methods in Medicine*, *2020*(1), 7187602.

Mamat, M., & Subiyanto, A. K. (2013). Mathematical model of cancer treatments using immunotherapy, chemotherapy and biochemotherapy. *Applied Mathematical Sciences*, *7*, 247–261.

Martins, M., Ferreira Jr, S., & Vilela, M. (2007). Multiscale models for the growth of avascular tumors. *Physics of Life Reviews*, *4*(2), 128–156.

Mattes, J., Hulett, M., Xie, W., Hogan, S., Rothenberg, M. E., Foster, P., & Parish, C. (2003). Immunotherapy of cytotoxic T cell–resistant tumors by T helper 2 cells: an eotaxin and STAT6-dependent process. *The Journal of Experimental Medicine*, *197*(3), 387–393.

Michalopoulos, G. K. (2007). Liver regeneration. *Journal of Cellular Physiology*, *213*(2), 286–300.

Min, L., Su, Y., & Kuang, Y. (2008). Mathematical analysis of a basic virus infection model with application to HBV infection. *The Rocky Mountain Journal of Mathematics*, *38*(5), 1573–1585.

Mueller, S. N., & Rouse, B. T. (2009). Immune responses to viruses. *Clinical Immunology*, *27*, 421–431.

Murray, J. M., & Goyal, A. (2015). In silico single cell dynamics of hepatitis B virus infection and clearance. *Journal of Theoretical Biology*, *366*, 91–102.

Nagy, J. D. (2005). The ecology and evolutionary biology of cancer: a review of mathematical models of necrosis and tumor cell diversity. *Mathematical Biosciences & Engineering*, *2*(2), 381–418.

Nelder, J. A., & Mead, R. (1965). A simplex method for function minimization. *The Computer Journal*, *7*(4), 308–313.

Nisar, K. S., Ahmad, A., Inc, M., Farman, M., Rezazadeh, H., Akinyemi, L., & Akram, M. M. (2022). Analysis of dengue transmission using fractional order scheme. *AIMS Mathematics*, *7*(5), 8408–8429.

Nowak, M. A., Bonhoeffer, S., Hill, A. M., Boehme, R., Thomas, H. C., & McDade, H. (1996). Viral dynamics in hepatitis B virus infection. *Proceedings of the National Academy of Sciences*, *93*(9), 4398–4402.

Ogunlaran, O. M., & Oukouomi Noutchie, S. C. (2016). Mathematical model for an effective management of HIV infection. *BioMed Research International*, *2016*(1), 4217548.

Ohga, S., Nomura, A., Takada, H., Tanaka, T., Furuno, K., Takahata, Y., ... Hara, T. (2004). Dominant expression of interleukin-10 and transforming growth factor-β genes in activated T-cells of chronic active epstein–barr virus infection. *Journal of Medical Virology*, *74*(3), 449–458.

Opoku, N. K.-D. O., & Mazandu, G. K. (2020). Modelling the human immune response dynamics during progression from mycobacterium latent infection to disease. *Applied Mathematical Modelling*, *80*, 217–237.

Packer, A., Forde, J., Hews, S., & Kuang, Y. (2014). Mathematical models of the interrelated dynamics of hepatitis D and B. *Mathematical Biosciences*, *247*, 38–46.

Pawelek, K. A., Huynh, G. T., Quinlivan, M., Cullinane, A., Rong, L., & Perelson, A. S. (2012). Modeling within-host dynamics of influenza virus infec-

tion including immune responses. *PLoS Computational Biology*, *8*(6), e1002588.

Peeridogaheh, H., Meshkat, Z., Habibzadeh, S., Arzanlou, M., Shahi, J. M., Rostami, S., ... Teimourpour, R. (2018). Current concepts on immunopathogenesis of hepatitis B virus infection. *Virus Research*, *245*, 29–43.

Perelson, A. S., Neumann, A. U., Markowitz, M., Leonard, J. M., & Ho, D. D. (1996). HIV-1 dynamics in vivo: virion clearance rate, infected cell lifespan, and viral generation time. *Science*, *271*(5255), 1582–1586.

Perez-Diez, A., Joncker, N. T., Choi, K., Chan, W. F., Anderson, C. C., Lantz, O., & Matzinger, P. (2007). CD4 cells can be more efficient at tumor rejection than CD8 cells. *Blood, The Journal of the American Society of Hematology*, *109*(12), 5346–5354.

Podlubny, I. (1998). *Fractional differential equations: an introduction to fractional derivatives, fractional differential equations, to methods of their solution and some of their applications*. San Diego, California 92101-4495, USA: Elsevier.

Qomlaqi, M., Bahrami, F., Ajami, M., & Hajati, J. (2017). An extended mathematical model of tumor growth and its interaction with the immune system, to be used for developing an optimized immunotherapy treatment protocol. *Mathematical Biosciences*, *292*, 1–9.

Rahib, L., Smith, B. D., Aizenberg, R., Rosenzweig, A. B., Fleshman, J. M., & Matrisian, L. M. (2014). Projecting cancer incidence and deaths to 2030: the unexpected burden of thyroid, liver, and pancreas cancers in the united states. *Cancer Research*, *74*(11), 2913–2921.

Ramsay, A. J., Ruby, J., & Ramshaw, I. A. (1993). A case for cytokines as effector molecules in the resolution of virus infection. *Immunology Today*, *14*(4), 155–157.

Revill, P. A., Chisari, F. V., Block, J. M., Dandri, M., Gehring, A. J., Guo, H., ... others (2019). A global scientific strategy to cure hepatitis B. *The Lancet Gastroenterology & Hepatology*, *4*(7), 545–558.

Roberts, P. A., Huebinger, R. M., Keen, E., Krachler, A.-M., & Jabbari, S. (2019). Mathematical model predicts anti-adhesion–antibiotic–debridement combination therapies can clear an antibiotic resistant infection. *PLoS Computational Biology*, *15*(7), e1007211.

Saifullah, S., Ali, A., Irfan, M., & Shah, K. (2021). Time-fractional klein–gordon equation with solitary/shock waves solutions. *Mathematical Problems in Engineering*, *2021*(1), 1–15.

Sanmamed, M. F., & Chen, L. (2018). A paradigm shift in cancer immunotherapy: from enhancement to normalization. *Cell*, *175*(2), 313–326.

Saraiva, M., & O'garra, A. (2010). The regulation of IL-10 production by immune cells. *Nature Reviews Immunology*, *10*(3), 170–181.

Sarkar, R. R., & Banerjee, S. (2005). Cancer self remission and tumor stability-a stochastic approach. *Mathematical Biosciences*, *196*(1), 65–81.

Schlicke, P., Kuttler, C., & Schumann, C. (2021). How mathematical modeling could contribute to the quantification of metastatic tumor burden under therapy: insights in immunotherapeutic treatment of non-small cell lung cancer. *Theoretical Biology & Medical Modelling*, *18*(1), 1–15.

Schulze, A., Gripon, P., & Urban, S. (2007). Hepatitis B virus infection initiates with a large surface protein–dependent binding to heparan sulfate proteoglycans. *Hepatology*, *46*(6), 1759–1768.

Sharma, S., & Samanta, G. (2013). Dynamical behaviour of a tumor-immune system with chemotherapy and optimal control. *Journal of Nonlinear Dynamics*, *2013*(1), 608598.

Sheena, B. S., Hiebert, L., Han, H., Ippolito, H., Abbasi-Kangevari, M., Abbasi-Kangevari, Z., ... Adane, M. M. (2022). Global, regional, and national burden of hepatitis B, 1990–2019: a systematic analysis for the Global Burden of Disease Study 2019. *The Lancet Gastroenterology & Hepatology*, *7*(9), 796–829.

Shepard, C. W., Simard, E. P., Finelli, L., Fiore, A. E., & Bell, B. P. (2006). Hepatitis B virus infection: epidemiology and vaccination. *Epidemiologic Reviews*, *28*(1), 112-125.

Shtylla, B., Gee, M., Do, A., Shabahang, S., Eldevik, L., & de Pillis, L. (2019). A mathematical model for DC vaccine treatment of type I diabetes. *Frontiers in Physiology*, *10*, 1107.

Spalding, K. L., Arner, E., Westermark, P. O., Bernard, S., Buchholz, B. A., Bergmann, O., ... Britton, T. (2008). Dynamics of fat cell turnover in humans. *Nature*, *453*(7196), 783–787.

Su, Y., Wen, Y., & Min, L. (2012). Analysis of a HBV infection model with ALT. In *2012 IEEE 6th International Conference on Systems Biology (ISB)* (pp. 97–100). Xi'an, China.

Sun, D., Liu, J., Su, X., & Pei, G. (2022). Fractional differential equation modeling of the HBV infection with time delay and logistic proliferation. *Frontiers in Public Health*, *10*, 1036901.

Sweilam, N. H., Al-Mekhlafi, S. M., Assiri, T., & Atangana, A. (2020). Optimal control for cancer treatment mathematical model using atangana–baleanu–caputo fractional derivative. *Advances in Difference Equations*, *2020*(1), 1–21.

Sypsa, V.-A., Mimidis, K., Tassopoulos, N. C., Chrysagis, D., Vassiliadis, T., Moulakakis, A., ... Hatzakis, A. (2005). A viral kinetic study using pegylated interferon alfa-2b and/or lamivudine in patients with chronic hepatitis B/HBeAg negative. *Hepatology*, *42*(1), 77–85.

Tacke, F. (2017). Targeting hepatic macrophages in liver disease. *Journal of Hepatology*, *66*(1), 123–131. Retrieved from https://pubmed.ncbi.nlm.nih.gov/28485309/ doi: 10.1016/j.jhep.2016.08.024

Takkenberg, R., Weegink, C., Zaaijer, H., & Reesink, H. (2010). New developments in antiviral therapy for chronic hepatitis B. *Vox Sanguinis*, *98*(4), 481–494.

Tao, Y., Guo, Q., & Aihara, K. (2010). A mathematical model of prostate tumor growth under hormone therapy with mutation inhibitor. *Journal of Nonlinear Science*, *20*(2), 219–240.

Taylor, A. E., & Lay, D. C. (1986). *Introduction to functional analysis*. USA: Krieger Publishing Co., Inc.

Tilahun, G. T., Makinde, O. D., & Malonza, D. (2018). Co-dynamics of pneumonia and typhoid fever diseases with cost effective optimal control analysis. *Applied Mathematics & Computation*, *316*, 438–459.

Vos, T., Barber, R. M., Bell, B., Bertozzi-Villa, A., Biryukov, S., Bolliger, I., ... Dicker, D. (2015). Global, regional, and national incidence, prevalence, and years lived with disability for 301 acute and chronic diseases and injuries in 188 countries, 1990–2013: a systematic analysis for the Global Burden of Disease Study 2013. *The Lancet*, *386*(9995), 743–800.

Walter, M. R. (2014). The molecular basis of IL-10 function: from receptor structure to the onset of signaling. *Interleukin-10 in Health & Disease*, *380*, 191–212.

Wan, X.-P., Zhang, X.-B., Li, Y., Zhao, L., Zhang, L., Zhang, X.-F., & Zhang, L.-X. (2014). Macrophage polarization in liver disease and hepatocellular carcinoma. *Hepatology*, *60*(2), 519–532. Retrieved from https://pubmed.ncbi.nlm.nih.gov/24975576/ doi: 10.1002/hep.27290

Webster, G. J., Hallett, R., Whalley, S. A., Meltzer, M., Balogun, K., Brown, D., ... others. (2000). Molecular epidemiology of a large outbreak of hepatitis B linked to autohaemotherapy. *The Lancet*, *356*(9227), 379–384.

Webster, G. J., Reignat, S., Maini, M. K., Whalley, S. A., Ogg, G. S., King, A., ... others. (2000). Incubation phase of acute hepatitis B in man: dynamic of cellular immune mechanisms. *Hepatology*, *32*(5), 1117–1124.

Whalley, S. A., Murray, J. M., Brown, D., Webster, G. J., Emery, V. C., Dusheiko, G. M., & Perelson, A. S. (2001). Kinetics of acute hepatitis B virus infection in humans. *The Journal of Experimental Medicine*, *193*(7), 847–854.

Wiah, E., Dontwi, I., & Adetunde, I. (2011). Using mathematical model to depict the immune response to hepatitis B virus infection. *Journal of Mathematics Research*, *3*(2), 157.

Wilson, J. N., Nokes, D. J., & Carman, W. F. (1998). Current status of HBV vaccine escape variants–a mathematical model of their epidemiology. *Journal of Viral Hepatitis*, *5*, 25–30.

World Health Organization. (2002). *Department of Communicable Diseases Surveillance and Response. Hepatitis B; 2002 Report* (Tech. Rep.). WHO/CDS/CSR/LYO. Retrieved from `http://www.who.int/emc`

World Health Organization. (2019). Hepatitis B vaccines: WHO position paper, july 2017–Recommendations. *Vaccine*, *37*(2), 223–225.

Yang, Z., Yang, C., Dong, Y., & Takeuchi, Y. (2020). Mathematical modelling of the inhibitory role of regulatory T cells in tumor immune response. *Complexity*, *2020*(1), 4834165.

Yousfi, N., Hattaf, K., & Tridane, A. (2011). Modeling the adaptive immune response in HBV infection. *Journal of Mathematical Biology*, *63*, 933–957.

Zhang, L., ur Rahman, M., Arfan, M., & Ali, A. (2021). Investigation of mathematical model of transmission co-infection TB in HIV community with a non-singular kernel. *Results in Physics*, *28*, 104559.

Zhang, S., Bernard, D., Khan, W. I., Kaplan, M. H., Bramson, J. L., & Wan, Y. (2009). $CD4^+$ T-cell-mediated anti-tumor immunity can be uncoupled from autoimmunity via the STAT4/STAT6 signaling axis. *European Journal of Immunology*, *39*(5), 1252–1259.

Zhang, Y., Wallace, D. L., De Lara, C. M., Ghattas, H., Asquith, B., Worth, A., ... Beverley, P. C. (2007). In vivo kinetics of human natural killer cells: the effects of ageing and acute and chronic viral infection. *Immunology*, *121*(2), 258–265.

APPENDIX

Patient Data

Table 14: HBV DNA Levels for Patient 1 at Various Time Points

Patient	Days	HBV DNA per ml
1	101	7.22×10^8
	107	6.15×10^9
	116	6.37×10^9
	117	6.69×10^9
	121	2.16×10^9
	128	1.58×10^8
	137	2.32×10^5
	145	6.79×10^4
	153	4.52×10^4
	159	4.8×10^2
	188	390

Table 15: HBV DNA Levels for Patient 2 at Various Time Points

Patient	Days	HBV DNA per ml
2	36	7.41×10^6
	48	4.16×10^8
	60	6.82×10^8
	69	4.16×10^8
	70	2.59×10^8
	72	2.01×10^8
	73	1.53×10^8
	74	1.44×10^8
	76	1.37×10^8
	78	5.35×10^7
	79	1.09×10^8
	80	6.31×10^8
	81	5.33×10^7
	85	1.55×10^7
	86	5.70×10^7
	87	1.81×10^7
	93	4.21×10^5
	95	2.52×10^5
	103	1.30×10^5
	105	7.27×10^4
	118	7.78×10^4
	123	6.61×10^4
	140	8.52×10^3
	155	1.40×10^3
	167	3.20×10^3

Table 16: HBV DNA Levels for Patient 3 at Various Time Points

Patient	Days	HBV DNA per ml
3	108	3.27×10^8
	120	2.25×10^7
	127	4.85×10^7
	161	3.69×10^4
	193	4.40×10^5
	205	7.68×10^3
	275	9.20×10^3

Table 17: HBV DNA Levels for Patient 4 at Various Time Points

Patient	Days	HBV DNA per ml
4	93	1.11×10^9
	106	7.24×10^7
	110	2.66×10^7
	117	6.06×10^6
	134	1.05×10^5
	151	1.99×10^4
	165	8.40×10^2
	190	1.12×10^3
	213	390
	226	390

Table 18: HBV DNA Levels for Patient 5 at Various Time Points

Patient	Days	HBV DNA per ml
5	66	6.78×10^7
	80	3.58×10^8
	96	1.16×10^9
	110	9.61×10^7
	123	1.35×10^6
	143	7.66×10^4
	172	1.99×10^4
	195	3×10^3
	240	1.6×10^3

Table 19: HBV DNA Levels for Patient 6 at Various Time Points

Patient	Days	HBV DNA per ml
6	99	1.4×10^8
	114	2.05×10^9
	116	4×10^9
	118	1.82×10^9
	120	2.12×10^9
	122	9.65×10^8
	127	1.25×10^9
	129	2.87×10^8
	132	1.88×10^8
	134	1.74×10^8
	136	1.11×10^8
	140	1.15×10^8
	143	4.26×10^7
	145	3.95×10^7
	149	2.59×10^7
	151	3.34×10^7
	157	1.35×10^7
	159	4.73×10^6
	161	4.58×10^6
	163	1.76×10^5
	171	1.14×10^4
	174	2.62×10^4
	177	1.95×10^4
	181	1.30×10^4
	186	6.60×10^3
	198	4.48×10^3
	280	1.22×10^4

Table 20: HBV DNA Levels for Patient 7 at Various Time Points

Patient	Days	HBV DNA per ml
7	95	6.86×10^9
	105	5.66×10^9
	120	5.77×10^9
	122	6.10×10^9
	124	9.15×10^9
	126	7.37×10^9
	128	1.43×10^9
	133	1.43×10^9
	135	9.50×10^9
	137	7.53×10^8
	150	1.94×10^9
	153	3.03×10^8
	155	3.81×10^9
	157	6.87×10^8
	159	1.91×10^8
	161	5.86×10^7
	165	1.22×10^8
	169	5.80×10^7
	172	4.85×10^7
	174	2.10×10^7
	179	1.46×10^7
	181	2.49×10^6
	190	1.38×10^7
	222	3.44×10^6
	223	2.32×10^6
	226	4.33×10^6
	234	1.81×10^6
	240	2.79×10^6
	263	3.16×10^6